THE UNIVERSITY OF QUEENSLAND

AUSTRALIA

Global metabolic effect of manipulating pyruvate dehydrogenase complex activity in mammalian cells

Maria Buchsteiner

(Dipl.-Ing., M. Sc.)

A thesis submitted for the degree of Doctor of Philosophy at The University of Queensland in 2014

Australian Institute of Bioengineering and Nanotechnology

Abstract

Aerobic glycolysis is an inefficient metabolic phenotype displayed by many rapidly proliferating cells during growth. It is characterized by high glycolytic activity and only partial oxidation of glucose resulting in the production of high amounts of lactate. This phenotype was originally reported by Otto Warburg in 1927 as a hallmark of cancer and – while it is now known to occur in other fast growing cells as well – it remains an interesting target for cancer therapy. Aerobic glycolysis also has major implications for biopharmaceutical production, since lactate accumulation can be growth inhibiting, limiting the cell density that can be achieved in culture.

Due to its association with various diseases and being an unfavorable metabolic phenotype in industrial applications, reducing the Warburg effect and analyzing accompanying effects on the cell as a whole are of great interest. Whereas in cancer therapy the objective is to kill cells relying on aerobic glycolysis, the aim in industrial applications is to reduce aerobic glycolysis without inducing cell death or inhibiting cell growth. Pyruvate dehydrogenase complex (PDC) is a mitochondrial gatekeeping enzyme determining how much pyruvate is converted to acetyl-CoA and subsequently enters the TCA cycle. PDC activity is regulated by reversible phosphorylation catalyzed by pyruvate dehydrogenase kinase (PDK) (phosphorylation → inactivation) and pyruvate dehydrogenase phosphatase (dephosphorylation → activation). PDC activity can be increased by inhibiting PDK using dichloroacetate (DCA) a known PDK inhibitor, hereby reducing aerobic glycolysis.

The objective in this thesis was twofold; i) analyzing metabolic as well as growth inhibitory effects of DCA in human embryonic kidney 293 (HEK293) cells, and ii) investigating the effects of a non growth inhibiting DCA concentration using Chinese hamster ovary (CHO) cells in industrial relevant bioprocesses. In both studies aerobic glycolysis decreased with increasing DCA concentration characterized by reduced glucose consumption and lactate production. At lower DCA concentrations cell growth was unaffected. Furthermore, no increase in oxidative metabolism was detected at low DCA concentration indicating that the cells adopt a more energy efficient metabolism without directing more pyruvate into the TCA cycle. However, it appears that the cytoplasmic pyruvate fraction is reduced as not only less lactate but also less alanine is produced. The metabolic changes observed were mostly attributable to post-translational regulation since transcriptomics and proteomics analyses revealed only minor changes to metabolic enzymes. However, in the absence of

increased TCA cycle activity, allosteric regulation of glycolytic enzymes did not readily explain reduced glycolysis.

Cell growth in HEK293 cells was reduced only at higher DCA concentration when increased cellular stress and TCA cycle activity were detected. Since DCA was found to depolarize mitochondria the increased TCA cycle activity may not result in higher ATP production and in fact the ATP yield may be insufficient leading to a “metabolic crisis” and reduced cell growth. Additionally, in the HEK293 study asparagine synthetase (ASNS) activity, amino acid transporter gene expression and mitochondrial one-carbon metabolism were increased in DCA cultures. Increased ASNS activity and one-carbon metabolism have been linked to various human diseases including cancer. However, further investigations are necessary to explain the upregulation of these reactions during increased PDC activity.

With regard to industrial applications, reduced aerobic glycolysis induced by DCA led to longer cultivation periods and higher final antibody titers in CHO cell cultures due to lower lactate accumulation and slower increase in osmolality. Cell specific productivity and antibody quality in terms of charge variants, aggregation and glycan pattern were unaffected by DCA.

In summary, we investigated the effects of increased PDC activity induced by DCA with regard to metabolic effects and growth inhibition. At lower DCA concentration the cells appear to have a more energy efficient metabolism and reduced aerobic glycolysis proved to be beneficial for culture performance and antibody production. However, the exact mechanisms leading to growth inhibition caused by DCA remain to be further investigated.

Declaration by author

This thesis is composed of my original work, and contains no material previously published or written by another person except where due reference has been made in the text. I have clearly stated the contribution by others to jointly-authored works that I have included in my thesis.

I have clearly stated the contribution of others to my thesis as a whole, including statistical assistance, survey design, data analysis, significant technical procedures, professional editorial advice, and any other original research work used or reported in my thesis. The content of my thesis is the result of work I have carried out since the commencement of my research higher degree candidature and does not include a substantial part of work that has been submitted to qualify for the award of any other degree or diploma in any university or other tertiary institution. I have clearly stated which parts of my thesis, if any, have been submitted to qualify for another award.

I acknowledge that an electronic copy of my thesis must be lodged with the University Library and, subject to the General Award Rules of The University of Queensland, immediately made available for research and study in accordance with the *Copyright Act 1968*.

I acknowledge that copyright of all material contained in my thesis resides with the copyright holder(s) of that material. Where appropriate I have obtained copyright permission from the copyright holder to reproduce material in this thesis.

Maria Buchsteiner

Publications during candidature

Oral presentations

Buchsteiner M, Quek LE, Gray P, Nielsen LK (2013) Improving Culture Performance and Antibody Production in CHO Cell Culture Processes by Reducing the Warburg Effect. Presented at BioProcessing Network Annual Conference 2013. October 22nd – 24th. Gold Coast, Australia.

Buchsteiner M, Quek LE, Gray P, Nielsen LK (2012) Characterization of Increased Pyruvate Dehydrogenase Complex Activity Caused by Dichloroacetate in HEK 293 Cells. Presented at School of Chemistry and Molecular Biosciences 8th Annual Research Students Symposium 2012. November 22nd. Brisbane, Australia

Poster presentations

Buchsteiner M, Quek LE, Gray P, Nielsen LK (2014) Improving culture performance and antibody production in CHO cell culture processes by reducing the Warburg effect. Presented at Cell Culture Engineering XIV, May 4th – 9th. Quebec, Canada

Buchsteiner M, Quek LE, Gray P, Nielsen LK (2012) Systems Level Characterisation of HEK293 Cells with Dichloroacetate Enhanced Pyruvate Dehydrogenase Activity. Presented at 23rd meeting of the European Society for Animal Cell Technology. June 23rd – 26th. Lille, France

Publications included in this thesis

No publications included

Contributions by others to the thesis

Chapter 3: Dynamic Metabolic Flux Analysis using B-splines to study the Effects of Temperature Shift on CHO Cell Metabolism

Contributor	Statement of contribution
Maria Buchsteiner (Candidate)	Designed experiments (30%) Performed experiments (100%) Analysed data (30%) Wrote chapter (30%) Edited chapter (10%)
Verónica Martínez	Designed experiments (30%) Developed software (90%) Analysed data (70%) Wrote chapter (70%) Edited chapter (19%)
Peter Gray	Edited chapter (1%)
Lake-Ee Quek	Designed experiments (10%) Developed software (10%) Edited chapter (40%)
Lars Keld Nielsen	Designed experiments (30%) Edited chapter (30%)

Chapter 4: Improving Culture Performance and Antibody Production in CHO Cell Culture Processes by Reducing the Warburg Effect

Contributor	Statement of contribution
Maria Buchsteiner (Candidate)	Designed experiments (80%) Performed experiments (97%) Analysed data (80%) Wrote chapter (100%) Edited chapter (20%)
Lake-Ee Quek	Analysed data (10%) Edited chapter (9%)
Verónica Martínez	Analysed data (10%)
Camila Orellana & Esteban Marcellin	Performed experiments (3%)
Peter Gray	Edited chapter (1%)
Lars Keld Nielsen	Designed experiments (20%) Edited chapter (70%)

Chapter 5: Characterization of Increased Pyruvate Dehydrogenase Complex Activity Induced by Dichloroacetate in HEK293 Cells at a Cellular System Level

Contributor	**Statement of contribution**
Maria Buchsteiner (Candidate)	Designed experiments (60%) Performed experiments (100%) Analysed data (90%) Wrote chapter (100%) Edited chapter (30%)
Lake-Ee Quek	Analysed data (10%)
Peter Gray	Edited chapter (1%)
Lars Keld Nielsen	Designed experiments (40%) Edited chapter (69%)

Appendix C: Metabolic Flux Analysis method

Contributor	**Statement of contribution**
Lake-Ee Quek	Developed software (100%) Wrote appendix (100%)

Appendix H: Generating a stable HEK293 cell line overexpressing resistin-like molecule β using a Tet-On 3G inducible expression system

Contributor	**Statement of contribution**
Maria Buchsteiner (Candidate)	Designed experiments (30%) Performed experiments (80%) Analysed data (100%) Wrote appendix (100%) Edited appendix (70%)
Stacey Anderson	Performed experiment (20%) Edited appendix (30%)
Lars Keld Nielsen	Designed experiments (70%)

Statement of parts of the thesis submitted to qualify for the award of another degree

None.

Acknowledgements

First and foremost, I would like to thank my supervisor Prof Lars Nielsen for giving me the opportunity to undertake my PhD in his group and sharing his extensive knowledge and continuing guidance allowing me to complete this thesis. I would like to thank both Prof Lars Nielsen and Prof Peter Gray for providing the resources required to perform the work in this thesis.

I would like thank Dr Lake-Ee Quek who was always ready to discuss mammalian cell metabolism and for his support in metabolic flux analysis. Many thanks also goes to Dr Mark Hodson, Dr Manuel Plan, Haryadi Sugiarto and Michael Wang for the LC-MS/MS and HPLC analysis. Thank you Dr Esteban Marcellin for introducing me to the world of proteomics and patiently answering all my questions. Thank you Dr Stefanie Dietmair for your help, especially during my first year. I would also like to thank my fellow students Veronica Salazar and Camila Orellana, it was a pleasure to work with you. Thank you to previous and current members of the Nielsen and Gray group for creating such a pleasant environment.

Ein dickes Dankeschön an die liebe Mama, Matthias, Opa Lothar, Oma Sigrid, Opa Achim, Opa Karli, Oma Gudrun und Oma Ursel für Eure Unterstützung Zeit meines Lebens. Ohne Euch hätte ich es nicht so weit geschafft. Vielen Dank auch für die vielen Hilfspakete, unzähligen Postkarten und aufmunternden Telefongespräche in die verschiedensten Ecken dieser Welt.

Last but not least, I would like to thank Efe. I am sure I would have finished this thesis without you, maybe even earlier. But I surely would have not enjoyed it as much. Thank you for your support and for forcing me from time to time to enjoy another critical part of being a PhD student: procrastinating. One out of three fulfilled.

This thesis would not have been possible without the financial support from The University of Queensland and the Australian Institute for Bioengineering and Nanotechnology (AIBN) in form of a University of Queensland International Scholarship – Fees, a University of Queensland Research Scholarship and an AIBN top-up scholarship.

Keywords

mammalian cell culture, metabolism, aerobic glycolysis, pyruvate dehydrogenase complex, dichloroacetate, systems biology

Australian and New Zealand Standard Research Classifications (ANZSRC)

ANZSRC code: 060104 Cell Metabolism, 40%

ANZSRC code: 60114 Systems Biology 50%

ANZSRC code: 100302 Bioprocessing, Bioproduction and Bioproducts 10%

Fields of Research (FoR) Classification

FoR code: 0601 Biochemistry and Cell Biology 90%

FoR code: 1003 Industrial Biotechnology 10%

Table of Contents

List of Figures

List of Tables

Selected Abbreviations and Symbols

2PG	2-phosphoglycerate
3PG	3-phosphoglycerate
5,10MTHF	5,10-methylenetetrahydrofolate
10-CHO-THF	10-formyl-THF
AA	Amino acid
Ab	Antibody
Ab2	IgG antibody Ab2
ACN	Acetonitrile
ACO	Aconitate
ACoA	Acetyl-CoA
Agj.p-val	Adjusted p value
ADP	Adenosine diphosphate
AEC	Adenylate energy charge
AMBIC	Ammonium bicarbonate
AMP	Adenosine monophosphate
AMPK	AMP-activated protein kinase
ANOVA	Analysis of Variance
ASNS	Asparagine synthetase (glutamine-hydrolyzing)
ATF4	Activating transcription factor
ATP	Adenosine triphosphate
B-DMFA	Dynamic metabolic flux analysis using B-splines
CARE	CCAAT/enhancer-binding protein (C/EBP)-ATF response element
CDW	Cell dry weight
CH^+-THF	5,10-methenyl-THF
CH_2-THF	5,10-methylene-THF
CHO	Chinese hamster ovary
CI	Confidence interval
CIT	Citrate
CoA	Coenzyme A
Ct	Cycle threshold
CTP	Cytidine triphosphate
DCA	Dichloroacetate
DDIT3	DNA damage-inducible transcript 3 protein
DDIT4	DNA damage-inducible transcript 4 protein
DHAP	Dihydroxyacetone phosphate
DMFA	Dynamic metabolic flux analysis
DOX	Doxycycline
E4P	Erythrose 4-phosphate
eIF2	Eukaryotic initiation factor 2
ER	Endoplasmic reticulum
ESI	Electrospray ionization
ETC	Electron transport chain
ETV4	ETS translocation variant 4
ETV5	ETS translocation variant 5

F16DP	Fructose 1,6-bisphosphate
F6P	Fructose 6-phophate
FA	Formic acid
FAD	Flavin adenine dinucleotide
FBA	Flux balance analysis
FC	Fold change
FDR	False discovery rate
FUM	Fumarate
FVA	Flux variability analysis
G1P	Glucose 1-phosphate
G6P	Glucose 6-phophate
GA3P	Glyceraldehy 3-phosphate
GCN2	general control nonderepressible 2
gDW	Gram dry weight
GeM	Genome-scale model
GO	Gene ontology
GOI	Gene of interest
GST	Glutathione S-transferase
GSTZ1	Glutathione S-transferase ζ1
HAS2AS	HAS2 antisense RNA 1
Hcys	Homocysteine
HEK293	Human embryonic kidney 293
HIF1α	Hypoxia-inducible factor 1-alpha
HIST1H4K	Histone H4
HIST2H2BE	Histone H2B type 2-E
HK	Hexokinase
HMOX	Heme oxygenase 1
HPLC	High performance liquid chromatography
IGFBP5	Insulin-like growth factor-binding protein 5
IgG	Immunoglobulin G
IHNBE	Inhibin beta E chain
ISO	Isocitrate
JNK	JUN NH_2-terminal kinase
kDa	Kilo Dalton
KGA	Oxoglutarate
KPYR	Pyruvate kinase isozymes L/R
L-DMFA	Linear DMFA
LAC	Lactate
LC	Liquid chromatography
LDH	Lactate dehydrogenase
LDHB	Lactate dehydrogenase B chain
LTBR	Tumor necrosis factor receptor superfamily member 3
μ	Cell-specific growth rate
mAb	Monoclonal antibody/antibodies
MAL	Malate
MDH	Malate dehydrogenase
MDHM	Mitochondrial malate dehydrogenase

ME	Malic enzyme
MFA	Metabolic flux analysis
MRM	Multiple reaction monitoring
mRNA	Messenger RNA
MS	Mass spectrometry
MTHFD1	Trifunctional C1-THF synthase
MTHFD1L	Monofunctional C1-tetrahydrofolate synthase
MTHFD2	Bifunctional methylenetetrahydrofolate dehydrogenase/cyclohydrolase
mTOR	Mammalian target of rapamycin
mTORC1	Mammalian target of rapamycin complex 1
MW	Molecular weight
MYOM2	Myomesin-2
NAD^+	Nicotinamide adenine dinucleotide
$NADP^+$	Nicotinamide adenine dinucleotide phosphate
OUR	Oxygen uptake rate
OXPHOS	Oxidative phosphorylation
PBS	Phosphate buffered saline
PC	Pyruvate carboxylase
pcd	Picogram(s) per cell per day
PCDH19	Protocadherin-19
PCK2	Phosphoenolpyruvate carboxykinase
PDC	Pyruvate dehydrogenase complex
PDK	Pyruvate dehydrogenase kinase
PDP	Pyruvate dehydrogenase phosphatase
PEP	Phosphoenolpyruvate
PERK	Protein kinase-like ER kinase
PFK	Phosphofructokinase
PGAM1	Phosphoglycerate mutase 1
PK	Pyruvate kinase
PPP	Pentose phosphate pathway
PYR	Pyruvate
Qp	Cell specific productivity
qRT-PCR	Quantitative real time polymerase chain reaction
R5P	Ribose 5-phosphate
rcf	Relative centrifugal force
RETNLB	Resistin like molecule beta
RL5P	ribulose 5-phosphate
RLU	Relative light unit
rpm	Rounds per minute
RT	Room temperature
SE	Standard error
SESN2	Sestrin-2
SHMT2	Mitochondrial serine hydroxymethyltransferase
siRNA	Small interfering RNA
SLC1A5	Solute Carrier Family 1, Member 5
SLC3A2	Solute Carrier Family 3, Member 2
SLC6A9	Solute Carrier Family 6, Member 9

SLC7A5	Solute Carrier Family 7, Member 5
SUC	Succinate
SWATH-MS	Sequential windowed data independent acquisition of the total high-resolution mass spectrometry
TCA cycle	Tricarboxylic acid cycle
TFA	Trifluoroacetic acid
THF	Tetrahydrofolate
TKTL1	Transketolase-like protein
TNFRSF12A	Tumor necrosis factor receptor superfamily member 12A
TNNT1	Troponin T
tRNA	Transfer RNA
TWEAK	TNF-Related Weak Inducer of Apoptosis
UDPG	UDP-glucose
UDPGA	UDP-glucuronic acid
UDPNAG	UDP N-acetylglucosamine
UPR	Unfolded protein response
VCD	Viable cell density
v/v	Volume per volume
w/v	Weight per volume
XL99-Ab2	Chinese hamster ovary cell line producing IgG antibody Ab2
Y	Yield

Chapter 1

General Introduction

1.1. Mammalian cell metabolism and the Warburg effect

Mammalian cell metabolism is highly structured, comprising of many pathways which are interlinked. Although strongly regulated mammalian metabolism provides the cell with a flexible metabolic structure to adapt to various energetic and biosynthetic demands and environmental conditions. The central metabolic pathways consist of glycolysis, pentose phosphate pathway, tricarboxylic acid (TCA) cycle, oxidative phosphorylation, glutaminolysis and metabolism of other amino acids. For energy generation in form of ATP, mammalian cells mainly rely on glycolysis and TCA cycle. Both pathways are spatially separated; glycolysis taking place in the cytosol while the TCA cycle is located in the mitochondrion; and are connected via the pyruvate dehydrogenase complex (PDC). The metabolic phenotype is determined by a variety of factors, one major determinant being oxygen availability. Mammalian cells either use glycolysis and TCA cycle with oxidative phosphorylation or mainly rely on glycolysis. If oxygen supply is sufficient, normal cells use glycolysis, TCA cycle and oxidative phosphorylation. In hypoxic conditions, oxygen as the final electron acceptor during oxidative phosphorylation is not available. Cells cannot use the TCA cycle but rely on glycolysis alone for ATP generation converting the glycolytic end-product, pyruvate, into lactate. During anaerobic glycolysis, less ATP per molecule glucose is produced and cells usually show a higher glycolytic rate to compensate for the lower energy yield. A third metabolic phenotype is aerobic glycolysis, also known as the Warburg effect. Cells performing aerobic glycolysis mostly rely on glycolysis and only little TCA cycle and oxidative phosphorylation are performed despite the presence of sufficient oxygen (Warburg, Wind & Negelein 1927). Similar to cells using anaerobic glycolysis a higher glycolytic rate and high lactate production are observed in these cells. Despite the fact that this metabolic phenotype is energy inefficient, many rapid proliferating cell types including many cancer cells, cells of embryonic tissue and cells used as production hosts in industrial applications prefer aerobic glycolysis, indicating that their similar metabolic and biosynthetic demands play a role (Hanahan & Weinberg 2011). At the same time, aerobic glycolysis has been associated to other congenital and age-related diseases in humans, such as congenital lactic acidosis or type-2 diabetes mellitus, and has been linked to impaired PDC activity (Stacpoole 2012). Due to its association with several diseases and being an unfavorable metabolic phenotype for industrial applications, reducing the Warburg effect and analyzing accompanying effects on the cell as a whole are of great interest.

Approaches to reduce the Warburg effect include reduction of glucose uptake, decrease of glycolytic rate as well as increase of pyruvate to acetyl-CoA conversion, latter being used in this work. PDC is the link between glycolysis and TCA cycle and its function plays a crucial role for the metabolism as it determines how much pyruvate enters the TCA cycle. PDC comprises of three components in multiple copies, pyruvate dehydrogenase (E1), dihydrolipoamide acetyltransferase (E2), and dihydrolipoamide dehydrogenase (E3), and is only active if unphosphorylated at three specific serine residues of E1-α subunit (Sale & Randle 1981; Teague et al. 1979; Yeaman et al. 1978). Phosphorylation (inactivation) and dephosphorylation (activation) are catalyzed by two enzymes, pyruvate dehydrogenase kinase (PDK) and pyruvate phosphatase, respectively.

Here, we use dichloroacetate (DCA), a known PDK inhibitor (Whitehouse, Cooper & Randle 1974), to indirectly increase PDC activity and hereby reduce the Warburg effect in two mammalian cell lines. First, the effects of increased PDC activity on culture performance and antibody production were explored using Chinese hamster ovary cells, the predominant cell line in industrial applications (Chapter 4). This was followed by investigations using human embryonic kidney 293 (HEK293) cells, as an example of a human cell line. DCA was found to have growth inhibitory and apoptotic effects on some cancer cells and has been investigated as a potential anti cancer drug. Using HEK293 cells the system wide effects of different DCA concentrations, metabolic effect with and without growth inhibition, were analyzed (Chapter 5). A systems biology approach was used to investigate the cellular changes during increased PDC activity using multiple omics technologies. A detailed literature review is provided in Chapter 2.

1.2. Systems biology

Cellular change in response to increased PDC activity can be at various functional levels (genes expression, protein abundance, or metabolite concentrations) and in order to investigate these changes various omics technologies (transcriptomics, proteomics, metabolomics, and fluxomics) can be used to obtain a detailed knowledge of the cell. Omics measurements and combining multiple omics technologies offer valuable information about the cell. Changes in transcriptome or proteome are not always reflected in the metabolic phenotype due to post-transcriptional or post-translational modifications as well as involvement of other regulators and degradation processes. Metabolite concentration and metabolic flux analysis are closer to the actual phenotype. However, changes in metabolite concentration may be the result of different metabolic activities and

transcriptomics and proteomics may be necessary to identify the corresponding enzyme activity. Therefore, the combination of transcriptomics and proteomics with metabolomics and fluxomics gives detailed information about the cell as a whole.

Transcriptomics is readily available for human cells, capable of measuring the complete set of RNAs. Similarly, proteomics analysis is well established for human cells. The release of the CHO cell genome in 2011 (Xu et al. 2011) provides the option to perform transcriptomics as well as proteomics analysis of CHO cell lines. Additionally, protocols for analysis of intracellular metabolite concentrations are available. Finally, metabolic flux analysis (MFA) can be used to estimate fluxes through central metabolic pathways on the basis of limited number of extracellular measurements.

Conventional MFA assumes a metabolic steady state, where intracellular fluxes are constant over time, and an average metabolic phenotype is estimated. This assumption though is only valid during mid exponential growth phase in batch cultures or continuous cultivations. In order to estimate intracellular fluxes over a complete cultivation or when variations in culture conditions occur, dynamic MFA (DMFA) approaches are necessary. An improved DMFA was developed based on current DMFA approaches by using B-splines performing higher order fit (B-DMFA, Chapter 3) and was subsequently used to calculate metabolic fluxes in a temperature shift experiment (Chapter 3) and in CHO cell cultures treated with DCA (Chapter 4).A temperature shift experiment was used as it provides a readily available tool to generate the required cell culture and metabolic data with changing metabolic rates needed to develop B-DMFA. Furthermore, mild hypothermia is widely used in industry to reduce the negative effects of the Warburg effect by reducing metabolic activity and therefore accumulation of toxic metabolites and increase of osmolality.

When specific enzyme activities in mammalian cells are investigated, genetic engineering is typically used to alter gene expression. The transfection is generally followed by selection for cells that have the introduced genomic modification. Genetic engineering can be time consuming and the clone obtained after single cell selection may not only have the desired genomic change but also may have other changes that were unknowingly selected (Dietmair et al. 2012). The obtained data from omics analysis would then not only give information about the effects of the intended but also of the unintentionally selected genomic modifications. In order to avoid this problem, either a cell line with an inducible expression system (Appendix H) can be generated or molecules that inhibit specific enzyme activity (if enzyme inhibition is pursued) can be used. Here, PDC activity was increased by using the small molecule PDK inhibitor DCA (Chapter 4 and 5).

1.3. Aims of this project

1. Develop dynamic metabolic flux analysis using B-splines to estimate metabolic fluxes in dynamic cell cultures and analysis of temperature shifted cultures compared to cultures maintained at a constant temperature (Chapter 3)
2. Analysis of increased PDC activity induced by DCA in CHO cells and its effect on culture performance and antibody production (Chapter 4)
3. Analysis of increased PDC activity induced by DCA in HEK293F cells at a cellular system level using different DCA concentrations (Chapter 5)

Chapter 2 provides a detailed literature review covering aerobic glycolysis, PDC and DCA. A contribution derived from research conducted during this thesis is the generation of a cell line with an inducible expression system as described in appendix H. However, this cell line was ultimately not used in the main investigations as DCA provided an easy and simple means to increase PDC activity. The cell line was subsequently used to investigate the effect of resistin-like molecule beta overexpression on glucose consumption in HEK293 cells.

Chapter 2

Literature Review

2.1. Mammalian cell central metabolism and ATP generation

Mammalian cell metabolism is highly complex and main metabolic pathways cannot be considered independent but rather as part of a complex and flexible structure. Additionally, mammalian cells are compartmentalized, particularly the cytosol and mitochondrion. The flexible network of metabolic pathways allows mammalian cells to adapt their metabolism to certain environmental conditions such as variations in nutrient or oxygen availability. The central metabolic pathways comprise of glycolysis, tricarboxylic acid (TCA) cycle, oxidative phosphorylation, pentose phosphate pathway (PPP), glutaminolysis and metabolism of other amino acids.

The displayed metabolic phenotype of mammalian cells is the combined result of different factors including, nutrient availability, nutrient transport, particularly glucose and glutamine into the cell, glycolysis, glutaminolysis, TCA cycle, oxidative phosphorylation, generation of cellular energy and regeneration of reducing power as well as metabolic flexibility of the cell and compartmentalization including further transport steps. The extracellular environment is also crucial with regard to altered metabolic phenotypes as many transport processes are concentration dependent.

In terms of energy generation in the form of ATP, glycolysis and TCA cycle are the two main sources. In glycolysis glucose is metabolized to pyruvate which can be further converted to CO_2 in the TCA cycle. Under aerobic conditions, mammalian cells use both glycolysis and TCA cycle for ATP generation while under anaerobic conditions the final electron acceptor during oxidative phosphorylation, oxygen, is not available and cells only use glycolysis and convert the glycolytic derived pyruvate into lactate. This is usually characterized by an increased glycolytic rate as more ATP needs to be derived from glycolytic pathway alone. However, even under conditions of sufficient oxygen availability, some cells prefer to convert pyruvate to lactate over using TCA cycle and oxidative phosphorylation. This metabolic phenotype is called aerobic glycolysis, was first observed by Otto Warburg, and is also known as the Warburg effect today (Warburg, Wind & Negelein 1927).

In this work we focused on glycolysis and TCA cycle as well as the connection between these two pathways with particular emphasis on aerobic glycolysis and possible approaches to reduce aerobic glycolysis in mammalian cells.

2.1.1. Glycolysis

The glucose metabolism is highly regulated, not only by activity of glycolytic enzymes but also the glucose transport across the cell membrane. Uptake of glucose is achieved by means of transport proteins (GLUT1, GLUT2, GLUT3, GLUT4, GLUT5, GLUT7) located in the cytoplasmic membrane as it is otherwise impermeable for polar molecules such as glucose. In most mammalian cells the glucose transport is a bidirectional diffusion driven by the concentration gradient across the cell membrane. Normally, the transport takes place in the uptake direction as free intracellular glucose concentrations are low due to rapid phosphorylation by hexokinases.

Once glucose is phosphorylated to glucose 6-phosphate it is further converted in three pathways: glycolysis, glycogen synthesis and PPP. In the main pathway glycolysis, glucose is converted to pyruvate via several intermediates some of which are also used for other biosynthetic pathways. Additionally, two ATP molecules and two NADH molecules are generated. Glucose 6-phosphate is also used for glycogen synthesis and can enter the PPP. In the PPP, NADPH molecules are generated required for cell anabolism and ribose 5-phosphate molecules for nucleic acid synthesis. Alternatively, ribose 5-phosphate can be converted to fructose 6-phosphate and glyceraldehyde 3-phosphate, both intermediates of glycolysis, providing metabolic flexibility in order to balance fluxes through these pathways. Fructose 6-phosphate itself is also required for amino sugar compound synthesis. Other glycolytic intermediates needed as precursors for biosynthesis are dihydroxyacetone-phosphate used for lipid synthesis via glycerol 3-phosphate and glycerate 3-phosphate used for serine and glycine synthesis.

Glycolytic enzyme abundance and activity are crucial for overall glycolytic activity. Allosteric regulation of glycolysis plays an important role for fast modulation of the glycolytic rate; the three regulatory enzymes being hexokinase (HK), phosphofructokinase (PFK), and pyruvate kinase (PK). HK catalyzes the first glycolytic reaction from glucose to glucose 6-phosphate consuming ATP and it is allosterically inhibited by its product glucose 6-phosphate (Regen et al. 1964). However, glucose 6-phosphate can also be generated from glycogen. Therefore, PFK rather than HK is considered the major regulatory glycolytic enzyme. PFK is also ATP-dependent and converts fructose 6-phosphate to fructose 1,6-bisphosphate. It is activated by AMP, ADP, and fructose 2,6-bisphosphate, while ATP and citrate are allosteric inhibitors reducing glycolytic rate when sufficient ATP or citrate for oxidation in TCA cycle are available (Costa Leite et al. 2007; Marinho-Carvalho et al. 2009; Zancan et al. 2007; Zancan et al. 2008). PK catalyzes the last step in glycolysis from

phosphoenolpyruvate to pyruvate producing ATP. It is activated by fructose 1,6-bisphosphate (PFK product) and inhibited by ATP, acetyl coenzyme A (acetyl-CoA) and alanine (Bailey, Stirpe & Taylor 1968; Tanaka et al. 1967; Weber 1969; Weber, Lea & Stamm 1967).

2.1.2. TCA cycle and oxidative phosphorylation

The TCA cycle has two main functions: it generates most of the metabolic energy in form of ATP and provides precursors for cell anabolism. It is spatially separated from the glycolysis as it takes place in the mitochondria and also plays a role in balancing the rate of glycolysis and glutaminolysis. TCA cycle and glycolysis are connected via pyruvate which is transported into the mitochondria and further converted to acetyl-CoA. Only part of the pyruvate enters the mitochondria as pyruvate is also converted to lactate, alanine, oxoglutarate and malate in the cytosol. On the other hand, acetyl-CoA can also be partially generated from amino acids tyrosine, leucine, isoleucine and lysine. The percentage of pyruvate entering the mitochondria reported in literature are quite different ranging from very low values (Fitzpatrick, Jenkins & Butler 1993; Neermann & Wagner 1996; Petch & Butler 1994), even less than 1%, to up to 40% (Sharfstein et al. 1994). The acetyl-CoA then reacts with oxaloacetate to citrate which can either be converted to isocitrate via aconitate or leave the mitochondria to be used for lipid formation with concomitant pyruvate production in the cytosol. If inflow of pyruvate into mitochondria is low and outflow of citrate is high, the TCA cycle can become depleted. In order to maintain the energy generation function of the TCA cycle it must be replenished which is done at the level of α-ketoglutarate using glutamine. Glutamine is converted to glutamate, generating ammonia, and further to α-ketoglutarate in the mitochondria. Therefore, glutamine's main function is to supply TCA cycle intermediates explaining the importance of this compound as a main carbon and energy source. Similar to glycolysis, several other TCA cycle intermediates are connected to other pathways. Oxaloacetate is also used for the synthesis of aspartate and asparagine. On the other hand, several amino acids can contribute to the TCA cycle. There can be inflow in form of succinyl-CoA derived from degradation of isoleucine, threonine, valine and methionine. Similarly, degradation of leucine and tyrosine to succinate can contribute to the TCA cycle as well. At the level of malate there is an important outflow to relieve any malate in excess from the cycle necessary to balance the fluxes within the TCA cycle. Malate is transported into the cytosol and converted to pyruvate. The NADH generated in the TCA cycle is used by the respiratory system located

in the internal mitochondrial membrane to produce ATP. NADH molecules are oxidized with oxygen being the final electron acceptor making sufficient oxygen availability essential for oxidative phosphorylation to take place.

Post-translational modulation of the TCA cycle is mainly determined by substrate availability and product inhibition. Availability of acetyl-CoA, citrate, and oxaloacetate as well as NAD^+/NADH ratio are important for TCA cycle regulation. NADH is the product of all dehydrogenases (except succinate dehydrogenase) and inhibits isocitrate dehydrogenase, α-ketoglutarate dehydrogenase, and citrate synthase, thereby reducing TCA cycle rate. Furthermore, α-ketoglutarate dehydrogenase is inhibited by its product succinyl-CoA. Succinyl-CoA also inhibits citrate synthase. Additionally, ATP downregulates α-ketoglutarate dehydrogenase activity, thereby reducing TCA cycle activity when sufficient energy is available (reviewed in (Williamson & Cooper 1980)).

2.1.3. Pyruvate dehydrogenase complex: connecting glycolysis and TCA cycle

Glucose utilization is highly regulated at several levels. This includes glucose uptake, glycolytic rate and entry of pyruvate into the TCA cycle in form of acetyl-CoA (Sugden, MC & Holness 2006). Pyruvate dehydrogenase complex (PDC) links glycolysis to the TCA cycle and is a multi-enzyme complex situated in the inner mitochondrial membrane catalyzing the irreversible oxidation of pyruvate to acetyl-CoA, CO_2 and NADH. There is no pathway in mammalian cells for the conversion of acetyl-CoA to pyruvate making PDC a key enzyme for the conversion of glucose to acetyl-CoA. Under aerobic conditions, activity of PDC is rate limiting for the oxidation of glucose and for metabolites, such as lactate and alanine, which are in equilibrium with pyruvate (Stacpoole et al. 1998). PDC also indirectly regulates the ATP yield from glucose by regulating the entry of acetyl-CoA into the TCA cycle, it controls the amount of malonyl-CoA available for fatty acid synthesis and plays an important role in the process of fuel selection in connection with the glucose fatty-acid cycle (Hue & Taegtmeyer 2009; Randle et al. 1963; Sugden, MC & Holness 2006).

PDC consists of three components in multiple copies, pyruvate dehydrogenase (E1), dihydrolipoamide acetyltransferase (E2), and dihydrolipoamide dehydrogenase (E3). The E1 component is a heterotetramer of two alpha and two beta subunits (α2β2). PDC is only active if unphosphorylated at three serine residues of E1α, serine-293 (phosphorylation site 1), serine-300 (phosphorylation site 2), and serine-232 (phosphorylation site 3), catalyzed by pyruvate dehydrogenase phosphatases (PDP) (Sale & Randle 1981; Teague et al. 1979; Yeaman et al. 1978). Pyruvate dehydrogenase kinases (PDKs) phosphorylate

PDC at these three serine residues and thereby inactivate PDC (Figure 2.1). PDP and PDK are the two enzymes that regulate PDC activity post-transcriptionally and each PDC complex contains two or three PDKs and PDPs that are tightly bound to E2 (Linn et al. 1972; Yang et al. 1998). PDC does not exist in a completely dephosphorylated (active) or phosphorylated (inactive) form but rather the relative activities of PDKs and PDPs determine the level of phosphorylation and therefore activity of PDC. Hence, changes in PDC phosphorylation and thereby its activity are determined by changes in PDK activity relative to PDP activity. PDKs phosphorylate the three serine residues however phosphorylation of any one site is sufficient to cause inactivation (Sugden, PH & Randle 1978). Phosphorylation rate of the sites differ with phosphorylation of site 1 being the fastest and phosphorylation of site 3 being the slowest (Korotchkina & Patel 1995; Sale & Randle 1981). Therefore, phosphorylation of site 1 appears to be more important for acute modulation according to metabolic demands. In contrast, rates of dephosphorylation were nearly identical for all sites indicating a random mechanism of dephosphorylation (Korotchkina & Patel 1995).

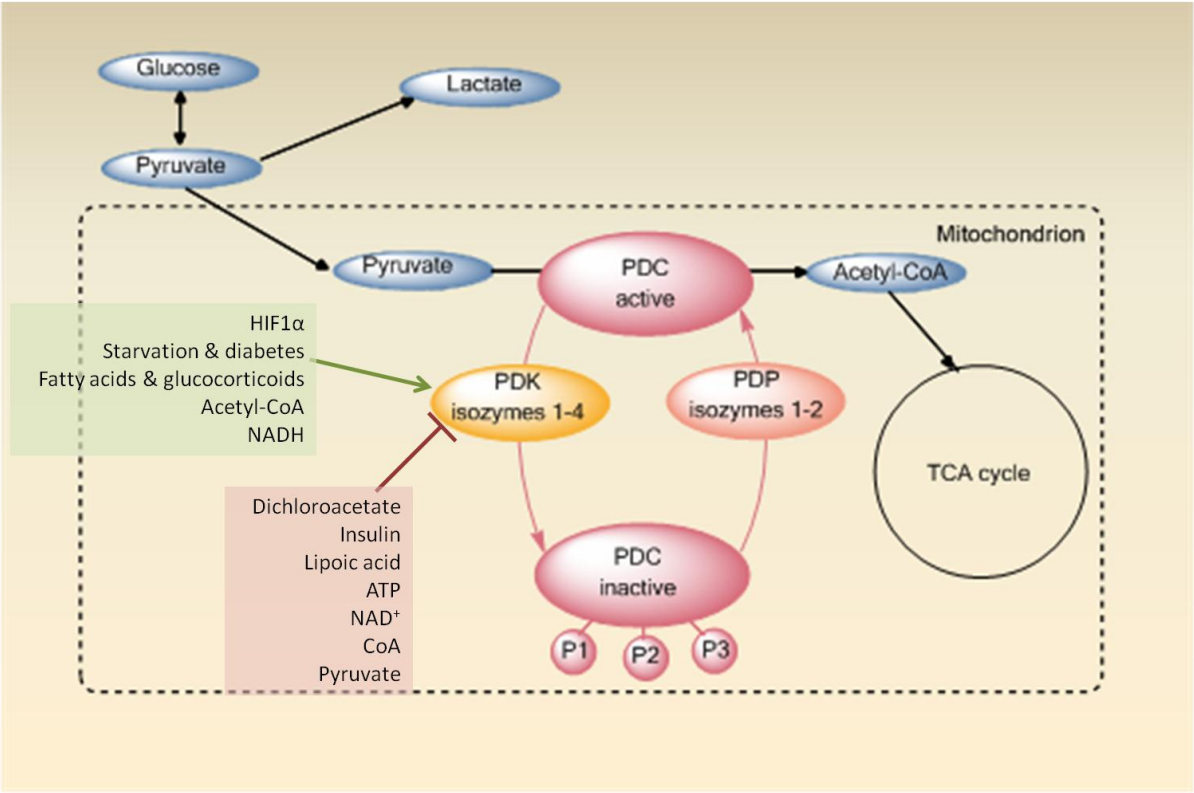

Figure 2.1: Regulation of pyruvate dehydrogenase complex (PDC) activity. PDC activity is regulated by pyruvate dehydrogenase kinases (PDKs) and pyruvate dehydrogenase phosphatases (PDPs). PDK activity is regulated by various factors and compounds; activators shown in green box and inhibitors shown in red box. The three phosphorylation sites are indicated by P1, P2 and P3. (Figure adapted from (Jeoung & Harris 2008)).

Four PDK isozymes have been identified in humans and rodents (PDK1, PDK2, PDK3, and PDK4) (Bowker-Kinley et al. 1998; Popov, Hawes & Harris 1997). Different PDKs are expressed in a tissue specific manner and not all PDKs are able to phosphorylate each of the three serine residues. All PDKs phosphorylate site 1 and 2 of E1α whereas site 3 is only phosphorylated by PDK1 (Kolobova et al. 2001; Korotchkina & Patel 2001). PDK2 is the most widely distributed PDK with high expression levels in liver, heart and kidney (Bowker-Kinley et al. 1998). PDK4 is also expressed in heart, kidney, oxidative skeletal muscle and liver (Bowker-Kinley et al. 1998; Sugden, MC et al. 2001; Sugden, MC, Langdown, et al. 2000; Wu, P et al. 1999; Wu, P et al. 1997; Wu et al. 2000). PDK1 and PDK3 are less distributed (Bowker-Kinley et al. 1998; Huang et al. 1998; Peters et al. 2001; Sugden, MC et al. 2001; Wu, F et al. 1997).

All four PDKs are transcriptionally regulated with PDK1 and PDK3 stimulated by Hypoxia-inducible factor 1-alpha (HIF1α) which is induced by low oxygen concentrations and often upregulated in cancer cells (Kim, JW et al. 2006; Lu et al. 2008; Papandreou et al. 2006) while PDK2 and PDK4 expression is controlled mostly by nutritional factors and hormones. Starvation, diabetes, fatty acids and glucocorticoids promote PDK activity (Abbot et al. 2005; Peters et al. 2001; Sugden, MC, Kraus, et al. 2000; Wu, P et al. 1999; Wu, P et al. 1997; Wu et al. 2000). The products of PDC (acetyl-CoA, NADH) increase PDK activity whereas PDC substrates (pyruvate, NAD^+, ADP, and CoA) inhibit PDK (Jeoung & Harris 2008; Roche & Hiromasa 2007). A high NADH/NAD^+ ratio and a high acetyl-CoA/CoA ratio, both caused by fatty acid oxidation, reduce the lipoyl moieties of E2 and promote acetylation of the reduced lipoyl moieties, respectively. Binding of PDK to an E2 lipoyl domain in which the lipoyl group is reduced and acetylated results in maximum PDK activity (Baker et al. 2000). PDKs are also inhibited by insulin, lipoic acid and dichloroacetate. PDKs and PDPs have a unique tissue dependent expression, different kinetic properties and sensitivities to regulatory molecules.

PDC has a crucial function in cell metabolism. Decreased PDC activity reduces glucose carbon flux into the TCA cycle and is linked to various age-related diseases such as glucose intolerance (Stacpoole, Moore & Kornhauser 1978), heart failure (Bersin & Stacpoole 1997), neurodegeneration (Stacpoole 1997), and cancer (reviewed in (Stacpoole 2012). An age-related decrease in glucose oxidation and oxygen consumption was observed in the brain (Kalpouzos et al. 2009; Martin et al. 1991) together with increased ketone body formation and aerobic glycolysis (Ross et al. 2010; Yao et al. 2010). Many neurodegenerative diseases, such as Alzheimer's disease, are associated with abnormal brain oxidative metabolism and data implicate up-regulated aerobic

glycolysis and reduced PDC activity (reviewed in (Coskun et al. 2012; Green, Galluzzi & Kroemer 2011). A decline in PDC activity may also contribute to the development of type 2 diabetes mellitus and increasing PDC activity in patients had a glucose and lactate lowering effect (Stacpoole, Moore & Kornhauser 1978). Additionally, many cancer cells mostly rely on aerobic glycolysis for energy generation (Gatenby & Gillies 2004). Therefore, PDC is considered a therapeutic target for many age-related diseases (Stacpoole 2012) and numerous studies have investigated PDC for anti-cancer therapy in recent years described in more detail below.

2.2. Aerobic glycolysis

2.2.1. Aerobic glycolysis: a metabolic phenotype mostly observed in rapid proliferating cells

More than 80 years ago, Otto Warburg observed that even under aerobic conditions cancer cells have an increased reliance on glycolysis for ATP generation and prefer lactate formation over oxidative phosphorylation (Warburg, Wind & Negelein 1927) (Figure 2.2). This phenomenon is called aerobic glycolysis, also known as the Warburg effect, and is characterized by increased glucose consumption and lactate production. This seems to be counterproductive since aerobic glycolysis yields less ATP per consumed glucose molecule than oxidative phosphorylation. However, adjusting the metabolism towards aerobic glycolysis is observed for many continuously proliferating cells such as cancer cells, rapidly dividing cells of embryonic tissue and cells used as production hosts in industrial applications.

In hypoxic environments, found in many solid tumors, increased glycolysis enables cancer cells to produce high amounts of ATP without the consumption of oxygen (Gatenby & Gillies 2004; Vander Heiden, Cantley & Thompson 2009). However, the fact that cancer cells under aerobic conditions and non-cancerous rapidly proliferating cells show a similar metabolic phenotype to hypoxic cancer cells indicate that their similar metabolic demands might play an important role as well (Hanahan & Weinberg 2011; Papandreou, Goliasova & Denko 2011). These cells must adjust their metabolism to meet the different energetic and biosynthetic requirements. Continuously dividing cells have a higher demand for nucleotides, amino acids and other cell components needed to assemble new cells and increased glycolysis allows the diversion of more glycolytic intermediates into other biosynthetic pathways to sustain rapid proliferation (Vander Heiden, Cantley & Thompson

2009). It was also shown in *in vitro* experiments using various cell lines that not only oxygen availability but also extracellular glucose concentration affects the glucose consumption rate (Altamirano et al. 2001; Cruz, Moreira & Carrondo 1999; Hayter et al. 1992; Miller, Blanch & Wilke 2000; Miller, Wilke & Blanch 1988) indicating a deregulated metabolism as cells consume more glucose than needed for cell growth. Different authors proposed that the increased lactate production from pyruvate is used by the cell to reduce NADH to NAD^+ in the cytosol for continued ATP production. High amounts of NADH are generated during increased glycolysis; however only NADH but not NAD^+, can pass through the mitochondrial membrane via the malate-aspartate shuttle system, the usual place of NAD^+ regeneration (Miller, Wilke & Blanch 1988; Sanfeliu et al. 1997; Wagner 1997). Additionally, deficiencies in some key enzymes connecting glycolysis to TCA cycle, such as PDC, phosphoenolpyruvate carboxykinase, and pyruvate carboxylase (PC) may elevate lactate production (Fitzpatrick, Jenkins & Butler 1993; Neermann & Wagner 1996; Petch & Butler 1994).

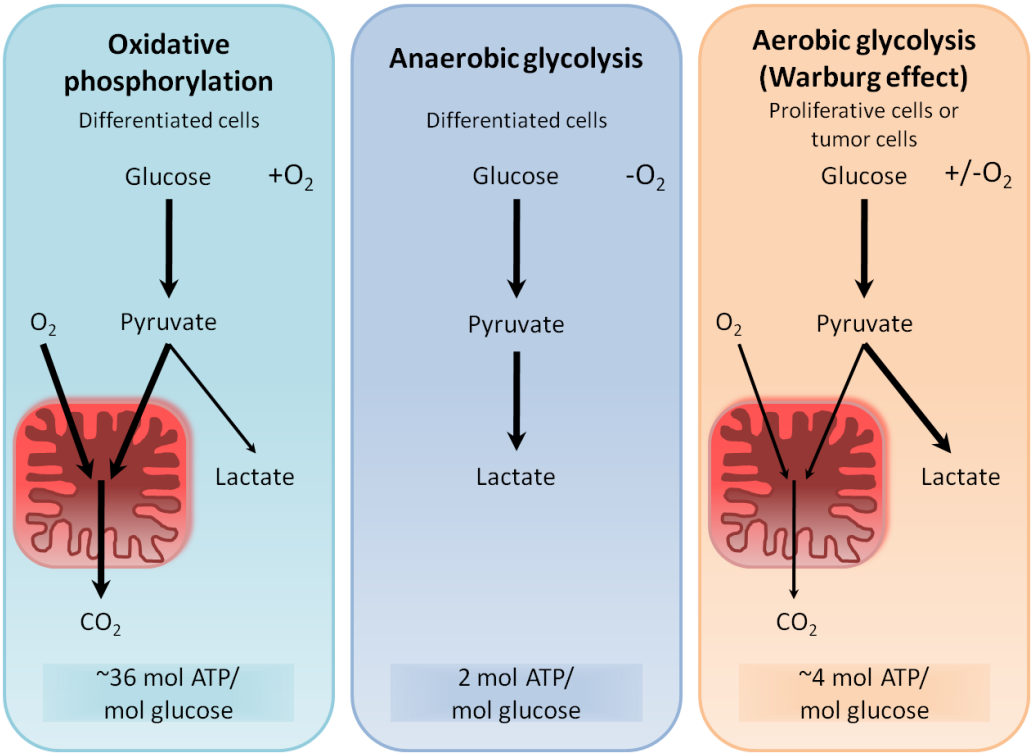

Figure 2.2: Differences between oxidative phosphorylation, anaerobic glycolysis and aerobic glycolysis. During oxidative phosphorylation cells first metabolize glucose to pyruvate in glycolysis followed by oxidation to CO_2 in the mitochondria if sufficient oxygen is available as it is essential being the final electron acceptor. When oxygen supply is limited cells can redirect glycolytic derived pyruvate away from mitochondrial oxidative phosphorylation by converting it to lactate during anaerobic glycolysis with a considerably lower ATP yield when compared to oxidative phosphorylation. During aerobic glycolysis, cells convert most glucose to lactate independent of oxygen availability. Mitochondria remain functional but only a smaller amount of pyruvate is oxidized making aerobic glycolysis less efficient for generating ATP than oxidative phosphorylation. (Figure adapted from (Vander Heiden, Cantley & Thompson 2009))

In order to compensate for the decrease in ATP yield per molecule glucose and for the increased need of glycolytic intermediates, cells activate a cellular response system, including regulation of glucose transporter and multiple enzymes of the glycolytic pathway (DeBerardinis et al. 2008; Hsu & Sabatini 2008; Jones & Thompson 2009; Kroemer & Pouyssegur 2008; Semenza 2010a, 2010b). PDK1 overexpression has been found in cancers such as head and neck, breast and lung cancers (Koukourakis et al. 2005; Lin, HJ et al. 2005). This is often associated with altered signaling pathways that involve oncogenes and tumor suppressor genes. Oncogenes that affect the central carbon metabolism are Akt1, cMyc, PKM2, and HIF1α. HIF1α is known to activate PDKs and thereby supporting pyruvate to lactate conversion observed in hypoxic cancer cells (Kim, JW et al. 2006; Lu et al. 2008; Wigfield et al. 2008). Overexprssion of PDKs is also associated with chemoresistance and PDK knockdown increased cytotoxicity of anticancer drugs (Lu et al. 2008) making PDC inactivation by PDK overexpression an important pro-survival pathway used by cancer cells.

Cancer cells and rapid proliferating non-cancerous cells share several characteristics and show a similar metabolic phenotype. However, the contribution and interplay of several factors, such as demand for biosynthetic precursors, extracellular environment, oncogene expression, and flexible structure between pathways, are very complex and many questions still remain. Due to the complex nature of the metabolic network several targets to affect the metabolic phenotype and lower the Warburg effect exist. Increasing PDC activity is promising as it directly links glycolysis to the TCA cycle and indirectly influences lactate production as well.

2.2.2. The Warburg effect in industrial relevant cell lines

Mammalian cell lines are the preferred production host for therapeutic proteins and the market of biopharmaceuticals is growing rapidly with annual sales exceeding USD 110 billion in 2011 (Ecker DM 2013). A great range of biologics, including vaccines, hormones, blood factors and monoclonal antibodies (mAbs) are produced in mammalian cell culture systems. As of December 2012, 154 biopharmaceuticals products have been approved for the US and EU market whereof 89 are produced in mammalian cell lines (Ecker DM 2013). There is a continuing need to develop technologies and approaches to achieve higher productivity and final antibody titers due to the increasing demand for biopharmaceuticals.

Despite their cost, difficulties and lower productivity, mammalian cells are the preferred production system for complex proteins, e.g. mAbs, because of their ability to correctly perform protein folding, assembly and post-translational modifications (e.g. glycosylation and phosphorylation) essential for safety and biologic efficacy (Durocher & Butler 2009; Walsh 2010; Wurm 2004). Those modifications are generally not correctly performed by microbial systems.

During the development of a production cell line the metabolic patterns of mammalian cell metabolism are altered considerably due to genetic changes during the immortalization process and stressful in vitro culture conditions leading to mammalian cell lines that exhibit a highly deregulated metabolism when cultured *in vitro* (Godia & Cairo 2006). Mammalian cell lines used as production hosts show a similar metabolic phenotype, aerobic glycolysis, to cancer cells, despite the fact that these cells are cultured in an environment very different from the environment in tumors, e.g. higher glucose concentration, higher oxygen concentration and all substrates in excess. They exhibit aerobic glycolysis resulting in an undesired high glucose and glutamine consumption in combination with high lactate and ammonia production leading to shorter culture periods and possible negative effects on cell growth, productivity, and product quality (Dietmair, Nielsen & Timmins 2011; Lim et al. 2010). Lactate is the main waste product that highly accumulates in both, batch and fed-batch processes, which can inhibit cell growth and protein production (Glacken, Huang & Sinskey 1989; Lao & Toth 1997). Additionally, to keep the pH constant, at high lactate production a large amount of base has to be added to the culture resulting in an increased osmolality which can inhibit cell growth and in turn can lead to lower productivity as well (Cruz et al. 2000; Irani et al. 1999; Langheinrich & Nienow 1999).

Intracellular pyruvate concentration influences the production of lactate and decreasing the available amount of cytoplasmic pyruvate by directing more pyruvate towards the TCA cycle could decrease lactate formation (Liu et al. 2009; Samuvel et al. 2009). Furthermore, enhancing the energy metabolism by increasing the ATP yield per glucose molecule consumed is promising because protein production is an extremely energy consuming process. A more efficient central carbon metabolism could also result in a decreased glucose and glutamine consumption as well as reduced ammonia production. The characterization, understanding and finally redistribution of the cellular metabolic behavior are essential to optimize the production systems and improve culture performance. Different approaches were tested to obtain modified cells with a more efficient metabolism such as alteration of culture conditions (e.g. media formulation, culture strategy) or metabolic engineering. Reduced lactate production was observed using optimized culture

conditions such as changing the balance of glucose and other nutrients (Nahapetian, Thomas & Thilly 1986) or exchanging glucose by other sugars such as galactose also in combination with replacing glutamine with glutamate (Altamirano, Illanes, Becerra, Cairó, et al. 2006; Altamirano et al. 2000; Altamirano et al. 2004). Strategic process control is another option keeping glucose concentrations low (Glacken, Fleischaker & Sinskey 1986) or lowering the culture pH (Gagnon et al. 2011).

Genetic engineering approaches either aim at reducing lactate production and glucose consumption or increase lactate consumption. Reduction of lactate dehydrogenase expression either by gene knock-out, siRNA or antisense RNA of lactate dehydrogenase (LDH) (Chen et al. 2001; Kim, SH & Lee 2007), knocking down glucose transporter (GLUT1) (Paredes et al. 1999), or transfection of fructose transporter (GLUT5) to enable growth on fructose (Wlaschin & Hu 2007) were used with varying results. Alternatively, directing more pyruvate into the TCA cycle by over-expression of yeast pyruvate carboxylase resulted in a reduced lactate production and glucose consumption (Fogolin et al. 2004; Irani et al. 1999) or simultaneous reduction of LDH and PDK using siRNA (Zhou, M et al. 2011). Inhibiting PDK activity and thereby increasing PDC activity is a promising target to reduce lactate production and to increase productivity in mammalian cell culture.

2.3. Dichloroacetate

2.3.1. Dichloroacetate indirectly increases PDC activity

Dichloroacetate (DCA) is an organohalide that is considered both, a potential environmental hazard and potential drug for the treatment of several metabolic, cardiovascular and cerebrovascular disorders (Stacpoole et al. 2008), as well as cancer (Michelakis et al. 2010). DCA is found in municipal drinking water as a by-product of water chlorination and the metabolism of chlorinated solvents, e.g. trichloroethylene, and pharmaceuticals, e.g. chloramphenicol, can result in *in vivo* formation of DCA (Stacpoole et al. 1998). In studies with in bred rodents it was shown that DCA has multiple organ toxicities and hepatocarcinogenicity after chronic exposure of doses in the range of 10 to 50 mg/kg/day (Stacpoole et al. 1998). However, similar doses were used for decades from the late 1970th onwards for short term or chronic treatment of diabetes, hyper lipoproteinemia, coronary heart diseases, congestive heart failure, or various acquired or congenital lactic acidosis, like PDC deficiency (Stacpoole, Nagaraja & Hutson 2003). It has mostly been used to lower blood lactate levels in children with different inborn

mitochondrial dysfunctions which lead to accumulation of lactate in the body (Stacpoole et al. 1998). Exposure to such high doses of DCA caused several reversible side effects in humans, such as mild increases in serum transaminases and mild to severe peripheral neuropathy (Kaufmann et al. 1999; Stacpoole et al. 1998; Stacpoole et al. 2008).

DCA is a pyruvate analog and the mitochondrion is considered the primary cellular site of DCA action. DCA enters the cell via the monocarboxylate transporter system that is located in the cell membrane and it enters the mitochondrial matrix via the mitochondrial pyruvate transporter (Stacpoole et al. 1998). Within the mitochondrial matrix, DCA inhibits PDK and thereby indirectly activates PDC. It was identified as a PDK inhibitor in 1973 using perfused rat heart (Whitehouse, Cooper & Randle 1974) and DCA occupies the pyruvate binding site in PDK2 (Roche et al. 2001). The PDK isozymes, identified in humans and rodents (PDK1, PDK2, PDK3, and PDK4), have different sensitivities to DCA; PDK2 is most sensitive to DCA, whereas PDK1 and PDK4 are relative sensitive and PDK3 is most resistant (Baker et al. 2000; Bowker-Kinley et al. 1998). Inside the cell, DCA can be dechlorinated to glyoxylate by glutathione S-transferase ζ1 (GSTZ1) the only enzyme known to metabolize DCA (Lantum et al. 2003; Li, WJ et al. 2011). GSTZ1 belongs to the cytosolic GST superfamily and is present in cytosol and mitochondria. Glyoxylate is then further metabolized in multiple pathways. DCA is also able to inhibit GSTZ1 activity in a broad range of doses in rats within days of continuous administration and thereby DCA can prevent its own degradation (Guo et al. 2006; Li, WJ et al. 2011).

Due to its effect on PDC activity, DCA has been coming into focus of cancer research and is considered a potential treatment. It was observed that DCA treatment increased PDC activity in tumors resulting in reduces glucose consumption and lactate production (Michelakis, Webster & Mackey 2008; Niewisch et al. 2012). However, DCA's lactate lowering activity can also be useful in other systems in which high lactate production is undesirable. In industrial applications where mammalian cells are used as production hosts, reducing lactate production is desirable as high lactate production can have negative effects on culture performance or product yield and it was shown that DCA can reduce lactate production in CHO cells (Follstat 2002).

2.3.2. Dichloroacetate in the focus of cancer research

In recent years, cancer research began to focus on the distinctive metabolism of glycolytic cancer cells as their metabolism is considered a new target for anti-cancer therapy (Hanahan & Weinberg 2011). Due to its lactate lowering activity, DCA has been receiving

attention as a potential anti-cancer drug and the majority of literature published in recent years regarding DCA is within the area of cancer research. Bonnet et al. published in 2007 that DCA inhibited the growth of A549 lung tumor xenocrafts in rats (Bonnet et al. 2007) and since then, numerous studies investigated the effect of DCA *in vitro* on mammalian cancer and non-cancerous cell lines and *in vivo*. The main focus in these studies has been cell survival and cause of cell death during DCA treatment. In addition, it was observed that DCA reduced lactate formation and aerobic glycolysis in non-cancerous and cancer cells (Bonnet et al. 2007; Michelakis et al. 2010; Stacpoole et al. 2008). However, DCA's affect on TCA cycle activity, measured by oxygen consumption, varied and appears to depend on factors such as cell line or HIF1α expression (Cairns et al. 2007; Niewisch et al. 2012). Additionally, DCA decreased E1α phosphorylation in UM-22A cells with increasing DCA concentration but had no effect on E1α phosphorylation in UM-22B cells (both are human neck squamous carcinoma cell lines) (McFate et al. 2008). Similarly, studies reported cytotoxic effects in different cancer cell lines but a broad range of concentration was necessary to induce toxicity, ranging from 0.5 mM to 100 mM affirming that different cell lines can respond very differently to DCA (Bonnet et al. 2007; Hanberry, Berger & Zastre 2014; Heshe et al. 2010; Stockwin et al. 2010).

Mitochondrial dysfunction contributes to apoptotic resistance in cancer cells and is believed to contribute to aerobic glycolysis (Kim, JW & Dang 2006). High mitochondrial membrane potential and low expression of K^+ channel Kv1.5, both characteristics of many cancer cells but not normal cells, were reported to be a selection criterion for the effect of DCA (Bonnet et al. 2007). Hyperpolarization of the mitochondrial membrane prevents the release of pro-apoptotic mediators from the mitochondria to the cytoplasm and thereby mediates apoptotic resistance. It was proposed that DCA is selective for cancer cells and "normalizes" the hyperpolarized mitochondrial membrane potential (MMP) which eventually leads to release of pro-apoptotic proteins and activation of apoptosis (Bonnet et al. 2007). More recently, an alternative mechanism as cause of cell death was reported. Several normal and cancerous cell lines of various tissues were investigated and the results indicated that DCA is not selective for cancer cells and the effect of DCA on MMP is the same for non-cancerous and cancer cells with a rather low influence of Kv1.5. Instead, DCA selectively targets cells with defects in their mitochondrial electron transport chain (ETC) (Stockwin et al. 2010). DCA inhibited cell growth of cells with impaired ETC and promoted oxidative phosphorylation. As a result ROS generation is increased; leading to increased cytochrome C release which ultimately leads to apoptosis (Garber 2006; Papandreou, Goliasova & Denko 2011).

However, the exact mechanisms that result in the tumoricidal effect of DCA need further investigation as DCA can inhibit tumor progression in several ways: i) increasing apoptosis without effect on cell proliferation was observed in endometrial cancer cells (Wong et al. 2008), ii) inhibiting cell proliferation without apoptosis induction or cell death was observed in lung, prostate and breast cancer (Stockwin et al. 2010; Sun et al. 2010), and iii) induction of apoptosis and inhibition of proliferation such as in lung and colorectal cancer (Bonnet et al. 2007; Madhok et al. 2010). Several studies reported an anti-tumor effect of DCA and decreased MMP and lactate production and increased production of reactive oxygen species (ROS) associated with induction of apoptosis and/or declined tumor cell proliferation were observed (Bonnet et al. 2007; Cao et al. 2008; Madhok et al. 2010; Michelakis et al. 2010; Niewisch et al. 2012; Ohashi et al. 2013; Shahrzad et al. 2010; Sorokina et al. 2011; Sun, Board & Blackburn 2011; Vella et al. 2012; Wong et al. 2008). However, reduced MMP and increased ROS were observed in several cancer cell lines without an apoptotic response (Stockwin et al. 2010). Others observed a decreased MMP and reduced cell proliferation without increased ROS production (Hanberry, Berger & Zastre 2014). Similarly, JNK1 activation and apoptosis was observed in A549 cancer cells without increase in ROS production (Ayyanathan et al. 2012). Induction of apoptosis together with alterations in expression of pro- and anti-apoptotic proteins such as p53 activation and HIF1α inhibition was reported as well (Kumar, A, Kant & Singh 2012, 2013; Michelakis et al. 2010; Sun, Board & Blackburn 2011).

While an increasing number of publications investigated DCA as an anti-cancer drug as sole treatment, it has also been considered for combination with established and novel cancer treatments (Ayyanathan et al. 2012; Fiebiger et al. 2011; Hur et al. 2013; Ishiguro et al. 2012; Kumar, K et al. 2013; Shen et al. 2013; Stockwin et al. 2010; Xie et al. 2011). Case studies of DCA treatment (Flavin 2010; Michelakis et al. 2010) as well as a phase I trial were published (Dunbar et al. 2013). A table summarizing the studies cited here can be found in Appendix I.

The metabolic effect of DCA, namely reduction of aerobic glycolysis, is well established. However, the exact mechanism by which increased PDC activity reduces the glycolytic rate needs further exploration. At the same time, the proliferation inhibiting and apoptotic effects are highly cell line dependent and it is still not fully understood what factors and mechanisms are responsible for apoptotic and anti-proliferating effects.

Chapter 3

Dynamic Metabolic Flux Analysis using B-splines to study the effects of temperature shift on CHO cell metabolism

Verónica S. Martínez*, Maria Buchsteiner*, Peter Gray, Lars K. Nielsen, and Lake-Ee Quek

* These authors contributed equally to this manuscript and should be considered as co-first authors.

This chapter was submitted to Metabolic Engineering on 17. September 2014

3.1. Abstract

Metabolic flux analysis (MFA) is widely used to estimate intracellular fluxes. Conventional MFA, however, is limited to continuous cultures and the mid-exponential growth phase of batch cultures. Dynamic MFA (DMFA) has emerged to characterize time-resolved metabolic fluxes for the entire culture period. Here, the linear DMFA approach was extended using B-spline fitting (B-DMFA) to estimate mass balanced fluxes. Smoother fits were achieved using reduced number of knots and parameters. Additionally, computation time was greatly reduced using a new heuristic algorithm for knot placement. B-DMFA revealed that Chinese hamster ovary cells shifted from 37°C to 32°C maintained a constant IgG volume-specific productivity, whereas the productivity for the controls peaked during mid-exponential growth phase and declined afterward. The observed 42% increase in product titer at 32°C was explained by a prolonged cell growth with high cell viability, a larger cell volume and a more stable volume-specific productivity.

3.2. Introduction

For over 20 years, metabolic flux analysis (MFA) has proven a powerful tool to quantitatively characterize cell metabolic phenotypes (Bonarius et al., 1996; Nielsen, 2003; Vallino and Stephanopoulos, 1993). MFA estimates intracellular fluxes using experimental measurements and mass balances. The quantification of metabolic fluxes has facilitated a better understanding of biological systems (Boghigian et al., 2010), including the identification of bottlenecks in product formation (Burleigh et al., 2011; Nyberg et al., 1999) and metabolic regulation (Fendt and Sauer, 2010). MFA is routinely used in media design (Altamirano et al., 2006; Martínez et al., 2010; Xing et al., 2011) and metabolic engineering (Becker et al., 2005) in order to improve metabolic phenotypes.

Conventional MFA assumes constant intracellular fluxes, a condition only satisfied by continuous cultures at steady state and during the mid-exponential phase of batch cultures. Most industrial cultures display dynamic metabolic changes (Matasci et al., 2008; Meadows et al., 2010), such as a gradual decline in cell-specific growth rate during batch and fed batch (Antoniewicz et al., 2007; Niklas et al., 2011) or diauxic growth (Mahadevan et al., 2002). Frequently, the most relevant metabolic behaviour occurs during transient conditions, where conventional MFA is no longer applicable.

Monoclonal antibody production by CHO cells illustrates the point. Conventional MFA has been used to study the Warburg effect observed during the initial growth phase, yet all

cultures display this phenotype during the initial exponential phase. What distinguishes successful cultures is the transition from exponential to stationary growth phase, whether the transition is invoked naturally (Ahn and Antoniewicz, 2011; Martínez et al., 2013), caused by medium design (Altamirano et al., 2006) or deliberate manipulation of culture conditions, such as a temperature shift (Bollati-Fogolin et al., 2005). A metabolic shift from lactate production to lactate consumption during this transition aids longevity and productivity of the culture (Altamirano et al., 2006; Ma et al., 2009; Martínez et al., 2013; Niklas et al., 2011; Young, 2013).

Several approaches have been used to estimate dynamic flux distributions (Antoniewicz, 2013). While all approaches assume pseudo-steady state for intracellular metabolism, i.e. the changes in internal metabolite concentrations are trivial compared to the fluxes (Varma and Palsson, 1994), they differ in terms of how dynamics in the data are captured. The simplest approach is to manually divide the time series data into distinct metabolic phases and estimate the flux profile of each phase by MFA (Ahn and Antoniewicz, 2011; Altamirano et al., 2006; Martínez et al., 2013; Niklas et al., 2011). This approach produces an average flux estimate for each phase but fails to capture the temporal evolution of metabolic fluxes. It is also difficult to maintain a homogenous precision among determined rates, which are dependent on the consistency and frequency of data points contained in each phase. Newer approaches overcome these limitations by first generating smooth functions to fit the measured metabolite concentrations and subsequently estimating instantaneous rates based on the functions' slope (Lequeux et al., 2010; Llaneras and Pico, 2007; Niklas et al., 2011). Then MFA is applied to each time point to generate a continuous flux distribution profile. The independent smoothing of individual concentration profiles followed by differentiation ignores mass conservation, potentially introducing significant bias into the flux estimates. Dynamic MFA (DMFA) overcomes this issue by using free fluxes as bases for the fitting functions and a least-square approach to fit the full dataset simultaneously (Leighty and Antoniewicz, 2011).

The original DMFA implementation uses piecewise linear functions to describe the time profile of free fluxes (Leighty and Antoniewicz, 2011). While simple in form, the linear assumption creates rates with unnatural, non-smooth breakpoints and struggle to fit higher-order dynamics, which do commonly occur since the time profile of absolute rates tend to trace a sigmoid curve (e.g., Monod model). In this study, we have extended the linear method by using B-spline functions when performing DMFA (B-DMFA), bringing in capabilities for higher order fit and the use of knot multiplicity. Knots are equivalent to the so-called DMFA time points (Leighty and Antoniewicz, 2011).

B-splines, or basis splines, are often used in computer-aided geometrical design and software packages to approximate data due to their rich mathematical structure and the robust numerical algorithms available (Prautzsch et al., 2002). B-splines and their integrals can be formulated such that they are linear with respect to the model parameters, and therefore all statistical and computational advantages shown in the linear DMFA (L-DMFA) implementation are retained (Leighty and Antoniewicz, 2011). Moreover, by exploiting the local support property of B-splines, a fast heuristic algorithm was developed for knot placement, which is by far the most time consuming task when performing DMFA. The performance of the B-DMFA algorithm was compared to the current L-DMFA approach (Leighty and Antoniewicz, 2011) using a simulated diauxic growth dataset of yeast fermentation (Sonnleitner and Kappeli, 1986). Demonstrating application to real data, B-DMFA was used to determine flux profiles of CHO cultures in order to investigate the effects of temperature shift on CHO metabolism.

3.3. Materials and Methods

3.3.1. Dynamic metabolic flux analysis (DMFA) using B-Spline fitting

Metabolic fluxes ($v(t)$) are calculated by performing mass balance around each metabolite in a metabolic network, which is represented by a stoichiometric matrix (S) for the internal metabolites (c_{int}) and a matrix R for the external metabolites (c_{ext}):

$$\frac{d\begin{bmatrix}c_{ext}\\c_{int}\end{bmatrix}}{dt} = \begin{bmatrix}R\\S\end{bmatrix} v(t) \tag{1}$$

Eq. (1) can be divided in balanced (internal) and not balanced (external) metabolites. It is assumed that internal metabolites are at pseudo steady-state, i.e., the fluxes to and away from any internal metabolite are far greater than the net accumulation of the metabolite itself (Varma & Palsson 1994a):

$$\frac{dc_{ext}}{dt} = R \cdot v(t) \tag{2}$$

$$S \cdot v(t) = 0 \tag{3}$$

In conventional MFA, metabolic fluxes are assumed to be constant, and the internal metabolite balances are mathematically formulated by Eq. (3) with constant v. In DMFA, metabolic fluxes are allowed to change over time to reflect the dynamics of the measured concentrations and rates.

The vector of fluxes ($v(t)$) can be expressed as a function of the null space of the balanced stoichiometric matrix S and a set of free fluxes ($u(t)$):

$$v(t) = K \cdot u(t); \quad \text{where } K = \text{null}(S) \tag{4}$$

Leighty and Antoniewicz calculated internal fluxes using a time-dependent $u(t)$ formulated as a linear spline function (Leighty and Antoniewicz, 2011). A smoother fit, however, can be achieved by formulating $u(t)$ using higher order B-splines as shown in Eq. (5) (Curry, H. B. & Schoenberg 1947; Curry, Haskell B & Schoenberg 1966).

$$u(t) = B_k(t) = \sum_{i=0}^{m-k-1} P_i \cdot \mathrm{N_{i,k}}(t) \tag{5}$$

Under B-spline terminology, m is the number of time points (called knots), k is the order of the polynomial segments of the B-spline (order k means that the curve is made of polynomial segments of degree k-1), P_i is the i^{th} control point, and $N_{i,k}(t)$ is the i^{th} normalized B-spline blending function of order k. The control points and blending functions define the shape of the B-spline (Prautzsch, Boehm & Paluszny 2002). The normalized blending functions are estimated by the Cox-de Boor recurrence relation (Cox 1972; De Boor 1972):

$$N_{i,k}(t) = \frac{\mathrm{t-t_i}}{\mathrm{t_{i+k-1}-t_i}} \mathrm{N_{i,k-1}}(t) + \frac{\mathrm{t_{i+k}-t}}{\mathrm{t_{i+k}-t_{i+1}}} \mathrm{N_{i+1,k-1}(t)} \tag{6}$$

$$\mathrm{N_{i,1}}(t) = \begin{cases} 1 & \text{if } t \in [t_i, t_{i+1}] \\ 0 & \text{otherwise} \end{cases} \tag{7}$$

In this study, a quadratic B-spline (k=3) was used to fit the free-flux vector, thus the metabolic fluxes were expressed as:

$$v(t) = K \cdot P \cdot N(t) \tag{8}$$

where $P = \left[\overrightarrow{P_0} \quad \ldots \quad \overrightarrow{P_{m-3}}\right]$ and $N(t) = \begin{bmatrix} \overrightarrow{N_{3,0}}(t) \\ \vdots \\ \overrightarrow{N_{3,m-3}}(t) \end{bmatrix}$

The time profiles of metabolite concentrations are described using the integral of Eq. (2), thus the integral of Eq. (8) is required. The indefinite integral of B-spline function of 3rd order is:

$$\int B_3(t) = \sum_j e_j \cdot N_{j,4}(t); \qquad e_j = \left(\frac{1}{3}\right) \cdot \left(\sum_{i=0}^{j} P_i \cdot (t_{i+3} - t_i)\right) \tag{9}$$

The B-spline functions for metabolite concentrations, after the rearrangement of e_j, can subsequently be expressed in matrix form as:

$$c(t) = c_0 + R \cdot K \cdot P \cdot \mathrm{M_e} \cdot IN(t) \tag{10}$$

where $M_e = \left(\frac{1}{3}\right) \cdot \begin{bmatrix} (t_3 - t_0) & \ldots & (t_3 - t_0) \\ 0 & \ddots & \vdots \\ 0 & 0 & (t_m - t_{m-3}) \end{bmatrix}$ and $IN(t) = \begin{bmatrix} N_{0,4}(t) \\ \vdots \\ N_{m-3,4}(t) \end{bmatrix}$

For a pre-determined knot series, the control points (matrix P) and the initial metabolite concentrations (vector c_0) are linear with respect to the model. The complete time-series of metabolic fluxes can be estimated by solving a single optimization problem (Antoniewicz 2013a). The optimization estimates free fluxes and initial metabolite concentrations by minimizing the variance-weighted sum of squared residuals (SSR) between estimated and measured external metabolite concentrations (c_i and $c_{i,m}$) and external rates (r_i and $r_{i,m}$) if available (Leighty & Antoniewicz 2011):

$$\min SSR = \sum_i \left[\overrightarrow{c_i} - \overrightarrow{c_{i,m}}\right]' \cdot W_i \cdot \left[\overrightarrow{c_i} - \overrightarrow{c_{i,m}}\right] + \sum_j \left[\overrightarrow{r_j} - \overrightarrow{r_{j,m}}\right]' \cdot W_{rj} \cdot \left[\overrightarrow{r_j} - \overrightarrow{r_{j,m}}\right] \tag{11}$$

$$s.t. \qquad \overrightarrow{c_i}(t) = \int S \cdot v(t) dt \tag{12}$$

$$\overrightarrow{r_j}(t) = R \cdot v(t) \tag{13}$$

where W_i and W_{rj} are diagonal matrices containing the inverse of measurement variances of metabolite i and external rates j for every time point, respectively.
The optimization is linear with respect to P and c_0 (problem parameters), thus the solution to the problem can be solved explicitly using the equation (Leighty & Antoniewicz 2011):

$$\begin{pmatrix} c_o \\ \underline{P} \end{pmatrix} = H^{-1} \cdot J \tag{14}$$

where H and J are the Hessian and Jacobian matrixes, respectively. From this point onwards, the formulation is identical to the L-DMFA approach (Leighty & Antoniewicz 2011), namely the method used to estimate standard deviations for the estimated metabolic fluxes. The B-DMFA algorithm was scripted in MATLAB, and is available from the corresponding author upon request.

3.3.2. Heuristic algorithm to determine the placement and number of knots

Finding the least-square solution of B-splines is a simple linear problem once the knots sequence has been specified, otherwise the problem is non-linear and difficult to solve. There are various parameterization approaches to specify the knot sequence, such as uniformly spaced or chord length (Prautzsch, Boehm & Paluszny 2002), however, these approaches are mainly designed to fit one curve at a time. Since we are simultaneously fitting a large number of curves using a single knot sequence, we developed a heuristic algorithm that uses the SSR within knot spans to guide the placement of knots (Appendix A). The algorithm was conceived based on the fact that the shape of B-splines can be controlled locally, i.e. adjusting positions of proximal knots have limited distal effects. Generally there are more time series data points than there are piecewise polynomials required to fit the experimental data. As such, the algorithm starts from no internal knots and progressively adds knots until the SSR is reduced to an acceptable threshold. A region of data with greater dynamic behaviour will correspondingly have higher density of knots. This avoids issues related to over-fitting and oscillation.
Briefly, the algorithm places a knot into the time span that has the largest contribution to the overall SSR (Figure 3.1A). The position of each added knot is determined by a greedy trial-and-error approach, guided by SSR trial calculations, the SSR of placing a knot in either the middle of the time span or the middle of the half right or left of the defined time interval is compared (Figure 3.1B).

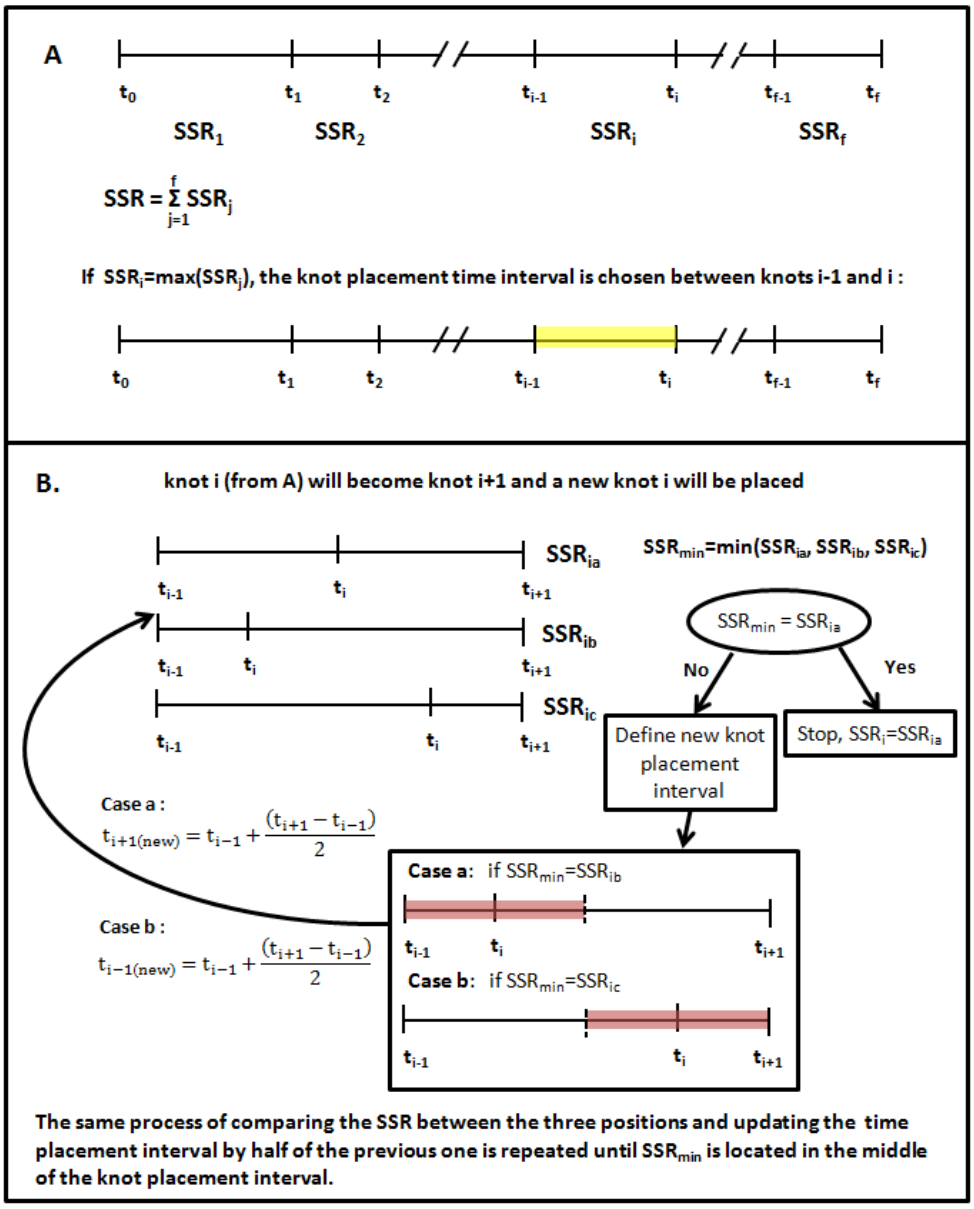

Figure 3.1: A. Selecting knot placement time interval. The time interval that has the greatest contribution to the total SSR is selected for placing a knot. **B. Placing knot i within the selected time interval.** The position of the knot i is determined by an iterative process. First, the SSRs of placing the knot in the middle of the knot placement time interval, or the middle of the left or right half of the knot placement time interval are compared. The process is stopped if placing the knot in the middle of the knot placement time interval gives the smallest SSR. Otherwise the knot placement time interval is updated to the right or left half of the initial time interval, depending on which knot position gives the smallest SSR. Then the process is repeated on the new reduced knot placement time interval.

If the smallest SSR is given by placing the knot in the middle position, then it is kept as part of the final knot sequence. Otherwise, the focus is shifted to the right or left half of the current time span, chosen based on the knot position that gives the smallest SSR. The previous smallest SSR is compared again with the options of placing the new knot in the middle of the right or left half of the new time span (half of the previous time interval), and the knot position that generates the smallest SSR is selected. The process is repeated,

with the time span segment becoming narrower, until the best knot position is found to be placed at the middle of the last defined time span. The algorithm starts again for the next knot. After the placement of the second and subsequent knots, the position of all knots are adjusted again to minimize SSR in order to account for the effects of other knots, whereby a better position for the i^{th} knot is checked between the time interval defined by $i\text{-}1^{th}$ knot and $i+1^{th}$ knot. The whole process terminates when the minimum SSR is below the chi-square threshold.

3.3.3. Metabolic model

The metabolic model was derived from the *Mus musculus* GeM (Quek & Nielsen 2008a) as previously described (Quek et al. 2010). The metabolic model contains the TCA cycle, non-oxidative pentose phosphate pathway (PPP) and pathways for the synthesis of essential biomass precursors (e.g., fatty acids, steroids, glycogen, and nucleotides). The mitochondrial malic enzyme and the oxidative PPP were removed such that NADPH is only produced by $NADP^+$ dependant malic enzyme. Further modifications were made to the model to reflect differences in substrate consumption and by-product formation: (1) the uptake of hypoxanthine, choline, myo-inositol and ethanolamine were removed; (2) proline degradation pathway was replaced by its biosynthetic pathway; and (3) an IgG1 antibody production reaction was added (IgG1 composition shown in Appendix B). L-alanyl-L-glutamine dipeptide was treated as free glutamine and alanine, and the decomposition of glutamine was assumed to be negligible since its extracellular accumulation is low. A biomass equation was used, with the precursor compositions obtained from a previous CHO cell culture study (Martínez, VS et al. 2013). The average dry weight for control cells at exponential growth phase was measured to be 350 [pg/cell].

3.3.4. Cell culture

The CHO cell line CHO-XL99, producing an IgG1 antibody (Ab2), is a derivative of CHO-K1 (ATCC 61-CCL) adapted from adherent growth in serum containing medium to suspension growth in EX-CELL302 serum free medium at the University of New South Wales. The CHO-XL99 cell line was further adapted to EX-CELL CD CHO Fusion (Sigma-Aldrich, Castle Hill, Australia) medium supplemented with 8 mM GlutaMAX (L-alanyl-L-glutamine; LifeTechnologies Australia, Mulgrave, Australia), 400 µg/ml Geneticin (LifeTechnologies Australia) and 0.2% v/v Anti-Clumping Agent (LifeTechnologies

Australia). CHO-XL99 cells were cultivated in four 1L shake flasks with a working volume of 200 ml in humidified Infors shaking incubators set at 37°C, 7.5% CO_2 and 130 rpm. After 72.5 hours two shake flasks were transferred to a humidified incubator set at 32°C with otherwise identical settings. Samples for viable cell density and cell diameter measurements as well as antibody and metabolite concentration analysis were taken twice a day. Cell number, viability and cell diameter were determined using a CedeX cell counter (Innovatis, Bielefeld, Germany). Ammonia concentrations were measured using a Nova Bioprofiler FLEX (Nova Biomedical, Waltham, USA). For extracellular metabolites and antibody analysis, 500 µl of cell suspension was removed from the cell cultures, centrifuged at 200 g for 5 min and supernatants were frozen on dry ice and stored at -80°C until further processing.

3.3.5. Extracellular metabolites and antibody concentration analysis

Glucose, lactate, L-alanyl-L-glutamine and amino acid concentrations were measured using HPLC as described previously (Dietmair, Timmins, Gray, Nielsen & Krömer 2010). Antibody concentrations were determined using surface plasmon resonance with a Biacore T-100 system (GE Healthcare, Mansfield, Australia) and the human antibody capture kit (GE Healthcare) was used for the immobilization of an Ab2 binding α-Hu IgG FC-specific antibody onto the CM5 sensor chips. Samples were diluted 5-10 times in a 96 well plate and protein-A purified Ab2 was used to obtain a standard curve for quantification.

3.4. Results and discussion

3.4.1. Comparing B-DMFA against L-DMFA

The implementation of L-DMFA is formally identical to B-DMFA with order (k) 2, except that L-DMFA uses an optimization algorithm to specify knot sequence (Leighty & Antoniewicz 2011). A diauxic growth model of yeast on glucose (Nielsen, Jens & Villadsen 2003; Sonnleitner & Kappeli 1986) was used to compare their performances (Figure 3.2). In the simulated batch culture, *S. cerevisiae* initially metabolize glucose by an oxidoreductive metabolism. While the uptake rate of glucose is described by Monod kinetics, the oxidation of glucose is additionally limited by the respiratory capacity. Excess pyruvate therefore overflows to ethanol. As glucose is consumed, its consumption rate

decreases to a point where spare respiratory capacity allows the reconsumption of ethanol. The uptake rate of ethanol is described by Monod kinetics that includes glucose inhibition. The complex dynamics of the oxygen consumption rate is shown in Figure 3.2.

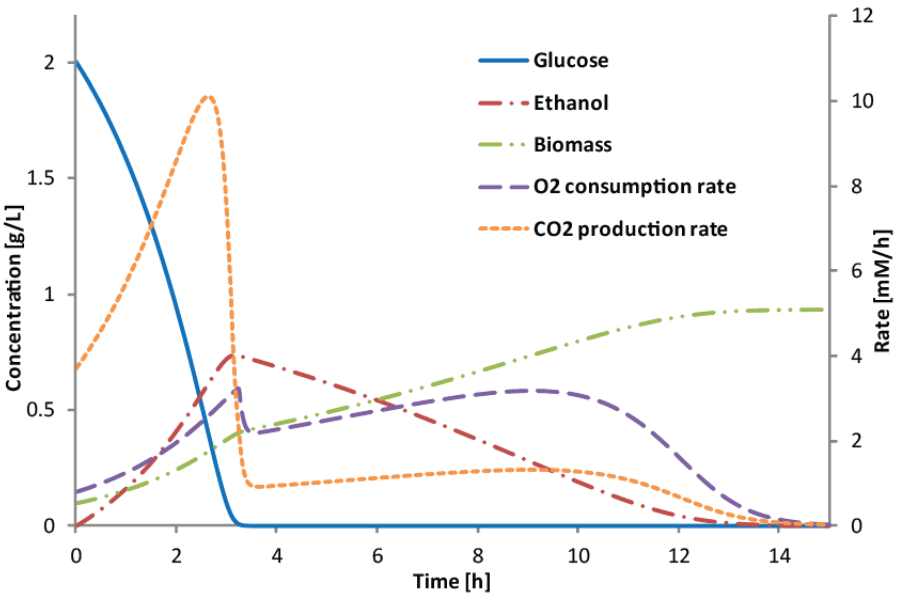

Figure 3.2: Simulated data of yeast diauxic growth in batch culture. Initially, cells metabolize glucose and produce ethanol and CO_2. Ethanol is consumed when glucose is depleted. Transients in the oxygen consumption rate and CO_2 production rate around the depletion of glucose and ethanol are shown.

The goodness of fit by L-DMFA (Leighty & Antoniewicz 2011) and by B-DMFA were compared using the described simulated dataset. The dataset consisted of concentrations of glucose, ethanol, biomass, and rates of oxygen and carbon dioxide at 30 minutes intervals from 0 to 15 hours. Initial glucose and biomass concentrations were set to 2 g/L and 0.1 g/L. Measurement errors were assumed to be 5% (Figure 3.3).

The two approaches were comparable in terms of the ability to fit concentration datasets (Figure 3.3 A, B and C). B-DMFA, however, gave a smoother fit for the oxygen and CO_2 rates, particularly at time points when glucose and ethanol approached depletion (Figure 3.3 D and E). Unlike L-DMFA, B-DMFA was able to trace the spike in the rates by allowing insertion of multiple knots at the same time point. Therefore, B-DMFA generates a better fitting for dynamic experimental rates that contain drastic changes in a short period of time. A quantitative comparison of the fitting between both approaches was carried out (Table 3.1). Particularly, we examined how sampling frequency would affect performance. B-DMFA and L-DMFA were performed on ten datasets for each sampling frequency (15, 30 and 60 minutes sampling intervals). Each dataset was generated by corrupting the simulated concentrations and rates with normally distributed random noise (5% standard deviation). Since the upper limit of SSR in DMFA vary depending on the number of knots,

a proxy for goodness-of-fit (SSRo) was used, which measures the discrepancy between the fitted and the noise-free models. This allows us to compare the goodness-of-fit for the various fitted models using the simulated noise-free dataset as a common basis. SSRo was found to be similar for both B-DMFA and L-DMFA. However, B-DMFA achieved this with a smaller number of internal knots (time points) and parameters than L-DMFA, demonstrating the higher fitting power achieved using B-spline fitting.

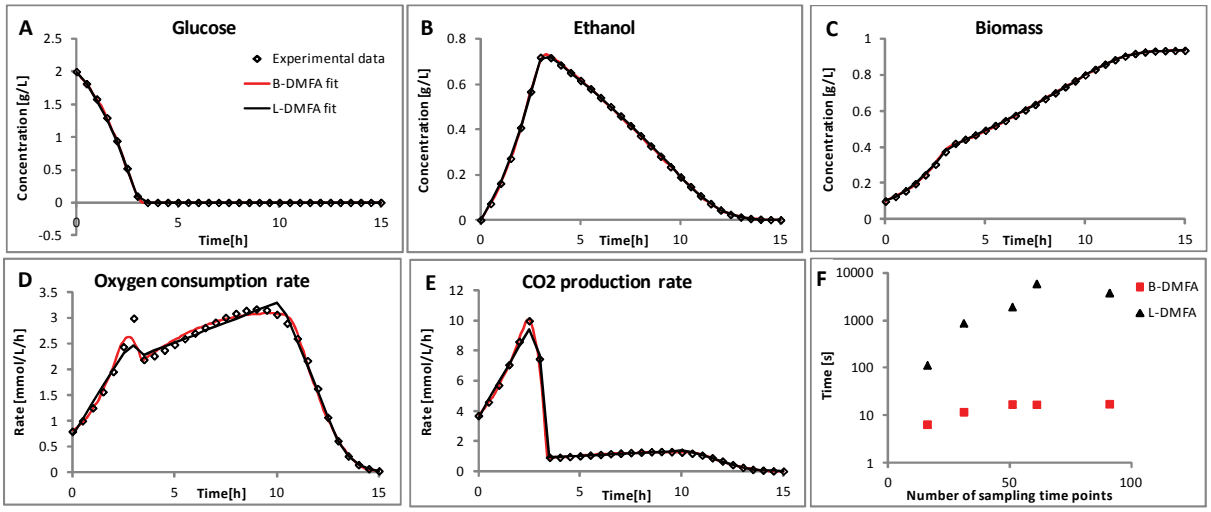

Figure 3.3: Fitting of simulated dataset of yeast diauxic growth by L-DMFA and B-DMFA, and simulations computation time. In A to E the simulated data points are represented by ◊, and the fitting of L-DMFA and B-DFMA are represented by black and red lines, respectively. In F, the computation time (in an Intel® Core™ i5 CPU with 8GB RAM) by L-DMFA and B-DMFA with increasing number of sampling points is shown.

B-DMFA was found to be significantly faster than L-DMFA (Table 3.1). We attributed this to the heuristic algorithm for knots placement. L-DMFA uses an optimization approach, which begins with a maximum potential DMFA time points (e.g., 29 in the 15 minute case) and removes one by one until the fit is still within the 95% confidence intervals (CI) (Leighty & Antoniewicz 2011), while the B-DMFA heuristic algorithm adds knots starting from zero. This was verified when the knot placement heuristic algorithm was implemented in the original L-DMFA approach, and as a consequence, the computation times were significantly improved. Interestingly the B-DMFA approach remains the fastest (Table 3.1). SSRo indicates that the resulting fits were similar to the original L-DFMA implementation. Nonetheless, B-DMFA remained the faster approach compared to the original L-DMFA with or without the heuristic algorithm, especially for datasets presenting in higher sampling frequency (Table 3.1).

Table 3.1: Comparison of B-DMFA, L-DMFA and L-DMFA using the knot insertion heuristic. For each sampling frequency ten datasets with noise (5% standard deviation) were simulated, for sampling every 15, 30 and 60 minutes. The datasets were analyzed with B-DMFA, L-DMFA and L-DMFA using the heuristic algorithm for knots placement. The SSR with respect to a dataset without noise (SSRo), the computation time (in an Intel® Core™ i5 CPU with 8GB RAM), the number of internal knots required for fitting and the number of parameters were determined. The goodness of fit was similar between the three approaches, however, B-DMFA required less parameters. B-DMFA is also a much faster approach than L-DMFA, mainly due to the knots placement heuristic algorithm.

		B-DMFA	L-DMFA	L-DMFA + heuristic algorithm
SSRo	15 min	94.8 ± 24.2	125.9 ± 32.8	97.1 ± 22.5
	30 min	65.1 ± 14.3	75.7 ± 18.0	65.5 ± 15.9
	1 hour	49.0 ± 12.6 *	51.1 ± 11.5 *	50.2 ± 12.2[#]
Time (sec)	15 min	23.2 ± 13.2	3,543 ± 3,119	36.3 ± 12.3
	30 min	9.5 ± 2.9	826.2 ± 413.4	22.5 ± 13.5
	1 hour	5.6 ± 3.0 *	140.5 ± 40.1 *	10.1 ± 8.0 [#]
N° Internal knots	15 min	7 ± 2	15 ± 15	9 ± 1
	30 min	6 ± 1	11 ± 7	9 ± 3
	1 hour	6 ± 1 *	8 ± 4 *	9 ± 4 [#]
N° Parameters	15 min	40 ± 6	69 ± 61	45 ± 6
	30 min	37 ± 4	51 ± 27	46 ± 12
	1 hour	36 ± 5 *	40 ± 14 *	46 ± 17 [#]

* One out of ten datasets did not converge with a 95% CI, thus the dataset was omitted from the analysis.
[#] Two out of ten datasets did not converge with a 95% CI, thus the datasets were omitted from the analysis.

Figure 3.3F shows that the B-DMFA approach is significantly less sensitive to the number of sampling time points than L-DMFA. At 16 time points, B-DMFA algorithm took 7 seconds to generate a statistically acceptable flux distribution, while L-DMFA took 115 seconds; at 91 sampling points, B-DMFA was two orders of magnitude faster (Figure 3.3F). The longest computation time using L-DMFA was approximately one hour. This computation time can be considered reasonable, however, when dealing with large models that describe the full cell metabolism (more than 100 reactions), and more experimental measurement (the full set of amino acids concentrations for a ten days cell culture) the computation time could be in the order of days.

The heuristic algorithm for knot placement was validated to be sound by a Monte Carlo approach. By randomly sampling 10,000 sets of knot sequences with a fixed number of knots, the best SSR was still 37% greater despite the Monte Carlo approach requiring 8.5 minutes to complete compared to the 12 seconds required by the heuristic algorithm. When sample size was increased to 100,000, the best SSR was 25% less than the

heuristic algorithm, but only four instances returned SSR better than the algorithm (Appendix A). The sets of statistically acceptable knot sequences randomly generated were not very different compared to the knot sequence determined by the algorithm. The largest difference was 6% of the full time span when compared to the best set. However, the Monte Carlo approach took 1.4 hours to completion.

3.4.2. Effects of temperature shift on cell size and productivity of CHO-XL99 cells

Growth profile, antibody concentration, mean cell diameter and cell specific productivity for the two control cultures (37°C) and two temperature-shifted cultures (32°C) are shown in Figure 3.4. The log plot of cell number (Figure 3.4A) showed that cell-specific growth rates for all four cultures were constant at about 0.025 to 0.029 h-1 during early exponential phase, but began to decline after 96 hours. This is expected for shake flask cultures as pH is not controlled. At 100 hours, the cell-specific growth rates for the temperature-shifted and control cultures were between 0.012 – 0.016 hr^{-1} and 0.020 – 0.023 hr^{-1}, respectively, suggesting a reduced growth rate and slower metabolism for the temperature-shifted cultures. A lower peak cell density was also observed for the temperature-shifted cultures. Both observations are consistent with the literature (Kumar, N, Gammell & Clynes 2007; Moore et al. 1997). Cultures reached peak cell density at 168 hours and 192 hours for the control and temperature-shifted cultures, respectively. Cell viabilities for all four cultures were above 90% for the remaining culture duration up to 240 hours. Cell viability was slightly higher for the temperature-shifted cultures than the control cultures. The reduction of culture temperature from 37°C to 32°C appears to have reduced the cell growth rate and overall metabolism.

The final antibody titer was on average 42% higher in the temperature-shifted cultures compared to the controls. As a consequence of a smaller integral viable cell density and a higher antibody titer, the average cell-specific productivity (Qp) appeared to be larger for the temperature-shifted cultures (Figure 3.4D). Cells in the temperature-shifted cultures, however, showed a significant increase in cell diameter compared to the controls despite all cultures showing similar cell sizes before the temperature shift (Figure 3.4C). Metabolic fluxes and antibody yields were therefore normalized to cell volume instead of cell number due to the observed differences in cell sizes. Since cell volume is proportional to cell mass (Frame & Hu 1990), it is more accurate to express metabolic fluxes and antibody yields in terms of cell volume instead of cell number when cell size varies (Nielsen, LK, Reid &

Greenfield 1997). The difference in average Qp was eliminated once Qp was normalized against cell volume (Figure 3.4D).

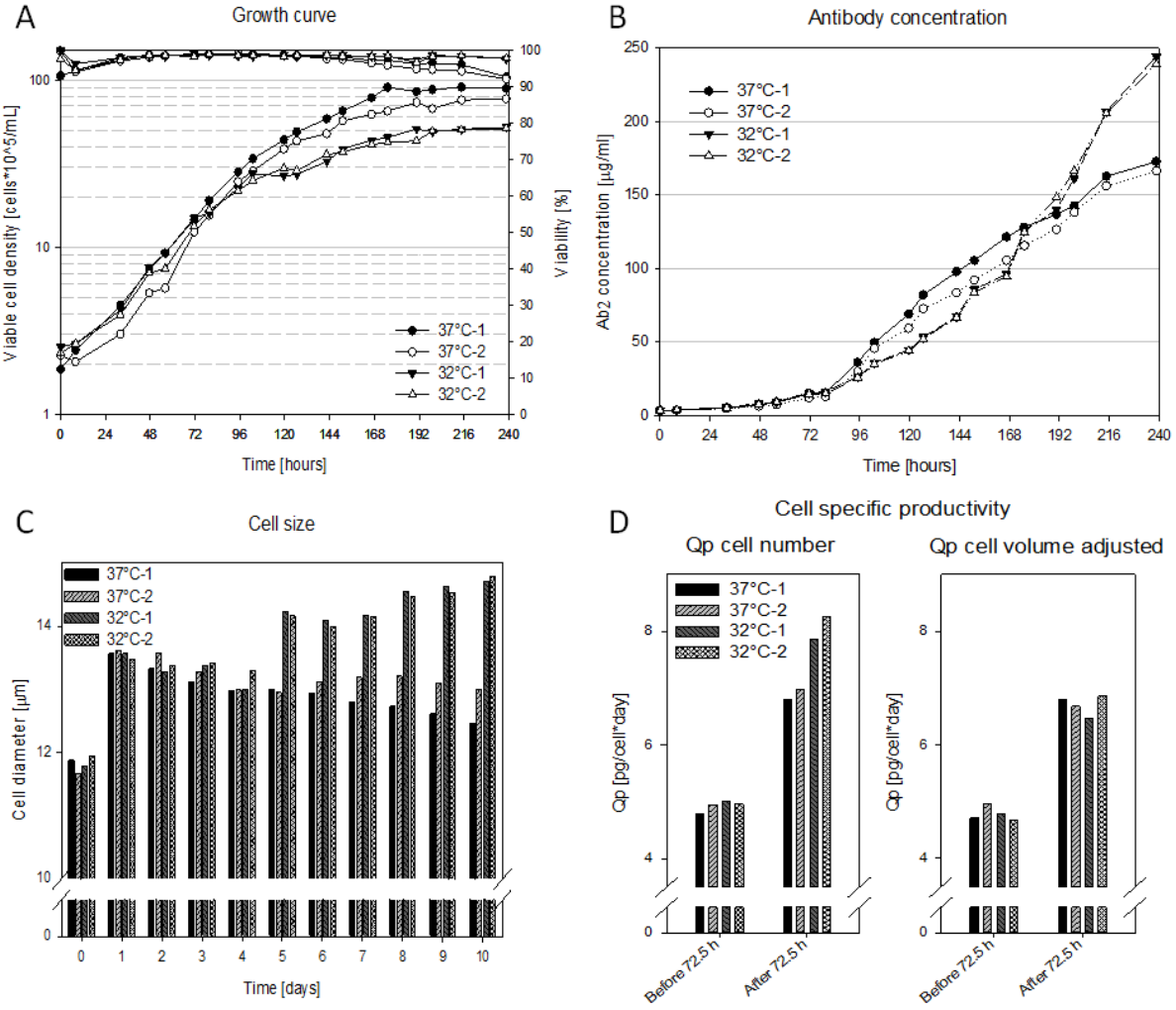

Figure 3.4: Viable cell density, antibody concentration, cell size and specific productivity. A: CHO-XL99 cells were cultivated in four shake flasks, two cultures were temperature-shifted at 72.5 hours (32°C-1 and 32°C-2) and the other two were maintained at 37°C throughout the whole experiment (37°C-1 and 37°C -2). Approximately 24 hours after the temperature shift the growth rate decreased and peak viable cell density was lower in temperature shifted cells compared to cells at 37°C. B: Final antibody titer was higher in temperature shifted cells by about 42%. C: An increase in cell diameter was observed for cells at 32°C on day 5, approximately two days after the temperature shift. D: Cell specific productivity (Qp) based on cell number increased for cells cultivated at 32°C while cell volume normalized Qp did not show an increased productivity for temperature shifted cells. Qp after 72.5 h was estimated until cells entered stationary phase.

Several studies of CHO cultures have reported an enhanced Qp when temperature was reduced from 37°C to mild hypothermia (Al-Fageeh et al. 2006; Bollati-Fogolin et al. 2005; Fox et al. 2004; Furukawa & Ohsuye 1998; Kumar, N, Gammell & Clynes 2007; Yoon, Song & Lee 2003), but none of these studies accounted for the role of cell size. Temperature-shifted CHO cells typically accumulate in the G1 phase (Kumar, N, Gammell & Clynes 2007; Moore et al. 1997), and might therefore be expected to be smaller in size

than cells in S or G2 phases. However, an increase in size has been observed for cells arrested in G1 phase by means other than temperature shift (Al-Rubeai et al. 1992; Bi, Shuttleworth & Ai-Rubeai 2004; Carvalhal, Marcelino & Carrondo 2003; Lloyd et al. 2000). It has previously been found that cell-specific productivity correlates with cell size (Bi, Shuttleworth & Ai-Rubeai 2004; Lloyd et al. 2000) and our data similarly showed that volumetric productivity was largely constant even with an almost 40% increase in observed cell volume.

3.4.3. B-DMFA captures dynamic metabolic changes caused by temperature shift

Dynamic flux analysis of CHO cell cultures was performed using the B-DMFA framework. The experimentally measured metabolite concentrations (amino acids, glucose, lactate and ammonia), antibody concentration and cell volume were used as input. Cell number was not used due to differences in cell diameter observed between the control and the temperature-shifted cultures (Figure 3.4C). The second control culture (37 °C-2) had a smaller inoculum concentration than the first (37 °C-2), thus the 37 °C-2 dataset was shifted back by 8.5 hours. A total of 408 measurements (24 concentrations $\times$ 17 time points) per culture were fitted (Figure 3.5). Since oxygen uptake was not measured, the measurement set has only one degree of redundancy with respect to the model inputs and outputs (Quek et al. 2010). The calculated residual error therefore reflects the consistency of nitrogen balance among the measurements.

The B-splines were generally able to accurately trace all of the measured concentrations for both control and temperature-shifted cultures (Figure 3.5). The number of internal knots used and parameters fitted ranged from 0 to 2 and 93 to 141, respectively, for the four cultures; computation times were less than 11 seconds. The knot selection was validated by a Monte Carlo approach using 100,000 random samples of knot sequence; SSR was improved by only 3% at most.

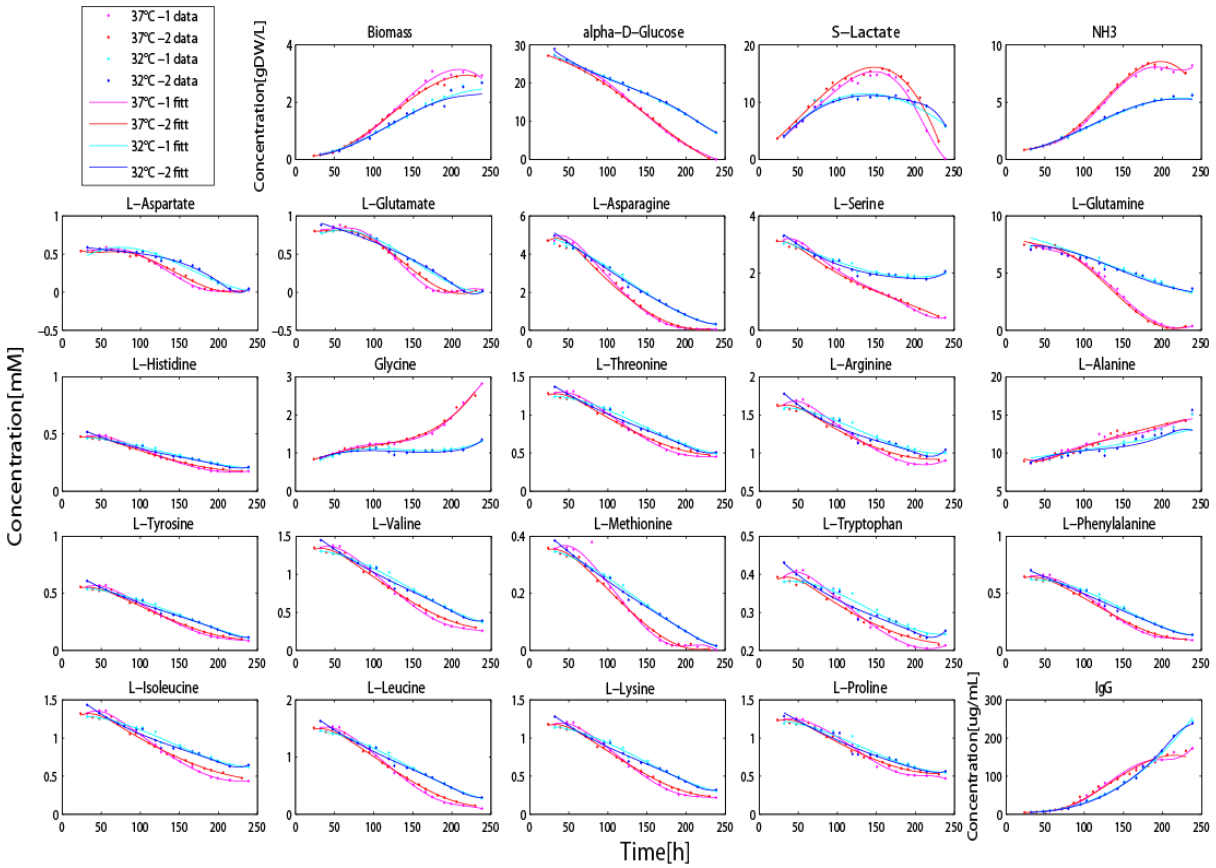

Figure 3.5: Fitted concentrations from CHO-XL99 cell cultures by B-DMFA. The experimental data are presented by points and the B-spline fit by lines. Data for cell cultures at constant 37°C are shown in pink (37°C-1) and red (37°C-2), and for temperature-shifted cultures in cyan (32°C-1) and blue (32°C-2)**.** Measurements before 24 hours were omitted from the analysis due to their high uncertainty.

Compared to the temperature-shifted cultures, the control cultures displayed faster depletion of glucose, glutamine and serine, and accumulation of lactate, ammonia and glycine (Figure 3.5). The time-resolved absolute fluxes estimated by B-DMFA were consistent with these general observations (Figures 3.6). The biomass precursor (glycogen, steroids, fatty acids and nucleotides) reactions presented the biggest difference in flux between control and temperature-shifted cultures, particularly between 80 and 180 hours a higher flux was observed for the cells at 37°C. The fluxes for serine aldolase (glycine production from serine) and glutaminase (glutamate production from glutamine) were also higher in a similar fashion to the biomass precursor reactions, but glycolytic fluxes were only marginally higher. Lactate dehydrogenase flux was higher for the control cultures; in agreement with the lactate concentration profile (Figures 3.5 and 3.7). TCA cycle flux was similar under both culture conditions. The absolute fluxes clearly showed the transient changes in metabolism as the cultures progress (Figure 3.6). Particularly in the control cultures, the glutamine consumption flux was elevated when cell-specific growth rate was beginning to decline at 100 hours, which coincided with the switch from lactate production to consumption (Figure 3.7).

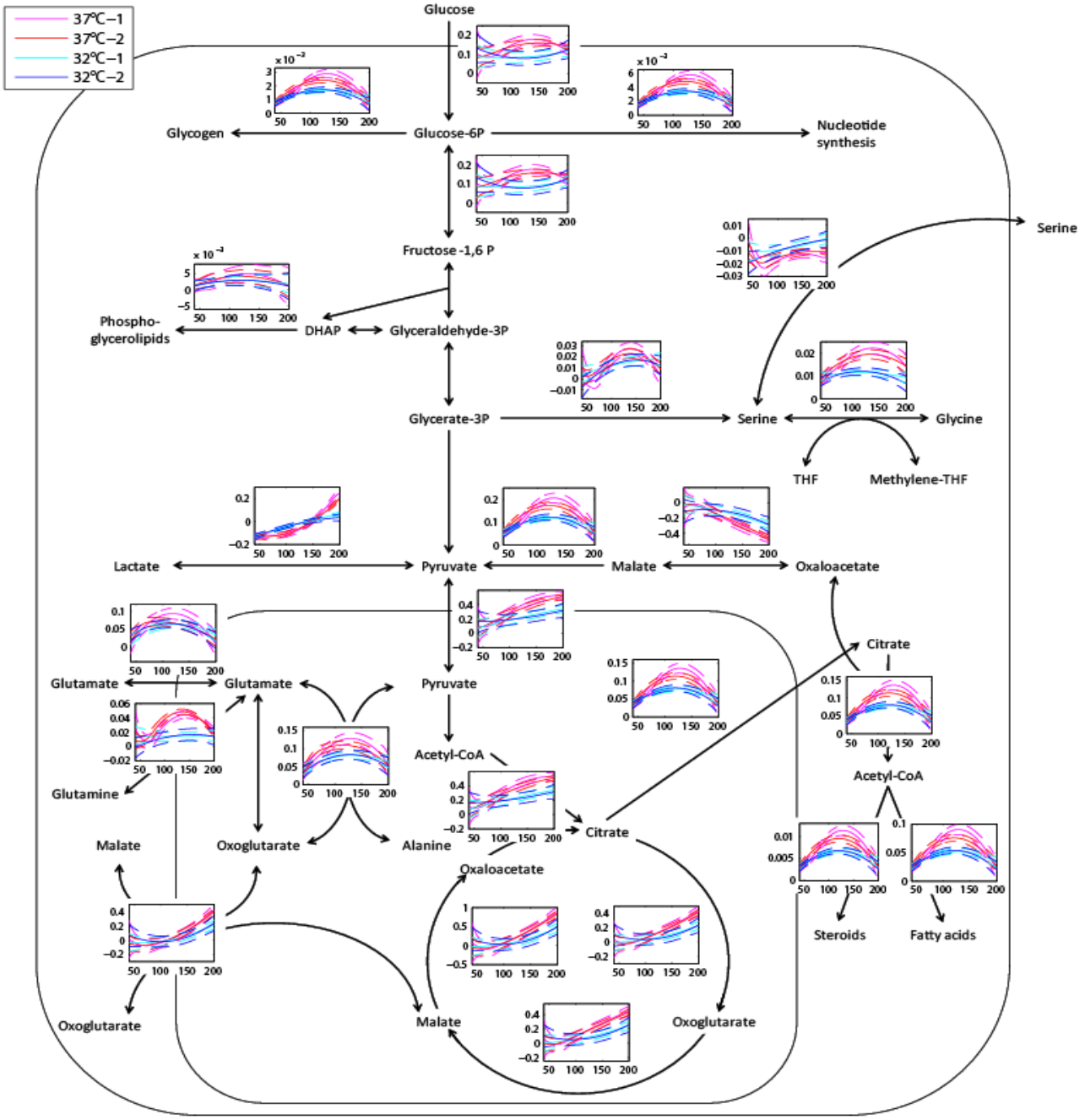

Figure 3.6: Absolute intracellular fluxes over time for control and temperature shifted cultures. Fluxes in [mM/h], time scale in hours. The figure shows the estimated dynamic fluxes from 40 to 200 h (Full time scale of the estimated fluxes in Appendix Figure A3). The CHO-XL99 cultures at constant 37°C are in pink (37°C-1) and red (37°C-2), the temperature shifted cultures in cyan (32°C-1) and blue (32°C-2). The fluxes calculated by B-DMFA are shown with solid lines and the 95% CIs are shown with dashed lines. Clear flux differences were observed between the control and temperature-shifted cultures. Especially for the biomass precursor reactions, control cultures showed higher fluxes than temperature-shifted cultures between 80 to 180 hours.

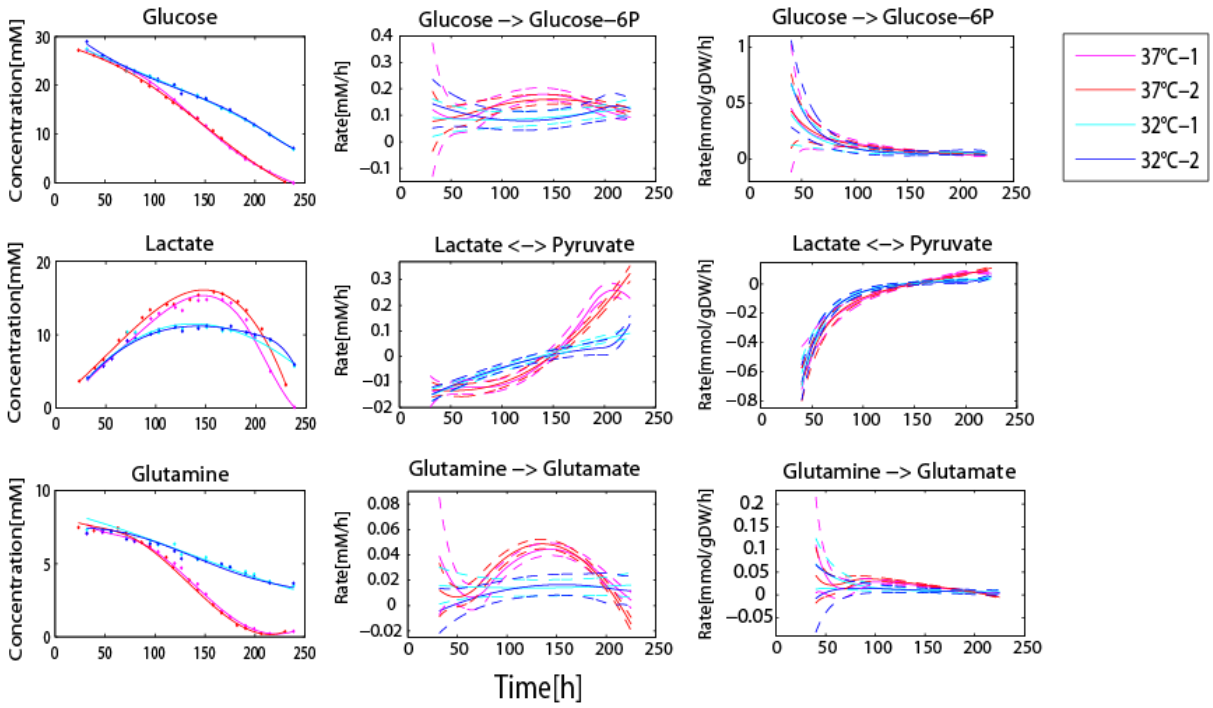

Figure 3.7: Concentration, absolute fluxes and volume specific fluxes for glucose, lactate and glutamine. Concentration in [mM], absolute fluxes in [mM/h], volume specific fluxes in [mmol/gDW/cell] and time scale in hours. The data for the control cultures are shown in pink (37°C-1) and red (37°C-2), and the temperature-shifted cultures in cyan (32°C-1) and blue (32°C-2). The glucose and glutamine consumption fluxes were higher for the control cultures, whereas they were more stable over time for the temperature-shifted cultures. Similarly, the lactate flux was higher for the control cultures until 168 hours. At stationary phase cells began to consume lactate. Differences in fluxes between the control and temperature-shifted cultures were reduced when fluxes were expressed as specific fluxes.

The differences in absolute fluxes between the two conditions can partially be attributed to differences in cell density, as cultures at 37°C grew faster than temperature-shifted cells and concomitantly accumulated more biomass. Volume-specific fluxes were therefore estimated to check if normalized fluxes were still different. While fluxes still showed transient behaviors, flux differences between the two culture conditions were diminished in general (Figure appendix A3). Glutaminase and lactate dehydrogenase fluxes for the control cultures were still significantly higher compared to the temperature-shifted cultures (Figure 3.8), but glycolytic fluxes were only marginally higher. The disparity between glycolytic and lactate fluxes suggests that, for the control cultures, a larger fraction of pyruvate was derived from other carbon sources in addition to glucose compared to temperature-shifted cultures. Biomass precursor reactions were kept at higher fluxes between 95 and 168 hours for the control cultures, which is proportional to the higher cell-specific growth rate of the control cultures during that period of time. Cells entered stationary phase at 168 hours, showing a reduction in their biomass precursor requirements and concomitantly most intracellular fluxes. An interesting exception are the TCA cycle fluxes, which appeared to be similar and constant throughout the whole culture

for both conditions. Yoon et al. (2003) showed no change in cell-specific glucose, glutamine and lactate fluxes when temperature of CHO cell culture was reduced from 37°C to 33°C, but a significant increase in all three fluxes when temperature was reduced to 30°C (Yoon, Song & Lee 2003).

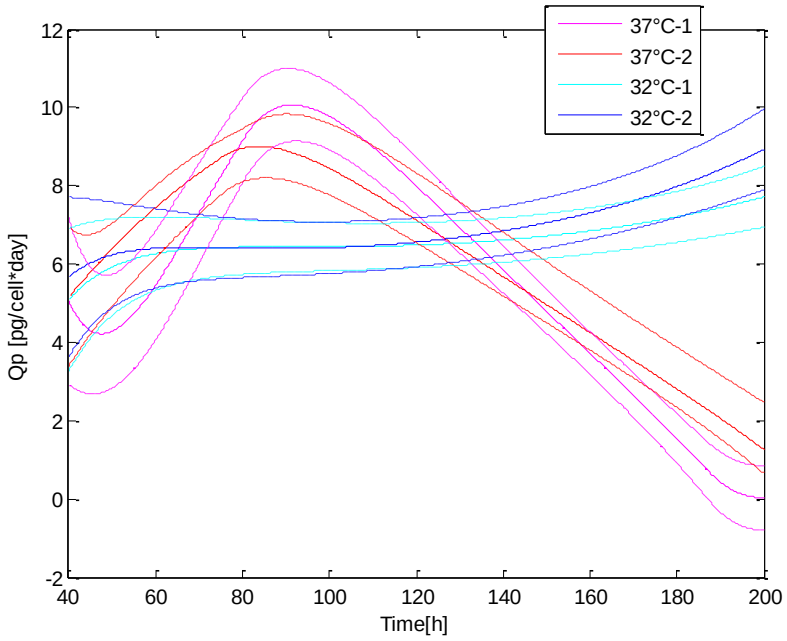

Figure 3.8: Volume specific productivity (Qp) over time for control and temperature-shifted cultures. The figure shows the estimated volume specific Qp from 40 to 200 h. The data for the control cultures are shown in pink (37°C-1) and red (37°C-2), and the temperature-shifted cultures in cyan (32°C-1) and blue (32°C-2). The cell number was normalized by cell volume. The temperature-shifted cultures have an almost constant volumetric Qp over the full culture. On the other hand, cells at constant temperature have a peak in volumetric Qp around 90 hours and then a decline. However, on average volumetric Qp is comparable in both conditions from 72.5 hours to 168 hours. Note that the 95% CIs of the Qp estimated by B-DMFA were large before the temperature shift due to the low cell number.

Although the average volumetric Qp was the same for the two conditions (Figure 3.4D) during exponential phase, the time-resolved volumetric Qp prolife revealed by B-DMFA was very different (Figure 3.7). The volumetric Qp for the temperature-shifted cultures was largely constant at about 6 - 7 pg cell^{-1}day^{-1} for the entire culture duration, despite the decline in cell-specific growth rate. In contrast, volumetric Qp for the control cultures peaked between 8 – 10 pg cell^{-1} day^{-1} at 90 hours, before gradually declining to 0. The higher titer achieved in the temperature-shifted cultures could be attributed to a more stable volumetric Qp (Figure 3.8).

Overall, B-DFMA was able to quantify changes in cell metabolism for the whole cell culture duration. While we expect the temperature shift to induce transient metabolic behaviors in

the cell cultures, B-DFMA was able to account for the gradual decline in cell-specific growth rate and dynamic consumption and production profiles. The changes observed in the latter were not expected for the control cultures. None of the metabolic fluxes were constant over time for any of the culture conditions (Figures 3.6, 3.7, A2 and A3). The gradual decline in cell-specific growth rate may be pH-related, and possibly due to the accumulation of lactate and ammonia. While B-DMFA was designed for resolving transient metabolic behaviors, it was crucial in showing that volume-specific productivity of IgG1 was significantly more stable in the temperature-shifted cultures compared to the controls. These observations would have been missed if average fluxes were used, highlighting the benefit of B-DMFA compared to conventional MFA.

3.5. Conclusions

We have demonstrated the usefulness of applying conventional B-spline notation and formulation to calculate dynamic fluxes without being restricted to any specific order of fitting. B-DMFA is capable of generating smooth fit for complete time series experimental data, as well as incorporating statistical estimation of dynamic metabolic fluxes in one step using redundant datasets. Using a higher-order fit, B-DMFA was shown to perform better in fitting dynamic external rates compared to L-DMFA. The heuristic algorithm developed to determine the knots sequence was validated to be accurate and was demonstrated to be much faster than the optimization method used in the L-DMFA approach (Leighty & Antoniewicz 2011). By resolving the dynamic changes in metabolic fluxes in temperature-shifted CHO-XL99 culture, we showed that the reduction of growth and overall metabolic rates by inducing mild hypothermia may have benefited the CHO cell culture in terms of enhancing the stability of recombinant protein production, leading to an observed increase in final antibody titer by 42%. This leaves room to speculate whether the slower cell metabolism and the reduced accumulation of lactate and ammonia have a positive effect on the stability of recombinant protein productivity.

Chapter 4

Improving Culture Performance and Antibody Production in CHO Cell Culture Processes by Reducing the Warburg Effect

Co-authors: Lake-Ee Quek, Peter Gray and Lars K. Nielsen

4.1. Abstract

Lactate is one of the key waste metabolites of mammalian cell culture. High lactate levels are caused by high aerobic glycolysis, also known as the Warburg effect, and are usually associated with adverse culture performance. Therefore, reducing lactate accumulation has been an ongoing challenge in cell culture development in order to improve growth, productivity and process robustness. The pyruvate dehydrogenase complex (PDC) plays a crucial role for the fate of pyruvate, as it converts pyruvate to acetyl-CoA. PDC activity can be indirectly increased by inhibiting the PDC inhibitor, pyruvate dehydrogenase kinase, using dichloroacetate (DCA); resulting in less pyruvate being available for lactate formation. Here, Chinese hamster ovary cells were cultivated either with 5 mM DCA or without DCA in various batch and fed-batch bioreactor processes. In all cultures, DCA increased peak viable cell density (VCD), culture length and final antibody titer. The strongest effect was observed in a fed-batch with media and glucose feeding in which peak VCD was increased by more than 50%, culture length was extended by over three days and final antibody titer increased by more than 2-fold. In cultures with DCA, lactate production and glucose consumption during exponential growth were on average reduced by about 40% and 35%, respectively. Reduced lactate production rate also reduced osmolality increase in DCA cultures due to smaller amount of base being added to the system. Metabolic flux analysis showed reduced glycolytic fluxes while fluxes in TCA cycle were not affected suggesting that cultures with DCA use glucose more efficiently. In proteomics analysis only few proteins were identified as being differentially expressed indicating that DCA acts on a post-translational level. Antibody quality in terms of aggregation, charge variant and glycosylation pattern was unaffected. Subsequent bioreactor experiments with sodium lactate and sodium chloride feeding indicated that lower osmolality, rather than lower lactate concentration itself, improved culture performance in DCA cultures. In conclusion, the addition of DCA to the cell culture improved culture performance and increased antibody titers without any disadvantages for cell specific productivity or antibody quality.

4.2. Introduction

Mammalian cells are the preferred production host for therapeutic proteins such as monoclonal antibodies due to their ability to perform post-translational modifications, which are essential for biological efficacy and safety (Durocher & Butler 2009; Wurm 2004). Most

cultured mammalian cells display aerobic glycolysis also known as the Warburg effect, i.e. inefficient energy metabolism, characterized by increased glucose consumption and lactate production (Warburg, Wind & Negelein 1927). Rapid lactate accumulation adversely effects culture performance and productivity (Dietmair, Nielsen & Timmins 2011; Gambhir et al. 2003; Lao & Toth 1997; Lim et al. 2010). In fermentation, pH is controlled and growth inhibition has been attributed to the concomitant osmolality increase (Cruz et al. 2000). Increased osmolality can also affect antibody quality (Li, J et al. 2012; Pacis et al. 2011).

Many strategies involving process optimization (Altamirano et al. 2004; Gagnon et al. 2011; Glacken, Fleischaker & Sinskey 1986; Kuwae et al. 2005) or genetic engineering (Fogolin et al. 2004; Irani et al. 1999; Wlaschin & Hu 2007; Zhou, M et al. 2011) have been explored to reduce lactate production and hereby improving cell growth, productivity and process robustness. Interestingly, while a knock-down of lactate dehydrogenase (LDH) reduces glucose consumption and lactate production (Kim, SH & Lee 2007), our attempt to perform a double knock-out of LDH failed presumably due to lethality; one allele was readily interrupted by a zing finger nuclease, but no double knock-out could be produced (unpublished). Correspondingly, Sanfeliu et al. concluded from experiments using oxamate, an LDH inhibitor, in hybridoma cells that LDH activity is essential for cell survival as LDH activity is necessary to reoxidise large amounts of NADH produced in glycolysis (Sanfeliu et al. 1997). It is possible that the TCA cycle is unable to absorb additional carbon. Consistent herewith, the glucose consumption declined in knock-down study and no additional carbon was redirected into the TCA cycle as lactate to glucose yield was unaltered.

The pyruvate dehydrogenase complex (PDC) plays a crucial role in glucose metabolism linking glycolysis to the TCA cycle as it converts pyruvate to acetyl-CoA. PDC activity is regulated by reversible phosphorylation of three serine residues; phosphorylation being catalyzed by pyruvate dehydrogenase kinase (PDK) which inactivates PDC (Yeaman et al. 1978). PDC activity can be indirectly increased by inhibiting PDK using dichloroacetate (DCA) (Whitehouse, Cooper & Randle 1974). DCA has been used for decades in the treatment of human diseases such as acquired or congenital lactic acidosis, congestive heart failure and ischemic heart disease due to its ability to lower blood lactate levels (Stacpoole et al. 1998). DCA has also been explored to improve mammalian cell culture. In hybridoma cell cultures without pH control, DCA improved peak viable cell density and final antibody titer by delaying glutamine depletion without any effect on glucose consumption or lactate production (Murray, Gull & Dickson 1996). In Chinese hamster

ovary (CHO) cultures without pH control, DCA reduced lactate production leading to higher viable cell density (Follstat 2002). However, no improvements in culture performance were observed in pH controlled bioreactor fermentations.

In this study, we successfully used DCA to reduce lactate production and glucose consumption in commercially relevant, pH controlled CHO fed batch cultures, in which no essential macronutrients were depleted. We compared cell growth as well as nutrient consumption and metabolite production, productivity and antibody quality. Proteomics, metabolomics and fluxomics were used to explore the system-wide effect of DCA. Finally, sodium lactate and sodium chloride feed experiments were performed to establish if lower lactate accumulation itself or lower osmolality levels are responsible for improvements in culture performance.

4.3. Material and Methods

4.3.1. Cell line and medium

CHO-XL99 is a derivative of CHO-K1 (ATCC 61-CCL) and expresses a full IgG1 antibody (Ab2). It was adapted to CD CHO medium supplemented with 8mM GlutaMAX, 400ug/ml Geneticin and 0.2% v/v Anti-Clumping Agent (all Invitrogen). Cells were routinely maintained in shake flask in humidified incubators set to 37°C, 7.5% CO_2 and 130 rpm. Sodium dichloroacetate (Sigma-Aldrich) was added to respective pre-cultures two days before transfer to the bioreactor. Two ml/l Pluronic F-68 (Invitrogen) was added to the medium used for bioreactor cultures. Separate shake flask experiments were performed for Western blot, DCA response curve and DCA stability in cell culture analysis.

4.3.2. Western blot

CHO-XL99 cells were cultivated using different DCA concentrations (0 – 10 mM DCA) for 48 hours. Approximately, 2 x 10^7 cells were collected, washed with 0.9% sodium chloride and lysed in RIPA buffer (0.1% SDS, 1% Triton-X100, 5 mM ethylenediaminetetraacetic acid, 0.5% sodium deoxycholate, 150 mM NaCl, 50 mM Tris-HCl, 2 mM dithiothreitol, supplemented with 1ug/mL leupeptin (Roche), 1ug/mL aprotinin (Roche), 1 mM sodium orthovanadate, 10 mM sodium fluoride). Cell lysates were incubated for 60 min on ice followed by centrifugation at 16,000 rcf, 4°C for 10 min. Protein concentration of the supernatant was determined using a 2D Quant Kit (GE Healthcare). Cell extracts

equivalent to 10 µg of protein were run on a 4-12% SDS-polyacrylamide gel and transferred to nitrocellulose membranes by standard procedures. Membranes were blocked with 5% nonfat milk in PBS/Tween for 1 hour followed by incubation with anti-human PDC E1-α subunit (phospho S293) (abcam) and anti-β-tubulin (Cell Signalling Technology) antibodies for 2 hours at RT. Immunoreactive bands were visualized using horseradish peroxidase-conjugated anti-rabbit antibody (Life Technologies) and Amersham ECL Western Blotting Detection Reagents (GE Healthcare Bio-Sciences). Densitometry was performed using a BIORAD ChemiDoc MP Imaging System (Bio-Rad Laboratories) and Image Lab 4.0.1 software (Bio-Rad Laboratories).

4.3.3. HPLC method for DCA quantification in cell culture

CHO-XL99 cells were cultivated with different DCA concentrations (0 – 10 mM DCA). Every two days, a 500 µl sample was collected, centrifuged at 500 rcf and supernatants were frozen and stored at -20°C until analysis. DCA concentrations were determined by reverse phase HPLC on an Agilent 1200 system equipped with a Kinetex C18-XB column (100 Å, 2.6 µm, 100 × 2.1 mm, Phenomenex) and a diode array detector. The column temperature was set at 30°C and the flow rate was 0.2 ml/min. Mobile phase A consisted of 10 mM tetrabutylammonium bisulfate (Sigma-Aldrich) in water and mobile phase B was 100% acetonitrile (Merck). The gradient started with 5% mobile phase B and was increased linear to 30% in 3 min followed by a hold at 30% for 5 min. Next, the concentration of mobile phase B was increased linear from 30% to 60% in 1 min followed by a hold of 60% mobile phase B for 5 min. Afterwards, the gradient was reversed from 60% to 5% mobile phase B in 1 min, followed by a hold at 5% mobile phase B for 5 min.

4.3.4. Bioreactor cell culture

A total of 12 bioreactor cultures were performed (Table 4.1). All cultures were carried out in a 3L sparged bioreactor (Applikon) with 1L initial working volume at 37°C, pO_2 at 50% air saturation, stirrer speed at 200 rpm, and pH 7.0 controlled by CO_2 sparging and addition of 1 M sodium bicarbonate. Oxygen uptake rate (OUR) was determined using the dynamic method (Singh 1996). In fed-batch cultivations, a 1:1 mixture of CHO CD EfficientFeed A and CHO CD EfficientFeed B (FeedAB) (Life Technologies) was fed four times: prior to inoculation (15% of volume) and after approximately 90 h (15%), 109 h (10%) and 118 h (10%) after inoculation. In the "*fed-batch plus glucose*" cultures

concentrated glucose (450g/l, Sigma) was added to the cell culture as needed to keep glucose concentration above 11 mM after the last FeedAB feed and until the end of the culture.

Sodium lactate (Ajax finechem) and sodium chloride (Sigma-Aldrich) feeding experiments were carried out, starting the bioreactor cultivation as the fed-batch cultures. One day after inoculation, sodium lactate (40 mM/day) or sodium chloride (30 mM/day) was fed continuously until the end of culture.

Table 4.1: Overview of experiments presented in this work.

Study	Conditions*	Cultures	No. of runs
Batch	CD CHO medium	5mM DCA	2
	No feeding	No DCA (control)	2
Fed-batch	CD CHO medium	5mM DCA	1
	FeedAB	No DCA (control)	1
Fed-batch plus glucose	CD CHO medium	5mM DCA	2
	FeedAB + glucose feed	No DCA (control)	2
Sodium lactate feed	CD CHO medium	No DCA	1
	FeedAB + sodium lactate		
Sodium chloride feed	CD CHO medium	No DCA	1
	FeedAB + sodium chloride		

* FeedAB = CHO CD Efficient Feed A & B (1:1)

4.3.5. Cell count, metabolite and IgG measurements

Viable cell density, viability and cell diameter were measured using a CedeX cell counter (Innovatis AG). Ammonia, Na^+, and glucose concentrations used to determine time points of glucose feeding were quantified using a Nova Bioprofiler FLEX (Nova Biomedical). Extracellular glucose, lactate, GlutaMAX^{TM} and amino acid concentrations were measured by HPLC as described previously (Dietmair, Timmins, Gray, Nielsen & Kromer 2010), while antibody titers were determined using surface plasmon resonance with a Biacore T-100 (GE Healthcare). A human antibody capture kit (GE Healthcare) was used for the immobilization of an Ab2 binding α-Hu IgG FC-specific antibody onto the CM5 sensor chips. Samples were diluted 5-10 times in HBS-EP buffer (GE healthcare) and protein-A purified Ab2 was used to obtain a standard curve for quantification. Selected intracellular metabolites from glycolysis, TCA cycle and pentose phosphate pathway were measured by HPLC-MS/MS (Dietmair, Timmins, Gray, Nielsen & Kromer 2010) in mid-exponential growth phase of fed-batch and fed-batch plus glucose cultivations (Figure 4.2).

4.3.6. Metabolic flux analysis

Metabolic fluxes during exponential growth were estimated using a metabolic model derived from *Mus musculus* GeM (Quek & Nielsen 2008b) as previously described (Quek et al. 2010). The average cell dry weight was measured to be 350 pg/cell and precursor compositions obtained from previous CHO cell studies (Martínez, VS et al. 2013) were used for the biomass equation. An Ab2 antibody production reaction was added (Ab2 amino acid composition shown Appendix B). GlutaMAX^{TM} (L-alanyl-L-glutamine dipeptide) was treated as free glutamine and alanine. Constrained weighted quadratic programming was used for consistency checking and flux variability analysis (Antoniewicz, Kelleher & Stephanopoulos 2006), while a Monte-Carlo approach was used to propagate errors in the primary concentration data into the calculated cell-specific rates (Goudar et al. 2009, Quek et al. 2014) (see also Appendix C). Estimated fluxes were also used for calculation of ATP production (Martínez, VS et al. 2013).

Dynamic metabolic flux analysis (DMFA) was used to determine metabolic fluxes over the complete culture period and is described in chapter 3 in detail. Briefly, metabolic fluxes are allowed to change over time to reflect the dynamics of the measured concentrations and rates. The complete time-series of metabolic fluxes can be estimated by solving a single optimization problem (Antoniewicz 2013b). Higher-order B-spline fitting was used to estimate mass balanced fluxes for the entire culture time and a fast heuristic algorithm was used to determine the position of the knots (time points) of the B-spline.

4.3.7. Proteomics

4.3.7.1. Sample preparation

Approximately 3 x 10^7 cells were collected during the mid-exponential growth phase of fed-batch and fed-batch plus glucose cultures (Figure 4.2). Cells were centrifuged at 500 rcf for 3 min, washed with 0.9% sodium chloride and cell pellets frozen on dry ice and stored at -80°C. Cells were lysed in 500 µl cell lysis buffer (8 M urea, 50 mM ammonium bicarbonate, 5 mM sodium orthovanadate, 10 mM sodium fluoride, 2.5 µg/ml leupeptin (Roche), 1.5 µg/ml aprotinin (Roche)) and disrupted using a 25G needle followed by 3 x 1 min sonication. 5 µl RNaseA (Thermo Fisher Scientific Inc.) and 5 µl DNaseI (Thermo Fisher Scientific Inc.) were added to the cell lysate followed by incubation at RT for 15 min. Cell lysate was centrifuged for 10 min at 16.000 rcf, 0°C and supernatant was collected,

frozen on dry ice and stored at -80°C. Protein concentration was determined using a 2D Quant Kit (GE Healthcare) according the manufacturer's instructions. To 100 µg of protein, six times the volume of -20°C cold acetone was added and incubated at -20°C for three hours. Samples were centrifuged for 2 min at 1000 rcf, 0°C and supernatant was removed from the tubes. 20 µl of Dissolution Buffer (iTRAQ reagents, Sciex) and 1 µl of Denaturant (iTRAQ reagents) were added to dissolve the sample. 2 µl of Reducing Reagent (iTRAQ reagents) were added and the samples were incubated at 60°C for one hour. 1 µl of Cysteine Blocking Reagent (iTRAQ reagents) was added to the sample and incubated for 10 min at RT followed by adding 10 µg of trypsin (Trypsin Gold, Promega) and incubation at 37°C overnight. Digested peptide samples were cleaned using ZipTip C18 (Millipore) and eluted with 70% (v/v) acetonitrile. Residual acetonitrile was removed using vacuum centrifugation (Eppendorf) and samples were resuspended in 0.1% formic acid.

4.3.7.2. LC-MS/MS analysis and quantification

Peptides were separated on a Shimadzu Prominence Nano-LC system equipped with a Vydec Everest C18 column (300 Å, 5 µm, 150 mm x 150 µm) at a flow rate of 1 µl/min using a gradient of 10-60% mobile phase B over 90 min; mobile phase A = 1% acetonitrile/0.1% formic acid and mobile phase B = 80% acetonitrile/ 0.1% formic acid. Eluted peptides were analyzed on a QSTAR-Elite (ABSciex) equipped with a nano-spray ESI source operated in positive mode. Analyst® software was used to scan for masses between 300 to 1800 Da followed by high sensitivity product ion scan. ProteinPilot v4.5 (ABSciex) and the Paragon Algorithm were used to analyze MS/MS data. The protein sequences for CHO-K1 were downloaded from the Chinese hamster genome database (http://www.chogenome.org). A false discovery rate of 5% was used. Only proteins identified with at least 2 peptides at 95% confidence were included in the statistical analysis. For SWATH-MS, MS/MS data was analyzed with the SWATH-MS processing script in PeakView v 1.2 (ABSciex) using discovery data as the spectra library for protein identification and fragment ion peak areas were used for quantification. Summed protein peak areas were used for statistical analysis. Raw data was first log2 transformed and quantile normalized. Data was then analyzed for statistically differentially expressed proteins using limma (Smyth 2005) in R (R Core Team 2013). Proteins with an adjusted p-value of < 0.05 were considered statistically significant different.

4.3.8. Antibody product quality analysis

Samples were collected during early stationary phase of fed-batch plus glucose cultivations (Figure 4.2). Cell culture was centrifuged at 500 rcf, RT for 5 min, followed by a 0.22 µm filtration. Supernatant was stored at -80°C until purification. Antibody was protein-A purified using an ÄKTA avant 150 (GE Healthcare) with a HiTrap Map Select 1 mL column (GE Healthcare). Antibody was eluted in 0.1 M glycine, pH 3.0. The purified antibody was then desalted using a HiTrap 5 mL column (GE Healthcare) and eluted in 1x Dulbecco's Phosphate-Buffered Saline (Dulbecco). A LabChip GXII (Caliper) was used to analyze charged variants (HT Protein Charge Variant Kit, Caliper) and various glycoforms (ProfilerPro Glycan Profiling Kit, Caliper). Except for a longer PNGase digestion step of 3 hours, the kits were used according to manufacturer's instructions. Antibody aggregation, monomer and fragment levels were determined using standard size exclusion chromatography on an Agilent HPLC system.

4.4. Results

4.4.1. DCA is stable in CHO cell culture, decreases PDC phosphorylation and reduces lactate formation

Shake flask experiments with different DCA concentrations were performed to analyze the effects of DCA on cell growth, lactate production and PDC phosphorylation. DCA can be degraded by glutathione S-transferase ζ1 (Lantum et al. 2003; Li, WJ et al. 2011) and we first established that DCA concentration in CHO culture decreased less than 5% of its initial concentration over a period of 12 days and no additional DCA supplementation is required (Figure 4.1C). Lactate production decreased with increasing DCA concentration, while the growth rate was unaffected up to a concentration of 5 mM DCA, and this concentration was chosen for subsequent bioreactor cultures. Western blot analysis confirmed a decrease in PDC E1α phosphorylation with increasing DCA concentration with a 17% reduction observed at 5 mM DCA (Figure 4.1D).

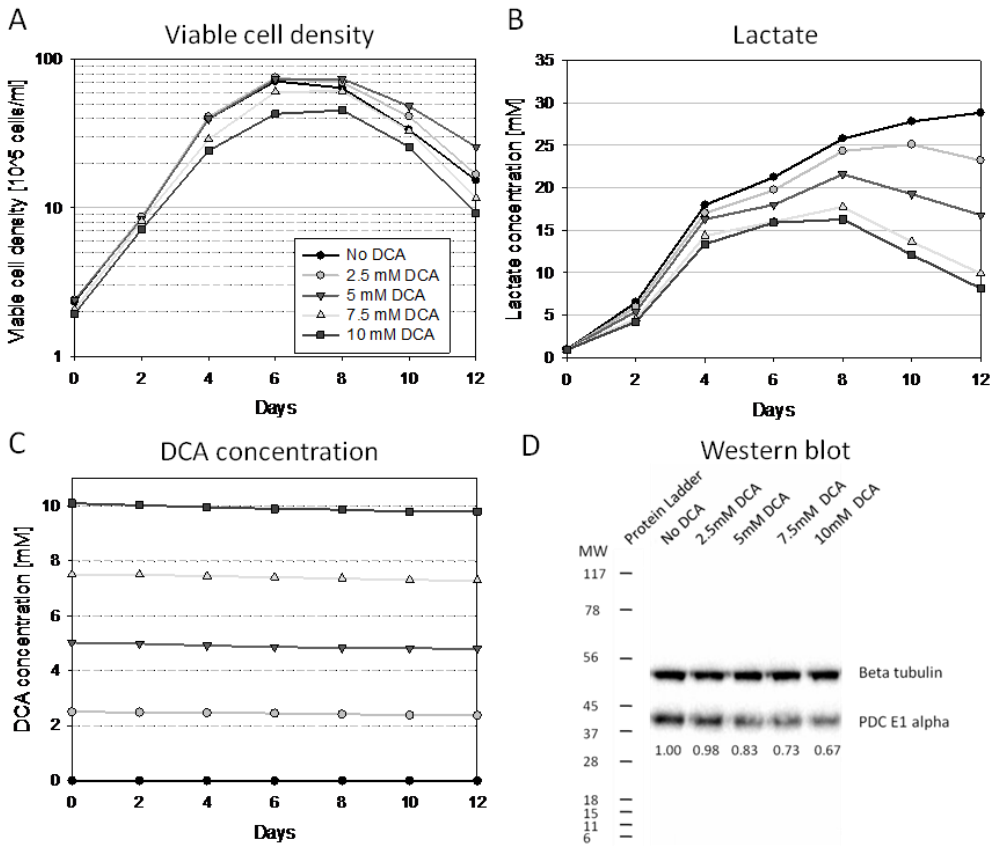

Figure 4.1: Growth curve, lactate and DCA concentration profile, and Western blot analysis. CHO cells were cultured in shake flask with different DCA concentrations. Growth rate was unaffected by DCA up to 5 mM and decreased at higher DCA concentrations (A). Lactate production decreased with increasing DCA concentration during exponential growth (B). DCA concentration decreased less than 5% in CHO cell culture over a 12 day culture period (C) and with increasing DCA concentration PDC E1α phosphorylation decreased (D).

4.4.2. Growth, glucose consumption, lactate production, and antibody titer profiles in different bioreactor culture processes

In batch fermentations, both control and 5 mM DCA, cell growth stopped once glucose was depleted (Figure 4.2, top panel). DCA delayed depletion, maintained high viability for an additional day and enhanced Ab2 titer (Table 4.2). Depletion can be avoided using fed-batch and we first used a rich feed to the maximum recommended total of 50% of culture volume (Figure 4.2, middle panel). While feeding extended the culture, cell growth stopped due to glucose depletion and DCA again extended the culture and increased titer (Table 4.2). Glucose depletion was avoided in the subsequent fed batch cultures by feeding glucose as required after completion of the rich medium feed (Figure 4.2, bottom panel). Surprisingly, glucose feeding had a greater benefit in DCA cultures extending these by 2.5 days compared to 1 day without DCA. The Ab2 titer improvement further increased to 105% (Table 4.2).

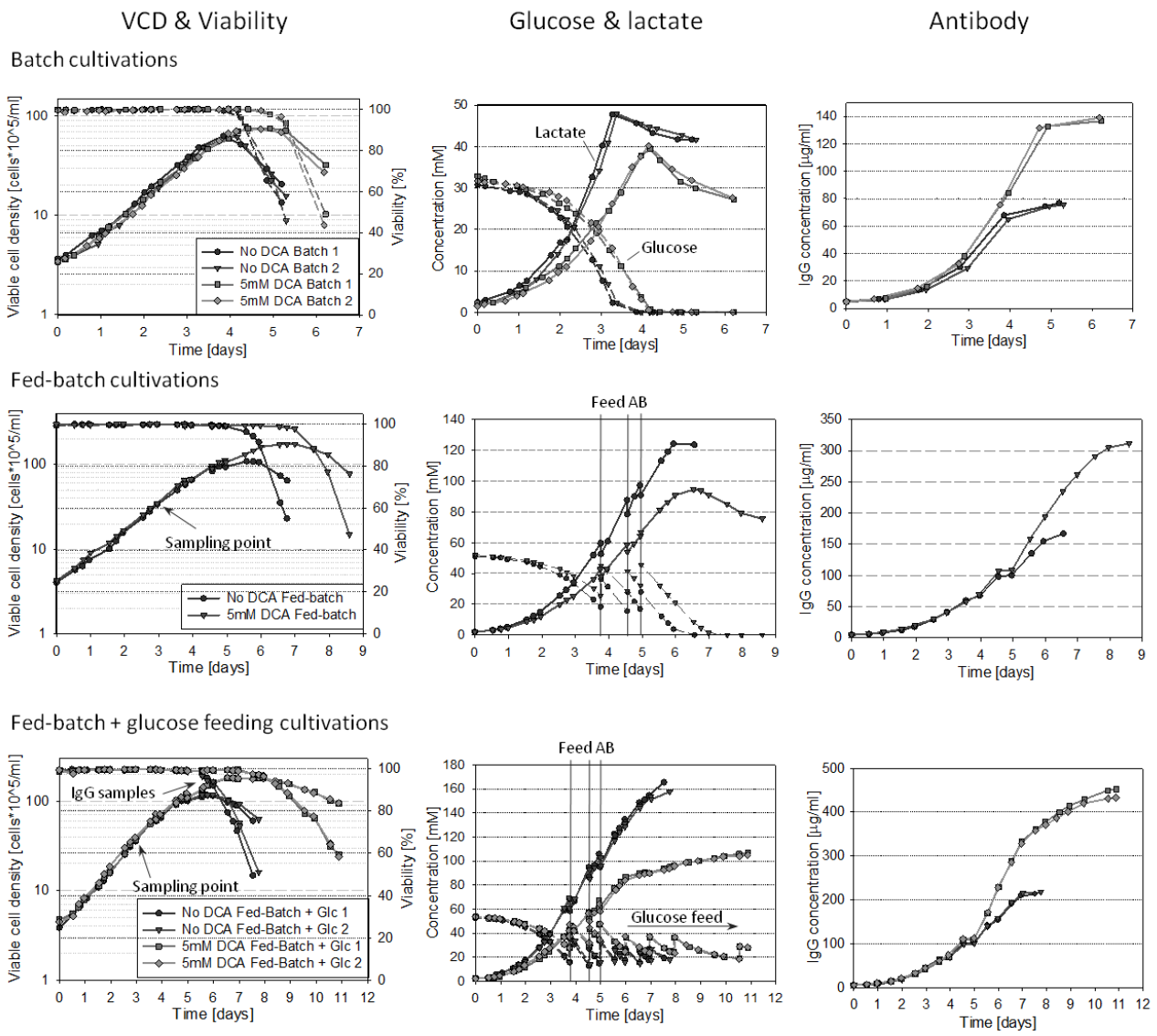

Figure 4.2: Impact of DCA on cell growth, glucose consumption, lactate production and antibody titer. CHO-XL99 cells were cultivated in a bioreactor with 1L initial working volume in batch, fed-batch and fed-batch plus glucose processes either with 5 mM dichloroacetate (DCA) or no DCA as control cultures. In fed-batch and fed-batch plus glucose the feeding medium (FeedAB) was added before inoculation followed by three more feedings during the cultivation. In fed-batch plus glucose cultures, glucose feeding started on day 6 and continued until the end of the culture as needed to keep glucose concentration above 11 mM. In all processes, DCA extended the culture time, led to a higher peak VCD, decreased glucose consumption and lactate production and increased final antibody titer. VCD = viable cell density.

During exponential growth, DCA reduced glucose consumption and lactate production by about 35.4 ± 3.4% and 40.2 ± 3.4%, respectively, resulting in a decrease in molar lactate to glucose yield of 7.43% (Table 4.2). The growth rate during exponential growth for all ten cultures was the same (0.0333 ± 0.0004 h^{-1}, $p = 0.30$, t-test). Similarly, there was no difference in the cell specific productivity (8.81 ± 0.05 pg/(cell*day), $p = 0.65$, t-test). Thus, the improved titers seen with DCA are exclusively attributable to maintaining cultures viable for longer.

Table 4.2: Culture length, peak viable cell density, lactate to glucose yield, and final antibody titer of cultures with DCA and control cultures in different processes.

	Culture time [days]	Peak VCD [*10^5 cells/ml]	$Y_{lactate/glucose}$	Final Ab2 conc. [ug/ml]	Ab2 conc. increase compared to control culture
Batch, no DCA	~4	62.52	1.75	77.15	
Batch, 5 mM DCA	~5	74.66	1.62	137.79	~78%
Fed-batch, no DCA	~7	108.52	1.74	167.27	
Fed-batch, 5 mM DCA	~8.5	172.85	1.61	311.54	~86%
Fed-batch + glucose, no DCA	~8	117.97	1.68	215.56	
Fed-batch + glucose, 5 mM DCA	~11	181.51	1.56	442.94	~105%

VCD = viable cell density

4.4.3. DCA does not affect antibody quality

The CHO-XL99 cell line expresses a full IgG1 antibody (Ab2). Change in culture conditions and cell metabolism can influence the antibody quality. DCA had no major impact on aggregation level, acidic and basic variants or glycoform pattern (Table 4.3). The percentage of monomers was slightly lower, while the percentage of dimers and multimers was higher. Similarly, a slight shift from basic to acidic variants was observed in DCA cultures. The glycan profile analysis was similar for both cultures and showed no change in % Man5, a variable previously found to be affected by osmolality (Pacis et al. 2011).

Table 4.3: Aggregation, charge variant and glycan profiles of control and DCA cultures. Samples (n=3 for each condition) were collected in early stationary phase (Figure 4.2) and analyzed for aggregation using SEC-HPLC, charge variants (HT Protein Charge Variant Kit, LabChip GX2) and glycoforms (ProfilerPro Glycan Profiling Kit, LabChip GX2).

	Aggregation					
	% Monomers		**% Dimers**		**% Multimers**	
Culture	Mean ± SD		Mean ± SD		Mean ± SD	
Control	**90.4**	0.25	**8.6**	0.35	**1.0**	0.10
5mM DCA	**88.4**	0.44	**10.2**	0.37	**1.4**	0.07

	Charge Variant					
	% Acidic		**% Main**		**% Basic**	
Culture	Mean ± SD		Mean ± SD		Mean ± SD	
Control	**12.5**	0.35	**50.0**	0.70	**37.5**	0.35
5mM DCA	**13.7**	0.80	**51.0**	0.57	**35.3**	0.23

	Glycan											
	Man5		**G0**		**G0f**		**G1f/G1f'**		**G2**		**G2f**	
Culture	Mean ± SD		Mean ± SD		Mean ± SD		Mean ± SD		Mean ± SD		Mean ± SD	
Control	**1.04**	0.12	**5.43**	0.49	**60.14**	4.98	**22.15**	2.12	**0.79**	0.053	**1.40**	0.32
5mM DCA	**1.15**	0.10	**5.31**	0.86	**59.76**	1.74	**22.38**	1.93	**0.81**	0.069	**1.41**	0.18

4.4.4. Growth cessation is caused by high osmolality

During fed-batch plus glucose cultures, cell growth slowed down and cultures entered stationary phase despite neither glucose nor any of the essential amino acids being

depleted. While depletion of a micronutrient is a possibility, a more likely explanation, given the effect of DCA, is the accumulation of growth inhibiting by-products. Comparing growth curves and lactate concentrations of control and DCA cultures showed that in both conditions growth started to slow down once lactate concentration reached about 90 mM (Figure 4.3, blue circle).

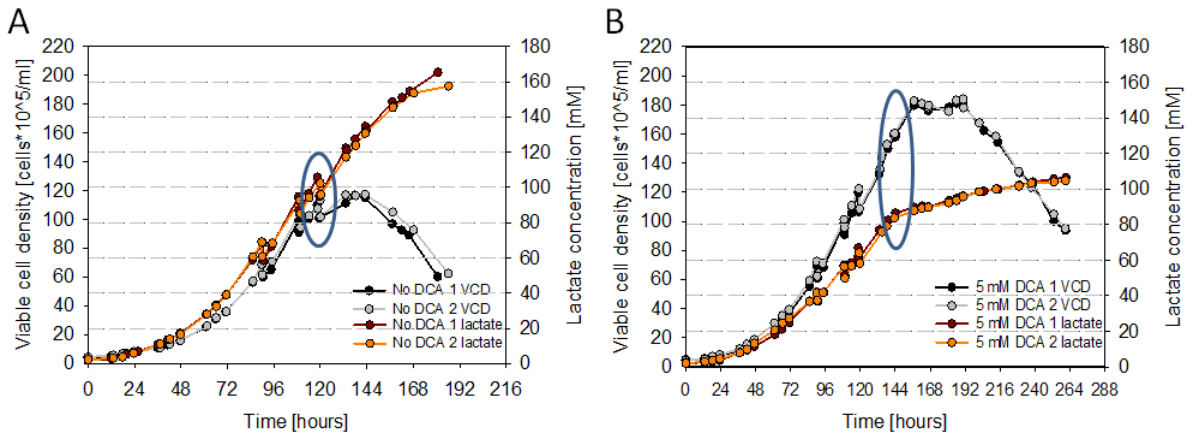

Figure 4.3: Viable cell density and lactate concentration of fed-batch plus glucose cultures. Viable cell density (VCD) and lactate concentration profile of fed-batch plus glucose control cultures (A) and with 5 mM DCA (B). Circles indicate start of growth rate reduction.

A sodium lactate feeding experiment was performed to confirm that high lactate concentration was responsible for growth inhibition (Figure 4.4A). Sodium lactate was fed at 40 mM/day, which is higher than the maximum volumetric lactate production rate observed in DCA cultures (~24 mM/day) but slightly lower than in control cultures (~42 mM/day).

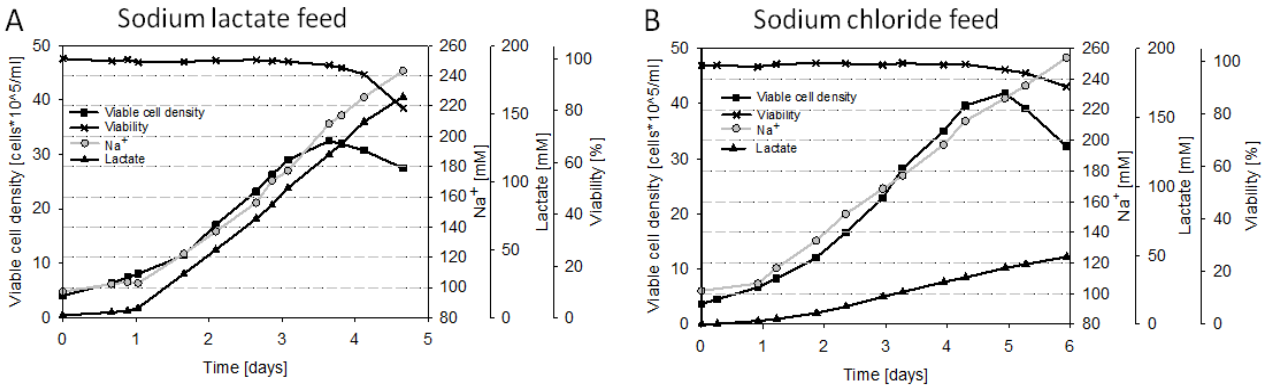

Figure 4.4: Impact of sodium lactate and sodium chloride feeding on cell growth. Culture had same starting conditions as fed-batch without DCA. One day after inoculation sodium lactate feeding (A, 40 mM/day) or sodium chloride feeding (B, 30 mM/day) started.

Early on day four during sodium lactate feed experiment, the lactate concentration reached 90 mM and cell growth slowed down, followed by stationary phase and entering death phase late on day four (Figure 4.4A). Na^+ concentration was around 180 mM when cell

growth rate decreased. Cells entered stationary phase at a Na^+ concentration of about 220 mM. Feeding sodium lactate to the culture not only increased the lactate concentration but also increased osmolality. Therefore it is not clear whether lactate itself or the increased osmolality caused growth inhibition.

A sodium chloride feeding experiment in which osmolality is increased at a higher rate while lactate concentration only increases at the rate produced by the cells was carried out to determine which factor is growth inhibitory (Figure 4.4B). The growth rate declined on day four at around 180 mM Na^+ however cell growth continued until day five. Cells started to die once Na^+ concentration reached about 220 mM. The Na^+ concentration were similar to concentrations observed in sodium lactate feeding experiment at time point of growth rate reduction, however lactate concentration was significantly lower (final lactate concentration was 49 mM) indicating that high osmolality, rather than the lactate concentration *per se*, was growth inhibitory in fed-batch plus glucose fermentations.

4.4.5. DCA significantly decreases lactate production without affecting oxidative metabolism

In order to understand global effects of DCA, a comprehensive omics comparison was performed during the exponential phase of fed batch cultures. Since this precedes post-inoculation feeding, data from fed batch cultures with and without glucose were used as biological replicates. Samples for proteomics and metabolomics were obtained on Day 3. Metabolic rates were determined between day ~1 and ~3.5 (Table 4.4) which were subsequently used for metabolic flux analysis (MFA) (Figure 4.5). Additionally, B-DMFA was performed for the complete cultivation period of fed-batch plus glucose fermentations (Figure 4.7). Samples for intracellular metabolite analysis were collected in triplicate from fed-batch plus glucose cultures. One of the DCA samples had varying results without a clear trend and was omitted from the analysis, leaving n = 5 for DCA cultures and n = 6 for control cultures. A total of 43 metabolites were measured whereof 14 were either not detected or below the lower limit of quantification in at least one of the samples (Figure 4.6). Using SWATH for quantitative proteomics, less than 1% (20) of 2016 identified proteins were differentially expressed (Appendix D) with the highest fold change being 2.31. None of the genes in central carbon metabolism appeared in the differentially expressed list, nor did gene enrichment analysis identify central metabolic processes such as glycolysis. Evidently both the direct and indirect effects of DCA are at a post-

translational level and observed metabolic changes are the result of post-translational regulation.

Table 4.4: Metabolic rates of CHO-XL99 cultures treated with 5 mM DCA and control cultures during exponential growth. Mean (n=3, fed-batch and fed-batch plus glucose) metabolic uptake and production rates of cultures with 5 mM DCA and control cultures during exponential growth. Rates are in µM/(gDW*h), growth rate is in h^{-1}, antibody (Ab2) production rate is in pg/(cell*day). Negative rates represent consumption while positive rates are production of the corresponding metabolite. The asterisks indicate rates which were statistically significantly different ($p < 0.05$, t-test) in cultures with DCA compared to control cultures. OUR = oxygen uptake rate, SE = standard error, Y = yield.

	No DCA		**5mM DCA**	
Metabolite	Rate ± SE		Rate ± SE	
Glucose*	-575.0	9.6	-371.6	8.7
Lactate*	1005	15	600	14
$Y_{lactate/glucose}$*	1.749	0.004	1.616	0.001
NH_4^+*	27.04	0.25	30.03	0.70
OUR	-291.4	3.5	-289.2	3.5
Consumed amino acids				
Asp*	-4.83	0.041	-3.83	0.087
Glu	-4.04	0.044	-3.82	0.17
Asn	-43.02	0.38	-42.30	0.54
Ser*	-47.95	0.23	-44.30	0.76
Arg*	-10.03	0.21	-8.44	0.13
Essential amino acids				
His	-4.45	0.13	-4.16	0.033
Thr	-10.70	0.25	-10.10	0.21
Tyr	-4.56	0.11	-4.76	0.21
Val	-13.89	0.23	-13.18	0.38
Met	-4.90	0.15	-4.79	0.065
Trp*	-3.67	0.090	-3.26	0.090
Phe*	-6.77	0.098	-5.52	0.12
Ile*	-11.43	0.12	-10.55	0.26
Leu	-17.79	0.23	-16.62	0.45
Lys*	-13.94	0.11	-13.05	0.25
Pro	-11.16	0.28	-11.88	0.31
Produced amino acids				
Gly*	23.73	0.30	16.61	0.24
Ala	97.4	1.4	95.0	1.9
Gln*	22.77	0.27	19.05	0.53
Glutamax*	-56.8	1.1	-50.8	1.4
Growth rate	0.0328	0.0004	0.0322	0.0007
Productivity	8.86	0.037	8.77	0.095

The metabolic rates for glucose consumption and lactate production were significantly reduced in DCA cultures, while the oxygen uptake rate (OUR) was unchanged indicating similar TCA cycle activity during exponential growth (Table 4.4). Several of the amino acid production and consumption rates as well as ammonia production were different between the two conditions ($p < 0.05$, t-test) with rates being lower in DCA cultures. The largest difference was observed for glycine production which was 30% lower in DCA cultures.

Intracellular metabolic fluxes (Figure 4.5) were estimated using total cell number, amino acids, glucose, lactate, ammonia measurements and Ab2 concentration as input data for MFA. As expected from reduced glucose consumption and lactate production (Table 4.4), glycolytic fluxes and flux through LDH were significantly lower in cultures with DCA (Figure 4.5). The concentration of glycolytic intermediates downstream of phosphofructokinase (PFK) and aldolase were lower in DCA culture compared to control cultures as were lactate. In contrast, glucose 6-phosphate, glucose 1-phosphate and fructose 6-phosphate were similar. MFA cannot resolve fluxes in the oxidative pentose phosphate pathway as the need for NADPH can also be met by the cytosolic malic enzyme (Quek et al. 2010). The concentrations of ribose 5-phosphate and ribulose 5-phosphate were higher in DCA cultures, suggesting a more active pentose phosphate pathway.

Apart from glycolysis, the only significant flux change was reduced flux in DCA cultures through the serine transhydroxymethyltransferase enzyme that converts serine and tetrahydrofolate (THF) to glycine and 5,10-methylene-THF, which is consistent with the reduced production of glycine observed in Table 4.4.

In both cultures, the majority of glycolytic derived pyruvate was converted to lactate though the percentage was lower for cultures with DCA (68% and 78% for DCA and control cultures, respectively). DCA reduces phosphorylation of PDC (Figure 4.1) and data does support a small shift in concentrations with lower pyruvate and higher acetyl-CoA (Figure 4.6). However, fluxes for pyruvate transport into the mitochondrion and the PDC reaction were unchanged (Figure 4.5), indicating that DCA cultures did not direct more pyruvate into the TCA cycle but rather reduced the flux to pyruvate and the fraction of pyruvate converted to lactate. Consistent herewith, the concentration of TCA cycle intermediates (citrate, aconitate, fumarate, and malate) were similar between the two conditions (Figure 4.6).

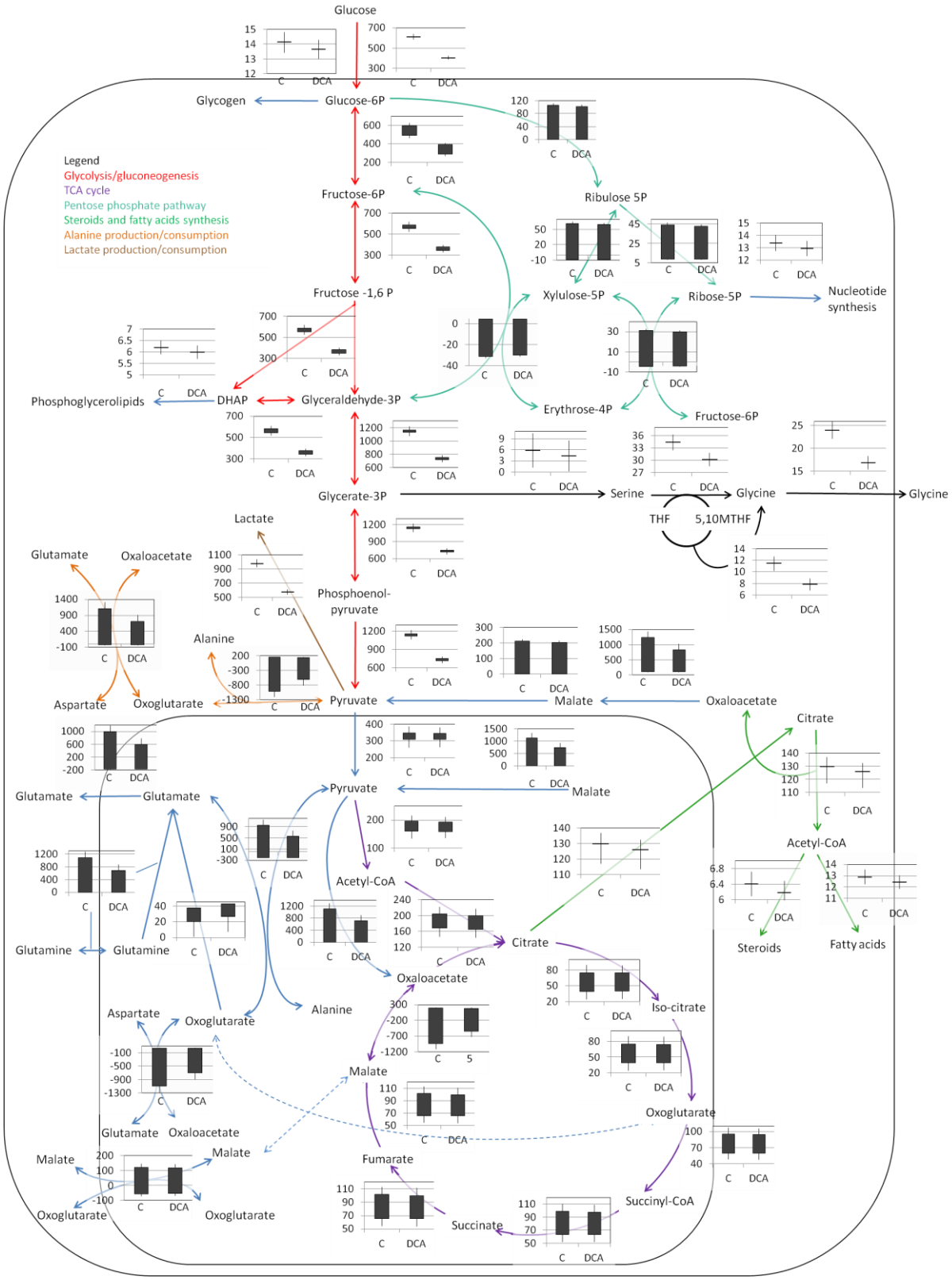

Figure 4.5: Metabolic flux analysis of CHO-XL99 cultures with 5 mM DCA and control cultures during exponential growth. Intracellular fluxes were estimated using metabolic flux analysis. Rates are shown as solid bars with 95% confidence intervals shown as vertical lines. While glycolytic fluxes, fluxes through lactate dehydrogenase and one carbon metabolism reaction were significantly lower in cultures with 5 mM DCA (DCA) compared to control cultures (C); fluxes through the TCA cycle, pentose phosphate pathway, and fatty acid and steroid production pathways were very similar. Rates are in µM/(gDW*h). THF = Tetrahydrofolate, 5,10MTHF = 5,10 Methylenetetrahydrofolate.

ATP production was calculated using the estimated optimum fluxes. ATP production via the TCA cycle was similar in both conditions. 1284 µmol/(gDW*h) and 1256 µmol/(gDW*h) for control and DCA cultures respectively, which is consistent with the unchanged OUR (Table 4.4). However, the amount of ATP generated in glycolysis is about 35% lower in DCA cultures, 1155 µM/(gDW*h) and 741 µM/(gDW*h) for control and DCA cultures, respectively. Accordingly, cultures with DCA produced 18% less ATP overall, 2440 µmol/(gDW*h) for control cultures and 1997 µmol/(gDW*h) for DCA cultures, despite having similar growth rates and cell specific productivity.

ATP concentration was lower in DCA cultures, however the adenylate energy charge (Atkinson & Walton 1967) was similar for control and DCA cultures with 0.91 ± 0.03 and 0.92 ± 0.01, respectively, indicating no lack of energy in either condition (Figure 4.6). Other nucleotides and nucleotide sugars were also elevated. $NADP^+$ concentrations were similar, while NAD^+ concentration was slightly reduced in DCA cultures (Figure 4.6). The latter may be attributed to reduced LDH activity in DCA cultures.

Similar to MFA, glucose, lactate, amino acids, ammonia measurements and Ab2 concentration data were used for B-DMFA (Figure 4.7). However, instead of cell number, cell volume was used as the cell diameter increased during the cultivation in both cultures. Since OUR was only measured once during the exponential growth, it was not used and the measurement set had only one degree of freedom (Quek et al. 2010). Therefore, the calculated residual error represents the consistency of the nitrogen balance among the measurements. The number of knots in control culture was two while three knots were necessary in DCA cultures. Data before 50 hours is not shown as the 95% CIs were very large due to low cell density increasing the error. However, MFA can be used during that period to estimate fluxes as steady state can be assumed during exponential growth.

The B-splines were mostly able to accurately trace the measured concentrations (Appendix Figure A1). The only difference was observed in stationary growth phase of 5 mM DCA cultures where the fitted biomass was lower than the measured values, meaning that more cells were generated than possible according to the nutrients consumed. This can be due to measurement errors of VCD at high cell densities, also indicated by the spreading of the measurements. Alternatively, another compound which was not measured was used as a nutrient by the cells.

Correlating with results from MFA, DCA cultures have a reduced flux in lactate production from pyruvate compared to control cultures. In control cultures, lactate production decreased over time for the whole cultivation period; while in DCA cultures, lactate production was constantly low after 150 hours when the cells entered stationary phase

which correlates with the reduced lactate production rate after day six (Figure 4.2). The fluxes from serine to glycine and glycolytic fluxes were also lower in DCA cultures, although the 95% CI overlap and the difference is only present until ~120 hours, when control cultures enter stationary phase. Interestingly, in both conditions TCA cycle fluxes were constant and similar, indicating a constant TCA cycle activity in 5 mM DCA and control cultures over the complete cultivation period.

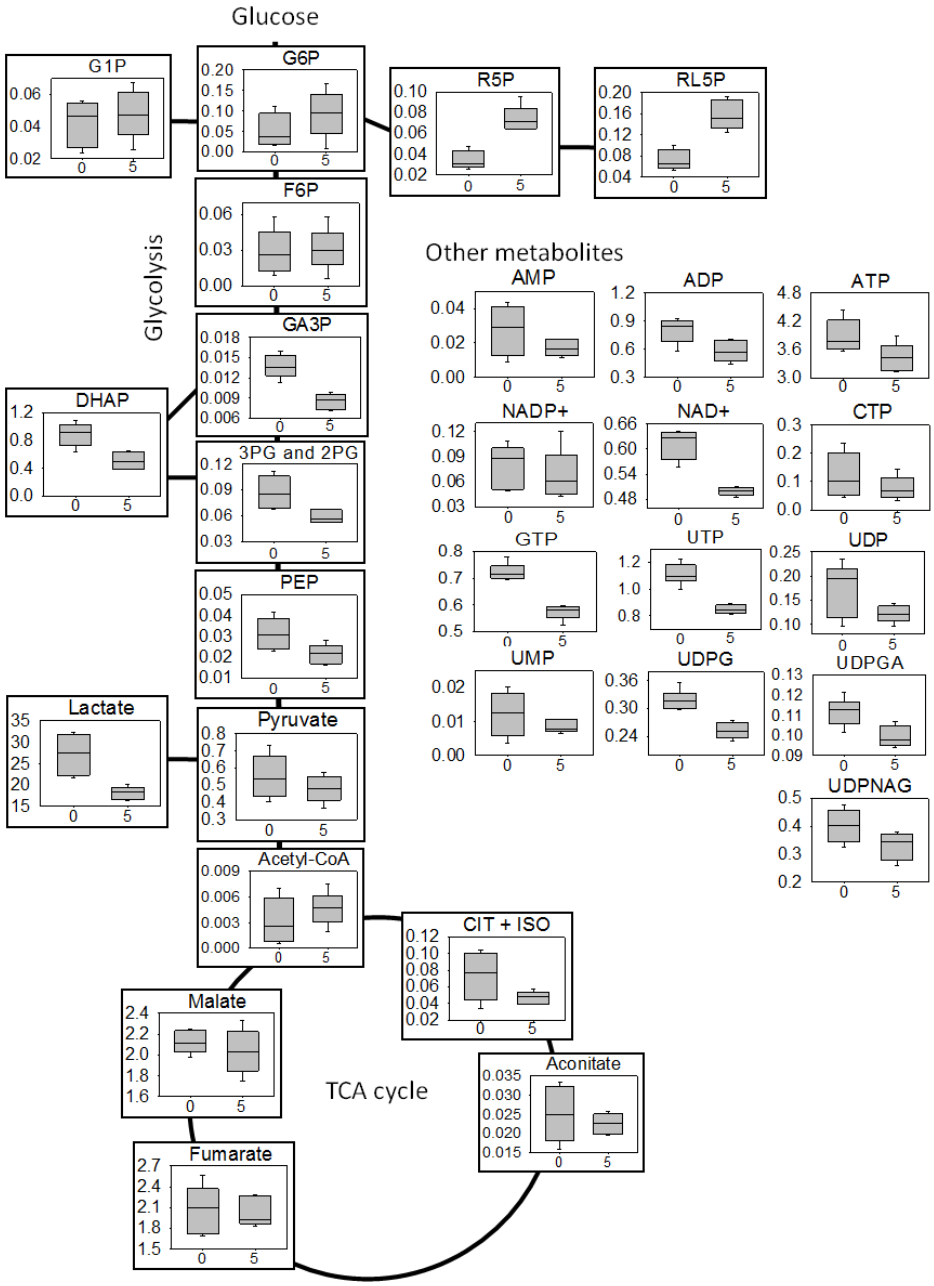

Figure 4.6: Comparison of intracellular metabolite concentrations. Concentrations are in fmol/cell. N=5 for DCA cultures, n=6 for control cultures. 3PG and 2PG = 3-phosphoglycerate and 2-phosphoglycerate, CIT + ISO = citrate and isocitrate, DHAP = dihydroxyacetone phosphate, F6P = fructose 6-phosphate, G1P = glucose 1-phosphate, G6P = glucose 6-phosphate, GA3P = glyceraldehyde 3-phosphate, PEP = phosphoenolpyruvate, PYR = pyruvate, R5P = ribose 5-phosphate, PL5P = ribulose 5-phosphate, UDPG = UDP-glucose, UDPGA = UDP-glucuronic acid, UDPNAG = UDP N-acetylglucosamine, 0 = control, 5 = 5 mM DCA.

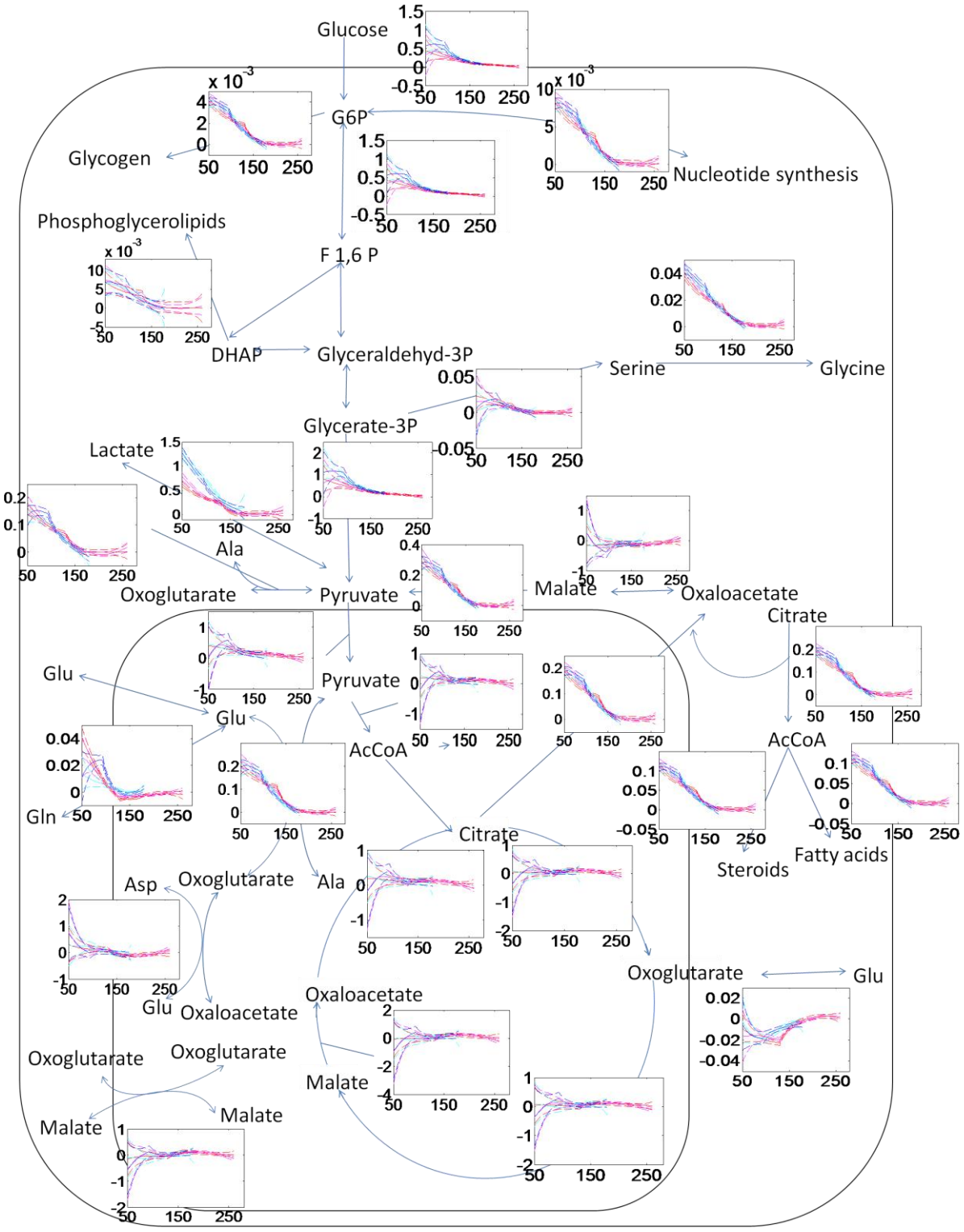

Figure 4.7: Intracellular fluxes over time for CHO-XL99 with 5mM DCA and control cultures. Fluxes are shown in [mM/(gDW*h)] and time scale is in hours. The estimated fluxes from 50 hours until 180 hours for control cultures and until 260 hours for DCA cultures are shown. The CHO-XL99 control cultures are shown in cyan and blue and the 5 mM DCA cultures are in pink and red. The calculated fluxes are shown as solid lines and the 95% confidence interval are shown as dashed lines. While most of the fluxes overlap, a difference can be observed for conversion of pyruvate to lactate and serine to glycine until ~120 hours. During that time, glycolytic fluxes of DCA cultures are also slightly lower however 95% CI overlap.

4.5. Discussion

4.5.1. DCA improves culture performance without affecting productivity and product quality

Cultured mammalian cells, such as CHO cells, consume glucose and glutamine beyond their stoichiometric needs and produce large amounts of waste products, such as lactate and ammonia (Altamirano et al. 2000; DeBerardinis et al. 2007; Warburg 1956). Lactate negatively impacts cell growth as well as antibody production and quality (Lao & Toth 1997; Ozturk et al. 1992; Cruz et al. 2000; Li, J et al. 2012; Pacis et al. 2011). In this study, we investigated the effects of a DCA-mediated increase of PDC activity on culture performance, cell metabolism as well as antibody production and antibody quality in a CHO cell line.

DCA inhibits PDK and thereby indirectly activates PDC. DCA reduced PDC phosphorylation in CHO-XL99 cells and cells were unable to degrade DCA ensuring exposure of the cells to a constant DCA concentration throughout the cultivation (Figure 4.1). PDC phosphorylation and lactate production were reduced in a dose-dependent manner, while cell growth was only affected at concentrations above 5 mM DCA, which was used in subsequent studies.

In all bioreactor fermentations, aerobic glycolysis was reduced and the lactate to glucose yield was about 7.4% lower in DCA cultures (Figure 4.2). DCA increased peak viable cell density, culture duration and final antibody titer. The largest effect was observed in fed-batch plus glucose cultures in which culture duration was extended by three days and final antibody titer doubled.

Culture conditions can impact productivity and antibody quality (Lao & Toth 1997; Li, J et al. 2012; Lim et al. 2010; Pacis et al. 2011). The cell specific productivity during exponential growth was the same in control and DCA cultures with 8.81 ± 0.05 pg/(cell*day) ($p > 0.05$, t-test). The differences seen between the two conditions regarding antibody quality were minor and within expected run-to-run variability (Table 4.3). We observed a small decrease in monomers, a slight reduction in basic charge variants and no change in glycan pattern (Table 4.3). In particular, no increase was observed in the Man5 fraction, a fraction that is readily cleared in the body (Goetze et al. 2011) and has previously been reported to increase in high osmolality conditions (Pacis et al. 2011). Reduced aerobic glycolysis induced by DCA does not affect cell specific productivity or antibody quality in CHO-XL99 cells.

4.5.2. Lactate inhibition mechanism on cell growth

Using fed batch, we demonstrated that the benefit of DCA is not merely to prevent depletion of glucose and amino acids. Indeed, the greatest improvement was observed in the fed-batch plus glucose culture. In both DCA and control cultures, the reduction of growth rate was observed around 90 mM lactate concentration (Figure 4.3), which is higher than previously reported growth inhibitory lactate concentrations (Lao & Toth 1997; Ozturk, Riley & Palsson 1992). Deliberately feeding sodium lactate, we confirmed that 90 mM lactate inhibits cell growth (Figure 4.4A). Sodium lactate was fed at a rate (40 mM/day) just below the maximum rate of lactate production observed in the culture, in order to prevent stress responses related to the rate of change (Newland et al. 1994).
Growth inhibition may be a direct effect of lactate itself or a result of the increased osmolality due to the lactic acid as well as the addition of base to neutralize the produced lactate (Cruz et al. 2000; Irani et al. 1999; Langheinrich & Nienow 1999). Feeding sodium lactate has the same effect on lactate and osmolality as cells producing lactic acid, which is neutralized by sodium bicarbonate addition. Feeding NaCl, we can separate the two effects and the Na^+ concentration is a surrogate measure for the culture osmolality. Deliberately feeding NaCl at 30 mM/day, growth inhibition commenced at about 180 mM Na^+ concentration with complete arrest around 220 mM Na^+ before onset of cell death (Figure 4.4B). These numbers are similar to those observed in the sodium lactate feeding experiment (Figure 4.4A), while the final lactate concentration was only 49 mM, about half observed in sodium lactate feeding experiments. It appears that high osmolality rather than lactate *per se* is the cause of growth inhibition and arrest. As DCA reduces lactate production and associated base addition, it delays growth inhibiting osmolality levels and increased antibody titer is a direct result of the extended cultures.

4.5.3. Warburg revisited

DCA reduces the production of lactate under aerobic conditions and may therefore provide insights into the Warburg effect. SWATH proteomics revealed only few differentially expressed proteins (20 out 2016 identified proteins) and none in central carbon metabolism. This indicates that at 5 mM, where DCA does not affect growth, both DCA and follow-on effects are at a post-translational level.
PFK is considered the major regulatory glycolytic enzyme (Schöneberg et al. 2013) and our data are consistent with control at the PFK node. Intracellular concentrations of

glycolytic intermediates before PFK were similar or slightly higher, while concentrations of glycolytic intermediates downstream of PFK were significantly lower in DCA treated cultures (Figure 4.6). Reduced PFK activity causes an accumulation of fructose 6-phosphate and glucose 6-phosphate, which inhibits hexokinase and reduces glucose assimilation.

Inhibition of PFK is normally attributed to high ATP and citrate levels reducing PFK activity when cells contain sufficient storage of ATP and oxidisable substrates (Costa Leite et al. 2007; Marinho-Carvalho et al. 2009; Zancan et al. 2007; Zancan et al. 2008). However, the ATP and citrate levels were lower under DCA conditions and there was no change the adenylate energy charge (Figure 4.6). Arguably, control is very tight and metabolomics is not sensitive enough to pick up the subtle concentration changes required for control. However, even at the most basic level the regulatory logic does not work; there is no evidence of increased PDC flux leading to more pyruvate through the TCA cycle (Figure 4.5) nor is there an increase in oxidative metabolism as measured by OUR (Table 4.4). The molecular link between de-repressed PDC and reduced glycolytic flux remains to be resolved.

The data does highlight that energy metabolism is inefficient under normal conditions. Without increasing oxidative metabolism, DCA caused a 35% reduction in glucose uptake, a 40% reduction in lactate production, a 30% reduction in glycine production and an 18% reduction in ATP production all without affecting adenylate energy charge, growth rate, or productivity. It is possible that the impact of DCA on cell growth at concentration greater than 5 mM (Figure 4.1) represents the limit of reduction possible given that aerobic metabolism apparently does not increase.

4.6. Conclusions

Lactate metabolism is one of the most important characteristics of industrial mammalian cell culture and due to its adverse effects on cell culture performance and productivity, reducing lactate production is a major focus in cell line and process development. Decreasing PDK activity using DCA is an easy and simple approach to increase PDC activity and thereby reduce aerobic glycolysis and decrease lactate production in an industrial relevant setting. Reduction in aerobic glycolysis had positive effects on cell culture performance and final antibody titer, while cell specific productivity and antibody quality were unaffected. The increase in final antibody titer in DCA cultures was the result of higher cell density and longer cultivation periods. DCA extended the culture duration by

reducing the lactate production rate, thereby the growth inhibiting osmolality level was reached later in DCA cultures. Additionally, the data demonstrate that the DCA concentration used here decreased glycolytic fluxes while the TCA cycle activity was unaffected and DCA mainly acted on a post-translational level.

Chapter 5

Characterization of Increased Pyruvate Dehydrogenase Complex Activity Induced by Dichloroacetate in HEK293 Cells at a Cellular System Level

Co-authors: Lake-Ee Quek, Peter Gray and Lars K. Nielsen

5.1. Abstract

Aerobic glycolysis, also known as the Warburg effect, is a metabolic phenotype characterized by cells preferring glycolysis and conversion of pyruvate to lactate over oxidative phosphorylation despite the presence of oxygen. This is observed not only in many cancer cells but also in other rapidly proliferating cells such as cell lines used as production hosts in industrial applications. Pyruvate dehydrogenase complex (PDC) plays a crucial role because it controls how much pyruvate derived from glycolysis enters the tricarboxylic acid cycle. PDC activity is inhibited by the enzyme pyruvate dehydrogenase kinase (PDK). Dichloroacetate is a known PDK inhibitor and thereby indirectly increases PDC activity. Here we analyzed the effects of increased PDC activity induced by DCA using multiple omics technologies. Human embryonic kidney 293 cells were cultivated with different DCA concentrations, 5mM and 10mM, and data for growth profile, nutrient consumption, metabolite production, gene expression, protein abundance and intracellular metabolite concentrations were obtained and metabolic flux analysis was performed. We observed a DCA concentration dependent reduction in aerobic glycolysis characterized by decreased glucose consumption and lactate production. An effect on cell growth was only observed at 10mM DCA. Further analysis revealed that the reduced aerobic glycolysis was mainly caused by post-translational effects of DCA. Additionally, an increased asparagine synthetase activity and increased mitochondrial one-carbon metabolism were observed. Metabolic flux analysis showed an increased TCA cycle activity in 10 mM DCA cultures and various genes linked to cellular stress were upregulated.

5.2. Introduction

In mammalian cells energy in the form of ATP is mainly derived from two sources, glycolysis in which glucose is metabolized to pyruvate and the tricarboxylic acid (TCA) cycle which converts pyruvate to CO_2. Under aerobic conditions normal cells use both glycolysis and TCA cycle for ATP generation. Under anaerobic conditions cells only use glycolysis and convert pyruvate to lactate as oxygen, the final electron acceptor in the electron transport chain, is not available. This is usually characterized by an elevated glycolytic rate resulting in increased glucose consumption and lactate production. Over 80 years ago, Warburg observed that even under aerobic conditions cancer cells prefer glycolysis and lactate formation over oxidative phosphorylation (OXPHOS) (Warburg, Wind & Negelein 1927). Aerobic glycolysis seems counterproductive because of its lower

ATP yield per glucose molecule compared to cells using OXPHOS however it enables hypoxic tumor cells to generate ATP without oxygen consumption. In order to counteract the lower ATP yield, cells often have a higher glycolytic rate during aerobic glycolysis. Additionally, a high glycolytic rate may allow cells to direct glycolytic intermediates into other biosynthetic pathways needed to assemble new cells (Vander Heiden, Cantley & Thompson 2009). Aerobic glycolysis is not only observed in many cancer cells but also in other rapid proliferating cells such as cell lines used as production hosts in industrial applications and cells of embryonic tissue, suggesting that similar energetic and biosynthetic demands play an important role (Hanahan & Weinberg 2011; Papandreou, Goliasova & Denko 2011).

Whether pyruvate derived from glycolysis enters the TCA cycle in the mitochondria or is available for lactate production in the cytosol is largely determined by the activity of pyruvate dehydrogenase complex (PDC). PDC is a key enzyme complex distributed heterogeneously within the mitochondrial matrix (Margineantu et al. 2002). It catalyzes the irreversible oxidation of pyruvate to acetyl-CoA and under aerobic conditions is rate-limiting for the elimination of pyruvate as well as alanine and lactate which are in equilibrium with pyruvate (Stacpoole et al. 1998). Hence, PDC deficiency or inhibition may lead to lactate accumulation and mitochondrial energy failure. PDC also indirectly regulates the ATP yield from glucose, controls the amount of malonyl-CoA available for fatty acid synthesis and plays an important role in the process of fuel selection in connection with the glucose fatty-acid cycle (Hue & Taegtmeyer 2009; Randle et al. 1963; Sugden, MC & Holness 2006).

PDC deficiency has been linked to various diseases and has been studied as a therapeutic target for cancer (Archer et al. 2008) and other age-related diseases such as glucose intolerance (Stacpoole, Moore & Kornhauser 1978), heart failure (Bersin & Stacpoole 1997) and neurodegeneration (Stacpoole 1997) (reviewed in (Stacpoole 2012)). A decline of PDC activity with increasing age was observed in several tissues (Gurd et al. 2008; Zhou, Q et al. 2009). This may contribute to development of type 2 diabetes mellitus as insulin secretion requires a coupled PDC-OXPHOS system and increasing PDC activity in patients had a glucose and lactate lowering effect (Stacpoole, Moore & Kornhauser 1978). In brain, an age-related decrease in glucose oxidation and oxygen consumption was observed (Kalpouzos et al. 2009; Martin et al. 1991) together with an increase of aerobic glycolysis and ketone body oxidation (Ross et al. 2010; Yao et al. 2010). Many neurodegenerative diseases, particularly Alzheimer's disease, are associated with abnormal brain oxidative metabolism and data implicate a reduced PDC activity and up-

regulation of aerobic glycolysis (reviewed in (Coskun et al. 2012; Green, Galluzzi & Kroemer 2011)). Furthermore, despite the differences between many cancers, they mostly rely on aerobic glycolysis for energy generation (Gatenby & Gillies 2004).

PDC activity is regulated by reversible phosphorylation of three serine residues by PDC kinases (PDKs) and PDC phosphatases (PDPs) (Sale & Randle 1981; Teague et al. 1979; Yeaman et al. 1978). Four PDK and two PDP isoforms were identified in humans and rodents with different tissue specific distributions (Bowker-Kinley et al. 1998; Linn, Pettit & Reed 1969; Popov, Hawes & Harris 1997). Acetyl-CoA and NADH, both end-products of the PDC reaction, as well as increase in intramitochondrial ATP increase PDK activity, resulting in phosphorylation and inhibition of PDC (reviewed in (Patel & Korotchkina 2006; Sugden, MC & Holness 2006). Inhibitors of PDK are pyruvate as well as dichloroacetate (DCA) which is a halogenated xenobiotic structurally similar to pyruvate (Li, J, Kato & Chuang 2009; Roche & Hiromasa 2007; Whitehouse, Cooper & Randle 1974). DCA occupies the pyruvate binding site and inhibits PDK thereby indirectly increasing PDC activity redirecting pyruvate towards the TCA cycle (Roche et al. 2001; Stacpoole et al. 1998). DCA has been explored for decades as a lactate lowering drug in treatment of various human diseases such as acquired or congenital lactic acidosis, diabetes, hypoxic pulmonary hypertension and congestive heart failure (Michelakis et al. 2002; Stacpoole, Moore & Kornhauser 1978; Stacpoole, Nagaraja & Hutson 2003).

In 2007, Bonnet et al. reported that DCA specifically induces apoptosis in cancer cells and since then numerous studies evaluated DCA's potential as an anti-cancer drug (reviewed in (Papandreou, Goliasova & Denko 2011)) and proof-of-concept was demonstrated in patients and a phase I trial was conducted (Dunbar et al. 2013; Flavin 2010; Michelakis et al. 2010). Bonnet et al. attributed the effect to the restoration of a normal mitochondrial membrane potential ($\Delta\Psi m$) in previously hyperpolarized mitochondria leading to increased H_2O_2 production, efflux of mitochondrial pro-apoptotic factors and activation of plasma membrane Kv1.5 potassium transporters, all together inducing apoptosis (Bonnet et al. 2007). However, a later study found that DCA has low activity and is not selective for cancer cells, but rather depolarizes mitochondria of both normal and cancer cells without induction of apoptosis (Stockwin et al. 2010). Growth suppression was greater in cells with defects in the mitochondrial electron transport chain (ETC) and DCA displayed synergistic effects with agents known to target mitochondria or interfere with glucose metabolism. They concluded that in cells with a defective ETC, DCA treatment results in "metabolic crisis" whereby cells are forced to generate ATP using a deficient pathway, resulting in a failure to meet metabolic demands. Interestingly, in some studies DCA reduces lactate

production without an increase in oxygen consumption, an indicator for TCA cycle activity. Oxygen consumption in response to DCA appears to depend on other factors such as cell line and HIF1α activity (Cairns et al. 2007; Niewisch et al. 2012).

In this study, a comprehensive evaluation of the metabolic effects of DCA was performed. Human embryonic kidney 293 (HEK293) cells were cultivated with different concentrations of DCA and a multi-omics approach was used to characterize the effects of increased PDC activity on gene expression, protein abundance, intracellular metabolite concentrations and metabolic fluxes.

5.3. Material and methods

5.3.1. Cell culture and extracellular metabolite analysis

HEK293F cells (Invitrogen) were cultivated in CD 293 medium (Invitrogen) supplemented with 4.5 mM glutamine (Invitrogen), 50 µg/ml dextran sulfate (Mw=5000Da, Sigma-Aldrich) and sodium dichloroacetate (DCA) (Sigma-Aldrich) at indicated concentrations. Cells were cultivated in vented shake flasks (Corning) with a working volume of 200 ml at 37°C, 5% CO_2, and 130 rpm. Single shake flask experiments were performed to analyze effects on growth, lactate production and PDC phosphorylation as well as DCA stability in HEK293F culture. Duplicate shake flasks experiments were performed for 14 days to obtain growth curve and extracellular metabolite concentration data. Samples were collected twice daily during the first seven days and at least once a day for the remaining culture period. Cell number and viability were measured using a CedeX cell counter (Roche Innovatis AG). Ammonia concentrations were determined using a Nova Bioprofiler FLEX (Nova Biomedical). Glucose, lactate and extracellular amino acid concentrations in culture supernatant were determined using HPLC as described in Dietmair et al. (Dietmair, Timmins, Gray, Nielsen & Kromer 2010). Additional shake flask cultures were cultivated in triplicates for 3 days and samples for transcriptomics, protein abundance and intracellular metabolite analysis were obtained.

5.3.2. Western blot

HEK293F cells (Invitrogen) were cultivated for 24 hours with different DCA concentrations (0 – 15 mM DCA). Approximately, 2 x 10^7 cells were collected, washed with 0.9% sodium chloride and lysed in RIPA buffer (0.1% SDS, 1% Triton-X100, 5 mM

ethylenediaminetetraacetic acid, 0.5% sodium deoxycholate, 150 mM NaCl, 50 mM Tris-HCl, 2 mM dithiothreitol, supplemented with 1ug/mL leupeptin (Roche), 1ug/mL aprotinin (Roche), 1 mM sodium orthovanadate, 10 mM sodium fluoride). Cell lysates were incubated for 60 min on ice followed by centrifugation at 16,000 rcf, 4°C for 10 min. Protein concentration of the supernatant was determined using a 2D Quant Kit (GE Healthcare). Cell extracts equivalent to 10 µg of protein were run on a 4-12% SDS-polyacrylamide gel and transferred to nitrocellulose membranes by standard procedures. Membranes were blocked with 5% nonfat milk in PBS/Tween for 1 hour followed by incubation with anti-PDC E1-α subunit (phospho S293) (abcam) and anti-β-tubulin (Cell Signalling Technology) antibodies for 2 hours at RT. Immunoreactive bands were visualized using horseradish peroxidase-conjugated anti-rabbit antibody (Life Technologies) and Amersham ECL Western Blotting Detection Reagents (GE Healthcare Bio-Sciences). Densitometry was performed using a BIORAD ChemiDoc MP Imaging System (Bio-Rad Laboratories) and Image Lab 4.0.1 software (Bio-Rad Laboratories).

5.3.3. DCA concentration in culture

HEK293F cells (Invitrogen) were cultivated in different DCA concentrations ranging from 0 – 20 mM DCA. Every two days, a sample of 500 µl was collected from the culture, centrifuged at 500 rcf and supernatants were frozen and stored at -20°C until further processing. An Agilent 1200 HPLC system (Agilent Technologies) equipped with a Kinetex C18-XB column (100 Å, 2.6 µm, 100 × 2.1 mm, Phenomenex) and a diode array detector was used to measure DCA concentrations. The column temperature was set at 30°C and the flow rate was 0.2 ml/min. Mobile phase A was of 10 mM tetrabutylammonium bisulfate in water and mobile phase B consisted of 100% acetonitrile far UV. The gradient began with 5% mobile phase B and was increased linear to 30% in 3 min followed by a hold at 30% for 5 min. The concentration of mobile phase B was then increased linear from 30% to 60% in 1 min followed by a hold of 60% mobile phase B for 5 min. Afterwards, the gradient was reversed from 60% to 5% mobile phase B in 1 min, followed by a hold at 5% mobile phase B for 5 min.

5.3.4. Transcriptomics analysis

5.3.4.1. Sample preparation

Cells were collected after three days and centrifuged at 200 rcf for 3 min. The supernatant was discarded and the pellet frozen on dry ice and stored at -80°C Total RNA from collected cells was extracted using an RNA Mini Kit (Qiagen) according to manufacturer's instructions including on-column DNA digestion using an RNase-Free DNase Set (Qiagen). RNA amount and purity were determined using an Agilent Bioanalyzer 2100 (Agilent Technologies). One sample per shake flask (n = 3 for each DCA concentration) was submitted to AGRF, Melbourne, Australia for gene expression analysis using Illumina HT12v4 chips (Illumina).

5.3.4.2. Data analysis

Background subtracted data from GenomeStudio was analyzed using lumi (Du, Kibbe & Lin 2008), a package for processing Illumina data in R (R Core Team 2012). A variance-stabilizing transformation and quantile normalization were performed (Lin, SM et al. 2008). Unexpressed genes were removed to reduce false positives and a nucleotide universal identifier (nuID) annotation system was used (Du, Kibbe & Lin 2007). Genes with a false discovery rate adjusted p-value of less than 0.01 were considered differentially expressed. The differentially expressed genes were analyzed manually and using HumanCyc Omics Viewer (http://humancyc.org/).

5.3.5. Targeted proteomics analysis

5.3.5.1. Sample preparation

Cells were collected after three days and centrifuged at 200 rcf for 3 min, washed with 0.9% sodium chloride and cell pellets stored at -80°C. Cell pellets were lysed in 8 M urea/50 mM ammonium bicarbonate (AMBIC) supplemented with 1 µg/ml aprotinin (Roche), 2.5 µg/ml leupeptin (Roche), 5 mM sodium orthovanadate, and 10 mM sodium fluoride. Cells were disrupted using a 22G needle and sonicated three times for 1 min. RNaseA (Thermo Fisher Scientific Inc.) and DNaseI (Thermo Fisher Scientific Inc.) were added to the samples according to manufacturer's instructions. After 15 min incubation at RT, samples were centrifuged at 16,000 rcf for 10 min at 0°C. Protein concentration of the

supernatant was determined using a 2D Quant kit (GE Healthcare Life Sciences) according to manufacturer's instructions. Dithiothreitol was added to 5 mM and samples were incubated at RT for 45 min, followed by addition of iodoacetamide to 25mM and incubation for 30 min at RT in the dark. Samples were diluted with 7 volumes of 50 mM AMBIC to obtain a final concentration of < 1M urea. Trypsin (Trypsin Gold, Promega) was added in a 1:50 enzyme:protein ratio and samples were incubated overnight at 37°C. The next morning samples were centrifuged at 16,000 rcf, 0°C for 10 min and 5% trifluoroacetic acid (TFA) was added to the sample until pH was below pH 4. Samples were desalted using Sep-Pak cartridges (Waters) equilibrated first with 100% acetonitrile (ACN), then 70% ACN/0.1%TFA, and finally 0.1% TFA. Equal volume of 0.1% TFA was added to the samples before loading them onto the column. The column was washed twice with 0.1% TFA and proteins were eluted with 70%ACN/0.1%TFA. Residual acetonitrile was removed by vacuum centrifugation (Eppendorf Group) and the sample was resuspended in 0.1% TFA and stored at -80°C until analysis.

5.3.5.2. HPLC-MS/MS

Mass spectrometry was performed as described elsewhere (Chang, RYK et al. 2014) with modified HPLC flow rate and gradient profile. Briefly, peptide samples were analyzed using an Agilent 1100/1200 HPLC system (Agilent Technologies) coupled to an ABSciex QTRAP 5500 mass spectrometer (ABSciex). Chromatographic separation was performed on an Agilent ZORBAX 300SB-C18, 5µm, 150 x 0.3 mm column (Agilent Technologies). Mobile phase A consisted of 5% ACN/0.1% formic acid (FA), mobile phase B was 99.9% ACN/0.1% FA (v/v) and the flow rate was set to 10 µl/min. The gradient elution profile was 10% buffer B 0-5 min, 10-40% buffer B 5-75 min, 40-90% buffer B 75-77 min, 90% buffer B 77-83 min, 90-10% buffer B 83-85 min, 10% buffer B 85-90 min.

The Agilent QTRAP 5500 was equipped with a TurboSpray ion source and set to Multiple Reaction Monitoring (MRM) scan type at unit resolution and peptide ionization was performed in positive mode. Skyline software (MacCross Lab Software) and SRM Atlas (http://www.srmatlas.org/) were used to build MRM methods and a list of analyzed proteins with peptide, precursor ion, product ion, and fragmentation can be found in Appendix Table F1.

5.3.5.3. Data analysis

Chromatograms were analyzed using Skyline software (MacCross Lab Software). All peaks were manually inspected and peak areas were used to calculate differences in relative protein abundance. The protein tubulin beta chain (UniProt ID P07437) was used as an internal standard as its abundance was confirmed to be constant across all three conditions using bovine alpha-S1-casein (Sigma-Aldrich) spiked samples. Relative protein abundance data was then statistically analyzed using the limma package (Smyth 2005) in R (R Core Team 2013).

5.3.6. Intracellular metabolite analysis

Cell suspension was collected after three days during exponential growth phase. Sample preparation and HPLC-MS/MS analysis to analyze glycolytic, TCA cycle and pentose phosphate pathway metabolites was performed according to Dietmair et al. 2010 (Dietmair, Timmins, Gray, Nielsen & Kromer 2010)

5.3.7. Metabolic flux analysis

A detailed description of the metabolic flux analysis is provided in Appendix C. Briefly, exchange rates were estimated using a yield approach over the exponential phase (Quek et al. 2010). The metabolic model used is a reduced version of the human genome scale model Recon 1 (Duarte et al. 2007), generated as described in (Quek & Nielsen 2008b). For consistency checking and flux variability analysis constrained weighted quadratic programming was used (Antoniewicz, Kelleher & Stephanopoulos 2006). A Monte Carlo approach was used to propagate errors in primary data (growth data and extracellular nutrient and metabolite data) into the calculated cell-specific rates (Goudar et al. 2009; Quek et al. 2014). The average dry weight was measured to be 515 pg/cell. Estimated fluxes were used for estimation of ATP production (Martínez, VS et al. 2013).

5.4. Results

5.4.1. DCA affects cell growth, lactate production and PDC phosphorylation and is stable in HEK293F cell culture

Shake flask experiments were carried out to investigate the effects of different DCA concentrations on cell growth, lactate production, and PDC phosphorylation (Figure 5.1). Since DCA can be degraded into glyoxylate by glutathione S-transferase ζ1 (Lantum et al. 2003; Li, WJ et al. 2011), the stability of DCA in HEK293F cell culture was analyzed first (Figure 5.1C). Over a culture period of twelve days DCA concentration in all cultures decreased by less than 5% of its initial concentration suggesting than HEK293F cells are unable to degrade DCA significantly and DCA supplementation is not required during the experiments.

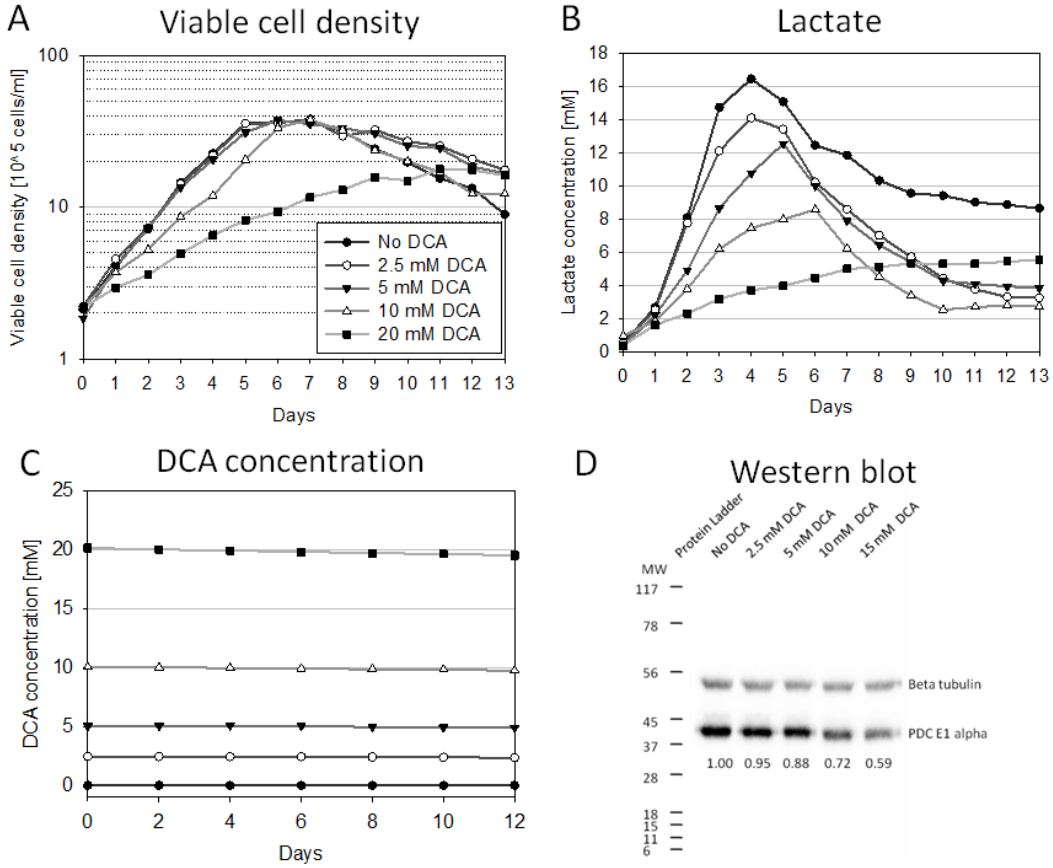

Figure 5.1: Growth curve, lactate concentration, DCA concentration, and Western blot analysis. HEK293F cells were cultured in shake flask with different DCA concentrations. Growth rate was unaffected by DCA up to 5 mM and decreased at higher DCA concentrations (A). Lactate production decreased with increasing DCA concentration during exponential growth (B). DCA concentration decreased less than 5% in HEK293F cell culture over a 12 day culture period (C) and with increasing DCA concentration PDC E1α phosphorylation decreased (D).

Growth during exponential phase was unaffected by DCA concentrations up to 5 mM. At higher DCA concentrations the growth rate decreased. Lactate production decreased with increasing DCA concentration and all cultures except 20 mM DCA culture used lactate as a carbon source later during the culture. Western blot analysis showed that PDC phosphorylation decreased with increasing DCA concentration indicating PDK inhibition and higher PDC activity.

For further experiments 5 mM and 10 mM DCA concentration were chosen to analyze DCA's effects on metabolism and cell growth. At 5 mM a clear metabolic effect is evident without a growth effect, while 10 mM DCA affects both metabolism and cell growth.

5.4.2. DCA reduces lactate production but affects oxidative metabolism only at higher concentrations

HEK293F cells were cultivated in duplicates with 5 mM, 10 mM DCA or no DCA (control) for 14 days and samples were collected twice a day during exponential and stationary growth phase and once a day during death phase. Viable cell density (VCD), viability, glucose and lactate concentrations (Figure 5.2) as well as extracellular amino acid concentrations were measured.

The average growth rates during exponential phase were similar between control and 5 mM DCA cultures, 0.0269 ± 0.0006 h^{-1} and 0.0254 ± 0.0005 h^{-1} for control and 5 mM DCA respectively ($p>0.20$ t-test), while the average growth rate of 10 mM DCA culture was 0.0218 ± 0.0004 h^{-1} and different compared to the control cultures ($p<0.02$ t-test). Viability was above 95% for all cultures until day 5 and viability as well as VCD decreased faster during death phase with increasing DCA concentration.

Glucose consumption as well as lactate production decreased with increasing DCA concentration during exponential growth phase (Figure 5.2 and Table 5.1), with mean glucose consumption rates being about 19% lower in 5 mM DCA cultures and about 23% lower in 10 mM DCA cultures. Similarly, the lactate production rate was lower in DCA cultures, about 27% in 5 mM DCA cultures and about 43% in 10 mM DCA cultures. This led to a decreased lactate to glucose yield with increasing DCA concentration; the ratios were 1.25 ± 0.02, 1.14 ± 0.02, and 0.94 ± 0.02 for control, 5 mM DCA, and 10 mM DCA, respectively. This corresponds to a reduction in lactate to glucose yield of 8.8% at 5 mM DCA and 24.8% at 10 mM DCA. During exponential growth the ammonia concentrations were similar for all DCA concentrations (Figure 5.3). However, due to the lower growth rate of the 10mM DCA cultures the ammonia production rates were higher (Table 5.1).

5.4.2.1. Cell growth and metabolite consumption and production

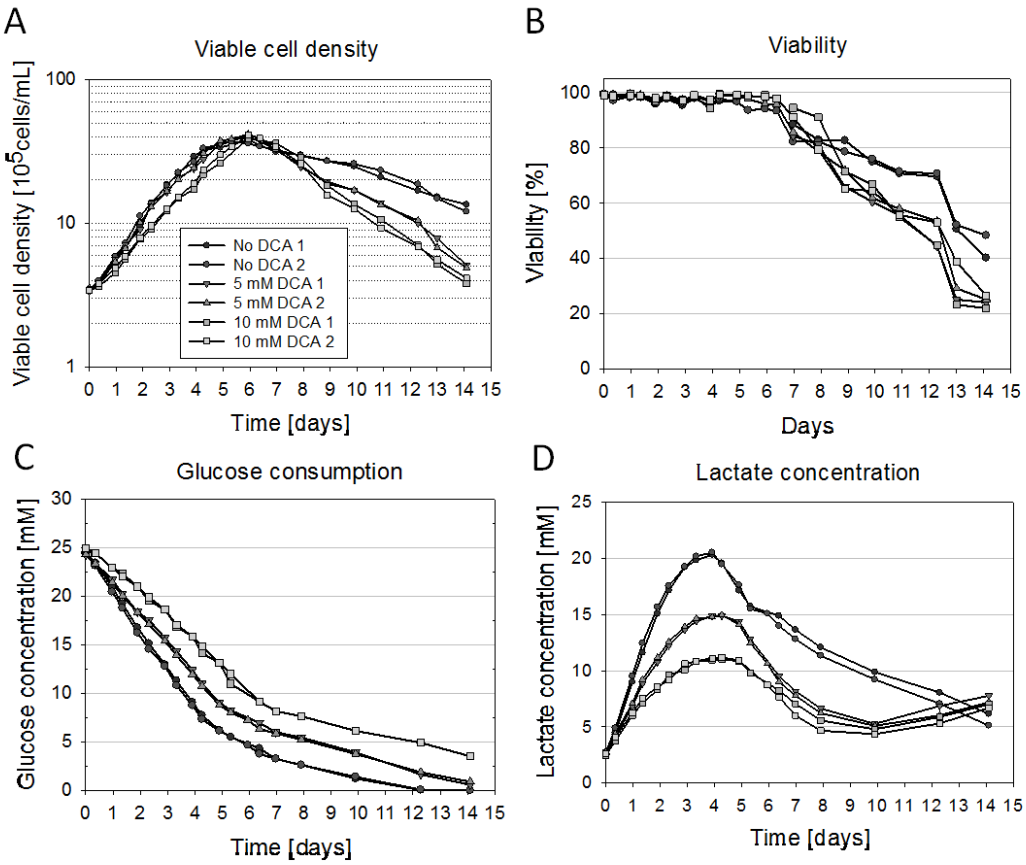

Figure 5.2: Viable cell density, viability, glucose and lactate concentration profiles. Duplicate cultures of HEK293F cells were cultivated with no, 5 mM or 10 mM DCA. DCA reduced glucose consumption (C) and lactate production (D) during exponential growth phase. Growth rate was only affected at 10 mM DCA (A) however viable cell density and viability decreased faster during death phase with increasing DCA concentration (A and B).

Although, several of the amino acid consumption and production rates were significantly different in DCA cultures compared to control cultures, the amino acid consumption pattern was similar with glutamine being the major consumed amino acid followed by serine, leucine, arginine, valine, and isoleucine (Table 5.1).

The amino acid production pattern differed between the three conditions. In control cultures alanine was the major product followed by proline, glutamate, and glycine. In cultures treated with 5 mM DCA the major product was glutamate followed by alanine, glycine, proline, and asparagine and in cultures treated with 10 mM DCA the major product was glutamate followed by glycine, alanine, proline, and asparagine. Major differences were observed for lysine and asparagine. In 10 mM DCA cultures, lysine consumption was more than 50% lower compared to control cells. Asparagine was consumed in control cultures; however it was produced in DCA cultures during exponential growth (Table 5.1).

Control cultures started to produce asparagine after 5 days while 10 mM DCA cultures mostly consumed asparagine after day 4 (Figure 5.3). 5 mM DCA cultures switched between asparagine consumption and production.

Table 5.1: Mean metabolic uptake and production rates during exponential growth. Mean (n = 2) metabolic uptake and production rates of control, 5 mM DCA and 10 mM DCA cultures during exponential growth. Rates are in µM/(gDW*h), growth rate in h^{-1}. Negative rates represent consumption and positive rates production. The asterisks indicate rates which were statistically significantly different ($p<0.05$ t-test) compared to the control cultures. Upregulated amino acid transporter in 10 mM DCA cultures identified in gene expression analysis. SE = standard error, Y = Yield.

Metabolite	**No DCA** Rate ± SE		**5 mM DCA** Rate ± SE		**10 mM DCA** Rate ± SE		**Upregulated transporter in 10 mM DCA**
Glucose	-297	1	-240*	9	-228*	11	
Lactate	373	5	273*	6	213*	5	
$Y_{lactate/glucose}$	1.25	0.02	1.14*	0.02	0.94*	0.02	
NH_4^{+*}	12.74	0.41	13.13	0.54	20.43*	1.37	
Consumed amino acids							
Asp	-4.48	0.12	-4.17	0.07	-4.40	0.04	SLC1A5
Gln	-61.3	0.8	-52.7*	1.4	-62.9	1.6	SLC7A5, SLC3A2, SLC1A5
Ser	-28	0.1	-28.2	0.4	-32.0*	0.9	SLC1A5
Arg	-12.04	0.45	-13.76	1.02	-15.77	0.85	SLC7A5, SLC3A2
Essential amino acids							
Tyr	-3.32	0.05	-2.93	0.14	-2.90*	0.05	SLC7A5, SLC3A2, SLC1A5
His	-2.41	0.09	-2.21	0.18	-1.95	0.17	
Thr	-6.36	0.02	-5.72	0.36	-5.67*	0.07	SLC1A5
Val	-10.17	0.17	-9.46	0.67	-12.02*	0.05	SLC1A5
Met	-3.62	0.16	-3.26	0.10	-3.53	0.30	SLC1A5
Trp	-1.15	0.004	-0.97*	0.001	-1.02	0.04	SLC7A5, SLC3A2, SLC1A5
Phe	-4.46	0.13	-3.56	0.21	-3.85*	0.01	SLC7A5, SLC3A2, SLC1A5
Ile	-8.92	0.28	-9.25	0.57	-10.89	0.38	SLC1A5
Leu	-13.57	0.32	-14.19	1.30	-15.51	0.98	SLC7A5, SLC3A2, SLC1A5
Lys	-7.36	0.28	-6.90	0.25	-3.50*	0.08	
Produced amino acids							
Glu	7.01	0.05	11.7	1.16	14.84*	0.22	
Gly	6.28	0.05	8.28*	0.10	11.91*	0.47	SLC6A9, SLC1A5
Ala	19.21	0.02	10.16*	0.22	10.43*	0.20	SLC1A5
Pro	11.53	0.62	6.89*	0.46	7.26*	0.71	SLC1A5
Consumed or produced amino acid							
Asn	-1.38	0.02	0.79*	0.10	2.99*	0.10	
Growth rate	0.0269	0.0006	0.0254	0.0005	0.0218*	0.0004	

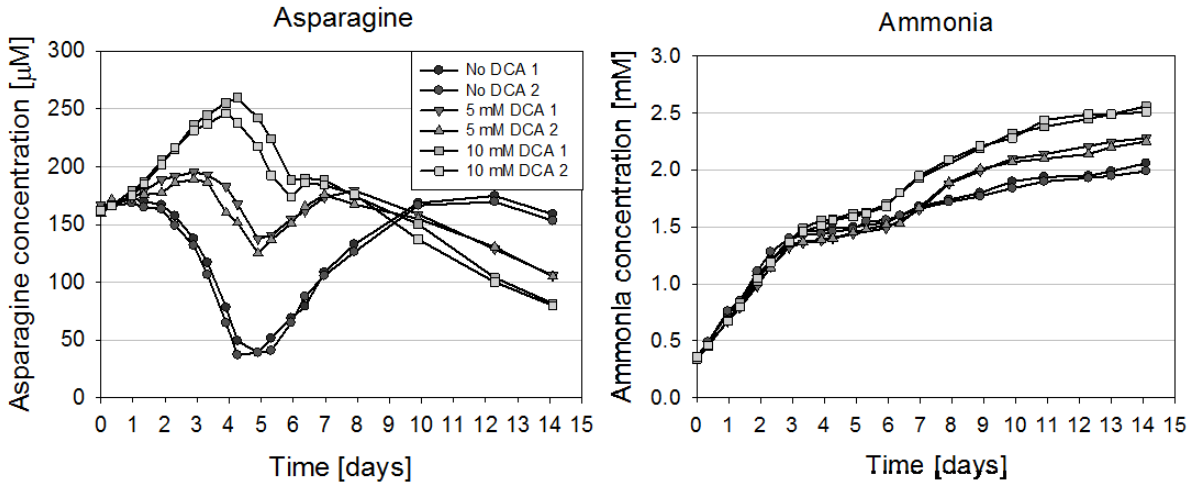

Figure 5.3: Asparagine and ammonia concentration profile in culture supernatant.

5.4.2.2. Differentially up-regulated amino acid transporters in 10 mM DCA cultures

A number of amino acid transporters were identified as significantly upregulated in 10 mM DCA cultures using gene expression analysis (Table 5.2). Together they cover the transport of almost all amino acids (Table 5.1). SLC3A2 is an amino acid transporter and binds to SLC7A5 (also upregulated). Together they are involved in sodium-independent transport of large neutral amino acids (Elorza et al. 2012; Ganapathy, Thangaraju & Prasad 2009). SLC3A2 is also linked to calcium concentrations either by responding to fluctuations in intracellular calcium concentrations or by regulating intracellular calcium levels (Chang, ACM, Jellinek & Reddel 2003; Jiang, Westberg & Andersson 2012; Nance et al. 2012). It was observed that DCA treatment led to lower free cytosolic calcium concentration in A549 cells (Bonnet et al. 2007). SLC1A5 can transport all neutral amino acids and mediates the net uptake of glutamine (Ganapathy, Thangaraju & Prasad 2009). SLC6A9 is a glycine transporter (Kim, KM et al. 1994) and absolute glycine production rate was almost doubled in 10 mM DCA cultures compared to control cultures. Although, amino acid transporters were up-regulated, for some amino acids the absolute amino acid consumption rate was not increased compared to control cultures. However, when metabolic rates are adjusted to growth rate (Appendix E), taking into account the significantly lower growth rate of 10 mM DCA cultures, the amino acid consumption rates of 10 mM DCA cultures agreed with the upregulation of the amino acid transporters suggesting an increased amino acid demand and potentially intracellular amino acid limitations.

Table 5.2: Up-regulated amino acid transporters in 10 mM DCA cultures compared to control cultures.

Transporter	Fold change	Description
SLC7A5	2.2279	Transport of large neutral amino acids such as phenylalanine, tyrosine, leucine, arginine and tryptophan, when associated with SLC3A2.
SLC3A2	2.2083	Transport of large neutral amino acids such as phenylalanine, tyrosine, leucine, arginine and tryptophan. Guiding and targeting of SLC7A5 and LAT2 to the plasma membrane.
SLC1A5	1.9640	Transport of all neutral amino acids, including glutamine, asparagine, and branched-chain and aromatic amino acids, excludes methylated amino acids, anionic amino acids, and cationic amino acids.
SLC6A9	1.7642	Sodium- and chloride-dependent glycine transporter

5.4.2.3. DCA affects several metabolic fluxes in a dose-dependent manner

Intracellular metabolic fluxes were estimated based on the cell specific consumption and production rates during exponential growth (23.25 – 69.5 hours) for all three conditions (n = 2). Although the majority of the flux ranges and 95% confidence intervals (CI) overlapped, several metabolic flux differences have been observed (Figure 5.4). Glucose uptake and glycolytic fluxes were lower in DCA cultures as expected from the reduced glucose consumption. Although, 10 mM DCA cultures consumed less glucose compared to 5 mM DCA cultures (Figure 5.2), 10 mM DCA glucose consumption rate (Table 5.1) and glycolytic fluxes (Figure 5.4) were only slightly lower compared to 5 mM DCA cultures and doubling the DCA concentration did not result in an equivalent decrease in absolute glycolytic fluxes. Fluxes through lactate dehydrogenase decreased with DCA. Fluxes towards biosynthetic precursors (fatty acids, nucleotides, and phosphoglycerolipids) and glycogen were similar between control and 5 mM DCA and lower for 10 mM DCA cultures, correlating with lower growth rate observed in 10 mM DCA cultures. Conversion of pyruvate to acetyl-CoA flux, catalyzed by PDC, was only increased in 10 mM DCA cultures and similar in 5 mM DCA cultures compared to control cultures. Correspondingly, fluxes in TCA cycle only increased in 10 mM DCA cultures indicating that 10 mM DCA cultures but not 5 mM DCA cultures have a more active TCA cycle. Fluxes through the pentose phosphate pathway (PPP) were similar in all three conditions. Glutamine uptake and conversion into glutamate was reduced for 5 mM DCA, however 10 mM DCA cultures had similar fluxes compared to control cultures, suggesting lower glutaminolysis in 5 mM DCA cultures. The fluxes through malate/oxoglutarate transport and conversion of aspartate and oxoglutarate to glutamate and oxaloacetate were increased in 10 mM DCA cultures. The fluxes from aspartate and glutamine to asparagine and glutamate, catalyzed by ASNS, increased with increasing DCA concentration which agrees with the observed

difference in asparagine consumption/production during exponential growth (Table 5.1 and Figure 5.3). Furthermore, glycine transport out of the cell increased with increasing DCA concentration indicating that glycine formation from serine by the one-carbon metabolism is increasing with DCA. The reaction from serine to glycine is catalyzed by the serine hydroxymethyltransferase (SHMT) which has also increased flux with increasing DCA concentrations. The one-carbon metabolism takes place in cytoplasm and mitochondria; however the metabolic model does not distinguish between these two pathways but gives the sum of both pathways. The formation of serine from glycerate 3-phosphate is lower for 10 mM DCA and similar for 5 mM DCA concentration compared to control cultures; while serine transport into the cell is increased in 10 mM cultures indicating that increased serine amount needed in the one-carbon metabolism is not supplied from glycolytic intermediates.

Using estimated metabolic fluxes maximum theoretical ATP production was calculated (Figure 5.5). Both DCA cultures derived about 20% less ATP from glycolysis compared to control culture correlating with reduced glycolytic fluxes (Figure 5.4) and reduced glucose consumption in DCA cultures (Figure 5.2 and Table 5.1). In 10 mM DCA cultures the ATP production potential in the TCA cycle was more than doubled compared to the control, in line with the increased TCA cycle fluxes observed only for the 10 mM DCA cultures.

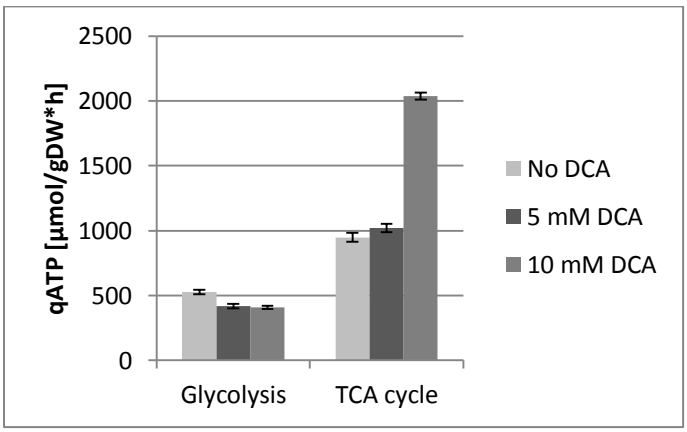

Figure 5.4: ATP production. Bars show mean optimal ATP production rate and whiskers indicate lower and upper optimal production range as estimated by metabolic flux analysis. DCA cultures produced less ATP via glycolysis while only 10 mM DCA cultures had increased ATP production from TCA cycle.

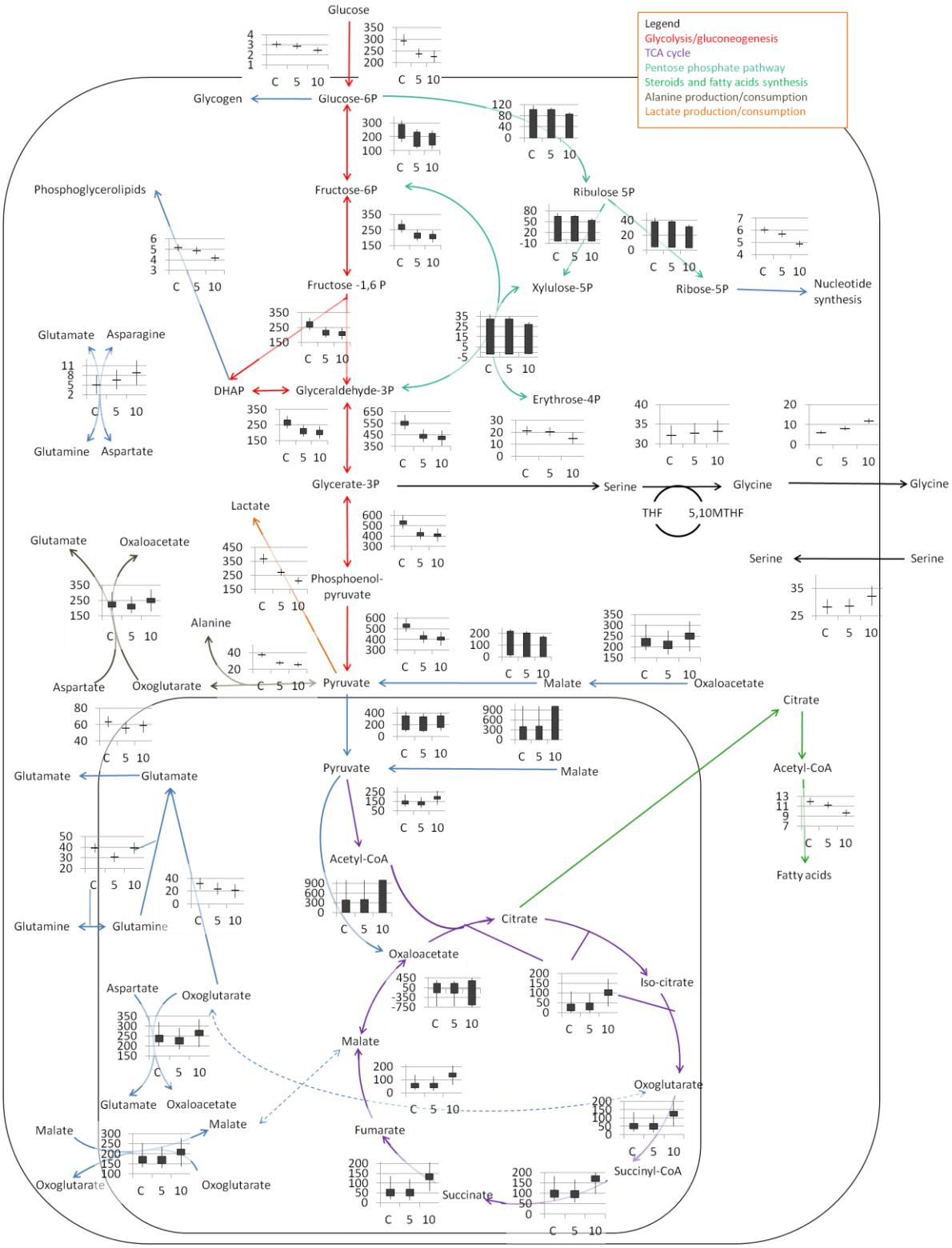

Figure 5.5: Metabolic flux analysis of HEK293F cultures in 5 mM DCA, 10 mM DCA and control cultures during exponential growth. Intracellular fluxes were estimated using metabolic flux analysis. Optimum rates are shown as solid bars with 95% confidence intervals shown as vertical lines. C = control, 5 = 5 mM DCA, 10 = 10 mM DCA. Rates are in µM/(gDW*h). THF = tetrahydrofolate, 5,10MTHF = 5,10-methylenetetrahydrofolate.

5.4.2.4. Intracellular metabolite concentrations

Samples for intracellular metabolite analysis were taken in triplicates after 3 days resulting in 9 samples for cells treated with 5 mM DCA, 10 mM DCA and control cells, respectively. 53 metabolites were measured using HPLC-MS/MS of which 24 were either not detected, not quantifiable due to insufficient calibration, below lower limit of quantification in at least one sample or the coefficient of variation of the pooled sample injections was higher than 25%. The majority of intracellular metabolite concentrations were not significantly different, however trends could be detected. Intracellular lactate concentrations decreased significantly with increasing DCA concentration correlating with the lower lactate production in DCA cultures. However, despite the lower glucose consumption in DCA cultures, glucose 6-phosphate (G6P) and fructose 1,6-bisphosphate (F16DP) concentrations were higher in DCA cultures; although differences were not significant. 3-phosphoglycerate and 2-phosphoglycerate (3PG + 2PG) and phosphoenolpyruvate (PEP) concentrations decreased with increasing DCA concentrations suggesting an increased glycolytic rate in the lower part of glycolysis. Dihydroxyacetone phosphate (DHAP) concentration was lower in DCA cultures as well. Concentrations of TCA cycle intermediates aconitate, citrate and isocitrate (CIT + ISO) were lower in 10 mM DCA cultures, while oxoglutarate (KGA) concentration increased with increasing DCA concentration. Succinate (SUC) concentrations were also slightly increased in DCA cultures, while fumarate were only lower in 10 mM DCA cultures and malate concentrations were similar in all conditions. Erythrose 4-phosphate (E4P) and xylulose 5-phosphate concentrations were lower in 10 mM DCA cultures. Ribulose 5-phosphate (RL5P) concentration decreased with increasing DCA concentration indicating lower pentose phosphate pathway activity. Pyruvate concentrations were similar for all conditions while acetyl-CoA concentrations increased with increasing DCA concentrations indicating a higher PDC activity. NAD^+ concentration were increased in DCA cultures while NADP concentration was similar in all conditions.

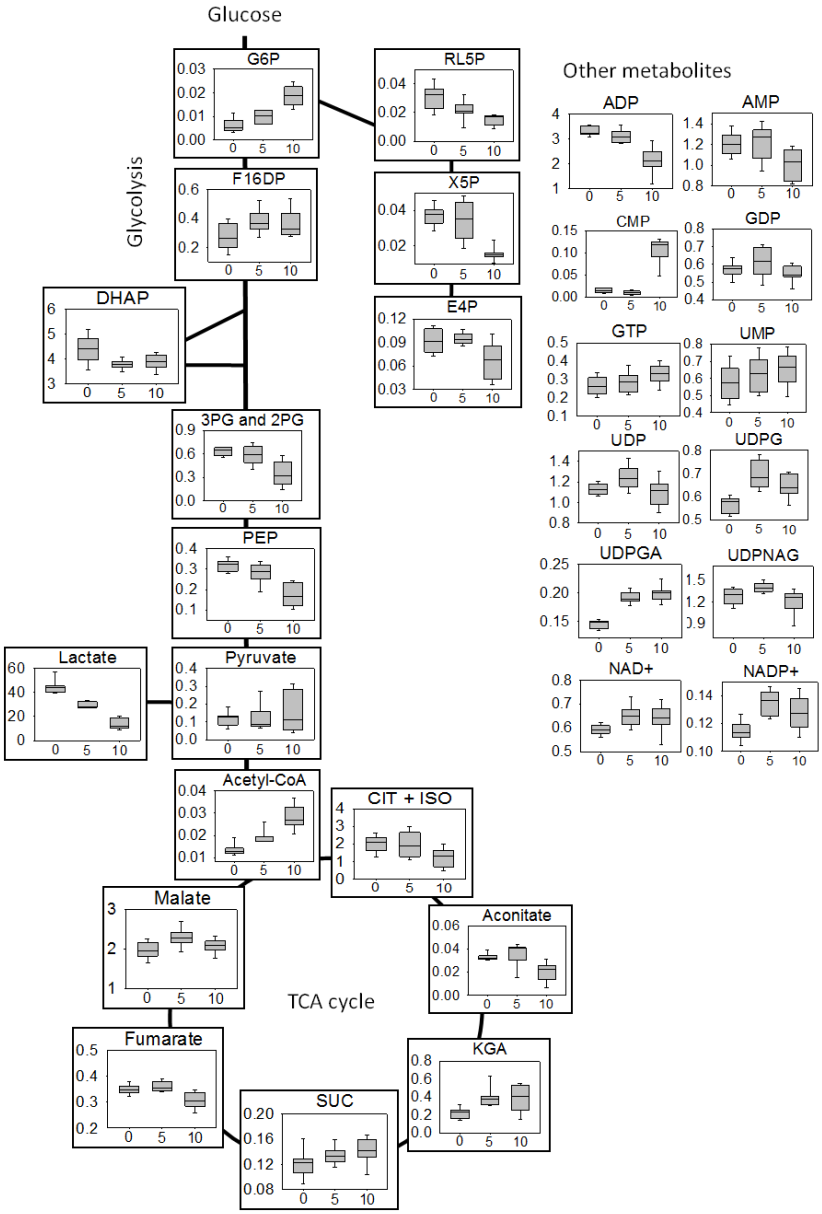

Figure 5.6: Mean intracellular metabolite concentrations in cells treated with DCA and control cells. Concentrations are in fmol/cell. N=9 for all three conditions. 3PG and 2PG = 3-phosphoglycerate and 2-phosphoglycerate, CIT + ISO = citrate and isocitrate, DHAP = dihydroxyacetone phosphate, E4P = erythrose 4-phosphate, F16DP = fructose 1,6-bisphosphate, G6P = glucose 6-phosphate, KGA = oxoglutarate, PEP = phosphoenolpyruvate, PL5P = ribulose 5-phosphate, SUC = succinate, UDPG = UDP glucose, UDPGA = UDP glucuronic acid, UDPNAG = UDP N-acetylglucosamine, X5P = Xylulose 5-phosphate. SE = standard error. 0 = control, 5 = 5 mM DCA, 10 = 10 mM DCA

5.4.3. Transcriptomics analysis

Samples for transcriptomics analysis were collected after 3 days from triplicate cell cultures to investigate the differences in gene expression between DCA cultures and control cultures. Transcript abundances were analyzed using an Illumina HT12 chip and 21,569 of the 47,317 entities were expressed.

Table 5.3: Significantly regulated genes in 10 mM DCA cultures involved in metabolism according to HumanCyc.

Gene name	Fold change	EC	Enzyme	Pathway
HMOX1	2.6297	1.14.99.3	Heme oxygenase 1	heme degradation
SGSH	2.2129	3.10.1.1	N-sulphoglucosamine sulphohydrolase	
IRAK1	2.1979	2.7.11.1	Interleukin-1 receptor-associated kinase 1	
LPPR2	2.0192	3.1.3.4	Lipid phosphate phosphatase-related protein type 2	triacylglycerol biosynthesis
BCAT1	1.9834	2.6.1.42	Branched-chain-amino-acid aminotransferase, cytosolic	leucine degradation I, valine degradation I, isoleucine degradation I
XYLB	1.9490	2.7.1.17	Xylulose kinase	
PCK2	1.9430	4.1.1.32	Phosphoenolpyruvate carboxykinase [GTP], mitochondrial	gluconeogenesis
SRXN1	1.9287	1.8.98.2	Sulfiredoxin-1	
ASNS	1.9173	6.3.5.4	Asparagine synthetase [glutamine-hydrolyzing]	asparagine biosynthesis I, citrulline biosynthesis, glutamine degradation I
CRMP1	1.9153	3.5.2.2	Dihydropyrimidinase-related protein 1	uracil degradation I (reductive), uracil degradation I (reductive), thymine degradation
ABCB1	1.8898	3.6.3.44	Multidrug resistance protein 3	ATP-dependent export of organic anions and drugs from the cytoplasm
ISG20	1.8575	3.1.13.1	Interferon-stimulated gene 20 kDa protein	
MTHFD1L	1.8506	6.3.4.3	Monofunctional C1-tetrahydrofolate synthase	folate polyglutamylation, folate transformations
MARS	1.8290	6.1.1.10	Methionyl-tRNA synthetase, cytoplasmic	tRNA charging
SPR	1.8118	1.1.1.153	Sepiapterin reductase 2	tetrahydrobiopterin de novo biosynthesis
CTH	1.7845	4.4.1.1	Cystathionine gamma-lyase 4	cysteine biosynthesis/homocysteine degradation, cysteine biosynthesis/homocysteine degradation
MTHFD2	1.7763	3.5.4.9	Methenyltetrahydrofolate cyclohydrolase 2	tetrahydrofolate salvage from 5,10-methenyltetrahydrofolate, folate transformations, histidine degradation III
TK1	1.7617	2.7.1.21/ 2.7.1.145	Thymidine kinase 1	pyrimidine deoxyribonucleosides salvage, pyrimidine deoxyribonucleosides salvage
FADS1	1.7563	1.14.19.-	Fatty acid desaturase 1	oleate biosynthesis II
AGPAT9	1.7173	2.3.1.15	Glycerol-3-phosphate acyltransferase 3	triacylglycerol biosynthesis, CDP-diacylglycerol biosynthesis
CBS	1.6837	4.2.1.22	Cystathionine beta-synthase 4	cysteine biosynthesis/homocysteine degradation
PPIF	1.6234	5.2.1.8	Peptidylprolyl isomerase F	
SHMT2	1.5782	2.1.2.1	Serine hydroxymethyltransferase 2	glycine biosynthesis I, dTMP de novo biosynthesis (mitochondrial), folate polyglutamylation, folate transformations, glycine betaine degradation
TKTL1	-2.3701	2.2.1.1	Transketolase-like protein 1	pentose phosphate pathway (non-oxidative branch)
CLYBL	-1.7420	4.1.3.6	Citrate lyase subunit beta-like protein, mitochondrial	
MRPL30	-1.7333	RXN0-5098	Lipoyltransferase 1, mitochondrial	lipoate biosynthesis and incorporation II, lipoate salvage I
LHPP	-1.6455	3.6.1.1	Phospholysine phosphohistidine inorganic pyrophosphate phosphatase	
PDK3	-1.6057	2.7.11.2	Pyruvate dehydrogenase kinase 3	
OSGEPL1	-1.5979	3.4.24.57	Probable O-sialoglycoprotein endopeptidase 2	

In 5 mM DCA samples no genes were differentially expressed compared to control cultures; however fold changes of up to 2.5 were detected indicating some variation between biological triplicates may led to the results being non-significant. In the 10 mM DCA samples 164 genes were differentially expressed of which 48 were down-regulated and 116 up-regulated (Appendix G). 163 and 51 genes had a fold change greater than 1.5 and 2, respectively. The complete data set was analyzed for enrichment of up- or down-regulated genes in metabolic pathways using HumanCyc (http://humancyc.org/). Differential expression was observed for 29 genes involved in metabolic reactions (Table 5.3) with mitochondrial one-carbon metabolism being the only significantly affected pathway. Evidently the observed metabolic differences between control and DCA cultures are caused mainly by post-transcriptional events rather than alterations in gene expression.

The up-regulated enzymes involved in one-carbon metabolism were monofunctional C1-tetrahydrofolate synthase (MTHFD1L), bifunctional methylenetetrahydrofolate dehydrogenase/cyclohydrolase (MTHFD2) and serine hydroxymethyltransferase (SHMT2). One-carbon metabolism takes place in the cytosol as well as in mitochondria (Figure 5.7). All three up-regulated enzymes are located in the mitochondria, suggesting that mitochondrial but not cytosolic one-carbon metabolism is increased in 10 mM DCA cultures.

Other metabolic enzymes with altered gene expression include asparagine synthetase (glutamine-hydrolyzing) (ASNS) which is up-regulated and is responsible for ATP-dependent synthesis of asparagine and glutamate from glutamine and aspartate. Additionally, mitochondrial phosphoenolpyruvate carboxykinase (PCK2) gene expression is also increased. This enzyme is used in the pathway of gluconeogenesis and converts oxaloacetate into phosphoenolpyruvate and CO_2. Somewhat surprising, pyruvate dehydrogenase kinase 3 (PDK3) gene expression was down-regulated. PDK3 is one of the four isozymes that inhibit PDC activity. As DCA is a PDK inhibitor, rather an up-regulation, if any, would have been expected to counteract the DCA induced PDK inhibition.

The majority of most up-regulated genes in 10 mM DCA cultures are linked to endoplasmic reticulum (ER) stress, oxidative stress, DNA damage or have been found to be associated with cancer (Table 5.4).

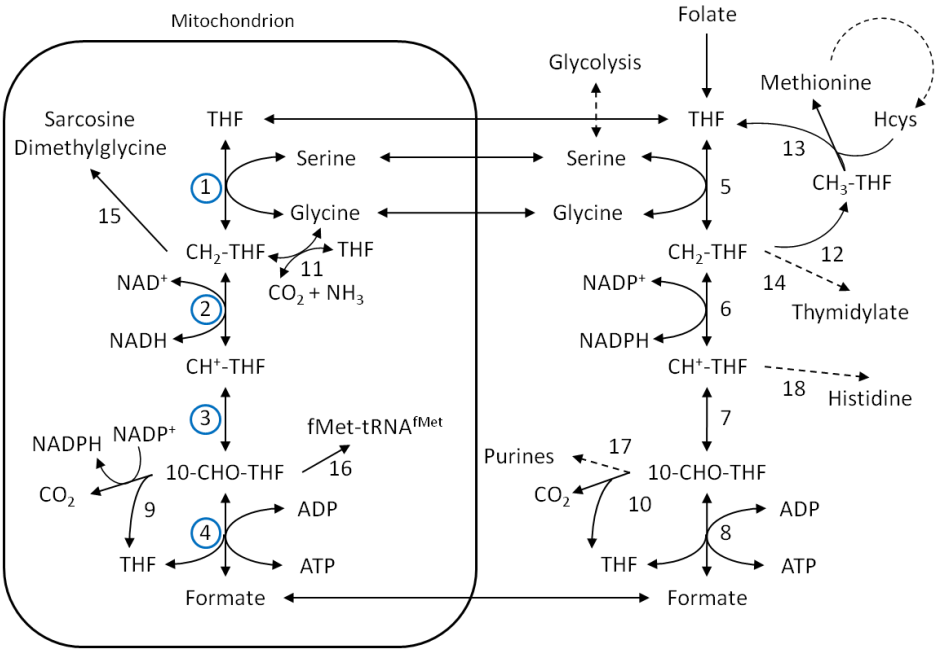

Figure 5.7: Simplified cytosolic and mitochondrial one-carbon metabolism. THF = tetrahydrofolate, CH_2-THF = 5,10-methylene-THF, CH^+-THF = 5,10-methenyl-THF, 10-CHO-THF = 10-formyl-THF, Hcys = homocysteine, fMet-tRNA^{fMet} = formylmethionyl-tRNA; Reactions: 1 = mitochondrial serine hydroxymethyltransferase (SHMT2), 2 & 3 = bifunctional methylenetetrahydrofolate dehydrogenase/ cyclohydrolase (MTHFD2), 4 = monofunctional C1-THF synthase (MTHFD1L), 5 = cytoplasmic serine hydroxymethyltransferase, 6 & 7 & 8 = trifunctional C1-THF synthase, 9 & 10 = 10-formyl-THF dehydrogenase, 11 = glycine cleavage system, 12 = 5,10-methylene-THF reductase, 13 = methionine synthase, 14 = thymidylate synthase, 15 = sarcosine dehydrogenase and dimethylglycine dehydrogenase, 16 = methionyl-tRNA formyl transferase, 17 = glycinamide ribonucleotide transformylase and aminoimidazole carboxamide, 18 = formiminotransferase-cyclodeaminase. Enzymes catalyzing reactions 1,2,3, and 4 were upregulated in 10 mM DCA cultures (blue circles).

Table 5.4: Most significantly up-regulated genes in 10 mM DCA cultures compared to control cultures.

Gene symbol	Protein	Fold change
Up-regulated		
INHBE	Inhibin beta E chain	5.1378
SESN2	Sestrin-2	3.6613
ETV5	ETS translocation variant 5	3.2484
TNFRSF12A	Tumor necrosis factor receptor superfamily member 12A	3.1621
TNNT1	Troponin T, slow skeletal muscle	2.9702
DDIT3	DNA damage-inducible transcript 3 protein	2.8866
ETV4	ETS translocation variant 4	2.8155
DDIT4	DNA damage-inducible transcript 4 protein	2.7388
LTBR	Tumor necrosis factor receptor superfamily member 3	2.6747
HMOX1	Heme oxygenase 1	2.6297

Inhibin beta E chain (IHNBE) is a peptide hormone and belongs to the growth factor-β super family. Treatment of cancer cells with ER stress inducing drugs resulted in increased IHNBE expression induced by up-regulation of activating transcription factor 4 (ATF4) (Brüning et al. 2012). IHNBE is also up-regulated by insulin in liver cells suggesting that it is involved in regulating glucose and energy metabolism (Hashimoto et al. 2009). Sestrin-2 (SESN2) activates AMP-activated protein kinase (AMPK) and thereby downregulates mammalian target of rapamycin (mTOR) which is downregulated in cells to slow down their metabolism (Budanov & Karin 2008; Yecies et al. 2011). SESN2 is linked to the cellular response to oxidative stress and DNA damage. By regenerating peroxiredoxins, SESN2 has a cytoprotective function and plays a role in the antioxidant defense of the cell (Essler, Dehne & Brüne 2009). ETS translocation variant 5 (ETV5) has been linked to cancer and overexpression increased cell proliferation (Rahim & Üren 2013). It also appears to be associated with glucose metabolism and obesity (Gutierrez-Aguilar et al. 2013). Tumor necrosis factor receptor superfamily member 12A (TNFRSF12A) is the receptor for TNF-Related Weak Inducer of Apoptosis (TWEAK). TWEAK has been shown to induce cell proliferation in several cell types (Gao et al. 2009; Girgenrath et al. 2006; Jakubowski et al. 2005; Sanz et al. 2009; Sugito et al. 2009) and TNFRSF12A gene and protein were overexpressed in several solid tumor types (Culp et al. 2010). Troponin T, slow skeletal muscle (TNNT1) is a subunit of troponin, a complex that regulates striated muscle contraction in response to fluctuations in intracellular calcium concentration (Mannherz & Goody 1974). DCA had a lowering effect on free cytosolic calcium concentration in A549 cells treated with DCA (Bonnet et al. 2007). DNA damage-inducible transcript 3 protein (DDIT3) is a multifunctional transcription factor induced by ER stress, oxidative stress, hypoxia and amino acid deprivation and promotes apoptosis (Lengwehasatit & Dickson 2002; Oyadomari & Mori 2004; Yamaguchi & Wang 2004). It is a negative regulator of ATF4-dependent transcriptional activation of asparagine synthetase (Su & Kilberg 2008). Although the adjusted p-value is just above the cut-off of 0.01 to be considered statistically significant, ATF4 was up-regulated in 10 mM DCA cultures with a fold change of 1.58 and could be responsible for increased asparagine production in 10 mM DCA cultures as well as increased IHNBE expression (see above). ETS translocation variant 4 (ETV4) is a transcriptional activator and linked to several cancers (Oh, Shin & Janknecht 2012). DNA damage-inducible transcript 4 protein (DDIT4) regulates cell growth, proliferation and survival via inhibition of mammalian target of rapamycin complex 1 (mTORC1) in response to cellular energy levels and cellular stress such as hypoxia and DNA damage (Corradetti, Inoki & Guan 2005; Ellisen et al. 2002;

Shoshani et al. 2002). Tumor necrosis factor receptor superfamily member 3 (LTBR) is also involved in promoting apoptosis and is an mTOR inhibitor (Sofer et al. 2005; Wu, MY et al. 1999). Heme oxygenase 1 (HMOX1) cleaves free heme to form biliverdin, Fe^{2+} and CO. Excess of free heme, caused by oxidative stress, can produce free radicals sensitizing cells to undergo apoptosis and HMOX1 expression is induced by oxidative stress (reviewed in (Gozzelino, Jeney & Soares 2010)).

5.4.4. Targeted proteomics analysis of central carbon metabolic enzyme

Samples for targeted proteomics were obtained after 3 days while cultures were in exponential growth phase (n = 3 for control, 5 mM DCA and 10 mM DCA, respectively). 62 metabolic proteins, mainly enzymes of glycolysis, TCA cycle and enzymes of connected metabolic pathways, were analyzed (Appendix F). In 5 mM DCA cultures no proteins were statistically differentially expressed. However, three proteins had an adjusted p-value of 0.0559, just above the cut-off of 0.05 (Appendix Table F3). Two proteins were up-regulated, asparagine synthetase (ASNS) (fold change 1.18) and pyruvate kinase PKLR (KPYR) (fold change 1.27). Mitochondrial malate dehydrogenase (MDHM) was downregulated (fold change 1.70). MDHM is an enzyme of the TCA cycle and reversibly catalyzes the oxidation of malate to oxaloacetate thereby reducing NAD^+ to NADH. Five of the 62 analyzed proteins were significantly differentially expressed in 10 mM DCA cultures compared to control cultures of which four proteins were upregulated and one downregulated (Table 5.5 and Appendix Table F2).

Table 5.5: Significantly differentially expressed proteins in 10 mM DCA cultures. Differentially expressed proteins in 10 mM DCA cultures compared to control cultures with an adjusted p-value of <0.05. Positive fold change indicates up-regulation and negative fold change down-regulation.

UniProt ID	Name	Fold change
P08243 ASNS_HUMAN	Asparagine synthetase [glutamine-hydrolyzing]	1.37
Q15119 PDK2_HUMAN	Pyruvate dehydrogenase kinase isozyme 2, mitochondrial	1.41
P07195 LDHB_HUMAN	L-lactate dehydrogenase B chain	1.37
P30613KPYR_HUMAN	Pyruvate kinase PKLR	1.22
P18669 PGAM1_HUMAN	Phosphoglycerate mutase 1	-1.35

ASNS was upregulated with a fold change of 1.36. ASNS converts glutamine and aspartate to glutamate and asparagine, using ATP. Pyruvate dehydrogenase 2 (PDK2),

which is one of the four PDK isozymes inhibited by DCA, was also upregulated with a fold change of 1.36. Lactate dehydrogenase B chain (LDHB) was upregulated with a fold change of 1.37 converting pyruvate to lactate. The forth upregulated enzyme was KPYR with a fold change of 1.22. It is one of the glycolytic key enzymes, converting phosphoenolpyruvate (PEP) to pyruvate generating one ATP. Only one enzyme was identified as being differentially downregulated, phosphoglycerate mutase 1 (PGAM1), which is also a glycolytic enzyme catalyzing the reversible reaction from 3-phosphoglycerate to 2-phosphoglycerate via 2,3-bisphosphoglycerate intermediate. The majority of the metabolic proteins analyzed were not differentially expressed in 10 mM DCA cultures and no proteins were identified as being differentially expressed in 5 mM DCA cultures, indicating that the reduced aerobic glycolysis induced by DCA is mainly the result of post-translational effects.

5.5. Discussion

This study investigated metabolic differences between HEK293F cells cultivated in different concentrations of DCA. PDK phosphorylates and thereby inactivates PDC, the enzyme complex that converts pyruvate to acetyl-CoA in the mitochondrion. DCA inhibits PDK resulting in PDC being less phosphorylated and therefore having higher activity. As expected, DCA reduced lactate production in a dose dependent manner (Figure 5.1). Up to 5 mM, DCA reduced aerobic glycolysis without affecting growth rate, while 10 mM and higher DCA concentrations not only reduced aerobic glycolysis but also affected cell growth negatively. In order to better understand the two effects of DCA, cells growing at these two conditions were compared and contrasted to control using a range of omics technologies, namely transcriptomics, targeted proteomics, fluxomics, and intracellular metabolite analysis.

5.5.1. Lactate production can be reduced without increased TCA cycle flux

DCA had a clear metabolic effect in HEK293F cells in a dose-dependent manner. The metabolic effect was also observed at lower DCA concentration where no growth inhibitory effect was evident. At lower DCA concentration, 5 mM, glucose consumption, lactate production and lactate to glucose yield were reduced indicating a more energy efficient metabolism (Table 5.1). Correspondingly, glycolytic fluxes were lower in DCA cultures indicating a reduced glycolytic rate leading to about 20% lower ATP yield from glycolytic

activity. PDC phosphorylation is reduced at 5 mM DCA and intracellular acetyl-CoA was increased indicating higher PDC activity. However, TCA cycle fluxes were not increased at 5 mM DCA and intracellular TCA cycle metabolite concentrations were mostly similar compared to control cultures. TCA cycle activity appears unaltered and no increase in oxidative metabolism was observed despite the increased acetyl-CoA formation. This has been observed before in neuroblastoma cells where glucose consumption and lactate production were reduced without increase in oxygen consumption indicating no increase in TCA cycle activity (Niewisch et al. 2012)

In addition to reduced lactate production, alanine formation from pyruvate is reduced as well in DCA cultures (Table 5.1 and Figure 5.4) suggesting lower cytosolic pyruvate levels. Intracellular pyruvate concentration was similar in DCA cultures compared to control (Figure 5.6). However, the measured pyruvate accounts for both, cytosolic and mitochondrial fraction. While DCA did not change the overall intracellular pyruvate concentration it may have affected the distribution of pyruvate between cytoplasm and mitochondrion reducing pyruvate availability for lactate and alanine formation in the cytosol.

It was previously shown that DCA depolarizes mitochondria even at concentrations that did not affect cell growth (Stockwin et al. 2010). Depolarization of mitochondria results in loss of oxidative phosphorylation capacity and therefore reduced ATP production from TCA cycle. However, it is not obvious how mitochondrial depolarization and reduced glycolysis can occur simultaneously without affecting cell growth. It appears that metabolic flexibility allows cells to adjust their metabolism at moderate PDC activity increase and the reduction in ATP production can be tolerated by the cells.

Furthermore, as no genes or proteins were significantly differentially expressed at 5 mM DCA and only a small number of metabolic genes and proteins were differentially expressed in 10 mM DCA cultures, the metabolic changes were mostly caused by post-translational events. Allosteric regulation plays an important role in modulation of the glycolytic rate with hexokinase, phosphofructokinase and pyruvate kinase being the three main regulatory enzymes. However, concentrations of allosteric regulators together with missing increase in TCA cycle activity do not support allosteric regulation. The reduced glycolytic activity is not readily explained and further investigations are necessary.

5.5.2. High DCA causes metabolic stress

At higher DCA concentration, 10 mM, the metabolic effect was stronger compared to control and 5 mM DCA cultures. Glucose consumption, lactate production and lactate to glucose yield were further reduced with peak lactate concentration being almost half compared to control cultures (Table 5.1 and Figure 5.2). Despite a strong reduction in aerobic glycolysis only a small number of metabolic genes and proteins involved in central carbon metabolism were upregulated (Table 5.3 and Table 5.5). Somewhat surprisingly, pyruvate dehydrogenase kinase 3 gene expression was downregulated. PDK3 is one of the isozymes inhibited by DCA and rather an upregulation, if any, would have been expected in order to antagonize the effects of DCA. Phosphoenolpyruvate carboxylase 2 (PCK2) gene expression was upregulated as well. PCK2 is part of the gluconeogenesis pathway converting oxaloacetate to phosphoenolpyruvate. However, PDK3 and PCK2 were not identified as being differentially expressed in targeted proteomics. In targeted proteomics, pyruvate dehydrogenase kinase 2 (PDK2) was upregulated without altered gene expression. Lactate dehydrogenase chain B (LDHB) protein was upregulated with a fold change of 1.37. LDHB converts pyruvate to lactate; however, no increased LDHB gene expression was detected and lactate production was significantly lower in 10 mM DCA cultures. Upregulation of PDK2 and LDHB could be the result of the cell counteracting PDC activation by DCA. The forth upregulated enzyme was pyruvate kinase isozyme L/R (KPYR) with a fold change of 1.22. It is one of the glycolytic key enzymes, converting phosphoenolpyruvate (PEP) to pyruvate generating one ATP. Intracellular PEP concentrations decreased with increasing DCA concentrations while pyruvate concentrations were similar correlating with higher pyruvate kinase activity (Figure 5.6). KPYR may be upregulated to provide more pyruvate needed as a substrate for PDC or to produce more ATP from glycolysis. PGAM1 was the only glycolytic enzyme identified as being downregulated catalyzing the reaction from 3-phosphoglycerate to 2-phosphoglycerate via 2,3-bisphosphoglycerate intermediate. However, gene expression of PGAM1 was not altered. As this reaction is reversible and not a site for major regulation of glycolysis the increased PGAM1 protein expression cannot be readily explained. A possible explanation for increased protein amount without increase in gene expression could be reduced PDK2, LDHB and KPYR protein degradation in response to increased PDC activity. Similarly, PGAM1 may be degraded at a higher rate. Taken together, the reduction in aerobic glycolysis even at growth inhibiting concentrations is mainly caused by post-translational regulation.

10 mM DCA significantly reduced exponential cell growth by about 19% in HEK293F without reduction in viability. In contrast to 5 mM DCA cultures, higher TCA cycle fluxes were estimated for 10 mM DCA cultures indicating increased oxidative metabolism. HEK293F cells appear to be unable to adjust their metabolism if PDC activity is increased past a threshold leading to higher TCA cycle activity. Due to the increased TCA cycle activity, a two-fold increase in theoretical ATP production from TCA was estimated. However, DCA can depolarize mitochondria which may reduce the ATP yield considerably leading to a “metabolic crisis” in which cells are unable to generate sufficient ATP and fail to meet metabolic demands. In gene expression analysis, the majority of the most upregulated genes respond to ER stress, oxidative stress, and DNA damage confirming cellular stress (Table 5.5). Additionally, four amino acid transporters were found to be upregulated together covering the transport of almost all amino acids suggesting intracellular amino acid limitation (Table 5.2 and Table 5.1). Correspondingly, ASNS gene and protein expression was increased in DCA culture corresponding with increased asparagine production during exponential growth. ASNS expression is activated in response to either amino acid limitation or cellular stress via pathways involving activating transcription factor 4 (ATF 4) which was also upregulated in the 10 mM DCA cultures with a fold change of 1.58 (adj. p-value 0.013). In response to amino acid deprivation the GCN2-eIF2-ATF4 pathway seems to be the predominant signaling pathway (Siu et al. 2002; Wek, Jiang & Anthony 2006; Zhang et al. 2002). Via this pathway ASNS mRNA expression cannot only be induced by asparagine limitation but also by limitation of other amino acids (Gong, Guerrini & Basilico 1991; Hutson & Kilberg 1994). GCN has also been linked to various diseases such as cancer and Alzheimer’s disease. In particular the GCN-eIF2-ATF4 pathway was found to be essential for maintaining metabolic homeostasis in tumor cells in response to nutrient deprivation (Ye et al. 2010). It was observed that pancreatic tumor cells exposed to low glucose had an increased ASNS gene expression which may protect the cells from apoptosis based on the observation that ASNS overexpression can suppress JUN NH_2-terminal kinase (JNK) activation and reduce apoptosis (Cui et al. 2007). The second factor regulating ASNS expression is cellular stress. ER stress results in activation of the double-stranded RNA-activated protein kinase-like ER kinase (PERK) as part of the unfolded rotein response which can be activated in response to various cellular stresses including oxidative stress and carbohydrate deprivation (Barbosa-Tessmann, Pineda, et al. 1999; Harding et al. 2000). Both, amino acid limitation and cellular stress result in activation of ATF4 either through GCN2-eIF2-ATF4 or PERK-eIF2-ATF4 pathway, both leading to transcriptional activation

of ATF4 responsive target genes, including ASNS (Barbosa-Tessmann, Chen, et al. 1999; Barbosa-Tessmann et al. 2000). However, the exact role that ASNS activation plays in response to increased PDC activity and whether amino acid limitations or ER stress are responsible need further exploration.

The only metabolic pathway found to be upregulated was mitochondrial one-carbon metabolism. In MFA, serine uptake and glycine production as well as flux through serine hydroxymethyltransferase (SHMT) were increased in 10 mM DCA cultures (Figure 5.4). The one-carbon metabolism comprises of a parallel cytoplasmic and mitochondrial pathway (Figure 5.7). Although the flux is shown in the cytosol, the flux in MFA is the sum of both, cytoplasmic and mitochondrial one-carbon metabolism. In gene expression analysis, only genes involved in mitochondrial part were upregulated, SHMT2, bifunctional methylenetetrahydrofolate dehydrogenase/ cyclohydrolase (MTHFD2), and monofunctional C1-tetrahydrofolate synthase (MTHFD1L) (Table 53 and Figure 5.7). The mitochondrial one-carbon metabolism and expression of MTHFD2 appear to be critical for cancer and knockdown of MTHFD2 results in death of human cancer cells (Nilsson et al. 2014). SHMT2 and MTHFD1L were also found to be upregulated in tumor cells (Sugiura et al. 2004; Tendler, Threadgill & Tisdale 1987) while MTHFD2 has been detected in tumor and transformed cells but not adult tissue (Di Pietro, Wang & MacKenzie 2004; Mejia & MacKenzie 1985; Peri & MacKenzie 1993; Smith et al. 1990). Folate deficiency or altered one-carbon metabolism was linked to several human diseases such as anemias, neural tube defects, cardiovascular disease, cancer, and Alzheimer's disease (Daly et al. 2005; Kim, YI 2003; Lucock 2000; Mattson & Shea 2003; Moat et al. 2004). Increased serine consumption, glycine production and equilibrium preferences suggest that the reactions are shifted towards 10-formyl-THF (Christensen & MacKenzie 2006; Kay et al. 1960; Pelletier & MacKenzie 1995). The oxidation of CH_2-THF to CH^+-THF and 10-formyl-THF to CO_2 generate NADH and NADPH respectively and are linked to the electron transport chain through Complex I. The exact role of one-carbon metabolism in cancer cell or embryonic cell metabolism is yet to be established. It was suggested that MTHFD2 expression may be necessary for detoxification processes unrelated to normal cell metabolism (Linster, Van Schaftingen & Hanson 2013; Nilsson et al. 2014).

5.6. Conclusions

Aerobic glycolysis (Warburg effect) is a distinct metabolic phenotype observed in many rapid proliferating cells including cancer cells. In this study we used DCA, a known PDK

inhibitor, to increase PDC activity and reverse the Warburg effect in HEK293F cells. Use of various omics technologies provided information necessary to analyze the cell as a whole as often the use of a single technology only gives limited information. A dose-dependent reduction of aerobic glycolysis was observed, leading to a more efficient metabolism in 5 mM DCA cultures. While higher DCA concentration (10 mM) reduced cell growth rate and increased TCA cycle activity resulting in increased cellular stress. Additionally, asparagine synthetase activity and mitochondrial one-carbon metabolism were increased in DCA cultures; however the relationship between reduced aerobic glycolysis and asparagine synthetase and one-carbon metabolism needs to be further investigated.

Chapter 6

General Discussion and Conclusions

6.1. Summary and general discussion

Mammalian cell metabolism is highly complex, organized in different cellular compartments and highly regulated. For the generation of energy in the form of ATP the cell mainly uses two pathways, glycolysis and TCA cycle. In glycolysis, glucose is converted to pyruvate which can be further used in the TCA cycle. However, both pathways are not always used as energy generation using TCA cycle (in connection with the electron transport chain) requires sufficient oxygen supply, as oxygen is the final electron acceptor. Therefore, under aerobic conditions, mammalian cells normally use both glycolysis and TCA cycle as it provides them with the maximum ATP yield per molecule glucose. Under anaerobic conditions, cells can only use glycolysis and convert excess pyruvate into lactate. This results in a lower ATP yield per consumed molecule glucose and is characterized by an increased glycolytic rate and lactate production. Otto Warburg observed over 80 years ago that cancer cells prefer glycolysis over oxidative phosphorylation even when sufficient oxygen is available, called aerobic glycolysis, also known as the Warburg effect (Warburg, Wind & Negelein 1927). This phenotype is observed in many cancer cells. However, it is not unique to cancer cells and was also observed in other rapid proliferating cells such as cell lines used in industrial applications indicating that similar metabolic and biosynthetic demands play a role (Hanahan & Weinberg 2011). Besides cancer, aerobic glycolysis is also associated with other age-related diseases such as type-2 diabetes mellitus or neurodegenerative diseases, such as Alzheimer's disease, and was linked to reduced pyruvate dehydrogenase complex (PDC) activity (Stacpoole 2012).

PDC is a crucial link between glycolysis and the TCA cycle as it converts pyruvate to acetyl-CoA. The activity of PDC is largely determined by reversible phosphorylation catalyzed by two enzymes, pyruvate dehydrogenase kinase (PDK, phosphorylation, inactivation) and pyruvate dehydrogenase phosphatase (PDP, dephosphorylation, activation) (reviewed in Chapter 2). One approach to reduce the Warburg effect is to increase the amount of pyruvate being converted to acetyl-CoA by increasing PDC activity, hereby decreasing the amount of pyruvate available for lactate formation. In this thesis, dichloroacetate (DCA) was used to inhibit PDK which in turn led to lower PDC phosphorylation and higher PDC activity. The majority of research in recent years regarding DCA focused on cancer cell apoptosis and growth inhibition as aerobic glycolysis is regarded a novel anti cancer target. However, the results regarding efficacy and underlying mechanism vary and appear to be highly cell line dependent (Chapter 2).

The focus of the main investigations in this thesis was twofold as aerobic glycolysis is an undesired phenotype in industrial applications and also associated with various diseases in humans. First, the effects of increased PDC activity induced by DCA on culture performance and antibody production using an industrial relevant cell line were investigated. Chinese hamster ovary cells were cultivated in bioreactor fermentations with 5 mM DCA improving cell's metabolism without affecting cell growth (Chapter 4). This was followed by an investigation using a human cell line, human embryonic kidney 293 (HEK293) cells, to obtain a detailed knowledge about the system wide effects of increased PDC activity (Chapter5). Specifically, two DCA concentrations were used, 5 mM DCA and 10 mM DCA. At 5 mM DCA only a metabolic effect was observed while at 10 mM DCA growth rate was reduced as well.

In CHO cell experiments, DCA at 5 mM reduced glucose consumption and lactate production in both batch and fed-batch processes (Chapter 4). This resulted in prolonged cultivation periods and increased final antibody titers, while growth rate and cell specific productivity were unaffected. The strongest effect was observed in fed-batch cultivations with glucose feeding to avoid glucose depletion during the cultivation. The cultivation period was prolonged by over three days and final antibody titer was doubled in DCA cultures. These cultures were not glucose or amino acid depleted suggesting another factor being responsible for the culture entering stationary phase and ultimately death phase. The data suggested that either lactate concentration or the associated high osmolality (due to adding base to the culture to neutralize lactate and keep pH constant) are the cause of growth inhibition. Results of sodium lactate and sodium chloride feeding experiments showed that high osmolality rather than the lactate concentration *per se* is responsible for the cultures stopping to grow. Due to lower lactate production in DCA cultures the increase in osmolality was slower which led to the longer cultivations. We also analyzed antibody quality in terms of glycan pattern, charge variants and aggregation finding only minor differences which are within run to run variability. MFA and B-DMFA were performed showing reduced glycolytic fluxes but similar TCA cycle fluxes in DCA cultures compared to control cultures indicating no change in oxidative metabolism. A lower one-carbon metabolism flux was observed as well. Combining conventional MFA for exponential growth phase and B-DMFA for later growth phases provides a good approach for flux analysis over a complete culture period. Additionally, proteomics using SWATH-MS analysis showed a lack of changes in core metabolism, thus indicating that reduction of the Warburg effect is attributable to post-translational events.

The metabolic effect of DCA was further studied in HEK293 cells. Two DCA concentrations were chosen; one to induce only a metabolic effect without growth inhibition (5 mM) and one to achieve both a metabolic effect and reduced cell growth (10 mM) (Chapter 5). Both concentrations reduced aerobic glycolysis; glucose consumption and lactate production were lower compared to control cultures. Lactate to glucose yield was lower as well, meaning that less glucose was converted to lactate. MFA analysis for exponential growth phase revealed reduced glycolytic fluxes in DCA cultures. In 10 mM DCA cultures an increased TCA cycle flux was observed indicating increased TCA cycle activity which would lead to an increase in ATP production. However, DCA was found to depolarize mitochondria which may reduce the ATP yield considerably leading to a "metabolic crisis" where amounts of generated ATP are insufficient to meet metabolic demands leading to cellular stress and reduced cell growth. Gene expression analysis revealed that several genes linked to cellular stress were upregulated while similar to the CHO cell experiment, only a small number of genes and proteins relating to metabolism were differentially expressed.

Besides reduced Warburg effect, two additional metabolic changes were observed in HEK293 cells with DCA: a) increased asparagine synthetase activity (ASNS) and b) increased mitochondrial one-carbon metabolism. Asparagine was produced in DCA cultures while consumed in control cultures during exponential growth and ASNS gene expression and protein expression were upregulated. ASNS catalyzes the ATP dependent conversion of aspartate and glutamine to asparagine and glutamate and hereby could also affect the glutamine content which is a major energy source. Two mechanisms are known to increase ASNS expression: amino acid limitation and cellular stress. Altered ASNS activity was also linked to certain cancers and metastasis. However, the exact role of higher ASNS activity and the advantage for the cell, especially during ER stress, remain to be investigated. Increased mitochondrial one-carbon metabolism was also upregulated. An increased flux through the serine hydroxymethyltransferase (SHMT) reaction was observed and cultures with DCA consumed more serine and produced more glycine. Transcriptomics analysis revealed that the genes for the mitochondrial enzymes involved in one-carbon metabolism were upregulated; SHMT2, MTHFD1L and MTHFD2. The flux estimated in MFA is the sum of both, cytosolic and mitochondrial, one-carbon metabolism. Without gene expression analysis it would not have been identified which pathway was upregulated, highlighting the importance of combining different omics technologies. Altered one-carbon metabolism was linked to several diseases as well as tumor cells. However, similar to upregulated ASNS activity, further investigations are needed as not much is

known about the regulation and purpose of increased mitochondrial one-carbon metabolism. An overview of expected and oberserved results of central metabolic pathways in both cell lines is given in Figure 6.1.

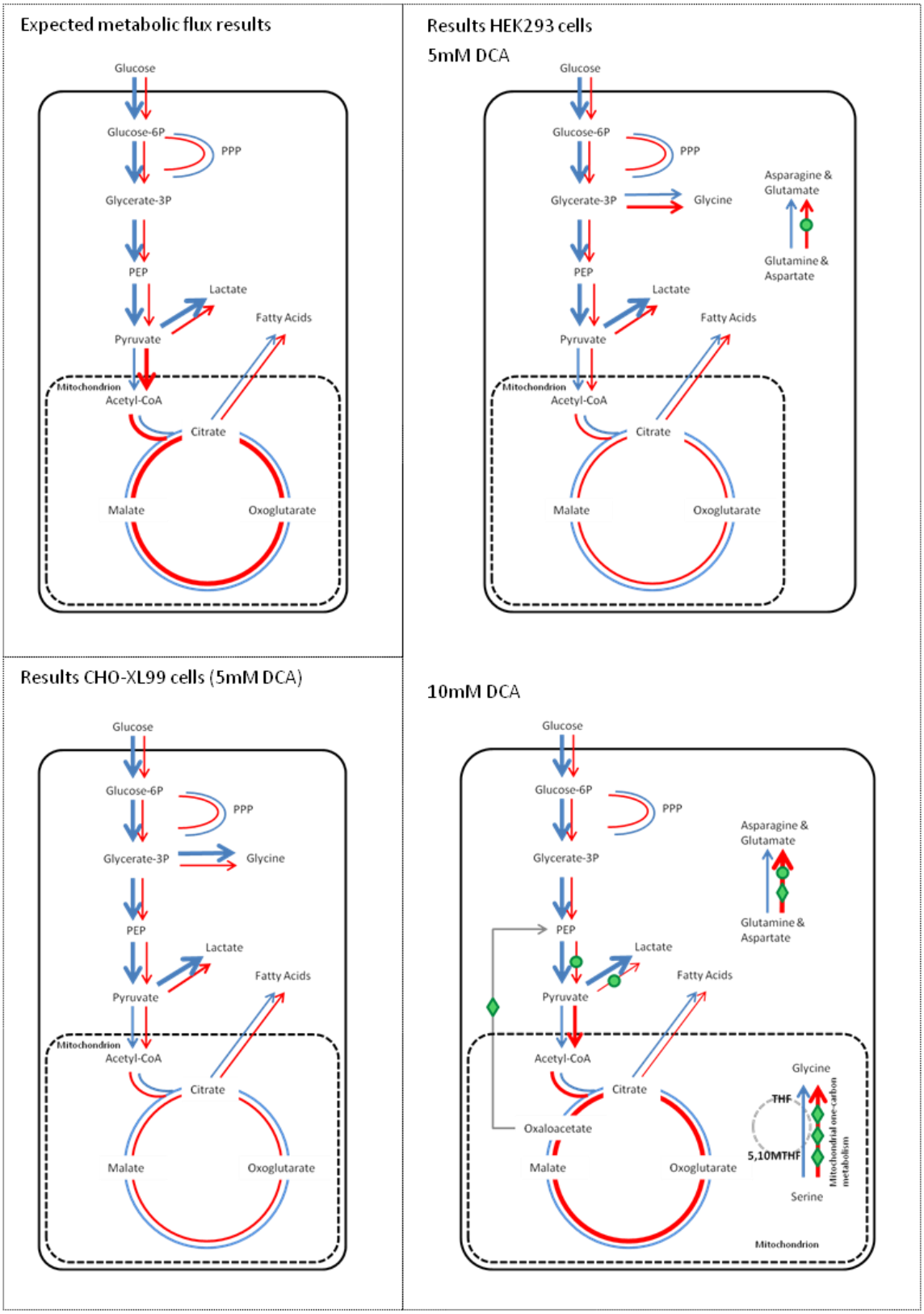

Figure 6.1: Summary of results from HEK293 and CHO-XL99 cells treated with DCA. Blue lines = control cell metabolic fluxes, red lines = DCA treatment metabolic fluxes, green circle = upregulated protein expression, green diamond = upregulated gene expression.

In summary, lower DCA concentrations can lead to a more efficient metabolism by reducing aerobic glycolysis resulting in lower glucose consumption and lactate production. On the other hand, higher DCA concentrations lead to reduced cell growth. It seems that mitochondrial depolarization at higher DCA concentrations may lead to a “metabolic crisis” with insufficient ATP production and hereby reduced cell growth.

Interestingly, while the one-carbon metabolism was lower in CHO DCA cultures it increased in HEK DCA cultures. This underlines what has been previously documented in literature, that different cell lines and also different culture conditions (different culture media with different nutrient concentrations, pH control vs. no pH control) may affect quite significantly the specific effects of increased PDC activity induced by DCA.

In both studies various omics technologies were used to analyze cellular changes in response to increased PDC activity as the effects could become apparent at different functional levels (gene expression, protein abundance, metabolites and metabolic fluxes). Transcriptomics and proteomics are well established and protocols for the analysis of intracellular metabolite concentrations are available. Metabolic flux analysis (MFA) can be used to estimate fluxes through central metabolic pathways using a limited number of extracellular measurements. However, conventional MFA assumes a steady state, which is only valid in continuous cultures or during mid exponential phase in batch cultures. In order to estimate metabolic fluxes over a complete cultivation period, dynamic MFA (DMFA) approaches are necessary. Therefore, an improved DMFA using B-splines (B-DMFA) was developed based on current DMFA approaches. Fluxes of a temperature shift experiment, an approach widely used to extend cultivations and achieve higher antibody titers, were estimated using B-DMFA (Chapter 3). Temperature shifted cultures showed a reduction in growth rate while control cultures entered death phase earlier. We observed an increased final antibody titer in temperature shifted cultures of about 42%. B-DMFA revealed that temperature shifted cultures maintained a constant volume specific antibody productivity, while productivity of control cultures declined after mid-exponential growth phase. The constant productivity together with the longer culture period at higher viability in temperature shifted cultures resulted in a higher final antibody titer. B-DMFA was also used to estimate fluxes of CHO cell fed-batch cultivations performed to examine DCA’s effects in industrial relevant processes (Chapter 4).

In order to manipulate the cellular metabolism, metabolic engineering is still the most widely used approach as the concept of using a specific enzyme inhibitor is not always available or desired. However, clonal variation from parental cell line can be a problem; especially in system wide investigations in response to a single genetic alteration (Dietmair

et al. 2012). Inducible expression systems have the advantage that only one cell clone is used and clonal variation from parental cell line introduced during selection process can be avoided. An HEK293 cell line was generated overexpressing resistin like molecule beta (RETNLB) in an inducible system (Appendix H). RETNLB was identified as being overexpressed in a cell line that had reduced glucose consumption (Dietmair et al. 2012). However, overexpression of RETNLB did not result in reduced glucose consumption in HEK293 cells, suggesting that increased RETNLB expression may not be the cause but rather a result of another factor that led to reduced glucose consumption. This underlines the difficulties related to picking successful targets for genetic engineering and further investigations are necessary to more effectively identify successful gene targets.

6.2. Achievements and future work

The main achievements of this thesis were i) analysis of increased PDC activity on culture performance and antibody production using industrial relevant cell line and processes (Chapter 4), ii) the comparative analysis of HEK293 cells with increased PDC activity induced by DCA using a combination of multiple omics technologies (Chapter 5), and iii) development of B-DMFA and analysis of metabolism of temperature shifted cells compared to cells maintained at constant temperature (Chapter 3).

A large amount of information was collected to analyze the system wide effects of increased PDC activity induced by DCA. While the aerobic glycolysis reducing effect of DCA was confirmed in all experiments there were also differences observed between HEK293 cell (Chapter 5) and CHO cell (Chapter 4) experiments. In both cell lines reduced aerobic glycolysis without growth inhibition was observed at lower DCA concentrations. It appears that the cells become more energy efficient as they produce less ATP without negative effects on growth or productivity. The observed reduction in glycolytic rate is not readily explained by allosteric regulation of glycolytic enzymes as concentrations of allosteric inhibitors such as ATP and citrate are not increased and further investigations are necessary. Higher DCA concentrations led to a reduced growth rate. Similarly, the mechanisms by which DCA becomes growth inhibitory or apoptotic need further explorations. It appears that increased TCA cycle activity leads to cellular stress however it is not clear why different cell lines respond very differently to DCA as documented in literature.

Metabolic differences between the two experiments were mainly in ASNS reaction and one-carbon metabolism which were both upregulated in HEK293 cultures with DCA but not

in CHO cultures with DCA. Apart from being different cell lines, the culture conditions were significantly different as well: different medium with different nutrient concentrations, shake flask without pH control (HEK293 cultures) or bioreactor with controlled pH and dO (CHO cultures), which could have considerably effect on the metabolic phenotypes observed. However, the increase in ASNS activity and one- carbon metabolism observed in HEK293 cells is not easily explained and further investigations are necessary. Genetic engineering experiments, preferably in an inducible system to avoid clonal variation, could give further insights into the importance of these reaction and pathway, especially during cellular stress such as ER and oxidative stress.

In the CHO cell experiment (Chapter 4) a clear advantage for cell culture performance and antibody productivity was observed using DCA without any effects on product quality. It would be of interest whether similar effects with regard to reduced aerobic glycolysis and unaffected product quality can be achieved using different production cell lines and cell lines producing other antibodies or biologics than IgG1. However, a current patent on using any PDK inhibitors for industrial applications, including DCA, exists (Follstat 2002) leaving only genetic engineering approaches, e.g. knocking-down of PDKs, to be used for commercial production processes.

The current B-DMFA method requires a model with degrees of redundancy to estimate metabolic fluxes (Chapter 3). Therefore, B-DMFA is not able to estimate fluxes of the pentose phosphate pathway unlike MFA. A method that is able to work with a metabolic model with residual degrees of freedom based on flux balance analysis would be required (Varma & Palsson 1994b).

References

Abbot, EL, McCormack, JG, Reynet, C, Hassall, DG, Buchan, KW & Yeaman, SJ 2005, 'Diverging regulation of pyruvate dehydrogenase kinase isoform gene expression in cultured human muscle cells', *FEBS Journal*, vol. 272, no. 12, pp. 3004-14.

Ahn, WS & Antoniewicz, MR 2011, 'Metabolic flux analysis of CHO cells at growth and non-growth phases using isotopic tracers and mass spectrometry', *Metabolic Engineering*, vol. 13, no. 5, pp. 598-609.

Al-Fageeh, MB, Marchant, RJ, Carden, MJ & Smales, CM 2006, 'The cold-shock response in cultured mammalian cells: Harnessing the response for the improvement of recombinant protein production', *Biotechnology and Bioengineering*, vol. 93, no. 5, pp. 829-35.

Al-Rubeai, M, Emery, AN, Chalder, S & Jan, DC 1992, 'Specific Monoclonal-Antibody Productivity and the Cell Cycle-Comparisons of Batch, Continuous and Perfusion Cultures', *Cytotechnology*, vol. 9, no. 1-3, pp. 85-97.

Altamirano, C, Illanes, A, Becerra, S, Cairo, JJ & Godia, F 2006, 'Considerations on the lactate consumption by CHO cells in the presence of galactose', *Journal of Biotechnology*, vol. 125, no. 4, pp. 547-56.

Altamirano, C, Illanes, A, Becerra, S, Cairó, JJ & Gòdia, F 2006, 'Considerations on the lactate consumption by CHO cells in the presence of galactose', *Journal of Biotechnology*, vol. 125, no. 4, pp. 547-56.

Altamirano, C, Illanes, A, Casablancas, A, Gámez, X, Cairó, JJ & Gòdia, C 2001, 'Analysis of CHO cells metabolic redistribution in a glutamate-based defined medium in continuous culture', *Biotechnology Progress*, vol. 17, no. 6, pp. 1032-41.

Altamirano, C, Paredes, C, Cairó, JJ & Gòdia, F 2000, 'Improvement of CHO cell culture medium formulation: Simultaneous substitution of glucose and glutamine', *Biotechnology Progress*, vol. 16, no. 1, pp. 69-75.

Altamirano, C, Paredes, C, Illanes, A, Cairó, JJ & Gòdia, F 2004, 'Strategies for fed-batch cultivation of t-PA producing CHO cells: Substitution of glucose and glutamine and rational design of culture medium', *Journal of Biotechnology*, vol. 110, no. 2, pp. 171-9.

Antoniewicz, MR 2013a, 'Dynamic metabolic flux analysis-tools for probing transient states of metabolic networks', *Current Opinion in Biotechnology*.

Antoniewicz, MR, Kelleher, JK & Stephanopoulos, G 2006, 'Determination of confidence intervals of metabolic fluxes estimated from stable isotope measurements', *Metab Eng*, vol. 8, no. 4, pp. 324-37.

Antoniewicz, MR, Kraynie, DF, Laffend, LA, Gonzalez-Lergier, J, Kelleher, JK & Stephanopoulos, G 2007, 'Metabolic flux analysis in a nonstationary system: Fed-batch fermentation of a high yielding strain of E. coli producing 1,3-propanediol', *Metabolic Engineering*, vol. 9, no. 3, pp. 277-92.

Archer, SL, Gomberg-Maitland, M, Maitland, ML, Rich, S, Garcia, JGN & Weir, EK 2008, 'Mitochondrial metabolism, redox signaling, and fusion: a mitochondria-ROS-HIF-1 alpha-

Kv1.5 O-2-sensing pathway at the intersection of pulmonary hypertension and cancer', *American Journal of Physiology-Heart and Circulatory Physiology*, vol. 294, no. 2, pp. H570-H8.

Atkinson, DE & Walton, GM 1967, 'Adenosine triphosphate conservation in metabolic regulation. Rat liver citrate cleavage enzyme', *Journal of Biological Chemistry*, vol. 242, no. 13, pp. 3239-41.

Ayyanathan, K, Kesaraju, S, Dawson-Scully, K & Weissbach, H 2012, 'Combination of sulindac and dichloroacetate kills cancer cells via oxidative damage', *Plos One*, vol. 7, no. 7.

Bailey, E, Stirpe, F & Taylor, CB 1968, 'Regulation of rat liver pyruvate kinase. The effect of preincubation, pH, copper ions, fructose 1,6-diphosphate and dietary changes on enzyme activity', *Biochemical Journal*, vol. 108, no. 3, pp. 427-36.

Baker, JC, Yan, X, Peng, T, Kasten, S & Roche, TE 2000, 'Marked differences between two isoforms of human pyruvate dehydrogenase kinase', *Journal of Biological Chemistry*, vol. 275, no. 21, pp. 15773-81.

Barbosa-Tessmann, IP, Chen, C, Zhong, C, Schuster, SM, Nick, HS & Kilberg, MS 1999, 'Activation of the unfolded protein response pathway induces human asparagine synthetase gene expression', *Journal of Biological Chemistry*, vol. 274, no. 44, pp. 31139-44.

Barbosa-Tessmann, IP, Chen, C, Zhong, C, Siu, F, Schuster, SM, Nick, HS & Kilberg, MS 2000, 'Activation of the human asparagine synthetase gene by the amino acid response and the endoplasmic reticulum stress response pathways occurs by common genomic elements', *Journal of Biological Chemistry*, vol. 275, no. 35, pp. 26976-85.

Barbosa-Tessmann, IP, Pineda, VL, Nick, HS, Schuster, SM & Kilberg, MS 1999, 'Transcriptional regulation of the human asparagine synthetase gene by carbohydrate availability', *Biochemical Journal*, vol. 339, no. 1, pp. 151-8.

Becker, J, Klopprogge, C, Zelder, O, Heinzle, E & Wittmann, C 2005, 'Amplified expression of fructose 1,6-bisphosphatase in Corynebacterium glutamicum increases in vivo flux through the pentose phosphate pathway and lysine production on different carbon sources', *Applied and Environmental Microbiology*, vol. 71, no. 12, pp. 8587-96.

Bersin, RM & Stacpoole, PW 1997, 'Dichloroacetate as metabolic therapy for myocardial ischemia and failure', *American Heart Journal*, vol. 134, no. 5 I, pp. 841-55.

Bi, JX, Shuttleworth, J & Ai-Rubeai, M 2004, 'Uncoupling of cell growth and proliferation results in enhancement of productivity in p21(C1P1)-arrested CHO cells', *Biotechnology and Bioengineering*, vol. 85, no. 7, pp. 741-9.

Boghigian, BA, Seth, G, Kiss, R & Pfeifer, BA 2010, 'Metabolic flux analysis and pharmaceutical production', *Metabolic Engineering*, vol. 12, no. 2, pp. 81-95.

Bollati-Fogolin, M, Forno, G, Nimtz, M, Conradt, HS, Etcheverrigaray, M & Kratje, R 2005, 'Temperature reduction in cultures of hGM-CSF-expressing CHO cells: Effect on productivity and product quality', *Biotechnology Progress*, vol. 21, no. 1, pp. 17-21.

Bonarius, HP, Hatzimanikatis, V, Meesters, KP, de Gooijer, CD, Schmid, G & Tramper, J 1996, 'Metabolic flux analysis of hybridoma cells in different culture media using mass balances', *Biotechnology and Bioengineering*, vol. 50, no. 3, pp. 299-318.

Bonnet, S, Archer, SL, Allalunis-Turner, J, Haromy, A, Beaulieu, C, Thompson, R, Lee, CT, Lopaschuk, GD, Puttagunta, L, Harry, G, Hashimoto, K, Porter, CJ, Andrade, MA, Thebaud, B & Michelakis, ED 2007, 'A mitochondria-K+ channel axis is suppressed in cancer and its normalization promotes apoptosis and inhibits cancer growth', *Cancer Cell*, vol. 11, no. 1, pp. 37-51.

Bowker-Kinley, MM, Davis, WI, Wu, P, Harris, RA & Popov, KM 1998, 'Evidence for existence of tissue-specific regulation of the mammalian pyruvate dehydrogenase complex', *Biochemical Journal*, vol. 329, no. 1, pp. 191-6.

Brüning, A, Matsingou, C, Brem, GJ, Rahmeh, M & Mylonas, I 2012, 'Inhibin beta E is upregulated by drug-induced endoplasmic reticulum stress as a transcriptional target gene of ATF4', *Toxicology and Applied Pharmacology*, vol. 264, no. 2, pp. 300-4.

Budanov, AV & Karin, M 2008, 'p53 Target Genes Sestrin1 and Sestrin2 Connect Genotoxic Stress and mTOR Signaling', *Cell*, vol. 134, no. 3, pp. 451-60.

Burleigh, SC, van de Laar, T, Stroop, CJ, van Grunsven, WM, O'Donoghue, N, Rudd, PM & Davey, GP 2011, 'Synergizing metabolic flux analysis and nucleotide sugar metabolism to understand the control of glycosylation of recombinant protein in CHO cells', *BMC Biotechnology*, vol. 11, p. 95.

Cairns, RA, Papandreou, I, Sutphin, PD & Denko, NC 2007, 'Metabolic targeting of hypoxia and HIF1 in solid tumors can enhance cytotoxic chemotherapy', *Proceedings of the National Academy of Sciences of the United States of America*, vol. 104, no. 22, pp. 9445-50.

Cao, W, Yacoub, S, Shiverick, KT, Namiki, K, Sakai, Y, Porvasnik, S, Urbanek, C & Rosser, CJ 2008, 'Dichloroacetate (DCA) sensitizes both wild-type and over expressing bcl-2 prostate cancer cells in vitro to radiation', *Prostate*, vol. 68, no. 11, pp. 1223-31.

Carvalhal, AV, Marcelino, I & Carrondo, MJT 2003, 'Metabolic changes during cell growth inhibition by p27 overexpression', *Applied Microbiology and Biotechnology*, vol. 63, no. 2, pp. 164-73.

Chang, ACM, Jellinek, DA & Reddel, RR 2003, 'Mammalian stanniocalcins and cancer', *Endocrine-Related Cancer*, vol. 10, no. 3, pp. 359-73.

Chang, RYK, Etheridge, N, Dodd, P & Nouwens, A 2014, 'Quantitative multiple reaction monitoring analysis of synaptic proteins from human brain', *Journal of Neuroscience Methods*, no. 0.

Chen, KQ, Liu, Q, Xie, LZ, Sharp, PA & Wang, DIC 2001, 'Engineering of a mammalian cell line for reduction of lactate formation and high monoclonal antibody production', *Biotechnology and Bioengineering*, vol. 72, no. 1, pp. 55-61.

Christensen, KE & MacKenzie, RE 2006, 'Mitochondrial one-carbon metabolism is adapted to the specific needs of yeast, plants and mammals', *BioEssays*, vol. 28, no. 6, pp. 595-605.

Corradetti, MN, Inoki, K & Guan, KL 2005, 'The stress-inducted proteins RTP801 and RTP801L are negative regulators of the mammalian target of rapamycin pathway', *Journal of Biological Chemistry*, vol. 280, no. 11, pp. 9769-72.

Coskun, P, Wyrembak, J, Schriner, SE, Chen, HW, Marciniack, C, Laferla, F & Wallace, DC 2012, 'A mitochondrial etiology of Alzheimer and Parkinson disease', *Biochimica et Biophysica Acta - General Subjects*, vol. 1820, no. 5, pp. 553-64.

Costa Leite, T, Da Silva, D, Guimarães Coelho, R, Zancan, P & Sola-Penna, M 2007, 'Lactate favours the dissociation of skeletal muscle 6-phosphofructo-1- kinase tetramers down-regulating the enzyme and muscle glycolysis', *Biochemical Journal*, vol. 408, no. 1, pp. 123-30.

Cox, MG 1972, 'The numerical evaluation of B-splines', *IMA Journal of Applied Mathematics*, vol. 10, no. 2, pp. 134-49.

Cruz, HJ, Freitas, CM, Alves, PM, Moreira, JL & Carrondo, MJT 2000, 'Effects of ammonia and lactate on growth, metabolism, and productivity of BHK cells', *Enzyme and Microbial Technology*, vol. 27, no. 1-2, pp. 43-52.

Cruz, HJ, Moreira, JL & Carrondo, MJT 1999, 'Metabolic shifts by nutrient manipulation in continuous cultures of BHK cells', *Biotechnology and Bioengineering*, vol. 66, no. 2, pp. 104-13.

Cui, H, Darmanin, S, Natsuisaka, M, Kondo, T, Asaka, M, Shindoh, M, Higashino, F, Hamuro, J, Okada, F, Kobayashi, M, Nakagawa, K & Koide, H 2007, 'Enhanced expression of asparagine synthetase under glucose-deprived conditions protects pancreatic cancer cells from apoptosis induced by glucose deprivation and cisplatin', *Cancer Research*, vol. 67, no. 7, pp. 3345-55.

Culp, PA, Choi, D, Zhang, Y, Yin, J, Seto, P, Ybarra, SE, Su, M, Sho, M, Steinle, R, Wong, MHL, Evangelista, F, Grove, J, Cardenas, M, James, M, Hsi, ED, Chao, DT, Powers, DB, Ramakrishnan, V & Dubridge, R 2010, 'Antibodies to TWEAK receptor inhibit human tumor growth through dual mechanisms', *Clinical Cancer Research*, vol. 16, no. 2, pp. 497-508.

Curry, HB & Schoenberg, IJ 1947, 'On Spline Distributions and Their Limits - the Polya Distribution Functions', *Bulletin of the American Mathematical Society*, vol. 53, no. 11, pp. 1114-.

Curry, HB & Schoenberg 1966, 'On Pólya frequency functions IV: the fundamental spline functions and their limits', *Journal d'analyse mathématique*, vol. 17, no. 1, pp. 71-107.

Daly, S, Cotter, A, Molloy, AE & Scott, J 2005, 'Homocysteine and folic acid: Implications for pregnancy', *Seminars in Vascular Medicine*, vol. 5, no. 2, pp. 190-200.

De Boor, C 1972, 'On calculating with B-splines', *Journal of Approximation Theory*, vol. 6, no. 1, pp. 50-62.

DeBerardinis, RJ, Mancuso, A, Daikhin, E, Nissim, I, Yudkoff, M, Wehrli, S & Thompson, CB 2007, 'Beyond aerobic glycolysis: Transformed cells can engage in glutamine metabolism that exceeds the requirement for protein and nucleotide synthesis', *Proceedings of the National Academy of Sciences of the United States of America*, vol. 104, no. 49, pp. 19345-50.

DeBerardinis, RJ, Sayed, N, Ditsworth, D & Thompson, CB 2008, 'Brick by brick: metabolism and tumor cell growth', *Current Opinion in Genetics & Development*, vol. 18, no. 1, pp. 54-61.

Di Pietro, E, Wang, XL & MacKenzie, RE 2004, 'The expression of mitochondrial methylenetetrahydrofolate dehydrogenase-cyclohydrolase supports a role in rapid cell growth', *Biochimica et Biophysica Acta - General Subjects*, vol. 1674, no. 1, pp. 78-84.

Dietmair, S, Hodson, MP, Quek, LE, Timmins, NE, Gray, P & Nielsen, LK 2012, 'A multi-omics analysis of recombinant protein production in Hek293 cells', *Plos One*, vol. 7, no. 8.

Dietmair, S, Nielsen, LK & Timmins, NE 2011, 'Engineering a mammalian super producer', *Journal of Chemical Technology and Biotechnology*, vol. 86, no. 7, pp. 905-14.

Dietmair, S, Timmins, NE, Gray, PP, Nielsen, LK & Kromer, JO 2010, 'Towards quantitative metabolomics of mammalian cells: Development of a metabolite extraction protocol', *Analytical Biochemistry*, vol. 404, no. 2, pp. 155-64.

Dietmair, S, Timmins, NE, Gray, PP, Nielsen, LK & Krömer, JO 2010, 'Towards quantitative metabolomics of mammalian cells: development of a metabolite extraction protocol', *Analytical Biochemistry*, vol. 404, no. 2, pp. 155-64.

Dorai, H, Yun, SK, Ellis, D, Kinney, C, Lin, C, Jan, D, Moore, G & Betenbaugh, MJ 2009, 'Expression of anti-apoptosis genes alters lactate metabolism of Chinese Hamster ovary cells in culture', *Biotechnology and Bioengineering*, vol. 103, no. 3, pp. 592-608.

Du, P, Kibbe, WA & Lin, SM 2007, 'NuID: A universal naming scheme of oligonucleotides for Illumina, Affymetrix, and other microarrays', *Biology Direct*, vol. 2.

Du, P, Kibbe, WA & Lin, SM 2008, 'lumi: A pipeline for processing Illumina microarray', *Bioinformatics*, vol. 24, no. 13, pp. 1547-8.

Duarte, NC, Becker, SA, Jamshidi, N, Thiele, I, Mo, ML, Vo, TD, Srivas, R & Palsson, BØ 2007, 'Global reconstruction of the human metabolic network based on genomic and bibliomic data', *Proceedings of the National Academy of Sciences of the United States of America*, vol. 104, no. 6, pp. 1777-82.

Dunbar, EM, Coats, BS, Shroads, AL, Langaee, T, Lew, A, Forder, JR, Shuster, JJ, Wagner, DA & Stacpoole, PW 2013, 'Phase 1 trial of dichloroacetate (DCA) in adults with recurrent malignant brain tumors', *Investigational New Drugs*, pp. 1-13.

Durocher, Y & Butler, M 2009, 'Expression systems for therapeutic glycoprotein production', *Current Opinion in Biotechnology*, vol. 20, no. 6, pp. 700-7.

Ecker DM, RT 2013, 'Mammalian Cell Culture Capacity for Biopharmaceutical Manufacturing', *Adv Biochem Eng Biotechnol*.

Ellisen, LW, Ramsayer, KD, Johannessen, CM, Yang, A, Beppu, H, Minda, K, Oliner, JD, McKeon, F & Haber, DA 2002, 'REDD1, a developmentally regulated transcriptional target of p63 and p53, links p63 to regulation of reactive oxygen species', *Molecular Cell*, vol. 10, no. 5, pp. 995-1005.

Elorza, A, Soro-Arnáiz, I, Meléndez-Rodríguez, F, Rodríguez-Vaello, V, Marsboom, G, de Cárcer, G, Acosta-Iborra, B, Albacete-Albacete, L, Ordóñez, A, Serrano-Oviedo, L, Giménez-Bachs, JM, Vara-Vega, A, Salinas, A, Sánchez-Prieto, R, Martín del Río, R, Sánchez-Madrid, F, Malumbres, M, Landázuri, MO & Aragonés, J 2012, 'HIF2α Acts as an mTORC1 Activator through the Amino Acid Carrier SLC7A5', *Molecular Cell*, vol. 48, no. 5, pp. 681-91.

Essler, S, Dehne, N & Brüne, B 2009, 'Role of sestrin2 in peroxide signaling in macrophages', *FEBS Letters*, vol. 583, no. 21, pp. 3531-5.

Fendt, SM & Sauer, U 2010, 'Transcriptional regulation of respiration in yeast metabolizing differently repressive carbon substrates', *Bmc Systems Biology*, vol. 4.

Fiebiger, W, Olszewski, U, Ulsperger, E, Geissler, K & Hamilton, G 2011, 'In vitro cytotoxicity of novel platinum-based drugs and dichloroacetate against lung carcinoid cell lines', *Clinical and Translational Oncology*, vol. 13, no. 1, pp. 43-9.

Fitzpatrick, L, Jenkins, HA & Butler, M 1993, 'Glucose and glutamine metabolism of a murine B-lymphocyte hybridoma grown in batch culture', *APPL.BIOCHEM.BIOTECHNOL.*, vol. 43, no. 2, pp. 93-116.

Flavin, DF 2010, 'Non-hodgkin's lymphoma reversal with dichloroacetate', *Journal of Oncology*.

Fogolin, MB, Wagner, R, Etcheverrigaray, M & Kratje, R 2004, 'Impact of temperature reduction and expression of yeast pyruvate carboxylase on hGM-CSF-producing CHO cells', *Journal of Biotechnology*, vol. 109, no. 1-2, pp. 179-91.

Follstat, B, D. 2002, *Improvement of cell culture performance*, patent, WO 02/04598 A2.

Fox, SR, Patel, UA, Yap, MGS & Wang, DIC 2004, 'Maximizing interferon-gamma production by Chinese hamster ovary cells through temperature shift optimization: Experimental and modeling', *Biotechnology and Bioengineering*, vol. 85, no. 2, pp. 177-84.

Frame, KK & Hu, WS 1990, 'Cell-Volume Measurement as an Estimation of Mammalian-Cell Biomass', *Biotechnology and Bioengineering*, vol. 36, no. 2, pp. 191-7.

Furukawa, K & Ohsuye, K 1998, 'Effect of culture temperature on a recombinant CHO cell line producing a C-terminal alpha-amidating enzyme', *Cytotechnology*, vol. 26, no. 2, pp. 153-64.

Gagnon, M, Hiller, G, Luan, YT, Kittredge, A, Defelice, J & Drapeau, D 2011, 'High-End pH-controlled delivery of glucose effectively suppresses lactate accumulation in CHO Fed-batch cultures', *Biotechnology and Bioengineering*, vol. 108, no. 6, pp. 1328-37.

Gambhir, A, Korke, R, Lee, J, Fu, PC, Europa, A & Hu, WS 2003, 'Analysis of cellular metabolism of hybridoma cells at distinct physiological states', *Journal of Bioscience and Bioengineering*, vol. 95, no. 4, pp. 317-27.

Ganapathy, V, Thangaraju, M & Prasad, PD 2009, 'Nutrient transporters in cancer: Relevance to Warburg hypothesis and beyond', *Pharmacology and Therapeutics*, vol. 121, no. 1, pp. 29-40.

Gao, HX, Campbell, SR, Burkly, LC, Jakubowski, A, Jarchum, I, Banas, B, Saleem, MA, Mathieson, PW, Berman, JW, Michaelson, JS & Putterman, C 2009, 'TNF-like weak inducer of apoptosis (TWEAK) induces inflammatory and proliferative effects in human kidney cells', *Cytokine*, vol. 46, no. 1, pp. 24-35.

Garber, K 2006, 'Energy deregulation: licensing tumors to grow', *Science*, vol. 312, no. 5777, pp. 1158-9.

Gatenby, RA & Gillies, RJ 2004, 'Why do cancers have high aerobic glycolysis?', *Nature Reviews Cancer*, vol. 4, no. 11, pp. 891-9.

Girgenrath, M, Weng, S, Kostek, CA, Browning, B, Wang, M, Brown, SAN, Winkles, JA, Michaelson, JS, Allaire, N, Schneider, P, Scott, ML, Hsu, YM, Yagita, H, Flavell, RA, Miller, JB, Burkly, LC & Zheng, TS 2006, 'TWEAK, via its receptor Fn14, is a novel regulator of mesenchymal progenitor cells and skeletal muscle regeneration', *EMBO Journal*, vol. 25, no. 24, pp. 5826-39.

Glacken, MW, Fleischaker, RJ & Sinskey, AJ 1986, 'REDUCTION OF WASTE PRODUCT EXCRETION VIA NUTRIENT CONTROL: POSSIBLE STRATEGIES FOR MAXIMIZING PRODUCT AND CELL YIELDS ON SERUM IN CULTURES OF MAMMALIAN CELLS', *Biotechnology and Bioengineering*, vol. 28, no. 9, pp. 1376-89.

Glacken, MW, Huang, C & Sinskey, AJ 1989, 'MATHEMATICAL DESCRIPTIONS OF HYBRIDOMA CULTURE KINETICS .3. SIMULATION OF FED-BATCH BIOREACTORS', *Journal of Biotechnology*, vol. 10, no. 1, pp. 39-65.

Godia, F & Cairo, JJ 2006, 'Cell Metabolism', in SS Ozturk & WS Hu (eds), *Cell Culture Technology for Pharmaceutical and Cell-Based Therapies*, CSC Press Taylor & Francis Group, Boca Raton.

Goetze, AM, Liu, YD, Zhang, Z, Shah, B, Lee, E, Bondarenko, PV & Flynn, GC 2011, 'High-mannose glycans on the Fc region of therapeutic IgG antibodies increase serum clearance in humans', *Glycobiology*, vol. 21, no. 7, pp. 949-59.

Gong, SS, Guerrini, L & Basilico, C 1991, 'Regulation of asparagine synthetase gene expression by amino acid starvation', *Molecular and Cellular Biology*, vol. 11, no. 12, pp. 6059-66.

Goudar, CT, Biener, R, Konstantinov, KB & Piret, JM 2009, 'Error propagation from prime variables into specific rates and metabolic fluxes for mammalian cells in perfusion culture', *Biotechnol Prog*, vol. 25, no. 4, pp. 986-98.

Gozzelino, R, Jeney, V & Soares, MP 2010, *Mechanisms of cell protection by heme Oxygenase-1*, 03621642 (ISSN), <http://www.scopus.com/inward/record.url?eid=2-s2.0-77949525185&partnerID=40&md5=f5dbe665448b3a33442de6e10afcf520>.

Green, DR, Galluzzi, L & Kroemer, G 2011, 'Mitochondria and the autophagy-inflammation-cell death axis in organismal aging', *Science*, vol. 333, no. 6046, pp. 1109-12.

Guo, X, Dixit, V, Liu, H, Shroads, AL, Henderson, GN, James, MO & Stacpoole, PW 2006, 'Inhibition and recovery of rat hepatic glutathione S-transferase zeta and alteration of tyrosine metabolism following dichloroacetate exposure and withdrawal', *Drug Metabolism and Disposition*, vol. 34, no. 1, pp. 36-42.

Gurd, BJ, Peters, SJ, Heigenhauser, GJF, LeBlanc, PJ, Doherty, TJ, Paterson, DH & Kowalchuk, JM 2008, 'O2 uptake kinetics, pyruvate dehydrogenase activity, and muscle deoxygenation in young and older adults during the transition to moderate-intensity exercise', *American Journal of Physiology - Regulatory Integrative and Comparative Physiology*, vol. 294, no. 2, pp. R577-R84.

Gutierrez-Aguilar, R, Kim, DH, Casimir, M, Dai, XQ, Pfluger, PT, Park, J, Haller, A, Donelan, E, D'Alessio, D, Woods, SC, MacDonald, PE & Seeley, RJ 2013, 'The role of the transcription factor ETV5 in insulin exocytosis', *Diabetologia*, pp. 1-9.

Hanahan, D & Weinberg, RA 2011, 'Hallmarks of Cancer: The Next Generation', *Cell*, vol. 144, no. 5, pp. 646-74.

Hanberry, BS, Berger, R & Zastre, JA 2014, 'High-dose vitamin B1 reduces proliferation in cancer cell lines analogous to dichloroacetate', *Cancer Chemotherapy and Pharmacology*, pp. 1-10.

Harding, HP, Zhang, Y, Bertolotti, A, Zeng, H & Ron, D 2000, 'Perk is essential for translational regulation and cell survival during the unfolded protein response', *Molecular Cell*, vol. 5, no. 5, pp. 897-904.

Hashimoto, O, Sekiyama, K, Matsuo, T & Hasegawa, Y 2009, 'Implication of activin E in glucose metabolism: Transcriptional regulation of the inhibin/activin βE subunit gene in the liver', *Life Sciences*, vol. 85, no. 13-14, pp. 534-40.

Hassell, T, Gleave, S & Butler, M 1991, 'Growth inhibition in animal cell culture - The effect of lactate and ammonia', *Applied Biochemistry and Biotechnology*, vol. 30, no. 1, pp. 29-41.

Hayter, PM, Curling, EMA, Baines, AJ, Jenkins, N, Salmon, I, Strange, PG, Tong, JM & Bull, AT 1992, 'Glucose-limited chemostat culture of Chinese hamster ovary cells producing recombinant human interferon-γ', *Biotechnology and Bioengineering*, vol. 39, no. 3, pp. 327-35.

Heshe, D, Hoogestraat, S, Brauckmann, C, Karst, U, Boos, J & Lanvers-Kaminsky, C 2010, 'Dichloroacetate metabolically targeted therapy defeats cytotoxicity of standard anticancer drugs', *Cancer Chemotherapy and Pharmacology*, pp. 1-9.

Hsu, PP & Sabatini, DM 2008, 'Cancer cell metabolism: Warburg and beyond', *Cell*, vol. 134, no. 5, pp. 703-7.

Huang, B, Gudi, R, Wu, P, Harris, RA, Hamilton, J & Popov, KM 1998, 'Isoenzymes of pyruvate dehydrogenase phosphatase. DNA-derived amino acid sequences, expression, and regulation', *Journal of Biological Chemistry*, vol. 273, no. 28, pp. 17680-8.

Hue, L & Taegtmeyer, H 2009, 'The Randle cycle revisited: A new head for an old hat', *American Journal of Physiology - Endocrinology and Metabolism*, vol. 297, no. 3, pp. E578-E91.

Hur, H, Xuan, Y, Kim, YB, Lee, G, Shim, W, Yun, J, Ham, IH & Han, SU 2013, 'Expression of pyruvate dehydrogenase kinase-1 in gastric cancer as a potential therapeutic target', *International Journal of Oncology*, vol. 42, no. 1, pp. 44-54.

Hutson, RG & Kilberg, MS 1994, 'Cloning of rat asparagine synthetase and specificity of the amino acid-dependent control of its mRNA content', *Biochemical Journal*, vol. 304, no. 3, pp. 745-50.

Irani, N, Wirth, M, Van Den Heuvel, J & Wagner, R 1999, 'Improvement of the primary metabolism of cell cultures by introducing a new cytoplasmic pyruvate carboxylase reaction', *Biotechnology and Bioengineering*, vol. 66, no. 4, pp. 238-46.

Ishiguro, T, Ishiguro, M, Ishiguro, R & Iwai, S 2012, 'Cotreatment with dichloroacetate and omeprazole exhibits a synergistic antiproliferative effect on malignant tumors', *Oncology Letters*, vol. 3, no. 3, pp. 726-8.

Jakubowski, A, Ambrose, C, Parr, M, Lincecum, JM, Wang, MZ, Zheng, TS, Browning, B, Michaelson, JS, Baestcher, M, Wang, B, Bissell, DM & Burkly, LC 2005, 'TWEAK induces liver progenitor cell proliferation', *Journal of Clinical Investigation*, vol. 115, no. 9, pp. 2330-40.

Jeoung, NH & Harris, RA 2008, 'Pyruvate dehydrogenase kinase-4 deficiency lowers blood glucose and improves glucose tolerance in diet-induced obese mice', *American Journal of Physiology - Endocrinology and Metabolism*, vol. 295, no. 1, pp. E46-E54.

Jiang, J, Westberg, JA & Andersson, LC 2012, 'Stanniocalcin 2, forms a complex with heme oxygenase 1, binds hemin and is a heat shock protein', *Biochemical and Biophysical Research Communications*, vol. 421, no. 2, pp. 274-9.

Jones, RG & Thompson, CB 2009, 'Tumor suppressors and cell metabolism: a recipe for cancer growth', *Genes & Development*, vol. 23, no. 5, pp. 537-48.

Kalpouzos, G, Chételat, G, Baron, JC, Landeau, B, Mevel, K, Godeau, C, Barré, L, Constans, JM, Viader, F, Eustache, F & Desgranges, B 2009, 'Voxel-based mapping of brain gray matter volume and glucose metabolism profiles in normal aging', *Neurobiology of Aging*, vol. 30, no. 1, pp. 112-24.

Kaufmann, H, Mazur, X, Fussenegger, M & Bailey, JE 1999, 'Influence of low temperature on productivity, proteome and protein phosphorylation of CHO cells', *Biotechnology and Bioengineering*, vol. 63, no. 5, pp. 573-82.

Kay, LD, Osborn, MJ, Hatefi, Y & Huennekens, FM 1960, 'The enzymatic conversion of N5-formyl tetrahydrofolic acid (folinic acid) to N10-formyl tetrahydrofolic acid', *The Journal of biological chemistry*, vol. 235, pp. 195-201.

Kim, JW & Dang, CV 2006, 'Cancer's molecular sweet tooth and the Warburg effect', *Cancer Research*, vol. 66, no. 18, pp. 8927-30.

Kim, JW, Tchernyshyov, I, Semenza, GL & Dang, CV 2006, 'HIF-1-mediated expression of pyruvate dehydrogenase kinase: A metabolic switch required for cellular adaptation to hypoxia', *Cell Metabolism*, vol. 3, no. 3, pp. 177-85.

Kim, KM, Kingsmore, SF, Han, H, Yang-Feng, TL, Godinot, N, Seldin, MF, Caron, MG & Giros, B 1994, 'Cloning of the human glycine transporter type 1: Molecular and pharmacological characterization of novel isoform variants and chromosomal localization of the gene in the human and mouse genomes', *Molecular Pharmacology*, vol. 45, no. 4, pp. 608-17.

Kim, SH & Lee, GM 2007, 'Down-regulation of lactate dehydrogenase-A by siRNAs for reduced lactic acid formation of Chinese hamster ovary cells producing thrombopoietin', *Applied Microbiology and Biotechnology*, vol. 74, no. 1, pp. 152-9.

Kim, YI 2003, 'Role of Folate in Colon Cancer Development and Progression', *Journal of Nutrition*, vol. 133, no. 11 SUPPL. 1, pp. 3731S-9S.

Kolobova, E, Tuganova, A, Boulatnikov, I & Popov, KM 2001, 'Regulation of pyruvate dehydrogenase activity through phosphorylation at multiple sites', *Biochemical Journal*, vol. 358, no. 1, pp. 69-77.

Korotchkina, LG & Patel, MS 1995, 'Mutagenesis studies of the phosphorylation sites of recombinant human pyruvate dehydrogenase. Site-specific regulation', *Journal of Biological Chemistry*, vol. 270, no. 24, pp. 14297-304.

Korotchkina, LG & Patel, MS 2001, 'Site Specificity of Four Pyruvate Dehydrogenase Kinase Isoenzymes toward the Three Phosphorylation Sites of Human Pyruvate Dehydrogenase', *Journal of Biological Chemistry*, vol. 276, no. 40, pp. 37223-9.

Koukourakis, MI, Giatromanolaki, A, Sivridis, E, Gatter, KC & Harris, AL 2005, 'Pyruvate dehydrogenase and pyruvate dehydrogenase kinase expression in non small cell lung cancer and tumor-associated stroma', *Neoplasia*, vol. 7, no. 1, pp. 1-6.

Kroemer, G & Pouyssegur, J 2008, 'Tumor cell metabolism: Cancer's Achilles' heel', *Cancer Cell*, vol. 13, no. 6, pp. 472-82.

Kumar, A, Kant, S & Singh, SM 2012, 'Novel molecular mechanisms of antitumor action of dichloroacetate against T cell lymphoma: Implication of altered glucose metabolism, pH homeostasis and cell survival regulation', *Chemico-Biological Interactions*, vol. 199, no. 1, pp. 29-37.

Kumar, A, Kant, S & Singh, SM 2013, 'Antitumor and chemosensitizing action of dichloroacetate implicates modulation of tumor microenvironment: A role of reorganized glucose metabolism, cell survival regulation and macrophage differentiation', *Toxicology and Applied Pharmacology*, vol. 273, no. 1, pp. 196-208.

Kumar, K, Wigfield, S, Gee, HE, Devlin, CM, Singleton, D, Li, JL, Buffa, F, Huffman, M, Sinn, AL, Silver, J, Turley, H, Leek, R, Harris, AL & Ivan, M 2013, 'Dichloroacetate reverses the hypoxic adaptation to bevacizumab and enhances its antitumor effects in mouse xenografts', *Journal of Molecular Medicine*, vol. 91, no. 6, pp. 749-58.

Kumar, N, Gammell, P & Clynes, M 2007, 'Proliferation control strategies to improve productivity and survival during CHO based production culture - A summary of recent methods employed and the effects of proliferation control in product secreting CHO cell lines', *Cytotechnology*, vol. 53, no. 1-3, pp. 33-46.

Kushiyama, A, Shojima, N, Ogihara, T, Inukai, K, Sakoda, H, Fujishiro, M, Fukushima, Y, Anai, M, Ono, H, Horike, N, Viana, AYI, Uchijima, Y, Nishiyama, K, Shimosawa, T, Fujita, T, Katagiri, H, Oka, Y, Kurihara, H & Asano, T 2005, 'Resistin-like molecule β activates MAPKs, suppresses insulin signaling in hepatocytes, and induces diabetes, hyperlipidemia, and fatty liver in transgenic mice on a high fat diet', *Journal of Biological Chemistry*, vol. 280, no. 51, pp. 42016-25.

Kuwae, S, Ohda, T, Tamashima, H, Miki, H & Kobayashi, K 2005, 'Development of a fed-batch culture process for enhanced production of recombinant human antithrombin by Chinese hamster ovary cells', *Journal of Bioscience and Bioengineering*, vol. 100, no. 5, pp. 502-10.

Langheinrich, C & Nienow, AW 1999, 'Control of pH in large-scale, free suspension animal cell bioreactors: Alkali addition and pH excursions', *Biotechnology and Bioengineering*, vol. 66, no. 3, pp. 171-9.

Lantum, HBM, Cornejo, J, Pierce, RH & Anders, MW 2003, 'Perturbation of maleylacetoacetic acid metabolism in rats with dichloroacetic acid-induced glutathione transferase zeta deficiency', *Toxicological Sciences*, vol. 74, no. 1, pp. 192-202.

Lao, MS & Toth, D 1997, 'Effects of ammonium and lactate on growth and metabolism of a recombinant Chinese hamster ovary cell culture', *Biotechnology Progress*, vol. 13, no. 5, pp. 688-91.

Leighty, RW & Antoniewicz, MR 2011, 'Dynamic metabolic flux analysis (DMFA): A framework for determining fluxes at metabolic non-steady state', *Metabolic Engineering*, vol. 13, no. 6, pp. 745-55.

Lengwehasatit, I & Dickson, AJ 2002, 'Analysis of the role of GADD153 in the control of apoptosis in NS0 myeloma cells', *Biotechnology and Bioengineering*, vol. 80, no. 7, pp. 719-30.

Lequeux, G, Beauprez, J, Maertens, J, Van Horen, E, Soetaert, W, Vandamme, E & Vanrolleghem, PA 2010, 'Dynamic Metabolic Flux Analysis Demonstrated on Cultures Where the Limiting Substrate Is Changed from Carbon to Nitrogen and Vice Versa', *Journal of Biomedicine and Biotechnology*.

Li, J, Kato, M & Chuang, DT 2009, 'Pivotal role of the C-terminal DW-motif in mediating inhibition of pyruvate dehydrogenase kinase 2 by dichloroacetate', *Journal of Biological Chemistry*, vol. 284, no. 49, pp. 34458-67.

Li, J, Wong, CL, Vijayasankaran, N, Hudson, T & Amanullah, A 2012, 'Feeding lactate for CHO cell culture processes: Impact on culture metabolism and performance', *Biotechnology and Bioengineering*, vol. 109, no. 5, pp. 1173-86.

Li, WJ, James, MO, McKenzie, SC, Calcutt, NA, Liu, C & Stacpoole, PW 2011, 'Mitochondrion as a Novel Site of Dichloroacetate Biotransformation by Glutathione Transferase zeta 1', *Journal of Pharmacology and Experimental Therapeutics*, vol. 336, no. 1, pp. 87-94.

Lim, Y, Wong, NSC, Lee, YY, Ku, SCY, Wong, DCF & Yap, MGS 2010, 'Engineering mammalian cells in bioprocessing - current achievements and future perspectives', *Biotechnology and Applied Biochemistry*, vol. 55, pp. 175-89.

Lin, HJ, Hsieh, FC, Song, H & Lin, J 2005, 'Elevated phosphorylation and activation of PDK-1/AKT pathway in human breast cancer', *British Journal of Cancer*, vol. 93, no. 12, pp. 1372-81.

Lin, SM, Du, P, Huber, W & Kibbe, WA 2008, 'Model-based variance-stabilizing transformation for Illumina microarray data', *Nucleic Acids Research*, vol. 36, no. 2.

Linn, TC, Pelley, JW, Pettit, FH, Hucho, F, Randall, DD & Reed, LJ 1972, 'α-Keto acid dehydrogenase complexes. XV. Purification and properties of the component enzymes of the pyruvate dehydrogenase complexes from bovine kidney and heart', *Archives of Biochemistry and Biophysics*, vol. 148, no. 2, pp. 327-42.

Linn, TC, Pettit, FH & Reed, LJ 1969, 'Alpha-keto acid dehydrogenase complexes. X. Regulation of the activity of the pyruvate dehydrogenase complex from beef kidney mitochondria by phosphorylation and dephosphorylation', *Proceedings of the National Academy of Sciences of the United States of America*, vol. 62, no. 1, pp. 234-41.

Linster, CL, Van Schaftingen, E & Hanson, AD 2013, 'Metabolite damage and its repair or pre-emption', *Nature Chemical Biology*, vol. 9, no. 2, pp. 72-80.

Liu, CL, Wu, J, Zhu, J, Kuei, C, Yu, JX, Shelton, J, Sutton, SW, Li, X, Yun, SJ, Mirzadegan, T, Mazur, C, Kamme, F & Lovenberg, TW 2009, 'Lactate Inhibits Lipolysis in Fat Cells through Activation of an Orphan G-protein-coupled Receptor, GPR81', *Journal of Biological Chemistry*, vol. 284, no. 5, pp. 2811-22.

Llaneras, F & Pico, J 2007, 'A procedure for the estimation over time of metabolic fluxes in scenarios where measurements are uncertain and/or insufficient', *BMC Bioinformatics*, vol. 8.

Lloyd, DR, Holmes, P, Jackson, LP, Emery, AN & Al-Rubeai, M 2000, 'Relationship between cell size, cell cycle and specific recombinant protein productivity', *Cytotechnology*, vol. 34, no. 1-2, pp. 59-70.

Lu, CW, Lin, SC, Chen, KF, Lai, YY & Tsai, SJ 2008, 'Induction of pyruvate dehydrogenase kinase-3 by hypoxia-inducible factor-1 promotes metabolic switch and drug resistance', *Journal of Biological Chemistry*, vol. 283, no. 42, pp. 28106-14.

Lucock, M 2000, 'Folic acid: Nutritional biochemistry, molecular biology, and role in disease processes', *Molecular Genetics and Metabolism*, vol. 71, no. 1-2, pp. 121-38.

Ma, NN, Ellet, J, Okediadi, C, Hermes, P, McCormick, E & Casnocha, S 2009, 'A Single Nutrient Feed Supports Both Chemically Defined NS0 and CHO Fed-Batch Processes: Improved Productivity and Lactate Metabolism', *Biotechnology Progress*, vol. 25, no. 5, pp. 1353-63.

Madhok, BM, Yeluri, S, Perry, SL, Hughes, TA & Jayne, DG 2010, 'Dichloroacetate induces apoptosis and cell-cycle arrest in colorectal cancer cells', *British Journal of Cancer*, vol. 102, no. 12, pp. 1746-52.

Mahadevan, R, Edwards, JS & Doyle, FJ 2002, 'Dynamic flux balance analysis of diauxic growth in Escherichia coli', *Biophysical Journal*, vol. 83, no. 3, pp. 1331-40.

Mannherz, HG & Goody, RS 1974, 'The molecular basis of contractility. Part I', *Basic Research in Cardiology*, vol. 69, no. 1, pp. 88-104.

Margineantu, DH, Brown, RM, Brown, GK, Marcus, AH & Capaldi, RA 2002, 'Heterogeneous distribution of pyruvate dehydrogenase in the matrix of mitochondria', *Mitochondrion*, vol. 1, no. 4, pp. 327-38.

Marinho-Carvalho, MM, Costa-Mattos, PV, Spitz, GA, Zancan, P & Sola-Penna, M 2009, 'Calmodulin upregulates skeletal muscle 6-phosphofructo-1-kinase reversing the inhibitory effects of allosteric modulators', *Biochimica et Biophysica Acta - Proteins and Proteomics*, vol. 1794, no. 8, pp. 1175-80.

Martin, AJ, Friston, KJ, Colebatch, JG & Frackowiak, RSJ 1991, 'Decreases in regional cerebral blood flow with normal aging', *Journal of Cerebral Blood Flow and Metabolism*, vol. 11, no. 4, pp. 684-9.

Martínez, V, Gerdtzen, ZP, Andrews, BA & Asenjo, JA 2010, 'Viral vectors for the treatment of alcoholism: Use of metabolic flux analysis for cell cultivation and vector production', *Metabolic Engineering*, vol. 12, no. 2, pp. 129-37.

Martínez, VS, Dietmair, S, Quek, LE, Hodson, MP, Gray, P & Nielsen, LK 2013, 'Flux balance analysis of CHO cells before and after a metabolic switch from lactate production to consumption', *Biotechnology and Bioengineering*, vol. 110, no. 2, pp. 660-6.

Matasci, M, Hacker, DL, Baldi, L & Wurm, FM 2008, 'Recombinant therapeutic protein production in cultivated mammalian cells: current status and future prospects', *Drug Discovery Today: Technologies*, vol. 5, no. 2-3, pp. e37-e42.

Mattson, MP & Shea, TB 2003, 'Folate and homocysteine metabolism in neural plasticity and neurodegenerative disorders', *Trends in Neurosciences*, vol. 26, no. 3, pp. 137-46.

McFate, T, Mohyeldin, A, Lu, H, Thakar, J, Henriques, J, Halim, ND, Wu, H, Schell, MJ, Tsang, TM, Teahan, O, Zhou, S, Califano, JA, Jeoung, NH, Harris, RA & Verma, A 2008, 'Pyruvate dehydrogenase complex activity controls metabolic and malignant phenotype in cancer cells', *Journal of Biological Chemistry*, vol. 283, no. 33, pp. 22700-8.

Meadows, AL, Karnik, R, Lam, H, Forestell, S & Snedecor, B 2010, 'Application of dynamic flux balance analysis to an industrial Escherichia coli fermentation', *Metabolic Engineering*, vol. 12, no. 2, pp. 150-60.

Mejia, NR & MacKenzie, RE 1985, 'NAD-dependent methylenetetrahydrofolate dehydrogenase is expressed by immortal cells', *Journal of Biological Chemistry*, vol. 260, no. 27, pp. 14616-20.

Michelakis, ED, McMurtry, MS, Wu, XC, Dyck, JRB, Moudgil, R, Hopkins, TA, Lopaschuk, GD, Puttagunta, L, Waite, R & Archer, SL 2002, 'Dichloroacetate, a metabolic modulator, prevents and reverses chronic hypoxic pulmonary hypertension in rats: Role of increased expression and activity of voltage-gated potassium channels', *Circulation*, vol. 105, no. 2, pp. 244-50.

Michelakis, ED, Sutendra, G, Dromparis, P, Webster, L, Haromy, A, Niven, E, Maguire, C, Gammer, TL, Mackey, JR, Fulton, D, Abdulkarim, B, McMurtry, MS & Petruk, KC 2010, 'Metabolic modulation of glioblastoma with dichloroacetate', *Science Translational Medicine*, vol. 2, no. 31.

Michelakis, ED, Webster, L & Mackey, JR 2008, 'Dichloroacetate (DCA) as a potential metabolic-targeting therapy for cancer', *British Journal of Cancer*, vol. 99, no. 7, pp. 989-94.

Miller, WM, Blanch, HW & Wilke, CR 2000, 'A kinetic analysis of hybridoma growth and metabolism in batch and continuous suspension culture: Effect of nutrient concentration, dilution rate, and pH (Reprinted from Biotechnology and Bioengineering, vol 32, pg 947-965, 1988)', *Biotechnology and Bioengineering*, vol. 67, no. 6, pp. 853-71.

Miller, WM, Wilke, CR & Blanch, HW 1988, 'TRANSIENT RESPONSES OF HYBRIDOMA METABOLISM TO CHANGES IN THE OXYGEN-SUPPLY RATE IN CONTINUOUS CULTURE', *Bioprocess Engineering*, vol. 3, no. 3, pp. 103-11.

Moat, SJ, Lang, D, McDowell, IFW, Clarke, ZL, Madhavan, AK, Lewis, MJ & Goodfellow, J 2004, 'Folate, homocysteine, endothelial function and cardiovascular disease', *Journal of Nutritional Biochemistry*, vol. 15, no. 2, pp. 64-79.

Moon, B, Kwan, JJM, Duddy, N, Sweeney, G & Begum, N 2003, 'Resistin inhibits glucose uptake in L6 cells independently of changes in insulin signaling and GLUT4 translocation', *American Journal of Physiology - Endocrinology and Metabolism*, vol. 285, no. 1 48-1, pp. E106-E15.

Moore, A, Mercer, J, Dutina, G, Donahue, CJ, Bauer, KD, Mather, JP, Etcheverry, T & Ryll, T 1997, 'Effects of temperature shift on cell cycle, apoptosis and nucleotide pools in CHO cell batch cultures', *Cytotechnology*, vol. 23, no. 1-3, pp. 47-54.

Murray, K, Gull, K & Dickson, AJ 1996, 'Dichloroacetate increases cell and antibody yields in batch cultures of a hybridoma cell line', *Biotechnology and Bioengineering*, vol. 49, no. 4, pp. 377-82.

Nahapetian, AT, Thomas, JN & Thilly, WG 1986, 'Optimization of environment for high density Vero cell culture: effect of dissolved oxygen and nutrient supply on cell growth and changes in metabolites', *Journal of Cell Science*, vol. 81, pp. 65-103.

Nance, JR, Dowling, JJ, Gibbs, EM & Bönnemann, CG 2012, 'Congenital myopathies: An update', *Current Neurology and Neuroscience Reports*, vol. 12, no. 2, pp. 165-74.

Neermann, J & Wagner, R 1996, 'Comparative analysis of glucose and glutamine metabolism in transformed mammalian cell lines, insect and primary liver cells', *Journal of Cellular Physiology*, vol. 166, no. 1, pp. 152-69.

Neilson, AP, Djuric, Z, Land, S & Kato, I 2011, 'Plasma levels of resistin-like molecule beta in humans', *Cancer Epidemiology*, vol. 35, no. 5, pp. 485-9.

Newland, M, Kamal, MN, Greenfield, PF & Nielsen, LK 1994, 'Communication to the editor ammonia inhibition of hybridomas propagated in batch, fed-batch, and continuous culture', *Biotechnology and Bioengineering*, vol. 43, no. 5, pp. 434-8.

Nielsen, J 2003, 'It is all about metabolic fluxes', *Journal of Bacteriology*, vol. 185, no. 24, pp. 7031-5.

Nielsen, J & Villadsen, J 2003, *Bioreaction engineering principles*, 2nd edn, Kluwer Academic/Plenum Publishers, New York; London.

Nielsen, LK, Reid, S & Greenfield, PF 1997, 'Cell cycle model to describe animal cell size variation and lag between cell number and biomass dynamics', *Biotechnology and Bioengineering*, vol. 56, no. 4, pp. 372-9.

Niewisch, MR, Kuçi, Z, Wolburg, H, Sautter, M, Krampen, L, Deubzer, B, Handgretinger, R & Bruchelt, G 2012, 'Influence of dichloroacetate (DCA) on lactate production and oxygen consumption in neuroblastoma cells: Is DCA a suitable drug for neuroblastoma therapy?', *Cellular Physiology and Biochemistry*, vol. 29, no. 3-4, pp. 373-80.

Niklas, J, Schrader, E, Sandig, V, Noll, T & Heinzle, E 2011, 'Quantitative characterization of metabolism and metabolic shifts during growth of the new human cell line AGE1.HN using time resolved metabolic flux analysis', *Bioprocess and Biosystems Engineering*, vol. 34, no. 5, pp. 533-45.

Nilsson, R, Jain, M, Madhusudhan, N, Sheppard, NG, Strittmatter, L, Kampf, C, Huang, J, Asplund, A & Mootha, VK 2014, 'Metabolic enzyme expression highlights a key role for MTHFD2 and the mitochondrial folate pathway in cancer.', *Nat Commun*.

Nyberg, GB, Balcarcel, RR, Follstad, BD, Stephanopoulos, G & Wang, DI 1999, 'Metabolic effects on recombinant interferon-gamma glycosylation in continuous culture of Chinese hamster ovary cells', *Biotechnology and Bioengineering*, vol. 62, no. 3, pp. 336-47.

Oh, S, Shin, S & Janknecht, R 2012, 'ETV1, 4 and 5: An oncogenic subfamily of ETS transcription factors', *Biochimica et Biophysica Acta - Reviews on Cancer*, vol. 1826, no. 1, pp. 1-12.

Ohashi, T, Akazawa, T, Aoki, M, Kuze, B, Mizuta, K, Ito, Y & Inoue, N 2013, 'Dichloroacetate improves immune dysfunction caused by tumor-secreted lactic acid and increases antitumor immunoreactivity', *International Journal of Cancer*, vol. 133, no. 5, pp. 1107-18.

Oyadomari, S & Mori, M 2004, 'Roles of CHOP/GADD153 in endoplasmic reticulum stress', *Cell Death and Differentiation*, vol. 11, no. 4, pp. 381-9.

Ozturk, SS & Palsson, BO 1990, 'Chemical decomposition of glutamine in cell culture media: effect of media type, pH, and serum concentration', *Biotechnol Prog*, vol. 6, no. 2, pp. 121-8.

Ozturk, SS, Riley, MR & Palsson, BO 1992, 'Effects of ammonia and lactate on hybridoma growth, metabolism, and antibody production', *Biotechnology and Bioengineering*, vol. 39, no. 4, pp. 418-31.

Pacis, E, Yu, M, Autsen, J, Bayer, R & Li, F 2011, 'Effects of cell culture conditions on antibody N-linked glycosylation-what affects high mannose 5 glycoform', *Biotechnology and Bioengineering*, vol. 108, no. 10, pp. 2348-58.

Papandreou, I, Cairns, RA, Fontana, L, Lim, AL & Denko, NC 2006, 'HIF-1 mediates adaptation to hypoxia by actively downregulating mitochondrial oxygen consumption', *Cell Metabolism*, vol. 3, no. 3, pp. 187-97.

Papandreou, I, Goliasova, T & Denko, NC 2011, 'Anticancer drugs that target metabolism: Is dichloroacetate the new paradigm?', *International Journal of Cancer*, vol. 128, no. 5, pp. 1001-8.

Paredes, C, Prats, E, Cairo, JJ, Azorin, F, Cornudella, L & Godia, F 1999, 'Modification of glucose and glutamine metabolism in hybridoma cells through metabolic engineering', *Cytotechnology*, vol. 30, no. 1-3, pp. 85-93.

Patel, MS & Korotchkina, LG 2006, 'Regulation of the pyruvate dehydrogenase complex', *Biochemical Society Transactions*, vol. 34, no. 2, pp. 217-22.

Pelletier, JN & MacKenzie, RE 1995, 'Binding and interconversion of tetrahydrofolates at a single site in the bifunctional methylenetetrahydrofolate dehydrogenase/cyclohydrolase', *Biochemistry*, vol. 34, no. 39, pp. 12673-80.

Peri, KG & MacKenzie, RE 1993, 'NAD+-dependent methylenetetrahydrofolate dehydrogenase-cyclohydrolase: Detection of the mRNA in normal murine tissues and transcriptional regulation of the gene in cell lines', *BBA - Gene Structure and Expression*, vol. 1171, no. 3, pp. 281-7.

Petch, D & Butler, M 1994, 'Profile of energy metabolism in a murine hybridoma: Glucose and glutamine utilization', *Journal of Cellular Physiology*, vol. 161, no. 1, pp. 71-6.

Peters, SJ, Harris, RA, Heigenhauser, GJF & Spriet, LL 2001, 'Muscle fiber type comparison of PDH kinase activity and isoform expression in fed and fasted rats', *American Journal of Physiology - Regulatory Integrative and Comparative Physiology*, vol. 280, no. 3 49-3, pp. R661-R8.

Popov, KM, Hawes, JW & Harris, RA 1997, 'Mitochondrial alpha-ketoacid dehydrogenase kinases: a new family of protein kinases', *Advances in second messenger and phosphoprotein research*, vol. 31, pp. 105-11.

Prautzsch, H, Boehm, W & Paluszny, M 2002, *Bezier and B-spline techniques*, Springer, Berlin.

Quek, LE, Dietmair, S, Kromer, JO & Nielsen, LK 2010, 'Metabolic flux analysis in mammalian cell culture', *Metabolic Engineering*, vol. 12, no. 2, pp. 161-71.

Quek, LE & Nielsen, LK 2008a, 'On the reconstruction of the Mus musculus genome-scale metabolic network model', *Genome Informatics*, vol. 21, pp. 89-100.

Quek, LE, Dietmair, S, Hanscho, M, Martinez, VS, Borth, N, Nilesen, LK 2014, 'Reducing Recon 2 for steady-state flux analysis of HEK cell culture', *Journal of Biotechnology*, vol. 184, pp. 172-178.

Rahim, S & Üren, A 2013, 'Emergence of ETS transcription factors as diagnostic tools and therapeutic targets in prostate cancer', *American Journal of Translational Research*, vol. 5, no. 3, pp. 254-68.

Rajala, MW, Obici, S, Scherer, PE & Rossetti, L 2003, 'Adipose-derived resistin and gut-derived resistin-like molecule-β selectively impair insulin action on glucose production', *Journal of Clinical Investigation*, vol. 111, no. 2, pp. 225-30.

Randle, PJ, Garland, PB, Hales, CN & Newsholme, EA 1963, 'THE GLUCOSE FATTY-ACID CYCLE ITS ROLE IN INSULIN SENSITIVITY AND THE METABOLIC DISTURBANCES OF DIABETES MELLITUS', *The Lancet*, vol. 281, no. 7285, pp. 785-9.

Regen, DM, Davis, WW, Morgan, HE & Park, CR 1964, 'THE REGULATION OF HEXOKINASE AND PHOSPHOFRUCTOKINASE ACTIVITY IN HEART', *The Journal of biological chemistry*, vol. 239, pp. 43-9.

Roche, TE, Baker, JC, Yan, X, Hiromasa, Y, Gong, X, Peng, T, Dong, J, Turkan, A & Kasten, SA 2001, *Distinct regulatory properties of pyruvate dehydrogenase kinase and phosphatase isoforms*, 00796603 (ISSN); 0125400705 (ISBN); 9780125400701 (ISBN), <http://www.scopus.com/inward/record.url?eid=2-s2.0-0035224979&partnerID=40&md5=033ccda55ccabc80c3efc3393eff1c5d>.

Roche, TE & Hiromasa, Y 2007, 'Pyruvate dehydrogenase kinase regulatory mechanisms and inhibition in treating diabetes, heart ischemia, and cancer', *Cellular and Molecular Life Sciences*, vol. 64, no. 7-8, pp. 830-49.

Ross, JM, Öberg, J, Brené, S, Coppotelli, G, Terzioglu, M, Pernold, K, Goiny, M, Sitnikov, R, Kehr, J, Trifunovic, A, Larsson, NG, Hoffer, BJ & Olson, L 2010, 'High brain lactate is a hallmark of aging and caused by a shift in the lactate dehydrogenase A/B ratio', *Proceedings of the National Academy of Sciences of the United States of America*, vol. 107, no. 46, pp. 20087-92.

Sale, GJ & Randle, PJ 1981, 'Analysis of site occupancies in [32P]phosphorylated pyruvate dehydrogenase complexes by aspartyl-prolyl cleavage of tryptic phosphopeptides', *European Journal of Biochemistry*, vol. 120, no. 3, pp. 535-40.

Samuvel, DJ, Sundararaj, KP, Nareika, A, Lopes-Virella, MF & Huang, Y 2009, 'Lactate boosts TLR4 signaling and NF-κB pathway-mediated gene transcription in macrophages via monocarboxylate transporters and MD-2 up-regulation', *Journal of Immunology*, vol. 182, no. 4, pp. 2476-84.

Sanfeliu, A, Paredes, C, Cairó, JJ & Gódia, F 1997, 'Identification of key patterns in the metabolism of hybridoma cells in culture', *Enzyme and Microbial Technology*, vol. 21, no. 6, pp. 421-8.

Sanz, AB, Sanchez-Niño, MD, Izquierdo, MC, Jakubowski, A, Justo, P, Blanco-Colio, LM, Ruiz-Ortega, M, Egido, J & Ortiz, A 2009, 'Tweak induces proliferation in renal tubular epithelium: A role in uninephrectomy induced renal hyperplasia', *Journal of Cellular and Molecular Medicine*, vol. 13, no. 9 B, pp. 3329-42.

Schöneberg, T, Kloos, M, Brüser, A, Kirchberger, J & Sträter, N 2013, 'Structure and allosteric regulation of eukaryotic 6-phosphofructokinases', *Biological Chemistry*, vol. 394, no. 8, pp. 977-93.

Schwartz, DR & Lazar, MA 2011, 'Human resistin: Found in translation from mouse to man', *Trends in Endocrinology and Metabolism*, vol. 22, no. 7, pp. 259-65.

Semenza, GL 2010a, 'Defining the role of hypoxia-inducible factor 1 in cancer biology and therapeutics', *Oncogene*, vol. 29, no. 5, pp. 625-34.

Semenza, GL 2010b, 'HIF-1: upstream and downstream of cancer metabolism', *Current Opinion in Genetics & Development*, vol. 20, no. 1, pp. 51-6.

Shahrzad, S, Lacombe, K, Adamcic, U, Minhas, K & Coomber, BL 2010, 'Sodium dichloroacetate (DCA) reduces apoptosis in colorectal tumor hypoxia', *Cancer Letters*, vol. 297, no. 1, pp. 75-83.

Sharfstein, ST, Tucker, SN, Mancuso, A, Blanch, HW & Clark, DS 1994, 'Quantitative in vivo nuclear magnetic resonance studies of hybridoma metabolism', *Biotechnology and Bioengineering*, vol. 43, no. 11, pp. 1059-74.

Sheikh, K, Forster, J & Nielsen, LK 2005, 'Modeling Hybridoma Cell Metabolism Using a Generic Genome-Scale Metabolic Model of *Mus musculus*', *Biotechnol Prog*, vol. 21, no. 1, pp. 112-21.

Shen, YC, Ou, DL, Hsu, C, Lin, KL, Chang, CY, Lin, CY, Liu, SH & Cheng, AL 2013, 'Activating oxidative phosphorylation by a pyruvate dehydrogenase kinase inhibitor overcomes sorafenib resistance of hepatocellular carcinoma', *British Journal of Cancer*, vol. 108, no. 1, pp. 72-81.

Shoshani, T, Faerman, A, Mett, I, Zelin, E, Tenne, T, Gorodin, S, Moshel, Y, Elbaz, S, Budanov, A, Chajut, A, Kalinski, H, Kamer, I, Rozen, A, Mor, O, Keshet, E, Leshkowitz, D, Einat, P, Skaliter, R & Feinstein, E 2002, 'Identification of a novel hypoxia-inducible factor 1-responsive gene, RTP801, involved in apoptosis', *Molecular and Cellular Biology*, vol. 22, no. 7, pp. 2283-93.

Singh, V 1996, 'On-line measurement of oxygen uptake in cell culture using the dynamic method', *Biotechnology and Bioengineering*, vol. 52, no. 3, pp. 443-8.

Siu, F, Bain, PJ, Leblanc-Chaffin, R, Chen, H & Kilberg, MS 2002, 'ATF4 is a mediator of the nutrient-sensing response pathway that activates the human asparagine synthetase gene', *Journal of Biological Chemistry*, vol. 277, no. 27, pp. 24120-7.

Škalamera, D, Dahmer, M, Purdon, AS, Wilson, BM, Ranall, MV, Blumenthal, A, Gabrielli, B & Gonda, TJ 2012, 'Generation of a Genome Scale Lentiviral Vector Library for EF1α Promoter-Driven Expression of Human ORFs and Identification of Human Genes Affecting Viral Titer', *Plos One*, vol. 7, no. 12.

Smith, GK, Banks, SD, Monaco, TJ, Rigual, R, Duch, DS, Mullin, RJ & Huber, BE 1990, 'Activity of an NAD-dependent 5,10-methylenetetrahydrofolate dehydrogenase in normal tissue, neoplastic cells, and oncogene-transformed cells', *Archives of Biochemistry and Biophysics*, vol. 283, no. 2, pp. 367-71.

Smyth, GK (ed.) 2005, *Limma: linear models for microarray data.*, Bioinformatics and Computational Biology Solutions using R and Bioconductor, Springer, New York.

Sofer, A, Lei, K, Johannessen, CM & Ellisen, LW 2005, 'Regulation of mTOR and cell growth in response to energy stress by REDD1', *Molecular and Cellular Biology*, vol. 25, no. 14, pp. 5834-45.

Sonnleitner, B & Kappeli, O 1986, 'Growth of Saccharomyces-Cerevisiae Is Controlled by Its Limited Respiratory Capacity - Formulation and Verification of a Hypothesis', *Biotechnology and Bioengineering*, vol. 28, no. 6, pp. 927-37.

Sorokina, LV, Pyatchanina, TV, Didenko, GV, Kaplia, AA & Khyzhnyak, SV 2011, 'The influence of sodium dichloroacetate on the oxidative processes in sarcoma 37', *Experimental Oncology*, vol. 33, no. 4, pp. 216-21.

Stacpoole, PW 1997, 'Lactic acidosis and other mitochondrial disorders', *Metabolism: Clinical and Experimental*, vol. 46, no. 3, pp. 306-21.

Stacpoole, PW 2012, 'The pyruvate dehydrogenase complex as a therapeutic target for age-related diseases', *Aging Cell*.

Stacpoole, PW, Henderson, GN, Yan, Z, Cornett, R & James, MO 1998, 'Pharmacokinetics, metabolism, and toxicology of dichloroacetate', *Drug Metabolism Reviews*, vol. 30, no. 3, pp. 499-539.

Stacpoole, PW, Kurtz, TL, Han, ZC & Langaee, T 2008, 'Role of dichloroacetate in the treatment of genetic mitochondrial diseases', *Advanced Drug Delivery Reviews*, vol. 60, no. 13-14, pp. 1478-87.

Stacpoole, PW, Moore, GW & Kornhauser, DM 1978, 'Metabolic effects of dichloroacetate in patients with diabetes mellitus and hyperlipoproteinemia', *New England Journal of Medicine*, vol. 298, no. 10, pp. 526-30.

Stacpoole, PW, Nagaraja, NV & Hutson, AD 2003, 'Efficacy of dichloroacetate as a lactate-lowering drug', *Journal of Clinical Pharmacology*, vol. 43, no. 7, pp. 683-91.

Steppan, CM, Bailey, ST, Bhat, S, Brown, EJ, Banerjee, RR, Wright, CM, Patel, HR, Ahima, RS & Lazar, MA 2001, 'The hormone resistin links obesity to diabetes', *Nature*, vol. 409, no. 6818, pp. 307-12.

Steppan, CM, Brown, EJ, Wright, CM, Bhat, S, Banerjee, RR, Dai, CY, Enders, GH, Silberg, DG, Wen, X, Wu, GD & Lazar, MA 2001, 'A family of tissue-specific resistin-like

molecules', *Proceedings of the National Academy of Sciences of the United States of America*, vol. 98, no. 2, pp. 502-6.

Stockwin, LH, Yu, SX, Borgel, S, Hancock, C, Wolfe, TL, Phillips, LR, Hollingshead, MG & Newton, DL 2010, 'Sodium dichloroacetate selectively targets cells with defects in the mitochondrial ETC', *International Journal of Cancer*, vol. 127, no. 11, pp. 2510-9.

Su, N & Kilberg, MS 2008, 'C/EBP homology protein (CHOP) interacts with activating transcription factor 4 (ATF4) and negatively regulates the stress-dependent induction of the asparagine synthetase gene', *Journal of Biological Chemistry*, vol. 283, no. 50, pp. 35106-17.

Sugden, MC, Bulmer, K, Augustine, D & Holness, MJ 2001, 'Selective modification of pyruvate dehydrogenase kinase isoform expression in rat pancreatic islets elicited by starvation and activation of peroxisome proliferator-activated receptor-α: Implications for glucose-stimulated insulin secretion', *Diabetes*, vol. 50, no. 12, pp. 2729-36.

Sugden, MC & Holness, MJ 2006, 'Mechanisms underlying regulation of the expression and activities of the mammalian pyruvate dehydrogenase kinases', *Archives of Physiology and Biochemistry*, vol. 112, no. 3, pp. 139-49.

Sugden, MC, Kraus, A, Harris, RA & Holness, MJ 2000, 'Fibre-type specific modification of the activity and regulation of skeletal muscle pyruvate dehydrogenase kinase (PDK) by prolonged starvation and refeeding is associated with targeted regulation of PDK isoenzyme 4 expression', *Biochemical Journal*, vol. 346, no. 3, pp. 651-7.

Sugden, MC, Langdown, ML, Harris, RA & Holness, MJ 2000, 'Expression and regulation of pyruvate dehydrogenase kinase isoforms in the developing rat heart and in adulthood: role of thyroid hormone status and lipid supply', *Biochemical Journal*, vol. 352, pp. 731-8.

Sugden, PH & Randle, PJ 1978, 'Regulation of pig heart pyruvate dehydrogenase by phosphorylation. Studies on the subunit and phosphorylation stoicheiometries', *Biochemical Journal*, vol. 173, no. 2, pp. 659-68.

Sugito, T, Mineshiba, F, Zheng, C, Cotrim, AP, Goldsmith, CM & Baum, BJ 2009, 'Transient TWEAK overexpression leads to a general salivary epithelial cell proliferation', *Oral Diseases*, vol. 15, no. 1, pp. 76-81.

Sugiura, T, Nagano, Y, Inoue, T & Hirotani, K 2004, 'A novel mitochondrial C1-tetrahydrofolate synthetase is upregulated in human colon adenocarcinoma', *Biochemical and Biophysical Research Communications*, vol. 315, no. 1, pp. 204-11.

Sun, RC, Board, PG & Blackburn, AC 2011, 'Targeting metabolism with arsenic trioxide and dichloroacetate in breast cancer cells', *Molecular Cancer*, vol. 10.

Sun, RC, Fadia, M, Dahlstrom, JE, Parish, CR, Board, PG & Blackburn, AC 2010, 'Reversal of the glycolytic phenotype by dichloroacetate inhibits metastatic breast cancer cell growth in vitro and in vivo', *Breast Cancer Research and Treatment*, vol. 120, no. 1, pp. 253-60.

Tanaka, T, Harano, Y, Sue, F & Morimura, H 1967, 'Crystallization, characterization and metabolic regulation of two types of pyruvate kinase isolated from rat tissues', *Journal of Biochemistry*, vol. 62, no. 1, pp. 71-91.

Teague, WM, Pettit, FH, Yeaman, SJ & Reed, LJ 1979, 'Function of phosphorylation sites on pyruvate dehydrogenase', *Biochemical and Biophysical Research Communications*, vol. 87, no. 1, pp. 244-52.

Tendler, SJB, Threadgill, MD & Tisdale, MJ 1987, 'Activities of serine hydroxymethyltransferase in murine tissues and tumours', *Cancer Letters*, vol. 36, no. 1, pp. 65-9.

Vallino, JJ & Stephanopoulos, G 1993, 'Metabolic Flux Distributions in Corynebacterium-Glutamicum during Growth and Lysine Overproduction', *Biotechnology and Bioengineering*, vol. 41, no. 6, pp. 633-46.

van der Heijden, RTJM, Romein, B, Heijnen, JJ, Hellinga, C & Luyben, KCAM 1994, 'Linear constraint relations in biochemical reaction systems: II. Diagnosis and estimation of gross errors', *Biotechnology and Bioengineering*, vol. 43, no. 1, pp. 11-20.

Vander Heiden, MG, Cantley, LC & Thompson, CB 2009, 'Understanding the Warburg Effect: The Metabolic Requirements of Cell Proliferation', *Science*, vol. 324, no. 5930, pp. 1029-33.

Varma, A & Palsson, BO 1994a, 'Metabolic Flux Balancing - Basic Concepts, Scientific and Practical Use', *Bio-Technology*, vol. 12, no. 10, pp. 994-8.

Varma, A & Palsson, BO 1994c, 'Stoichiometric flux balance models quantitatively predict growth and metabolic by-product secretion in wild-type Escherichia coli W3110', *Applied and Environmental Microbiology*, vol. 60, no. 10, pp. 3724-31.

Vella, S, Conti, M, Tasso, R, Cancedda, R & Pagano, A 2012, 'Dichloroacetate inhibits neuroblastoma growth by specifically acting against malignant undifferentiated cells', *International Journal of Cancer*, vol. 130, no. 7, pp. 1484-93.

Wagner, R 1997, *Metabolic control of animal cell culture processes*, Mammalian Cell Biotechnology in Protein Production, Walter de Gruyter, Berlin.

Walsh, G 2010, 'Biopharmaceutical benchmarks 2010', *Nature Biotechnology*, vol. 28, no. 9, pp. 917-24.

Wang, NS & Stephanopoulos, G 1983, 'Application of macroscopic balances to the identification of gross measurement errors', *Biotechnology and Bioengineering*, vol. 25, no. 9, pp. 2177-208.

Warburg, O 1956, 'ORIGIN OF CANCER CELLS', *Science*, vol. 123, no. 3191, pp. 309-14.

Warburg, O, Wind, F & Negelein, E 1927, 'The metabolism of tumors in the body', *Journal of General Physiology*, vol. 8, no. 6, pp. 519-30.

Weber, G 1969, 'Regulation of pyruvate kinase', *Advances in Enzyme Regulation*, vol. 7, no. C, pp. 15-40.

Weber, G, Lea, MA & Stamm, NB 1967, 'Inhibition of pyruvate kinase and glucokinase by acetyl CoA and inhibition of glucokinase by phosphoenolpyruvate', *Life Sciences*, vol. 6, no. 22, pp. 2441-52.

Wek, RC, Jiang, HY & Anthony, TG 2006, 'Coping with stress: EIF2 kinases and translational control', *Biochemical Society Transactions*, vol. 34, no. 1, pp. 7-11.

Whitehouse, S, Cooper, RH & Randle, PJ 1974, 'Mechanism of activation of pyruvate dehydrogenase by dichloroacetate and other halogenated carboxylic acids', *Biochemical Journal*, vol. 141, no. 3, pp. 761-74.

Wigfield, SM, Winter, SC, Giatromanolaki, A, Taylor, J, Koukourakis, ML & Harris, AL 2008, 'PDK-1 regulates lactate production in hypoxia and is associated with poor prognosis in head and neck squamous cancer', *British Journal of Cancer*, vol. 98, no. 12, pp. 1975-84.

Williamson, JR & Cooper, RH 1980, 'Regulation of the citric acid cycle in mammalian systems', *FEBS Letters*, vol. 117, Supplement 1, no. 0, pp. K73-K85.

Wlaschin, KF & Hu, WS 2007, 'Engineering cell metabolism for high-density cell culture via manipulation of sugar transport', *Journal of Biotechnology*, vol. 131, no. 2, pp. 168-76.

Wong, JYY, Huggins, GS, Debidda, M, Munshi, NC & De Vivo, I 2008, 'Dichloroacetate induces apoptosis in endometrial cancer cells', *Gynecologic Oncology*, vol. 109, no. 3, pp. 394-402.

Wu, F, Bergstrom, M, Stridsberg, M, Orlefors, H, Eriksson, B, Oberg, K, Watanabe, Y & Langstrom, B 1997, 'Effect of 6-diazo-5-oxo-1-norleucine (DON) on human carcinoid tumor cell aggregates', *Anticancer Research*, vol. 17, no. 4A, pp. 2363-7.

Wu, MY, Wang, PY, Han, SH & Hsieh, SL 1999, 'The cytoplasmic domain of the lymphotoxin-β receptor mediates cell death in HeLa cells', *Journal of Biological Chemistry*, vol. 274, no. 17, pp. 11868-73.

Wu, P, Inskeep, K, Bowker-Kinley, MM, Popov, KM & Harris, RA 1999, 'Mechanism responsible for inactivation of skeletal muscle pyruvate dehydrogenase complex in starvation and diabetes', *Diabetes*, vol. 48, no. 8, pp. 1593-9.

Wu, P, Sato, J, Zhao, Y, Jaskiewicz, J, Popov, KM & Harris, RA 1997, 'Starvation and diabetes increase the amount of pyruvate dehydrogenase kinase isozyme 4 in rat heart', *Faseb Journal*, vol. 11, no. 9, p. 2911.

Wu, PF, Blair, PV, Sato, J, Jaskiewicz, J, Popov, KM & Harris, RA 2000, 'Starvation increases the amount of pyruvate dehydrogenase kinase in several mammalian tissues', *Archives of Biochemistry and Biophysics*, vol. 381, no. 1, pp. 1-7.

Wurm, FM 2004, 'Production of recombinant protein therapeutics in cultivated mammalian cells', *Nature Biotechnology*, vol. 22, no. 11, pp. 1393-8.

Xie, J, Wang, BS, Yu, DH, Lu, Q, Ma, J, Qi, H, Fang, C & Chen, HZ 2011, 'Dichloroacetate shifts the metabolism from glycolysis to glucose oxidation and exhibits synergistic growth

inhibition with cisplatin in HeLa cells', *International Journal of Oncology*, vol. 38, no. 2, pp. 409-17.

Xing, ZZ, Kenty, B, Koyrakh, I, Borys, M, Pan, SH & Li, ZJ 2011, 'Optimizing amino acid composition of CHO cell culture media for a fusion protein production', *Process Biochemistry*, vol. 46, no. 7, pp. 1423-9.

Xu, X, Nagarajan, H, Lewis, NE, Pan, S, Cai, Z, Liu, X, Chen, W, Xie, M, Wang, W, Hammond, S, Andersen, MR, Neff, N, Passarelli, B, Koh, W, Fan, HC, Wang, J, Gui, Y, Lee, KH, Betenbaugh, MJ, Quake, SR, Famili, I, Palsson, BO & Wang, J 2011, 'The genomic sequence of the Chinese hamster ovary (CHO)-K1 cell line', *Nat Biotech*, vol. 29, no. 8, pp. 735-41.

Yamaguchi, H & Wang, HG 2004, 'CHOP is involved in endoplasmic reticulum stress-induced apoptosis by enhancing DR5 expression in human carcinoma cells', *Journal of Biological Chemistry*, vol. 279, no. 44, pp. 45495-502.

Yang, DQ, Gong, XM, Yakhnin, A & Roche, TE 1998, 'Requirements for the adaptor protein role of dihydrolipoyl acetyltransferase in the up-regulated function of the pyruvate dehydrogenase kinase and pyruvate dehydrogenase phosphatase', *Journal of Biological Chemistry*, vol. 273, no. 23, pp. 14130-7.

Yao, J, Hamilton, RT, Cadenas, E & Brinton, RD 2010, 'Decline in mitochondrial bioenergetics and shift to ketogenic profile in brain during reproductive senescence', *Biochimica et Biophysica Acta - General Subjects*, vol. 1800, no. 10, pp. 1121-6.

Ye, J, Kumanova, M, Hart, LS, Sloane, K, Zhang, H, De Panis, DN, Bobrovnikova-Marjon, E, Diehl, JA, Ron, D & Koumenis, C 2010, 'The GCN2-ATF4 pathway is critical for tumour cell survival and proliferation in response to nutrient deprivation', *EMBO Journal*, vol. 29, no. 12, pp. 2082-96.

Yeaman, SJ, Hutcheson, ET, Roche, TE, Pettit, FH, Brown, JR, Reed, LJ, Watson, DC & Dixon, GH 1978, 'SITES OF PHOSPHORYLATION ON PYRUVATE-DEHYDROGENASE FROM BOVINE KIDNEY AND HEART', *Biochemistry*, vol. 17, no. 12, pp. 2364-70.

Yecies, JL, Zhang, HH, Menon, S, Liu, S, Yecies, D, Lipovsky, AI, Gorgun, C, Kwiatkowski, DJ, Hotamisligil, GS, Lee, CH & Manning, BD 2011, 'Akt stimulates hepatic SREBP1c and lipogenesis through parallel mTORC1-dependent and independent pathways', *Cell Metabolism*, vol. 14, no. 2, p. 280.

Yoon, SK, Song, JY & Lee, GM 2003, 'Effect of low culture temperature on specific productivity, transcription level, and heterogeneity of erythropoietin in chinese hamster ovary cells', *Biotechnology and Bioengineering*, vol. 82, no. 3, pp. 289-98.

Young, JD 2013, 'Metabolic flux rewiring in mammalian cell cultures', *Current Opinion in Biotechnology*.

Zancan, P, Almeida, FVR, Faber-Barata, J, Dellias, JM & Sola-Penna, M 2007, 'Fructose-2,6-bisphosphate counteracts guanidinium chloride-, thermal-, and ATP-induced dissociation of skeletal muscle key glycolytic enzyme 6-phosphofructo-1-kinase: A structural mechanism for PFK allosteric regulation', *Archives of Biochemistry and Biophysics*, vol. 467, no. 2, pp. 275-82.

Zancan, P, Marinho-Carvalho, MM, Faber-Barata, J, Dellias, JMM & Sola-Penna, M 2008, 'ATP and fructose-2,6-bisphosphate regulate skeletal muscle 6-phosphofructo-1-kinase by altering its quaternary structure', *IUBMB Life*, vol. 60, no. 8, pp. 526-33.

Zhang, P, McGrath, BC, Reinert, J, Olsen, DS, Lei, L, Gill, S, Wek, SA, Vattem, KM, Wek, RC, Kimball, SR, Jefferson, LS & Cavener, DR 2002, 'The GCN2 eIF2α kinase is required for adaptation to amino acid deprivation in mice', *Molecular and Cellular Biology*, vol. 22, no. 19, pp. 6681-8.

Zheng, LD, Yang, CL, Qi, T, Qi, M, Tong, L & Tong, QS 2012, 'Effects of resistin-like molecule β over-expression on gastric cancer cells in vitro', *World Journal of Gastroenterology*, vol. 18, no. 8, pp. 754-66.

Zhou, M, Crawford, Y, Ng, D, Tung, J, Pynn, AFJ, Meier, A, Yuk, IH, Vijayasankaran, N, Leach, K, Joly, J, Snedecor, B & Shen, A 2011, 'Decreasing lactate level and increasing antibody production in Chinese Hamster Ovary cells (CHO) by reducing the expression of lactate dehydrogenase and pyruvate dehydrogenase kinases', *Journal of Biotechnology*, vol. 153, no. 1-2, pp. 27-34.

Zhou, Q, Lam, PY, Han, D & Cadenas, E 2009, 'Activation of c-Jun-N-terminal kinase and decline of mitochondrial pyruvate dehydrogenase activity during brain aging', *FEBS Letters*, vol. 583, no. 7, pp. 1132-40.

Appendices

Appendix A: B-DMFA Supplementary Material

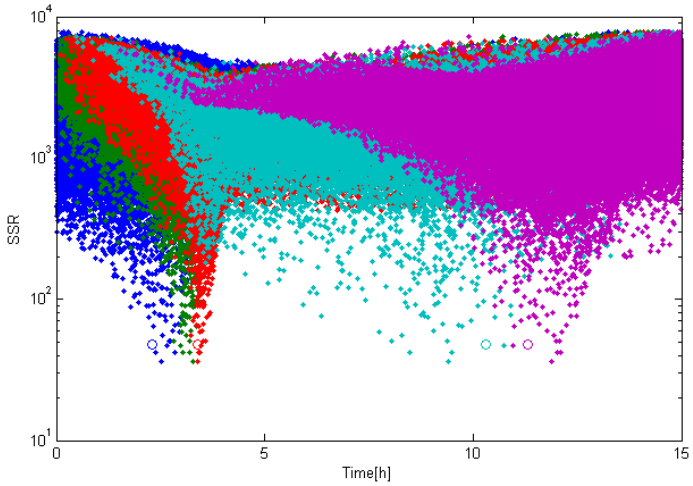

Figure A1: Results of Monte Carlo simulations and heuristic algorithm. The solution of sampling 100,000 sets of knot sequences. The solutions are organized by the SSR. Each colour represents one of the knots of the knot sequence. The solution of the heuristic algorithm is presented with circles, where the second and third knot are located in the same time point (green and red).

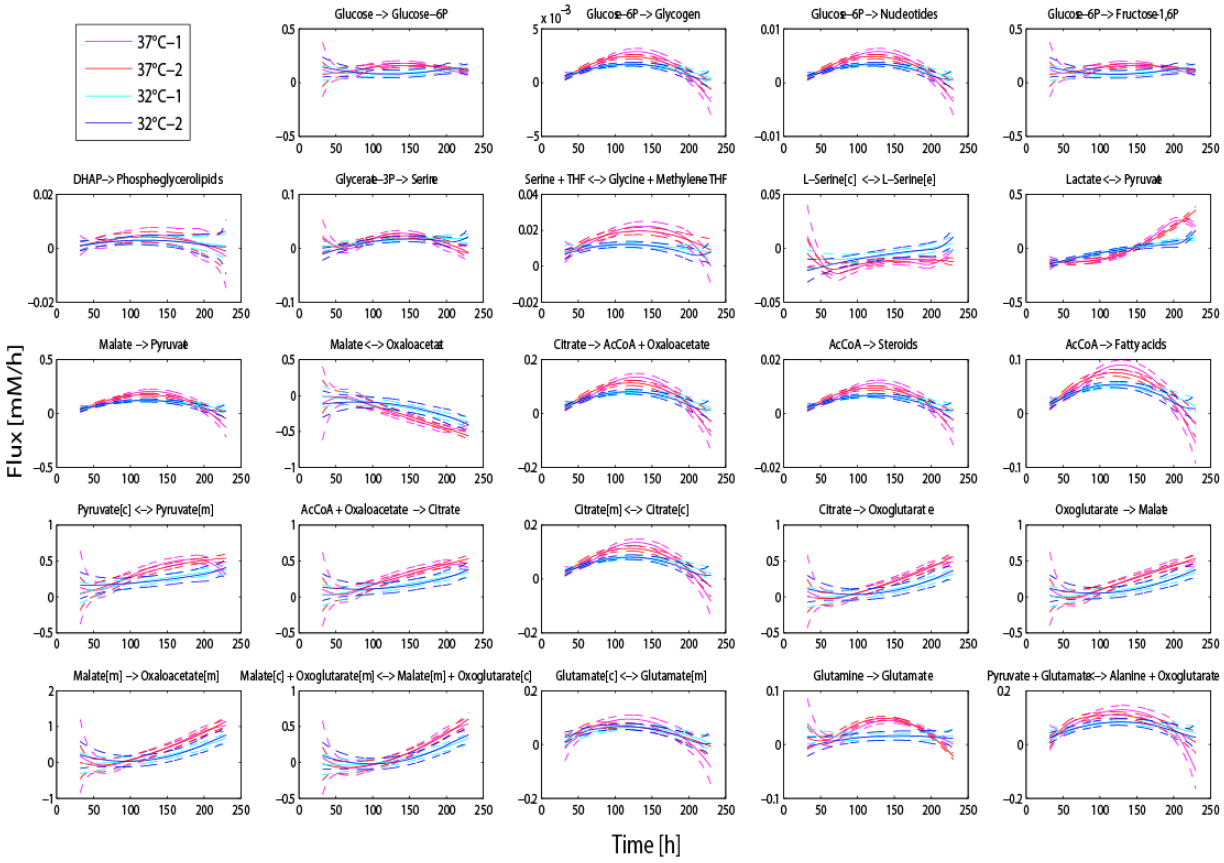

Figure A2: Dynamic intracellular fluxes for cell cultures at 37°C and temperature shifted cells. The estimated dynamic fluxes are presented. The cultures at constant 37°C are in pink (37°C-1) and red (37°C-2), the temperature shifted cultures in cyan (32°C-1) and blue (32°C-2). The fluxes calculated by B-DMFA are shown with solid lines and the 95% confidence intervals are shown with dashed lines.

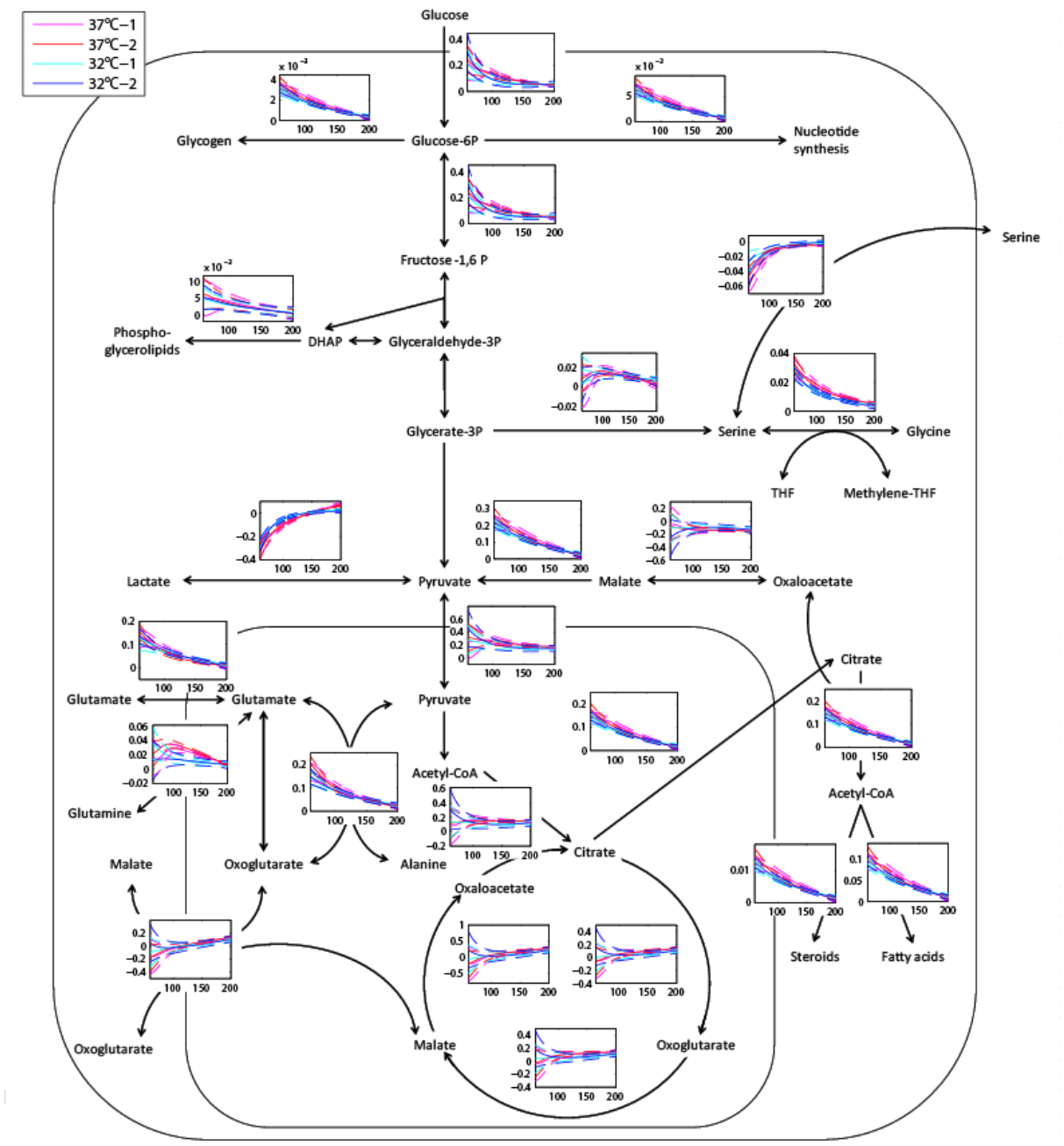

Figure A3: Volume specific dynamic intracellular fluxes for cell cultures at 37°C and temperature shifted cells. Fluxes in [mmol/gDW/h], time scale in hours. The figure shows the specific dynamic fluxes between 60 and 200 hours. The CHO cultures at constant 37°C are in pink (37°C-1) and red (37°C-2), the temperature shifted cultures in cyan (32°C-1) and blue (32°C-2). The volume specific fluxes are shown with solid lines and their 95% CIs are shown with dashed lines. A difference between fluxes of cells at constant temperature and the temperature shifted cultures is observed for biomass precursors' reactions, lactate dehydrogenase and serine/glycine metabolism.

Algorithm to determine knots sequence

A heuristic algorithm to determine the position and number of knots to describe the dynamic of the measured data was developed (Figure A5). In short, the algorithm place a new knot in the "knot placement time interval", which is defined as a continuous segment of the time span bounded by two knots but does not contain any knots in-between. The knot is initially placed in the middle of the knot placement time interval and then the sum of squared residuals (SSR) of this scenario is compared with the SSR of the option of placing the knot in the middle of the left or the right half of the knot placement time interval, whichever one gives the smallest SSR. The knot placement interval is successively reduced by half until the SSR no longer decreases. After the placement of the second and subsequent knots, the position of all knots are adjusted again to minimize SSR in order to account for the effects of other knots, whereby a better position for the i^{th} knot is checked between the time interval defined by $i\text{-}1^{th}$ knot and $i+1^{th}$ knot. The process is described as follow:

1. Start with the knot placement time interval defined by the full time span (i.e., with three knots in the initial time point and three in the end time point, but no internal knots). Stop if SSR is within the χ^2 cutoff
2. Calculate SSR with a knot in the middle of the knot placement time interval.
3. Calculate SSR of adding the knot in the middle of the time interval before or after the knot position defined in step 2.
4. Select the knot position with the smallest SSR between the SSR calculated in steps 2 and 3 (keep that SSR value). If the selected knot is the middle one, go to step 7. Otherwise, update the knot placement time interval to the half of the previous knot placement time interval which contains the selected knot.
5. Iteratively perform steps 3 and 4 until the SSR of the knot placed in the middle of the knot placement time interval is the smallest, and therefore, it is kept as the first inserted knot.
6. Stop if SSR is within the χ^2 cutoff.
7. Calculate SSR for each of the knot placement time intervals. Select the knot placement time interval that gives the biggest SSR. Similar to what was done with one knot (steps 2 to 4) a second knot is added in the new knot placement time interval.

8. Relocate one by one the position of the internal knots, starting from the smallest to the biggest one. For each of the i knots, select as knot placement time interval, the time interval from knot i-1 to knot i+1. Follow the procedure to chose the best position of each knot:
   8.1 Calculate SSR of moving the knot in the middle between the previous knot and the actual knot position or the middle between the actual knot position and the next knot.

   8.2 Find the smallest SSR between the one keeping the position of the knot and the calculated in 8.1, keep that solution. If moving the knot position does not reduce SSR, keep the knot position and move the next knot. Otherwise, chose as new knot placement time interval the half of the knot placement time interval that contains the selected knot and go back to 8.1.
9. Stop if SSR is within the χ^2 cutoff.
10. Add iteratively extra knots following steps 7 and 8 until the solution SSR is within the χ^2 cutoff.

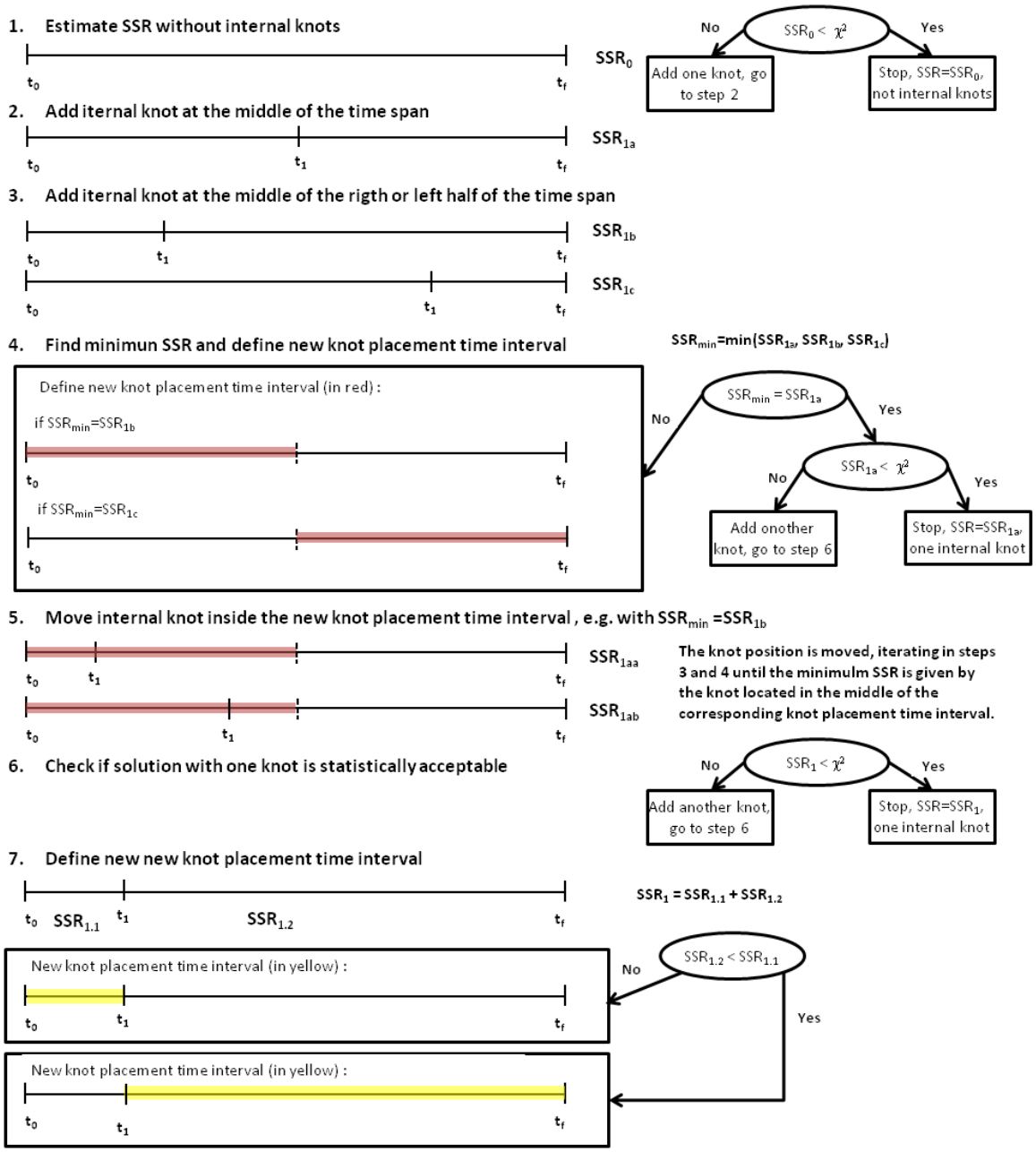

Figure A4: Initial steps of the knot placement algorithm.

Appendix B: Ab2 amino acid composition

Table B1: Ab2 amino acid composition. The Ab2 amino acids composition was estimated based on the sequence of heavy and light chains by the software ProtParam (from Expasy: http://web.expasy.org/protparam/).

Amino Acid	Mass fraction	Molecular Weight
Ala	4.6%	89
Arg	2.3%	174
Asn	3.7%	132
Asp	4.1%	133
Cys	2.6%	121
Gln	4.6%	146
Glu	4.4%	147
Gly	6.1%	75
His	1.9%	155
Ile	2.7%	131
Leu	7.9%	131
Lys	6.6%	146
Met	1.0%	149
Phe	3.4%	165
Pro	6.9%	115
Ser	12.4%	105
Thr	9.6%	119
Trp	2.0%	204
Tyr	4.6%	181
Val	8.7%	117

Appendix C: Metabolic flux analysis method (Quek et al. 2014)

C.1. Transforming primary data into flux constraints

Instead of the conventional MFA approach used in consistency checking (Goudar et al. 2009; van der Heijden et al. 1994; Wang & Stephanopoulos 1983), we used a Monte-Carlo approach for error propagation, and quadratic programming for error checking, flux calculation and sensitivity analysis. Cell number and cell culture concentrations were transformed into rates by a yield approach. Simple linear regression can be used for the transformation process by selectively performing MFA on growth phases that show steady-state metabolic behavior (Quek et al. 2010). A Monte-Carlo approach was used to propagate errors in the primary concentration data into the calculated cell-specific rates (Goudar et al. 2009). Constrained weighted quadratic programming was used for consistency checking and flux variability analysis (Antoniewicz, Kelleher & Stephanopoulos 2006).

C.1.1. Gross growth parameters

For batch cultures, the accumulation of biomass X (gDW/ml) and the change in metabolite concentrations M (μmol/ml) can be described by a series of differential equations shown as Eqs. 1 and 2, where μ is the cell specific growth rate (1/hr), and $r_{xm,i}$ is the cell specific productivity of metabolite *i* (μmol/gDW/hr).

$$\frac{dX}{dt} = \mu X \tag{1}$$

$$\frac{dM_i}{dt} = r_{xm,i} X \text{ for metabolite } i \tag{2}$$

The calculation for μ is different if the loss of viable cells is significant. By distinguishing dead and viable cells (X_{dead}, X_{viable}), the actual growth rate μ becomes the sum of cell specific death rate k_d (1/hr) and the apparent growth rate $\mu_{apparent}$ as shown by Eqs. 3, 4 and 5. It is assumed that dead cells are inert and have negligible effect on the medium upon lysis.

$$\frac{dX_{viable}}{dt} = \mu_{apparent} X_{viable} \quad (3)$$

$$\frac{dX_{dead}}{dt} = k_d X_{viable} \quad (4)$$

$$\mu = \mu_{apparent} + k_d \quad (5)$$

The differential equations can be solved directly for parameters $\mu_{apparent}$, k_d and $r_{xm,i}$ by regression or optimization approaches (Leighty & Antoniewicz 2011). A simpler process of estimating $r_{xm,i}$ is to assume that cells are at exponential growth and metabolic steady-state. This requires that all growth parameters within the growth phase MFA is performed are constant. Then $r_{xm,i}$ can be estimated using a yield approach and by simple linear regression using Eqs. 7, 8 and 9.

$$r_{xm,i} = \pm Y_{xm,i}\mu + r_{xm,i}^{non-growth} \approx \pm Y_{xm,i}^{apparent}\mu \quad (6)$$

where

$$\hat{Y}_{xm,i}^{apparent} = \left|\frac{\Delta M_i}{\Delta X_{total}}\right| \text{ for metabolite } i \quad (7)$$

$$\ln|X_{viable}| = \ln\left|\hat{X}_{viable}^{0}\right| + \hat{\mu}_{apparent} t \quad (8)$$

$$X_{dead} = \frac{\hat{k}_d}{\hat{\mu}_{apparent}} X_{viable} \quad (9)$$

The time-independent yield approach is based on the premise that when cells are at steady-state growth, the depletion and accumulation of metabolites in the media is linearly correlated with biomass concentration. Eq. 7, however, gives apparent cell-specific yields $Y_{xm,i}^{apparent}$ (μmol/gDW) instead of true yields $Y_{xm,i}$. As shown in Eq. 6, included in apparent yields is a small but potentially significant non-growth associated maintenance term

$r_{xm,i}^{non-growth}$ (μmol/gDW/hr), which can only be separately estimated by performing a series of flux experiments at different growth rates (e.g., chemostat) (Varma & Palsson 1994c).

For batch cultures, however, it is possible to assume that $Y_{xm}\mu >> r_{xm,i}^{non-growth}$ since cells are growing at the maximum rate ($\mu \to \mu_{\max}$); this assumption implies that cell metabolism mainly serves biosynthesis, and non-growth associated consumption or production is negligible. Flux constraints can then be formulated using either $r_{xm,i}$ or $Y_{xm,i}^{apparent}$, since both parameters are in proportional by the scaling factor μ.

Slow growing or growth arrested ($\mu \to 0$) mammalian cells, however, often maintain significant productivity and metabolic activity. $r_{xm,i}^{non-growth}$ is therefore significant and $Y_{xm,i}^{apparent}$ would over-estimate actual biosynthetic demands. It then becomes necessary to separately estimate $r_{xm,i}^{non-growth}$ (Sheikh, Forster & Nielsen 2005), and to formulate flux constraints using $r_{xm,i}$.

C.1.2. Glutamine decomposition

Free glutamine in the medium can decompose into ammonia and pyrrolidonecarboxylic acid. The actual cell-specific consumption of glutamine $r_{xm,GLN}$ and production of ammonia $r_{xm,\mathrm{NH3}}$ were calculated separately, since apparent glutamine uptake rate can almost double the actual consumption rate (Ozturk & Palsson 1990).

$$\frac{dM_{GLN}}{dt} = -kM_{GLN} + r_{xm,GLN}X_{viable} \tag{10}$$

$$\frac{dM_{\mathrm{NH3}}}{dt} = kM_{GLN} + r_{xm,\mathrm{NH3}}X_{viable} \tag{11}$$

$$\ln\left|\mathrm{M_{Gln}}\right| = \ln\left|\mathrm{M_{GLN}^{0}}\right| + kt \tag{12}$$

The rate of glutamine decomposition is taken at first-order with respect to glutamine concentration in Eq. 10. A similar adjustment is made to ammonia production as well using Eq. 11. The rate constant k (1/hr) is affected by pH and media composition (Ozturk & Palsson 1990), and was separately determined for the blank medium at the same cell

culture condition (e.g., temperature and pH) using Eq. 12. Assuming the parameters μ, k, $r_{xm,\mathrm{GLN}}$ and $r_{xm,\mathrm{NH3}}$ are constant (i.e., cells are at exponential growth and metabolic steady-state), integration-by-parts followed by linear regression can be used to estimate $r_{xm,\mathrm{GLN}}$ and $r_{xm,\mathrm{NH3}}$ using Eqs. 13 and 14. Note that $\hat{\mu}$ and $\hat{X}^0_{viable}$ were first determined, followed by $\hat{r}_{xm,\mathrm{GLN}}$ and then $\hat{r}_{xm,\mathrm{NH3}}$.

$$M_{GLN} - M^0_{\mathrm{GLN}} e^{-kt} = -\hat{r}_{xm,\mathrm{GLN}} \left(\hat{X}^0_{viable} \frac{e^{-kt} - e^{\hat{\mu}t}}{k + \hat{\mu}} \right) \tag{13}$$

$$M_{\mathrm{NH3}} - M^0_{\mathrm{NH3}} - \left(M^0_{\mathrm{GLN}} - \frac{\hat{r}_{xm,GLN} \hat{X}^0_{viable}}{\hat{\mu} + k} \right) \left(1 - e^{-kt}\right) - \frac{\hat{X}^0_{viable}}{\hat{\mu}} \left(e^{\hat{\mu}t} - 1\right) \frac{\hat{r}_{xm,\mathrm{GLN}} k}{\hat{\mu} + k} = \hat{r}_{xm,\mathrm{NH3}} \frac{\hat{X}^0_{viable}}{\hat{\mu}} \left(e^{\hat{\mu}t} - 1\right) \tag{14}$$

C.1.3. Error propagation by Monte-Carlo

It is important to gain a sense of accuracy for the MFA results considering the presence of experimental errors. Errors for the cell-specific rates (μ, $r_{xm,i}$) were therefore calculated from the primary data (X, M) by a Monte-Carlo approach. Since the system of equations is linear under the yield approach (Eq. 7), Monte-Carlo, used in conjunction with linear regression, is a fast and convenient technique to propagate errors, especially considering that both X and M contain errors, and the difficulty of processing Eqs. 13 and 14. The means and standard deviations were computed from 10,000 simulated samples of μ and $r_{xm,i}$ generated by corrupting the primary data with normally distributed random errors. There is also the opportunity to generate an error covariance matrix (CoV) used for subsequent least-square optimization, which accounts for potential biases arising from fitting cell-specific rates that are not independent of each other.

Based on repeated cell counts, a minimum error for cell number of 5% is used. We adopted an aggressive error estimate here because the error for all cell-specific rates will be at least 5% as well. Errors for metabolite concentrations ($s_{e,M}$) determined by HPLC were calculated from the respective mean squared errors (s_e^2) obtained from each metabolite's standard (linear) calibration curve (Eqs. 15, 16 and 17). If the number of

calibration points (n) is large, and that analyte responses are well within the calibration range, then Eq. 18 can be used to specify the minimum error $s^{\min}_{e,M_{\text{sample}}}$ for each type of metabolite.

$$\hat{y} = b_0 + b_1 x \tag{15}$$

$$\text{where } b_1 = \frac{\sum_i^n x_i y_i - n\overline{xy}}{\sum_i^n x_i^2 - n\overline{x}^2} \text{ and } b_0 = \overline{y} - b_1 \overline{x}$$

$$s_e^2 = \frac{\sum_i^n y_i^2 - b_0 \sum_i^n y_i - b_1 \sum_i^n x_i y_i}{n-2} \tag{16}$$

$$s_{e,M_{\text{sample}}} = s_e \left(1 + \frac{1}{n} + \frac{\left(x_{\text{sample}} - \overline{x}\right)^2}{\sum_i^n x_i^2 - n\overline{x}^2} \right)^{\frac{1}{2}} \cdot \text{dilution} \tag{17}$$

$$s^{\min}_{e,M_{\text{sample}}} = s_e \cdot \text{dilution} \tag{18}$$

C.1.4. Flux analysis by quadratic programming

The stoichiometric matrix (S) contains a set of reactions, a result of reducing Recon 1. The nullspace matrix (NS) of matrix S , for which Eq. 19 is satisfied, contains the basis vectors spanning the flux solution space ($\overline{v}$) (Eq. 20). By arranging reactions in S such that the leading reactions are all the input and output (measured) reactions, two sub-sections of NS will appear as shown in Eq. 21. The number of redundant measurements is indicated by the number of rows in A_1. Reaction rows spanned by non-zero values of I_2 and A_4 are underdetermined.

$$S' \cdot \overline{v} = 0 \tag{19}$$

$$\overline{v} = NS \cdot \overline{t} \tag{20}$$

$$NS = rref\left(null\left(S'\right)\right) = \begin{bmatrix} NS_{mea} \\ NS_{calc} \end{bmatrix} = \begin{bmatrix} I_1 & 0 \\ A_1 & 0 \\ A_2 & 0 \\ 0 & I_2 \\ A_3 & A_4 \end{bmatrix} \tag{21}$$

$$\text{where } NS_{mea} = \begin{bmatrix} I & 0 \\ A_1 & 0 \end{bmatrix}$$

Weighted least-square optimization was performed by quadratic programming to calculate the optimum flux distribution for the set of mean and variance of μ and $r_{xm,i}$ generated by the Monte-Carlo approach. Cell-specific rates were assumed to be independent, therefore only the diagonal elements of CoV were used. During the optimization, irreversible reactions were constrained such that their fluxes are zero or positive. The values in the boundary vectors ($\overline{lb}$, $\overline{ub}$) for the optimized variables ($\overline{t}$) was arbitrarily set to -1000 and 1000 respectively. The optimum flux distribution is calculated using Eq. 20.

$$\text{minimize}\left(\overline{t}' \cdot Q \cdot \overline{t} + f' \cdot \overline{t} + c\right) \tag{22}$$

subject to

$$\overline{lb} \le \overline{t} \le \overline{ub},\ NS_{\text{irreversible rxn}} \cdot \overline{t} \ge \overline{0}$$

where

$$Q = \frac{NS_{mea}' \cdot NS_{mea}}{CoV},\ f = \frac{\begin{bmatrix} \overline{\mu} & \overline{r}_{xm,i} \end{bmatrix} \cdot \begin{bmatrix} \overline{\mu} \\ \overline{r}_{xm,i} \end{bmatrix}}{CoV},\ c = \frac{-2 \cdot \begin{bmatrix} \overline{\mu} & \overline{r}_{xm,i} \end{bmatrix} \cdot NS_{mea}}{CoV}$$

The 95% confidence intervals of the optimum fluxes were calculated as a form sensitivity analysis. This is accomplished by finding the minimum and maximum flux of every reaction such that the increase in residual error from the minimum error is less than a certain threshold. This threshold is specified by the chi-square value taken at 5% significance and with a degrees-of-freedom (DoF) equal to the number of redundant measurements.

$$\text{minimize or maximize} \left(NS_{\text{rxn row } j} \cdot t \right) \tag{23}$$

subject to

$$\overline{lb} \le \bar{t} \le \overline{ub}, \; NS_{\text{irreversible rxn}} \cdot \bar{t} \ge \bar{0}, \; t' \cdot Q \cdot t + f' \cdot t + c \le \min \text{ error} + \chi^2 \left(0.05, DoF \right)$$

The optimum ranges of underdetermined reactions were separately calculated using the above optimization, except that the residual error threshold is set to zero.

C.2. Software

Both linear programming and quadratic programming were performed using Gurobi Optimizer (Gurobi Optimization, Inc., Houston TX) in MATLAB R2010a (MathWorks Inc., Natick, MA).

Appendix D: CHO-XL99 SWATH-MS proteomics

Table D1: Differentially expressed proteins in 5 mM DCA CHO-XL99 cell cultures compared to control cultures. 20 proteins out of 2016 identified protein were differentially expressed. Negative fold change indicates downregulation and positive fold change upregulation.

Gene ID	adj. P-value	Fold change	Cricetulus griseus (Chinese hamster) predicted protein name (GO biological process or function)
gi|354494438	0.00039	2.11	sulfated glycoprotein 1
gi|354505255	0.00051	-2.17	ubiquitin-conjugating enzyme E2 D3-like (apoptosis, metabolic process)
gi|354495660	0.00051	-1.91	calponin-3-like (system process)
gi|354499660	0.00057	2.10	profilin-2-like (profilin binds to actin and affects the structure of the cytoskeleton)
gi|354475569	0.00336	-1.70	peptidyl-prolyl cis-trans isomerase FKBP1A-like (apoptosis, cell communication, cell cycle, cellular process, immune system process, metabolic process, response to stimulus, system process) (immunoregulation and basic cellular processes involving protein folding and trafficking)
gi|354484974	0.00725	-1.56	60S ribosomal protein L27-like (metabolic process)
gi|354500469	0.00894	-1.78	60S ribosomal protein L10-like (metabolic process)
gi|354505902	0.00920	-1.58	40S ribosomal protein S15a-like (metabolic process)
gi|354492481	0.01717	-2.31	LOW QUALITY PROTEIN: deoxyribonucleoside 5'-monophosphate N-glycosidase-like
gi|354493803	0.01934	-1.93	SUMO-activating enzyme subunit 1-like (cell communication, cellular process, metabolic process)
gi|354503001	0.01934	-1.54	flap endonuclease 1-like (cell cycle, cellular process, metabolic process)(DNA replication, repair , and recombination)
gi|354492646	0.02102	1.54	integrin beta-1 (cell adhesion, cell communication, cellular process, immune system process, response to stimulus)
gi|354489238	0.02696	2.01	adapter molecule crk-like (cell communication, cellular process)
gi|354499904	0.02696	2.27	exosome complex component RRP43-like, partial (metabolic process)
gi|354497793	0.02841	-1.39	heterogeneous nuclear ribonucleoprotein D0-like
gi|354504522	0.02841	2.02	serine/threonine-protein phosphatase 2A activator-like, partial (metabolic process)
gi|354472305	0.03182	-1.44	heterogeneous nuclear ribonucleoprotein A3-like
gi|354485024	0.03623	-1.45	synaptic vesicle membrane protein VAT-1 homolog, partial
gi|354505599	0.04970	-1.41	cytosolic acyl coenzyme A thioester hydrolase
gi|354473527	0.04970	1.66	hypothetical protein LOC100757682

Appendix E: HEK293 cells growth rate adjusted metabolic rates (chapter 5)

Table E1: Growth rate adjusted metabolic rates and differentially expressed amino acid transporters. Mean (n = 2) growth rate adjusted nutrient and metabolite production and consumption rates for HEK293F cell control, 5 mM DCA, and 10 mM DCA cultures and upregulated amino acid transporters in 10 mM DCA cultures. Rates are in mM/(gDW*h), growth rate in h^{-1}. Negative rates represent consumption and positive rates production.

Metabolite	No DCA Rate	5 mM DCA Rate	10 mM DCA Rate	Upregulated transporter on 10 mM DCA
Glucose	-297.47	-254.15	-281.66	
Lactate	373.23	289.09	263.30	
NH_4^+	12.74	13.93	25.26	
Consumed amino acids				
Asp	-4.48	-4.42	-5.44	SLC1A5
Gln	-61.34	-55.87	-77.80	SLC7A5, SLC3A2, SLC1A5
Ser	-27.95	-29.87	-39.62	SLC1A5
Arg	-12.04	-14.59	-19.50	SLC7A5, SLC3A2
Tyr	-3.32	-3.11	-3.59	SLC7A5, SLC3A2, SLC1A5
Essential amino acids				
His	-2.41	-2.35	-2.41	
Thr	-6.36	-6.06	-7.01	SLC1A5
Val	-10.17	-10.03	-14.86	SLC1A5
Met	-3.62	-3.46	-4.36	SLC1A5
Trp	-1.15	-1.03	-1.26	SLC7A5, SLC3A2, SLC1A5
Phe	-4.46	-3.77	-4.76	SLC7A5, SLC3A2, SLC1A5
Ile	-8.92	-9.81	-13.46	SLC1A5
Leu	-13.57	-15.05	-19.18	SLC7A5, SLC3A2, SLC1A5
Lys	-7.36	-7.32	-4.33	
Produced amino acids				
Glu	7.01	12.41	18.35	
Gly	6.28	8.79	14.73	SLC6A9, SLC1A5
Ala	19.21	10.78	12.90	SLC1A5
Pro	11.53	7.31	8.98	SLC1A5
Consumed or produced amino acid				
Asn	-1.38	0.84	3.70	
Growth rate	0.0269	0.0269	0.0269	

Appendix F: HEK293 cell targeted proteomics (chapter 5)

Table F1: Proteins, peptides and transitions used in targeted proteomics

Protein Name	Peptide Sequence	Precursor Mz	Precursor Charge	Product Mz	Product Charge	Fragmentation
sp|O00757|F16P2_HUMAN	GTGELTQLLNSMLTAIK	895.490044	2	1103.649293	1	y10
sp|O00757|F16P2_HUMAN	GTGELTQLLNSMLTAIK	895.490044	2	432.28166	1	y4
sp|O00757|F16P2_HUMAN	YFDAATTEYVQK	718.340632	2	1125.542245	1	y10
sp|O00757|F16P2_HUMAN	YFDAATTEYVQK	718.340632	2	537.303124	1	y4
sp|O00757|F16P2_HUMAN	YFDAATTEYVQK	718.340632	2	568.240189	1	b5
sp|O43837|IDH3B_HUMAN	AAAVPVEFQEHHLSEVQNMASEEK	894.093903	3	823.402086	2	b15
sp|O43837|IDH3B_HUMAN	AAAVPVEFQEHHLSEVQNMASEEK	894.093903	3	872.936293	2	b16
sp|O43837|IDH3B_HUMAN	NIANPTAMLLSASNMLR	908.974038	2	620.318456	1	y5
sp|O43837|IDH3B_HUMAN	NIANPTAMLLSASNMLR	908.974038	2	1039.560478	1	b10
sp|O75390|CISY_HUMAN	DILADLIPK	499.30005	2	656.397753	1	y6
sp|O75390|CISY_HUMAN	DILADLIPK	499.30005	2	244.165568	1	y2
sp|O75390|CISY_HUMAN	DILADLIPK	499.30005	2	229.118283	1	b2
sp|O75390|CISY_HUMAN	GLVYETSVLDPDEGIR	881.946523	2	914.457787	1	y8
sp|O75390|CISY_HUMAN	GLVYETSVLDPDEGIR	881.946523	2	801.373723	1	y7
sp|O75874|IDHC_HUMAN	LVSGWVKPIIIGR	479.969528	3	213.159754	1	b2
sp|O75874|IDHC_HUMAN	LVSGWVKPIIIGR	479.969528	3	642.360973	1	b6
sp|O75874|IDHC_HUMAN	TVEAEAAHGTVTR	671.341497	2	571.283451	2	y11
sp|O75874|IDHC_HUMAN	TVEAEAAHGTVTR	671.341497	2	506.762154	2	y10
sp|P00338|LDHA_HUMAN	DLADELALVDVIEDK	829.430175	2	1001.551353	1	y9
sp|P00338|LDHA_HUMAN	DLADELALVDVIEDK	829.430175	2	930.514239	1	y8
sp|P00338|LDHA_HUMAN	GEMMDLQHGSLFLR	545.265687	3	724.362864	2	y12
sp|P00338|LDHA_HUMAN	GEMMDLQHGSLFLR	545.265687	3	658.842622	2	y11
sp|P00558|PGK1_HUMAN	ALESPERPFLAILGGAK	590.336716	3	792.940847	2	y15
sp|P00558|PGK1_HUMAN	ALESPERPFLAILGGAK	590.336716	3	728.419551	2	y14
sp|P00558|PGK1_HUMAN	VLNNMEIGTSLFDEEGAK	983.974955	2	1153.537159	1	y11
sp|P00558|PGK1_HUMAN	VLNNMEIGTSLFDEEGAK	983.974955	2	1096.515696	1	y10
sp|P04075|ALDOA_HUMAN	GILAADESTGSIAK	666.853906	2	1049.510944	1	y11
sp|P04075|ALDOA_HUMAN	GILAADESTGSIAK	666.853906	2	978.473831	1	y10
sp|P04075|ALDOA_HUMAN	FSHEEIAMATVTALR	838.427247	2	933.518613	1	y9
sp|P04075|ALDOA_HUMAN	FSHEEIAMATVTALR	838.427247	2	721.377025	2	y13
sp|P04406|G3P_HUMAN	LVINGNPITIFQER	807.454122	2	1003.557107	1	y8
sp|P04406|G3P_HUMAN	LVINGNPITIFQER	807.454122	2	579.288536	1	y4
sp|P04406|G3P_HUMAN	GALQNIIPASTGAAK	706.398815	2	815.462144	1	y9
sp|P04406|G3P_HUMAN	GALQNIIPASTGAAK	706.398815	2	597.335487	1	b6
sp|P05062|ALDOB_HUMAN	ELSEIAQSIVANGK	729.893563	2	688.398815	1	y7
sp|P05062|ALDOB_HUMAN	ELSEIAQSIVANGK	729.893563	2	389.214309	1	y4
sp|P05062|ALDOB_HUMAN	ALQASALAAWGGK	622.343312	2	447.235044	1	y4
sp|P05062|ALDOB_HUMAN	ALQASALAAWGGK	622.343312	2	726.414465	1	b8
sp|P06733|ENOA_HUMAN	DATNVGDEGGFAPNILENK	980.965976	2	1159.610599	1	y11

sp|P06733|ENOA_HUMAN	DATNVGDEGGFAPNILENK	980.965976	2	827.462144	1	y7
sp|P06733|ENOA_HUMAN	YISPDQLADLYK	713.366649	2	1149.57863	1	y10
sp|P06733|ENOA_HUMAN	YISPDQLADLYK	713.366649	2	1062.546602	1	y9
sp|P06744|G6PI_HUMAN	NLVTEDVMR	538.773873	2	306.159436	1	y2
sp|P06744|G6PI_HUMAN	NLVTEDVMR	538.773873	2	228.134267	1	b2
sp|P06744|G6PI_HUMAN	TLAQLNPESSLFIIASK	916.511834	2	1191.661966	1	y11
sp|P06744|G6PI_HUMAN	TLAQLNPESSLFIIASK	916.511834	2	527.318774	1	b5
sp|P07195|LDHB_HUMAN	LIAPVAEEEATVPNNK	847.951609	2	472.251423	1	y4
sp|P07195|LDHB_HUMAN	LIAPVAEEEATVPNNK	847.951609	2	699.348988	2	y13
sp|P07195|LDHB_HUMAN	MVVESAYEVIK	634.333764	2	1037.551353	1	y9
sp|P07195|LDHB_HUMAN	MVVESAYEVIK	634.333764	2	231.116175	1	b2
sp|P07205|PGK2_HUMAN	LGDVYVNDAFGTAHR	545.602232	3	761.357679	2	y14
sp|P07205|PGK2_HUMAN	LGDVYVNDAFGTAHR	545.602232	3	625.799268	2	y11
sp|P07205|PGK2_HUMAN	VSHVSTGGGASLELLEGK	580.975735	3	688.387582	1	y6
sp|P07205|PGK2_HUMAN	VSHVSTGGGASLELLEGK	580.975735	3	559.344989	1	y5
sp|P07437|TBB5_HUMAN	AILVDLEPGTMDSVR	808.42163	2	1219.562328	1	y11
sp|P07437|TBB5_HUMAN	AILVDLEPGTMDSVR	808.42163	2	862.408728	1	y8
sp|P07437|TBB5_HUMAN	GHYTEGAELVDSVLDVVR	653.66545	3	601.366787	1	y5
sp|P07437|TBB5_HUMAN	GHYTEGAELVDSVLDVVR	653.66545	3	488.282723	1	y4
sp|P07864|LDHC_HUMAN	SIIPAIVHYSPDCK	771.902876	2	948.424378	1	y8
sp|P07864|LDHC_HUMAN	SIIPAIVHYSPDCK	771.902876	2	231.604486	2	y4
sp|P07864|LDHC_HUMAN	SIIPAIVHYSPDCK	771.902876	2	994.572029	1	b9
sp|P07864|LDHC_HUMAN	VIGSGCNLDSAR	596.292961	2	546.758754	2	y11
sp|P07864|LDHC_HUMAN	VIGSGCNLDSAR	596.292961	2	490.216722	2	y10
sp|P07864|LDHC_HUMAN	VIGSGCNLDSAR	596.292961	2	213.159754	1	b2
sp|P07864|LDHC_HUMAN	EELFLSIPCVLGR	738.399969	2	1104.623412	1	y10
sp|P07864|LDHC_HUMAN	EELFLSIPCVLGR	738.399969	2	644.354842	1	y6
sp|P07864|LDHC_HUMAN	EELFLSIPCVLGR	738.399969	2	322.681059	2	y6
sp|P07954|FUMH_HUMAN	THTQDAVPLTLGQEFSGYVQQVK	849.434365	3	897.475251	2	y16
sp|P07954|FUMH_HUMAN	THTQDAVPLTLGQEFSGYVQQVK	849.434365	3	1087.03165	2	b20
sp|P07954|FUMH_HUMAN	IYELAAGGTAVGTGLNTR	882.467957	2	817.452642	1	y8
sp|P07954|FUMH_HUMAN	IYELAAGGTAVGTGLNTR	882.467957	2	560.315085	1	y5
sp|P08237|K6PF_HUMAN	SEWSDLLSDLQK	710.851363	2	703.398481	1	y6
sp|P08237|K6PF_HUMAN	SEWSDLLSDLQK	710.851363	2	590.314417	1	y5
sp|P08237|K6PF_HUMAN	DLQANVEHLVQK	697.37534	2	753.425364	1	y6
sp|P08237|K6PF_HUMAN	DLQANVEHLVQK	697.37534	2	624.382771	1	y5
sp|P08243|ASNS_HUMAN	LAVVDPLFGMQPIR	778.436886	2	1173.60849	1	y10
sp|P08243|ASNS_HUMAN	LAVVDPLFGMQPIR	778.436886	2	1058.581547	1	y9
sp|P08243|ASNS_HUMAN	DVPLHALYDNVEK	756.88828	2	880.441074	1	y7
sp|P08243|ASNS_HUMAN	DVPLHALYDNVEK	756.88828	2	649.840602	2	y11
sp|P08559|ODPA_HUMAN	EILAELTGR	1001.562586	1	646.351865	1	y6
sp|P08559|ODPA_HUMAN	EILAELTGR	1001.562586	1	556.297704	1	b5
sp|P08559|ODPA_HUMAN	EILAELTGR	1001.562586	1	827.45091	1	b8
sp|P08559|ODPA_HUMAN	YGMGTSVER	500.231841	2	490.261987	1	y4
sp|P08559|ODPA_HUMAN	YGMGTSVER	500.231841	2	390.189445	2	y7
sp|P08559|ODPA_HUMAN	YGMGTSVER	540.215007	2	570.228318	1	y4

sp|P08559|ODPA_HUMAN	YGMGTSVER	540.215007	2	430.172611	2	y7
sp|P08559|ODPA_HUMAN	YHGHSMSDPGVSYR	796.849163	2	1098.488435	1	y10
sp|P08559|ODPA_HUMAN	YHGHSMSDPGVSYR	796.849163	2	880.415922	1	y8
sp|P08559|ODPA_HUMAN	YHGHSMSDPGVSYR	796.849163	2	301.129516	1	b2
sp|P08559|ODPA_HUMAN	YHGHSMSDPGVSYR	876.815494	2	660.346385	1	y6
sp|P08559|ODPA_HUMAN	YHGHSMSDPGVSYR	876.815494	2	661.270517	1	y5
sp|P08559|ODPA_HUMAN	YHGHSMSDPGVSYR	876.815494	2	897.330812	1	b8
sp|P08559|ODPA_HUMAN	YHGHSMSDPGVSYR	836.832329	2	1178.454766	1	y10
sp|P08559|ODPA_HUMAN	YHGHSMSDPGVSYR	836.832329	2	758.323281	1	y6
sp|P08559|ODPA_HUMAN	YHGHSMSDPGVSYR	836.832329	2	505.18064	1	y3
sp|P08559|ODPA_HUMAN	YHGHSMSDPGVSYR	836.832329	2	793.383893	1	y7
sp|P08559|ODPA_HUMAN	YHGHSMSDPGVSYR	836.832329	2	678.35695	1	y6
sp|P08559|ODPA_HUMAN	YHGHSMSDPGVSYR	836.832329	2	706.312217	2	y13
sp|P08559|ODPA_HUMAN	YHGHSMSDPGVSYR	836.832329	2	995.307708	1	b8
sp|P08559|ODPA_HUMAN	MVNSNLASVEELK	717.368866	2	1203.621558	1	y11
sp|P08559|ODPA_HUMAN	MVNSNLASVEELK	717.368866	2	775.41961	1	y7
sp|P08559|ODPA_HUMAN	MVNSNLASVEELK	717.368866	2	518.282054	1	y4
sp|P09104|ENOG_HUMAN	IVIGMDVAASEFYR	785.900333	2	701.325316	1	y5
sp|P09104|ENOG_HUMAN	IVIGMDVAASEFYR	785.900333	2	870.475351	1	b9
sp|P09104|ENOG_HUMAN	YITGDQLGALYQDFVR	929.970333	2	827.404629	1	y6
sp|P09104|ENOG_HUMAN	YITGDQLGALYQDFVR	929.970333	2	791.896637	2	y14
sp|P09467|F16P1_HUMAN	YVGSMVADVHR	617.305872	2	597.310334	1	y5
sp|P09467|F16P1_HUMAN	YVGSMVADVHR	617.305872	2	411.246278	1	y3
sp|P09467|F16P1_HUMAN	YVGSMVADVHR	617.305872	2	486.240001	2	y9
sp|P09467|F16P1_HUMAN	TLVYGGIFLYPANK	778.429584	2	965.545479	1	y8
sp|P09467|F16P1_HUMAN	TLVYGGIFLYPANK	778.429584	2	592.308937	1	y5
sp|P09467|F16P1_HUMAN	TLVYGGIFLYPANK	778.429584	2	429.245609	1	y4
sp|P09467|F16P1_HUMAN	APVILGSPDDVLEFLK	856.977095	2	1075.567003	1	y9
sp|P09467|F16P1_HUMAN	APVILGSPDDVLEFLK	856.977095	2	381.249632	1	b4
sp|P09467|F16P1_HUMAN	APVILGSPDDVLEFLK	856.977095	2	551.355159	1	b6
sp|P09467|F16P1_HUMAN	APVILGSPDDVLEFLK	571.653822	3	649.391939	1	y5
sp|P09467|F16P1_HUMAN	APVILGSPDDVLEFLK	571.653822	3	536.307875	1	y4
sp|P09467|F16P1_HUMAN	APVILGSPDDVLEFLK	571.653822	3	538.287139	2	y9
sp|P09622|DLDH_HUMAN	NLGLEELGIELDPR	784.419945	2	799.430844	1	y7
sp|P09622|DLDH_HUMAN	NLGLEELGIELDPR	784.419945	2	272.171716	1	y2
sp|P09622|DLDH_HUMAN	FPFAANSR	909.457727	1	665.336549	1	y6
sp|P09622|DLDH_HUMAN	FPFAANSR	909.457727	1	518.268135	1	y5
sp|P09972|ALDOC_HUMAN	GVVPLAGTDGETTTQGLDGLSER	758.380037	3	846.431572	1	y8
sp|P09972|ALDOC_HUMAN	GVVPLAGTDGETTTQGLDGLSER	758.380037	3	561.299101	1	y5
sp|P09972|ALDOC_HUMAN	TPSALAILENANVLAR	826.970136	2	1112.642233	1	y10
sp|P09972|ALDOC_HUMAN	TPSALAILENANVLAR	826.970136	2	886.474105	1	y8
sp|P11413|G6PD_HUMAN	NSYVAGQYDDAASYQR	904.397729	2	1088.464329	1	y9
sp|P11413|G6PD_HUMAN	NSYVAGQYDDAASYQR	904.397729	2	624.31	1	y5
sp|P11413|G6PD_HUMAN	NSYVAGQYDDAASYQR	904.397729	2	365.14556	1	b3
sp|P11413|G6PD_HUMAN	IFGPIWNR	501.779619	2	475.241192	1	y3
sp|P11413|G6PD_HUMAN	IFGPIWNR	501.779619	2	371.70338	2	y6

sp|P11413|G6PD_HUMAN	IFGPIWNR	501.779619	2	261.159754	1	b2
sp|P13929|ENOB_HUMAN	TAIQAAGYPDK	567.79312	2	650.314417	1	y6
sp|P13929|ENOB_HUMAN	TAIQAAGYPDK	567.79312	2	481.750724	2	y9
sp|P13929|ENOB_HUMAN	VNQIGSVTESIQACK	526.271495	3	440.21566	2	y8
sp|P13929|ENOB_HUMAN	VNQIGSVTESIQACK	526.271495	3	455.234381	3	y13
sp|P14618|KPYM_HUMAN	LDIDSPPITAR	599.327327	2	856.452307	1	y8
sp|P14618|KPYM_HUMAN	LDIDSPPITAR	599.327327	2	654.393336	1	y6
sp|P14618|KPYM_HUMAN	GADFLVTEVENGGSLGSK	890.441605	2	1177.569522	1	y12
sp|P14618|KPYM_HUMAN	GADFLVTEVENGGSLGSK	890.441605	2	848.410836	1	y9
sp|P15104|GLNA_HUMAN	VQAMYIWIDGTGEGLR	904.953629	2	1216.632063	1	y11
sp|P15104|GLNA_HUMAN	VQAMYIWIDGTGEGLR	904.953629	2	1103.547999	1	y10
sp|P15104|GLNA_HUMAN	VQAMYIWIDGTGEGLR	904.953629	2	804.384622	1	y8
sp|P15104|GLNA_HUMAN	VQAMYIWIDGTGEGLR	904.953629	2	689.357679	1	y7
sp|P15104|GLNA_HUMAN	VQAMYIWIDGTGEGLR	904.953629	2	706.359259	1	b6
sp|P15104|GLNA_HUMAN	VQAMYIWIDGTGEGLR	904.953629	2	1005.522636	1	b8
sp|P15104|GLNA_HUMAN	DIVEAHYR	501.753798	2	475.241192	1	y3
sp|P15104|GLNA_HUMAN	DIVEAHYR	501.753798	2	229.118283	1	b2
sp|P15104|GLNA_HUMAN	LTGFHETSNINDFSAGVANR	1075.516699	2	821.426427	1	y8
sp|P15104|GLNA_HUMAN	LTGFHETSNINDFSAGVANR	1075.516699	2	866.405888	2	y16
sp|P15259|PGAM2_HUMAN	ALPFWNEEIVPQIK	842.458873	2	485.308209	1	y4
sp|P15259|PGAM2_HUMAN	ALPFWNEEIVPQIK	842.458873	2	750.398284	2	y12
sp|P15259|PGAM2_HUMAN	TLWAILDGTDQMWLPVVR	705.374953	3	769.471921	1	y6
sp|P15259|PGAM2_HUMAN	TLWAILDGTDQMWLPVVR	705.374953	3	822.908158	2	b14
sp|P15259|PGAM2_HUMAN	ALPFWNEEIVPQIK	842.458873	2	485.308209	1	y4
sp|P15259|PGAM2_HUMAN	ALPFWNEEIVPQIK	842.458873	2	750.398284	2	y12
sp|P17858|K6PL_HUMAN	SEWGSLLEELVAEGK	823.917235	2	987.535703	1	y9
sp|P17858|K6PL_HUMAN	SEWGSLLEELVAEGK	823.917235	2	874.451639	1	y8
sp|P17858|K6PL_HUMAN	SEWGSLLEELVAEGK	823.917235	2	715.879924	2	y13
sp|P17858|K6PL_HUMAN	TNVLGHLQQGGAPTPFDR	954.489755	2	1173.564711	1	y11
sp|P17858|K6PL_HUMAN	TNVLGHLQQGGAPTPFDR	954.489755	2	534.267073	1	y4
sp|P17858|K6PL_HUMAN	TNVLGHLQQGGAPTPFDR	954.489755	2	735.4148	1	b7
sp|P18669|PGAM1_HUMAN	FSGWYDADLSPAGHEEAK	660.630516	3	838.405357	1	y8
sp|P18669|PGAM1_HUMAN	FSGWYDADLSPAGHEEAK	660.630516	3	419.706317	2	y8
sp|P18669|PGAM1_HUMAN	ALPFWNEEIVPQIK	842.458873	2	485.308209	1	y4
sp|P18669|PGAM1_HUMAN	ALPFWNEEIVPQIK	842.458873	2	750.398284	2	y12
sp|P18669|PGAM1_HUMAN	ALPFWNEEIVPQIK	842.458873	2	485.308209	1	y4
sp|P18669|PGAM1_HUMAN	ALPFWNEEIVPQIK	842.458873	2	750.398284	2	y12
sp|P19367|HXK1_HUMAN	GDFIALDLGGSSFR	727.867348	2	951.489421	1	y9
sp|P19367|HXK1_HUMAN	GDFIALDLGGSSFR	727.867348	2	838.405357	1	y8
sp|P19367|HXK1_HUMAN	GDFIALDLGGSSFR	727.867348	2	610.29435	1	y6
sp|P19367|HXK1_HUMAN	LVDEYSLNAGK	604.81151	2	752.39373	1	y7
sp|P19367|HXK1_HUMAN	LVDEYSLNAGK	604.81151	2	589.330401	1	y6
sp|P21399|ACOC_HUMAN	ANYLASPPLVIAYAIAGTIR	1037.588407	2	864.493778	1	y8
sp|P21399|ACOC_HUMAN	ANYLASPPLVIAYAIAGTIR	1037.588407	2	945.048386	2	y18
sp|P21399|ACOC_HUMAN	YQQAGLPLIVLAGK	735.937576	2	810.544751	1	y8
sp|P21399|ACOC_HUMAN	YQQAGLPLIVLAGK	735.937576	2	292.129182	1	b2

sp|P21399|ACOC_HUMAN	YQQAGLPLIVLAGK	735.937576	2	661.330401	1	b6
sp|P21912|DHSB_HUMAN	AGDKPHMQTYEVDLNK	615.964842	3	588.335152	1	y5
sp|P21912|DHSB_HUMAN	AGDKPHMQTYEVDLNK	615.964842	3	737.853383	2	y12
sp|P21912|DHSB_HUMAN	AGDKPHMQTYEVDLNK	615.964842	3	606.299435	1	b6
sp|P21912|DHSB_HUMAN	QQYLQSIEER	647.325316	2	761.378808	1	y6
sp|P21912|DHSB_HUMAN	QQYLQSIEER	647.325316	2	433.204138	1	y3
sp|P23368|MAOM_HUMAN	DPFYMGLYQK	631.299724	2	608.340238	1	y5
sp|P23368|MAOM_HUMAN	DPFYMGLYQK	631.299724	2	360.155397	1	b3
sp|P23368|MAOM_HUMAN	ALTSQLTDEELAQGR	816.41539	2	431.236107	1	y4
sp|P23368|MAOM_HUMAN	ALTSQLTDEELAQGR	816.41539	2	360.198993	1	y3
sp|P24752|THIL_HUMAN	TPIGSFLGSLSLLPATK	851.492913	2	729.450516	1	y7
sp|P24752|THIL_HUMAN	TPIGSFLGSLSLLPATK	851.492913	2	529.334424	1	y5
sp|P24752|THIL_HUMAN	TPIGSFLGSLSLLPATK	851.492913	2	416.25036	1	y4
sp|P24752|THIL_HUMAN	EAYMGNVLQGGEGQAPTR	626.631863	3	373.219394	1	y3
sp|P24752|THIL_HUMAN	EAYMGNVLQGGEGQAPTR	626.631863	3	500.743962	2	y10
sp|P24752|THIL_HUMAN	EAYMGNVLQGGEGQAPTR	626.631863	3	753.338097	2	b15
sp|P30613|KPYR_HUMAN	STSIIATIGPASR	637.359159	2	772.431178	1	y8
sp|P30613|KPYR_HUMAN	STSIIATIGPASR	637.359159	2	701.394064	1	y7
sp|P30613|KPYR_HUMAN	STSIIATIGPASR	637.359159	2	487.262322	1	y5
sp|P30613|KPYR_HUMAN	STSIIATIGPASR	637.359159	2	844.477459	1	b9
sp|P30613|KPYR_HUMAN	GSQVLVTVDPAFR	694.880258	2	805.420279	1	y7
sp|P30613|KPYR_HUMAN	GSQVLVTVDPAFR	694.880258	2	584.340238	1	b6
sp|P30613|KPYR_HUMAN	FGVEHGVDIVFASFVR	889.964854	2	1053.572757	1	y9
sp|P30613|KPYR_HUMAN	FGVEHGVDIVFASFVR	889.964854	2	938.545814	1	y8
sp|P30613|KPYR_HUMAN	FGVEHGVDIVFASFVR	889.964854	2	570.267073	1	b5
sp|P31040|DHSA_HUMAN	LGANSLLDLVVFGR	737.424833	2	918.540728	1	y8
sp|P31040|DHSA_HUMAN	LGANSLLDLVVFGR	737.424833	2	805.456664	1	y7
sp|P31040|DHSA_HUMAN	IDEYDYSKPIQGQQK	604.631857	3	727.867348	2	y12
sp|P31040|DHSA_HUMAN	IDEYDYSKPIQGQQK	604.631857	3	646.335684	2	y11
sp|P35557|HXK4_HUMAN	LVDESSANPGQQLYEK	889.43378	2	1076.5371	1	y9
sp|P35557|HXK4_HUMAN	LVDESSANPGQQLYEK	889.43378	2	702.330461	1	b7
sp|P35557|HXK4_HUMAN	LVDESSANPGQQLYEK	889.43378	2	816.373388	1	b8
sp|P35557|HXK4_HUMAN	LVDENLLFHGEASEQLR	657.337444	3	505.26344	3	y13
sp|P35557|HXK4_HUMAN	LVDENLLFHGEASEQLR	657.337444	3	571.272218	1	b5
sp|P35557|HXK4_HUMAN	LVDENLLFHGEASEQLR	657.337444	3	472.758018	2	b8
sp|P36957|ODO2_HUMAN	ASAFALQEQPVVNAVIDDTTK	739.718102	3	791.414525	1	y7
sp|P36957|ODO2_HUMAN	ASAFALQEQPVVNAVIDDTTK	739.718102	3	713.869891	2	b14
sp|P36957|ODO2_HUMAN	GLVVPVIR	852.566549	1	484.324194	1	y4
sp|P36957|ODO2_HUMAN	GLVVPVIR	852.566549	1	466.302396	1	b5
sp|P40925|MDHC_HUMAN	DLDVAILVGSMPR	462.586755	3	547.265692	1	y5
sp|P40925|MDHC_HUMAN	DLDVAILVGSMPR	462.586755	3	490.244229	1	y4
sp|P40925|MDHC_HUMAN	DLDVAILVGSMPR	462.586755	3	627.334818	1	b6
sp|P40925|MDHC_HUMAN	FVEGLPINDFSR	697.359159	2	638.289265	1	y5
sp|P40925|MDHC_HUMAN	FVEGLPINDFSR	697.359159	2	574.290745	2	y10
sp|P40925|MDHC_HUMAN	FVEGLPINDFSR	697.359159	2	546.292225	1	b5
sp|P40926|MDHM_HUMAN	VAVLGASGGIGQPLSLLLK	598.368016	3	783.533852	1	y7

sp|P40926|MDHM_HUMAN	VAVLGASGGIGQPLSLLLK	598.368016	3	705.919383	2	y15
sp|P40926|MDHM_HUMAN	MISDAIPELK	558.802099	2	872.472374	1	y8
sp|P40926|MDHM_HUMAN	MISDAIPELK	558.802099	2	486.292225	1	y4
sp|P48163|MAOX_HUMAN	DMAAFNERPIIFALSNPTSK	741.380656	3	546.288202	1	y5
sp|P48163|MAOX_HUMAN	DMAAFNERPIIFALSNPTSK	741.380656	3	795.410868	2	b14
sp|P48163|MAOX_HUMAN	QITDNIFLTTAEVIAQQVSDK	778.744428	3	704.357344	1	y6
sp|P48163|MAOX_HUMAN	QITDNIFLTTAEVIAQQVSDK	778.744428	3	1037.046769	2	b19
sp|P48735|IDHP_HUMAN	VAKPVVEMDGDEMTR	838.902747	2	1182.47655	1	y10
sp|P48735|IDHP_HUMAN	VAKPVVEMDGDEMTR	838.902747	2	1083.408136	1	y9
sp|P48735|IDHP_HUMAN	DQTDDQVTIDSALATQK	924.944709	2	1047.568065	1	y10
sp|P48735|IDHP_HUMAN	DQTDDQVTIDSALATQK	924.944709	2	802.321353	1	b7
sp|P50213|IDH3A_HUMAN	TPIAAGHPSMNLLLR	530.964337	3	497.281777	3	y14
sp|P50213|IDH3A_HUMAN	TPIAAGHPSMNLLLR	530.964337	3	464.930856	3	y13
sp|P50213|IDH3A_HUMAN	TPYTDVNIVTIR	696.380091	2	1030.589135	1	y9
sp|P50213|IDH3A_HUMAN	TPYTDVNIVTIR	696.380091	2	715.4461	1	y6
sp|P51553|IDH3G_HUMAN	GNIETNHNLPPSHK	779.392053	2	565.309272	1	y5
sp|P51553|IDH3G_HUMAN	GNIETNHNLPPSHK	779.392053	2	706.339289	2	b13
sp|P51553|IDH3G_HUMAN	DIDILIVR	478.792392	2	500.355494	1	y4
sp|P51553|IDH3G_HUMAN	DIDILIVR	478.792392	2	229.118283	1	b2
sp|P52789|HXK2_HUMAN	GLGATTHPTAAVK	612.340769	2	586.355888	1	y6
sp|P52789|HXK2_HUMAN	GLGATTHPTAAVK	612.340769	2	527.288005	2	y11
sp|P52789|HXK2_HUMAN	NVELVEGEEGR	615.801674	2	547.247065	1	y5
sp|P52789|HXK2_HUMAN	NVELVEGEEGR	615.801674	2	684.356282	1	b6
sp|P52790|HXK3_HUMAN	EQQTLQVAVATGGR	729.388979	2	560.315085	1	y6
sp|P52790|HXK3_HUMAN	EQQTLQVAVATGGR	729.388979	2	461.246672	1	y5
sp|P52790|HXK3_HUMAN	QLGLDQGILLNWTK	799.948672	2	1072.614956	1	y9
sp|P52790|HXK3_HUMAN	QLGLDQGILLNWTK	799.948672	2	944.556378	1	y8
sp|P53597|SUCA_HUMAN	QGTFHSQQALEYGTK	565.609276	3	597.287868	1	y5
sp|P53597|SUCA_HUMAN	QGTFHSQQALEYGTK	565.609276	3	468.245275	1	y4
sp|P53597|SUCA_HUMAN	MGHAGAIIAGGK	541.7924	2	686.419551	1	y8
sp|P53597|SUCA_HUMAN	MGHAGAIIAGGK	541.7924	2	326.128136	1	b3
sp|P55809|SCOT1_HUMAN	QYLSGELEVELTPQGTLAER	745.04974	3	436.235241	2	y8
sp|P55809|SCOT1_HUMAN	QYLSGELEVELTPQGTLAER	745.04974	3	631.319168	2	b11
sp|P55809|SCOT1_HUMAN	QYLSGELEVELTPQGTLAER	745.04974	3	681.843007	2	b12
sp|P55809|SCOT1_HUMAN	GGHVDLTMLGAMQVSK	822.415825	2	720.370886	1	y7
sp|P55809|SCOT1_HUMAN	GGHVDLTMLGAMQVSK	822.415825	2	765.394361	2	y14
sp|P55809|SCOT1_HUMAN	GGHVDLTMLGAMQVSK	822.415825	2	811.3767	1	b8
sp|P55809|SCOT1_HUMAN	GMGGAMDLVSSAK	1223.57587	1	719.393395	1	y7
sp|P55809|SCOT1_HUMAN	GMGGAMDLVSSAK	1223.57587	1	832.369171	1	b9
sp|P60174|TPIS_HUMAN	QSLGELIGTLNAAK	707.898648	2	1086.61535	1	y11
sp|P60174|TPIS_HUMAN	QSLGELIGTLNAAK	707.898648	2	900.551293	1	y9
sp|P60174|TPIS_HUMAN	QSLGELIGTLNAAK	707.898648	2	787.467229	1	y8
sp|P60174|TPIS_HUMAN	QSLGELIGTLNAAK	707.898648	2	674.383165	1	y7
sp|P60174|TPIS_HUMAN	VVLAYEPVWAIGTGK	801.948141	2	1220.631	1	y11
sp|P60174|TPIS_HUMAN	VVLAYEPVWAIGTGK	801.948141	2	928.525078	1	y9
sp|Q01813|K6PP_HUMAN	DLQSNVEHLTEK	706.854437	2	855.457058	1	y7

sp|Q01813|K6PP_HUMAN	DLQSNVEHLTEK	706.854437	2	756.388644	1	y6
sp|Q01813|K6PP_HUMAN	NVIFQPVAELK	629.363713	2	931.524744	1	y8
sp|Q01813|K6PP_HUMAN	NVIFQPVAELK	629.363713	2	522.808042	2	y9
sp|Q02218|ODO1_HUMAN	SSENGVDYVIMGMPHR	896.411271	2	1103.548867	1	y9
sp|Q02218|ODO1_HUMAN	SSENGVDYVIMGMPHR	896.411271	2	409.230627	1	y3
sp|Q02218|ODO1_HUMAN	LLDTAFDLDVFK	698.871568	2	736.387582	1	y6
sp|Q02218|ODO1_HUMAN	LLDTAFDLDVFK	698.871568	2	508.276575	1	y4
sp|Q15118|PDK1_HUMAN	AIYDFTDTVIR	657.340435	2	851.462144	1	y7
sp|Q15118|PDK1_HUMAN	AIYDFTDTVIR	657.340435	2	488.319108	1	y4
sp|Q15118|PDK1_HUMAN	AIYDFTDTVIR	657.340435	2	565.279846	2	y9
sp|Q15118|PDK1_HUMAN	AVPLAGFGYGLPISR	759.427376	2	862.478128	1	y8
sp|Q15118|PDK1_HUMAN	AVPLAGFGYGLPISR	759.427376	2	674.374612	2	y13
sp|Q15119|PDK2_HUMAN	HNDVVPTMAQGVLEYK	900.951086	2	466.204472	1	b4
sp|Q15119|PDK2_HUMAN	HNDVVPTMAQGVLEYK	900.951086	2	1249.599382	1	b12
sp|Q15119|PDK2_HUMAN	ATVESHESSLILPPIK	860.977627	2	567.38646	1	y5
sp|Q15119|PDK2_HUMAN	ATVESHESSLILPPIK	860.977627	2	454.302396	1	y4
sp|Q15120|PDK3_HUMAN	LFNYMYSTAPRPSLEPTR	715.026213	3	941.959442	2	y16
sp|Q15120|PDK3_HUMAN	LFNYMYSTAPRPSLEPTR	715.026213	3	884.937979	2	y15
sp|Q15120|PDK3_HUMAN	AAPLAGFGYGLPISR	745.411726	2	1066.568006	1	y10
sp|Q15120|PDK3_HUMAN	AAPLAGFGYGLPISR	745.411726	2	642.393336	1	y6
sp|Q16654|PDK4_HUMAN	HHNVVPTMAQGIIEYK	612.985689	3	587.304855	1	b5
sp|Q16654|PDK4_HUMAN	NAPLAGFGYGLPISR	766.914632	2	862.478128	1	y8
sp|Q16654|PDK4_HUMAN	NAPLAGFGYGLPISR	766.914632	2	642.393336	1	y6
sp|Q16654|PDK4_HUMAN	NAPLAGFGYGLPISR	766.914632	2	472.287808	1	y4
sp|Q16665|HIF1A_HUMAN	ITELMGYEPEELLGR	875.44002	2	1034.48631	1	b9
sp|Q16665|HIF1A_HUMAN	ITELMGYEPEELLGR	875.44002	2	1163.528903	1	b10
sp|Q16665|HIF1A_HUMAN	ITELMGYEPEELLGR	875.44002	2	469.220411	2	b8
sp|Q16665|HIF1A_HUMAN	GQVTTGQYR	505.256705	2	824.426093	1	y7
sp|Q16665|HIF1A_HUMAN	GQVTTGQYR	505.256705	2	544.272552	1	b6
sp|Q16798|MAON_HUMAN	GLFITIHDK	522.297841	2	726.414465	1	y6
sp|Q16798|MAON_HUMAN	GLFITIHDK	522.297841	2	437.245078	2	y7
sp|Q16798|MAON_HUMAN	GHLATMLNSWPEDNIK	913.44871	2	724.347934	2	y12
sp|Q16798|MAON_HUMAN	GHLATMLNSWPEDNIK	913.44871	2	1111.535325	1	b10
sp|Q96I99|SUCB2_HUMAN	FFVADTANEALEAAK	798.898845	2	1203.585172	1	y12
sp|Q96I99|SUCB2_HUMAN	FFVADTANEALEAAK	798.898845	2	1132.548058	1	y11
sp|Q96I99|SUCB2_HUMAN	DPNVVGQLAK	520.790381	2	327.12991	1	b3
sp|Q96I99|SUCB2_HUMAN	DPNVVGQLAK	520.790381	2	426.198324	1	b4
sp|Q99798|ACON_HUMAN	IVYGHLDDPASQEIER	921.455047	2	1044.495629	1	y9
sp|Q99798|ACON_HUMAN	IVYGHLDDPASQEIER	921.455047	2	913.441408	1	b8
sp|Q99798|ACON_HUMAN	NAVTQEFGPVPDTAR	801.399543	2	812.426093	1	y8
sp|Q99798|ACON_HUMAN	NAVTQEFGPVPDTAR	801.399543	2	559.283451	1	y5
sp|Q9NR19|ACSA_HUMAN	SAHVPSLQR	994.542854	1	699.4148	1	y6
sp|Q9NR19|ACSA_HUMAN	SAHVPSLQR	994.542854	1	395.203744	1	b4
sp|Q9NR19|ACSA_HUMAN	SAHVPSLQR	994.542854	1	820.431178	1	b8
sp|Q9NR19|ACSA_HUMAN	IGPIATPDYIQNAPGLPK	933.012001	2	847.959237	2	y16
sp|Q9NR19|ACSA_HUMAN	IGPIATPDYIQNAPGLPK	933.012001	2	452.286745	1	b5

sp|Q9NR19|ACSA_HUMAN	IGPIATPDYIQNAPGLPK	933.012001	2	553.334424	1	b6
sp|Q9NUB1|ACS2L_HUMAN	GIVHTQAGYLLYAALTHK	652.694903	3	803.441014	1	y7
sp|Q9NUB1|ACS2L_HUMAN	GIVHTQAGYLLYAALTHK	652.694903	3	640.377686	1	y6
sp|Q9NUB1|ACS2L_HUMAN	GIVHTQAGYLLYAALTHK	652.694903	3	562.970256	3	y15
sp|Q9NUB1|ACS2L_HUMAN	MDDVINISGHR	628.806236	2	683.358347	1	y6
sp|Q9NUB1|ACS2L_HUMAN	MDDVINISGHR	628.806236	2	569.31542	1	y5
sp|Q9NUB1|ACS2L_HUMAN	MDDVINISGHR	628.806236	2	456.231356	1	y4
sp|Q9UI32|GLSL_HUMAN	VVQESSSGGLLDR	673.849155	2	1020.495629	1	y10
sp|Q9UI32|GLSL_HUMAN	VVQESSSGGLLDR	673.849155	2	804.421007	1	y8
sp|Q9UI32|GLSL_HUMAN	VVQESSSGGLLDR	673.849155	2	630.35695	1	y6

Table F2: Targeted proteomics analysis of 10 mM DCA cultures compared to control cultures

UniProt ID	adj.P.Val	Fold change	UniProt ID	adj.P.Val	Fold change
sp|P08243|ASNS_HUMAN	0.0040	1.37	sp|O43837|IDH3B_HUMAN	0.2459	1.06
sp|Q15119|PDK2_HUMAN	0.0105	1.41	sp|Q15120|PDK3_HUMAN	0.2556	1.20
sp|P07195|LDHB_HUMAN	0.0285	1.37	sp|P09104|ENOG_HUMAN	0.2905	1.14
sp|P18669|PGAM1_HUMAN	0.0349	-1.35	sp|P09622|DLDH_HUMAN	0.3608	1.13
sp|P30613|KPYR_HUMAN	0.0395	1.22	sp|P06744|G6PI_HUMAN	0.3608	-1.16
sp|P60174|TPIS_HUMAN	0.0544	-1.43	sp|P00338|LDHA_HUMAN	0.3608	1.13
sp|P05062|ALDOB_HUMAN	0.0550	1.19	sp|P48735|IDHP_HUMAN	0.3608	1.07
sp|P04406|G3P_HUMAN	0.0720	-1.42	sp|Q02218|ODO1_HUMAN	0.3629	-1.10
sp|Q9NR19|ACSA_HUMAN	0.0726	1.55	sp|Q15118|PDK1_HUMAN	0.4310	-1.08
sp|Q96I99|SUCB2_HUMAN	0.0726	1.38	sp|Q16798|MAON_HUMAN	0.4461	-1.13
sp|P48163|MAOX_HUMAN	0.0784	-1.63	sp|P24752|THIL_HUMAN	0.4520	1.04
sp|P00558|PGK1_HUMAN	0.0784	-1.26	sp|P23368|MAOM_HUMAN	0.4538	1.09
sp|P19367|HXK1_HUMAN	0.1002	1.26	sp|Q16654|PDK4_HUMAN	0.4726	1.18
sp|P09467|F16P1_HUMAN	0.1076	1.23	sp|P11413|G6PD_HUMAN	0.4761	1.09
sp|P07205|PGK2_HUMAN	0.1081	1.26	sp|P07954|FUMH_HUMAN	0.4761	1.09
sp|Q99798|ACON_HUMAN	0.1230	1.23	sp|P08559|ODPA_HUMAN	0.4803	1.09
sp|P13929|ENOB_HUMAN	0.1230	1.13	sp|P07864|LDHC_HUMAN	0.4815	-1.03
sp|P15259|PGAM2_HUMAN	0.1230	-1.24	sp|P14618|KPYM_HUMAN	0.4846	1.08
sp|Q9UI32|GLSL_HUMAN	0.1230	1.12	sp|P36957|ODO2_HUMAN	0.4999	1.07
sp|P08237|K6PF_HUMAN	0.1427	1.18	sp|P35557|HXK4_HUMAN	0.4999	1.05
sp|P52790|HXK3_HUMAN	0.1489	1.11	sp|P06733|ENOA_HUMAN	0.5355	-1.16
sp|Q01813|K6PP_HUMAN	0.1489	1.18	sp|P31040|DHSA_HUMAN	0.5732	1.10
sp|P40925|MDHC_HUMAN	0.1495	1.26	sp|P50213|IDH3A_HUMAN	0.6132	-1.05
sp|P15104|GLNA_HUMAN	0.1536	1.23	sp|P52789|HXK2_HUMAN	0.7760	-1.02
sp|P04075|ALDOA_HUMAN	0.1635	1.35	sp|P51553|IDH3G_HUMAN	0.7814	-1.03
sp|P17858|K6PL_HUMAN	0.1723	1.20	sp|P53597|SUCA_HUMAN	0.8446	-1.03
sp|O00757|F16P2_HUMAN	0.1738	1.16	sp|O75874|IDHC_HUMAN	0.8613	1.02
sp|P55809|SCOT1_HUMAN	0.1875	1.35	sp|P09972|ALDOC_HUMAN	0.8881	-1.04
sp|P21399|ACOC_HUMAN	0.2293	1.25	sp|Q9NUB1|ACS2L_HUMAN	0.9899	1.00
sp|O75390|CISY_HUMAN	0.2339	-1.27	sp|P21912|DHSB_HUMAN	0.9899	1.01
sp|Q16665|HIF1A_HUMAN	0.2361	1.11	sp|P40926|MDHM_HUMAN	1.0000	1.01

Table F3: Targeted proteomics analysis of 5 mM DCA cultures compared to control cultures

UniProt ID	adj.P.Val	Fold change	UniProt ID	adj.P.Val	Fold change
sp|P08243|ASNS_HUMAN	0.0559	1.18	sp|P00338|LDHA_HUMAN	0.8944	1.08
sp|P30613|KPYR_HUMAN	0.0559	1.27	sp|Q16654|PDK4_HUMAN	0.8944	1.10
sp|P40926|MDHM_HUMAN	0.0559	-1.70	sp|P21399|ACOC_HUMAN	0.8944	1.09
sp|Q15119|PDK2_HUMAN	0.4210	1.21	sp|P36957|ODO2_HUMAN	0.8944	1.05
sp|O75390|CISY_HUMAN	0.5480	0.65	sp|P06744|G6PI_HUMAN	0.8944	1.03
sp|P18669|PGAM1_HUMAN	0.5480	-1.09	sp|Q99798|ACON_HUMAN	0.9551	1.05
sp|P55809|SCOT1_HUMAN	0.5480	1.39	sp|Q16798|MAON_HUMAN	0.9551	-1.07
sp|P31040|DHSA_HUMAN	0.5705	-1.37	sp|P00558|PGK1_HUMAN	0.9551	-1.05
sp|P04075|ALDOA_HUMAN	0.6751	1.43	sp|P21912|DHSB_HUMAN	0.9551	1.04
sp|O43837|IDH3B_HUMAN	0.7705	1.06	sp|P07195|LDHB_HUMAN	0.9566	1.04
sp|Q96I99|SUCB2_HUMAN	0.7705	1.19	sp|P14618|KPYM_HUMAN	0.9576	1.05
sp|P48735|IDHP_HUMAN	0.7705	1.09	sp|P50213|IDH3A_HUMAN	0.9576	1.03
sp|P08237|K6PF_HUMAN	0.7705	1.11	sp|P15104|GLNA_HUMAN	0.9621	1.04
sp|P09467|F16P1_HUMAN	0.8742	1.11	sp|P07954|FUMH_HUMAN	0.9708	1.03
sp|P09622|DLDH_HUMAN	0.8944	-1.12	sp|Q02218|ODO1_HUMAN	0.9708	-1.03
sp|P19367|HXK1_HUMAN	0.8944	1.10	sp|P08559|ODPA_HUMAN	0.9708	-1.03
sp|P13929|ENOB_HUMAN	0.8944	1.06	sp|P23368|MAOM_HUMAN	0.9708	1.02
sp|Q16665|HIF1A_HUMAN	0.8944	1.17	sp|P17858|K6PL_HUMAN	0.9708	1.03
sp|O75874|IDHC_HUMAN	0.8944	-1.04	sp|P24752|THIL_HUMAN	1.0000	1.01
sp|Q9NR19|ACSA_HUMAN	0.8944	1.17	sp|Q15118|PDK1_HUMAN	1.0000	-1.01
sp|P60174|TPIS_HUMAN	0.8944	-1.10	sp|P09972|ALDOC_HUMAN	1.0000	1.04
sp|P53597|SUCA_HUMAN	0.8944	-1.07	sp|P07864|LDHC_HUMAN	1.0000	1.01
sp|P51553|IDH3G_HUMAN	0.8944	1.05	sp|P35557|HXK4_HUMAN	1.0000	1.01
sp|P15259|PGAM2_HUMAN	0.8944	-1.04	sp|Q9UI32|GLSL_HUMAN	1.0000	-1.01
sp|Q15120|PDK3_HUMAN	0.8944	1.11	sp|P52789|HXK2_HUMAN	1.0000	-1.00
sp|P11413|G6PD_HUMAN	0.8944	1.04	sp|P48163|MAOX_HUMAN	1.0000	-1.01
sp|P05062|ALDOB_HUMAN	0.8944	1.04	sp|O00757|F16P2_HUMAN	1.0000	1.01
sp|Q01813|K6PP_HUMAN	0.8944	1.06	sp|P06733|ENOA_HUMAN	1.0000	1.01
sp|Q9NUB1|ACS2L_HUMAN	0.8944	-1.06	sp|P04406|G3P_HUMAN	1.0000	-1.00
sp|P07205|PGK2_HUMAN	0.8944	1.06	sp|P52790|HXK3_HUMAN	1.0000	1.00
sp|P09104|ENOG_HUMAN	0.8944	1.07	sp|P40925|MDHC_HUMAN	1.0000	-1.00

Appendix G: Results of HEK293 cell transcriptomics

Table G1: Differentially regulated genes in 10 mM DCA cultures compared to control cultures.

Down-regulated Gene symbol	Protein name	Adj p-value	Fold change
SNORA12	small nucleolar RNA, H/ACA box 12	0.00026	3.6540
IGFBP5	insulin-like growth factor binding protein 5	0.00003	3.1069
MYOM2	myomesin (M-protein) 2, 165kDa	0.00013	2.9970
HS.572495	CDNA clone IMAGE:5268658	0.00012	2.5257
HS.170035	Transcribed locus	0.00135	2.4412
HS.335413	Uncharacterized LOC100134361	0.00103	2.4008
TKTL1	transketolase-like 1	0.00258	2.3701
HIST1H4K	histone cluster 1, H4k	0.00189	2.3352
HS.192506	Transcribed locus	0.00218	2.3072
HIST2H2BE	histone cluster 2, H2be	0.00256	2.2746
C10ORF140	chromosome 10 open reading frame 140	0.00384	2.1327
SNORD13	small nucleolar RNA, C/D box 13	0.00709	2.0989
HAS2AS	HAS2 antisense RNA (non-protein coding)	0.00189	2.0168
GAS1	growth arrest-specific 1	0.00452	1.9843
C18ORF56	chromosome 18 open reading frame 56	0.00632	1.9747
PCDH19	protocadherin 19	0.00189	1.9663
LOC100134361	Uncharacterized LOC100134361	0.00105	1.9648
C3ORF31	chromosome 3 open reading frame 31	0.00288	1.9432
SSPO	SCO-spondin homolog (Bos taurus)	0.00560	1.9408
C7ORF68	Hypoxia Inducible Lipid Droplet-Associated	0.00740	1.9315
ASB9	ankyrin repeat and SOCS box containing 9	0.00462	1.8770
HS.444913	Transcribed locus	0.00384	1.8620
VASH2	vasohibin 2	0.00432	1.8203
NOL12	nucleolar protein 12	0.00560	1.7881
C9ORF169	chromosome 9 open reading frame 169	0.00505	1.7871
LYPD1	LY6/PLAUR domain containing 1	0.00189	1.7704
ZNF2	zinc finger protein 2	0.00323	1.7560
SCNN1D	sodium channel, non-voltage-gated 1, delta subunit	0.00813	1.7535
CLYBL	citrate lyase beta like	0.00372	1.7420
GAL3ST4	galactose-3-O-sulfotransferase 4	0.00484	1.7400
MRPL30	mitochondrial ribosomal protein L30	0.00646	1.7333
LQK1	putative uncharacterized protein LQK1	0.00396	1.7127
KIF15	kinesin family member 15	0.00996	1.7071
LYRM7	Lyrm7 homolog (mouse)	0.00560	1.6829
CCDC45	centrosomal protein of 95 kDa	0.00973	1.6691
ARL17P1	ADP-Ribosylation Factor-Like 17A	0.00989	1.6611
TCEA2	transcription elongation factor A (SII), 2	0.00452	1.6571
BTBD12	SLX4 Structure-Specific Endonuclease Subunit	0.00996	1.6501
LOC286467	Family With Sequence Similarity 195, Member A Pseudogene	0.00560	1.6475
LHPP	phospholysine phosphohistidine inorganic pyrophosphate phosphatase	0.00699	1.6455
C20ORF7	chromosome 20 open reading frame 7	0.00651	1.6348
IFIT1	interferon-induced protein with tetratricopeptide repeats 1	0.00755	1.6248
PDK3	pyruvate dehydrogenase kinase, isozyme 3	0.00996	1.6057

LOC439949	PRKCQ Antisense RNA 1	0.00989	1.6013
OSGEPL1	O-sialoglycoprotein endopeptidase-like 1	0.00740	1.5979
ALDH4A1	aldehyde dehydrogenase 4 family, member A1	0.00997	1.5973
CTSL2	cathepsin L2	0.00976	1.5805
FLJ39827	APC membrane recruitment protein 1	0.00996	1.5438
Up-regulated Gene symbol	Protein name	Adj p-value	Fold change
INHBE	inhibin, beta E	0.00002	5.1378
SESN2	sestrin 2	0.00189	3.6613
ETV5	ets variant 5	0.00008	3.2484
TNFRSF12A	tumor necrosis factor receptor superfamily, member 12A	0.00218	3.1621
TNNT1	troponin T type 1 (skeletal, slow)	0.00560	2.9702
DDIT3	DNA-damage-inducible transcript 3	0.00065	2.8866
ETV4	ets variant 4	0.00406	2.8155
LOC387763	Chromosome 11 open reading frame 96	0.00007	2.7634
DDIT4	DNA-damage-inducible transcript 4	0.00005	2.7388
LTBR	lymphotoxin beta receptor (TNFR superfamily, member 3)	0.00126	2.6747
MIR1974	microRNA 1974	0.00168	2.6678
HMOX1	heme oxygenase (decycling) 1	0.00026	2.6297
MICALL1	MICAL-like 1	0.00065	2.5090
SLC4A2	solute carrier family 4, anion exchanger, member 2	0.00972	2.4845
IRF2BP1	interferon regulatory factor 2 binding protein 1	0.00626	2.4165
INA	internexin neuronal intermediate filament protein, alpha	0.00013	2.4057
STC2	stanniocalcin 2	0.00026	2.2996
CHAC1	ChaC, cation transport regulator homolog 1	0.00462	2.2851
ULBP1	UL16 binding protein 1	0.00168	2.2554
PLAGL1	pleiomorphic adenoma gene-like 1	0.00679	2.2505
IRX4	iroquois homeobox 4	0.00084	2.2310
SLC7A5	solute carrier family 7 (amino acid transporter light chain, L system), member 5	0.00042	2.2279
GDF15	growth differentiation factor 15	0.00505	2.2220
SGSH	N-sulfoglucosamine sulfohydrolase	0.00218	2.2129
SLC3A2	solute carrier family 3 (activators of dibasic and neutral amino acid transport), member 2	0.00084	2.2083
IRAK1	interleukin-1 receptor-associated kinase 1	0.00189	2.1979
CEBPB	CCAAT/enhancer binding protein (C/EBP), beta	0.00117	2.1597
LOC392437	Ferritin, Light Polypeptide Pseudogene	0.00158	2.1308
PLP2	proteolipid protein 2 (colonic epithelium-enriched)	0.00189	2.0884
CYBASC3	cytochrome b, ascorbate dependent 3	0.00202	2.0738
KCNK12	potassium channel, subfamily K, member 12	0.00967	2.0733
TMEM54	transmembrane protein 54	0.00524	2.0527
GADD45B	growth arrest and DNA-damage-inducible, beta	0.00189	2.0473
ANXA3	annexin A3	0.00318	2.0430
ORMDL3	ORM1-like 3 (S. cerevisiae)	0.00258	2.0297
LPPR2	lipid phosphate phosphatase-related protein type 2	0.00772	2.0192
CHGB	chromogranin B (secretogranin 1)	0.00524	2.0126
SCAMP5	secretory carrier membrane protein 5	0.00452	2.0098
BCAT1	branched chain amino-acid transaminase 1, cytosolic	0.00228	1.9834

EPR1	effector cell peptidase receptor 1 (non-protein coding)	0.00682	1.9806
CDC42EP1	CDC42 effector protein (Rho GTPase binding) 1	0.00190	1.9794
XKR8	XK, Kell blood group complex subunit-related family, member 8	0.00276	1.9786
SLC1A5	solute carrier family 1 (neutral amino acid transporter), member 5	0.00354	1.9640
XYLB	xylulokinase homolog (H. influenzae)	0.00491	1.9490
PCK2	phosphoenolpyruvate carboxykinase 2 (mitochondrial)	0.00646	1.9430
LOC143666	Uncharacterized LOC143666	0.00189	1.9316
SRXN1	sulfiredoxin 1	0.00189	1.9287
ZNF416	zinc finger protein 416	0.00920	1.9223
SYP	synaptophysin	0.00505	1.9201
ASNS	asparagine synthetase (glutamine-hydrolyzing)	0.00105	1.9173
MORC2	MORC family CW-type zinc finger 2	0.00258	1.9172
CRMP1	collapsin response mediator protein 1	0.00189	1.9153
NPLOC4	nuclear protein localization 4 homolog (S. cerevisiae)	0.00920	1.9009
IFRD1	interferon-related developmental regulator 1	0.00189	1.8929
ABCB1	ATP-binding cassette, sub-family B (MDR/TAP), member 1	0.00709	1.8898
EMP3	epithelial membrane protein 3	0.00258	1.8806
NFE2L1	nuclear factor (erythroid-derived 2)-like 1	0.00326	1.8710
ISG20	interferon stimulated exonuclease gene 20kDa	0.00189	1.8575
SAPS1	protein phosphatase 6, regulatory subunit 1	0.00632	1.8559
S100P	S100 calcium binding protein P	0.00462	1.8533
MTHFD1L	methylenetetrahydrofolate dehydrogenase (NADP+ dependent) 1-like	0.00168	1.8506
CHPF2	chondroitin polymerizing factor 2	0.00740	1.8475
CYTH1	cytohesin 1	0.00646	1.8444
CORO1B	coronin, actin binding protein, 1B	0.00740	1.8313
MARS	methionyl-tRNA synthetase	0.00189	1.8290
EPCAM	epithelial cell adhesion molecule	0.00362	1.8180
SPR	sepiapterin reductase (7,8-dihydrobiopterin:NADP+ oxidoreductase)	0.00920	1.8118
C19ORF51	chromosome 19 open reading frame 51	0.00524	1.8026
ZNF766	zinc finger protein 766	0.00920	1.7969
LOC100132139	similar to methylenetetrahydrofolate dehydrogenase (NADP+ dependent) 1-like	0.00644	1.7945
CTH	cystathionase (cystathionine gamma-lyase)	0.00189	1.7845
PERP	PERP, TP53 apoptosis effector	0.00632	1.7800
ZNF502	zinc finger protein 502	0.00432	1.7764
MTHFD2	methylenetetrahydrofolate dehydrogenase (NADP+ dependent) 2, methenyltetrahydrofolate cyclohydrolase	0.00218	1.7763
LOC644132	similar to basic-leucine zipper transcription factor MafG	0.00524	1.7714
SLC6A9	solute carrier family 6 (neurotransmitter transporter, glycine), member 9	0.00500	1.7642
TK1	thymidine kinase 1, soluble	0.00452	1.7617
XBP1	X-box binding protein 1	0.00208	1.7602
GLIPR1	GLI pathogenesis-related 1	0.00578	1.7578
FADS1	fatty acid desaturase 1	0.00996	1.7563
BSPRY	B-box and SPRY domain containing	0.00996	1.7531
MID1IP1	MID1 interacting protein 1	0.00552	1.7521
TRIB3	tribbles homolog 3 (Drosophila)	0.00475	1.7453
FKBPL	FK506 binding protein like	0.00989	1.7382

GTF3C1	general transcription factor IIIC, polypeptide 1, alpha 220kDa	0.00462	1.7283
AGPAT9	1-acylglycerol-3-phosphate O-acyltransferase 9	0.00709	1.7173
SLC35D2	solute carrier family 35, member D2	0.00740	1.7130
HSD17B14	hydroxysteroid (17-beta) dehydrogenase 14	0.00704	1.6997
CBS	cystathionine-beta-synthase	0.00560	1.6837
NR0B1	nuclear receptor subfamily 0, group B, member 1	0.00570	1.6819
ARAP3	ArfGAP with RhoGAP domain, ankyrin repeat and PH domain 3	0.00646	1.6814
CYR61	cysteine-rich, angiogenic inducer, 61	0.00835	1.6802
FLNC	filamin C, gamma	0.00740	1.6798
TRIP6	thyroid hormone receptor interactor 6	0.00681	1.6792
SREBF1	sterol regulatory element binding transcription factor 1	0.00996	1.6694
STX3	syntaxin 3	0.00975	1.6685
ZNF134	zinc finger protein 134	0.00646	1.6551
MTA2	metastasis associated 1 family, member 2	0.00892	1.6515
CD44	CD44 molecule (Indian blood group)	0.00976	1.6492
MBD3	methyl-CpG binding domain protein 3	0.00864	1.6487
TAC1	tachykinin, precursor 1	0.00453	1.6457
SH2B3	SH2B adaptor protein 3	0.00835	1.6418
RIMS3	regulating synaptic membrane exocytosis 3	0.00424	1.6351
LOC645166	lymphocyte-specific protein 1 pseudogene	0.00646	1.6302
DHRS2	dehydrogenase/reductase (SDR family) member 2	0.00835	1.6255
SEZ6L2	seizure related 6 homolog (mouse)-like 2	0.00940	1.6235
PPIF	peptidylprolyl isomerase F	0.00989	1.6234
LOC342979	paralemmin 3	0.00989	1.6204
ZNF763	zinc finger protein 763	0.00659	1.5933
ADORA2B	adenosine A2b receptor	0.00524	1.5825
SLC45A3	solute carrier family 45, member 3	0.00975	1.5801
SHMT2	serine hydroxymethyltransferase 2 (mitochondrial)	0.00644	1.5782
HERPUD1	homocysteine-inducible, endoplasmic reticulum stress-inducible, ubiquitin-like domain member 1	0.00644	1.5630
SPINT2	serine peptidase inhibitor, Kunitz type, 2	0.00922	1.5417
ZNF274	zinc finger protein 274	0.00996	1.5175
KCTD15	potassium channel tetramerisation domain containing 15	0.00996	1.4912

Appendix H: Generating a stable HEK293 cell line overexpressing resistin-like molecule β using a Tet-On 3G inducible expression system

H.1. Introduction

Transfection of cells is usually followed first by a selection for cells that incorporated the gene of interest (GOI) in their genome and then by a single cell selection to obtain single cell clones with desired GOI expression from a pool of transfected cells. In Dietmair et al. an HEK293F cell line was transfected to express a recombinant protein and the obtained single cell clone showed also reduced glucose consumption. Transcriptomics analysis of that clone revealed an about 66 times higher expression of resistin-like molecule beta (RETNLB) mRNA (Dietmair et al. 2012). RETNLB belongs to a family of Cysteine rich sercreted protein composed of resisitn, resisitn like α and RETNLB (Steppan, Brown, et al. 2001). These proteins, particularly resisitin, have been linked to insulin resistance and diabetes (Kushiyama et al. 2005; Rajala et al. 2003; Schwartz & Lazar 2011; Steppan, Bailey, et al. 2001). It was hsown that RETNLB over expression I rate skeletal muscle cells reduced glucose uptake (Moon et al. 2003). However, the role of RETNLB in humans or human cell lines has been hardly investigated (Neilson et al. 2011; Zheng et al. 2012) and further explorations are needed to clearly elucidate RETNLB metabolic role.

Single cell clone selection can lead to the selection of a clone that is different from the parental cell line in addition to the GOI and that can be a problem if the effect of a single gene is investigated. One possible approach to avoid the unintended selection for other cellular characteristics is to use an inducible expression system. A cell line is first transfected with a transactivator protein followed by the transfection of the GOI together with the inducible promoter. Using a tetracycline-controlled transcriptional activation system only one cell line is generated in which the expression of the GOI can be induced by adding doxycycline (Dox) to the cell culture (Figure H1). Here, an HEK293 cell line was transfected with a Tet-On 3G transactivator protein followed by the transfection with RETNLB that is under the control of a TRE3G promoter (P_{TRE3G}).

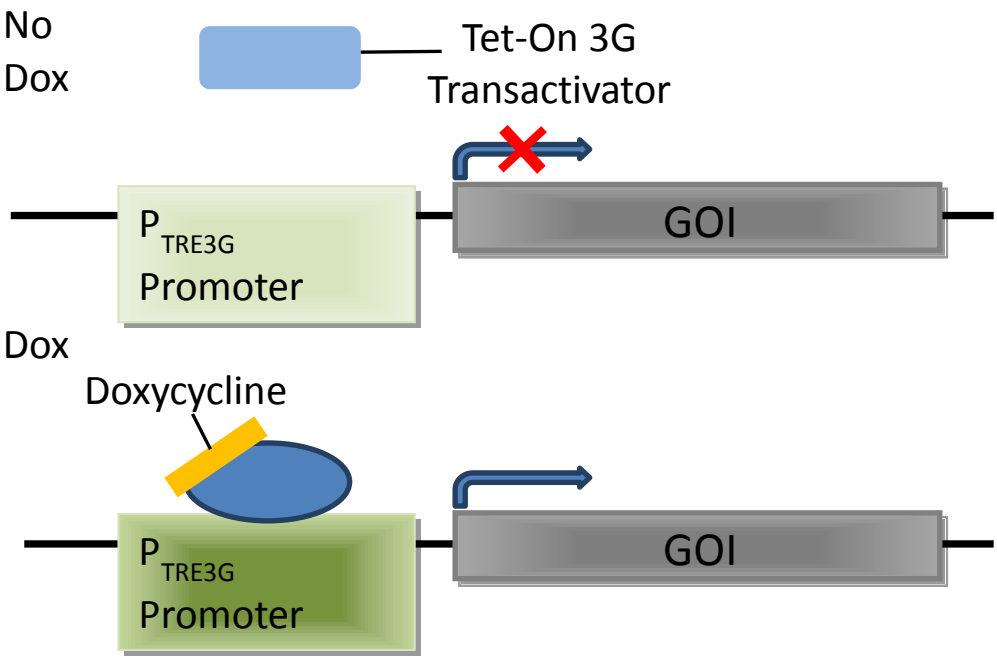

Figure H1: Tet-On 3G system allows inducible gene expression. Cells constantly express the Tet-On 3G transactivator protein. Dox binds to the Tet-On 3G transactivator causing a conformational change allowing it to bind to the tet operator sequence located in the TRE3G promoter (P_{TRE3G}) activating the expression of the GOI (figure adapted from Tet-On 3G Inducible Expression Systems User Manual (Clontech)).

H.2. Material and methods

H.2.1. Cell culture, transfection and single cell selection

HEK293F cells (LifeTechnologies) were cultivated in Freestyle 293 expression medium (LifeTechnologies) supplemented with 4 mM GlutaMAX (LifeTechnologies), 0.2% v/v Anti-Clumping agent (LifeTechnologies) and 5% v/v fetal calf bovine serum (Thermo Scientific). Cells were cultivated in vented shake flasks in humidified incubators set to 37°C, 7.5% CO_2, and 130 rpm. Cells were first transfected with the pCMV-Tet3G plasmid using FreeStyle MAX reagent (LifeTechnologies) according to manufacturer's instructions. Geneticin (LifeTechnologies) was used to select for cells that integrated the plasmid. Single cell selection was performed using limited dilution and 47 single cell clones were obtained of which 18 were tested for Tet-On transactivator mRNA expression using qRT-PCR. RNA was extracted using the RNA Mini Kit (Qiagen) with on-column DNA digestion using the RNase-Free DNase Set (Qiagen). cDNA was synthesized using the ProtoScript M-MuLV First Strand cDNA Synthesis Kit (New England BioLabs) and subjected to qRT-PCR described below.

Five clones with the highest Tet-On transactivator mRNA expression were transiently transfected with the pTRE3G-Luc plasmid (Clontech) using FreeStyle MAX reagent. 500 ng/ml doxycycline (Dox) was added 4 hours after transfection to the cell culture and incubated for 24 hours. Cells were harvested and luciferase activity was analyzed using the Luciferase Assay System (Promega) according to manufacturer's instructions. The clone with highest fold change in luciferase assay was then transfected with the pTRE3G-RETNLB plasmid and Linear Puromycin Marker (Clontech) using FreeStyle MAX reagent. After 96 hours, puromycin dihydrochloride (LifeTechnologies) was added to the cell culture to select for cells with integrated puromycin marker. Before single cell selection, a sample from the transfected pool was analyzed for inducible RETNLB mRNA expression. Cells were cultivated in a 6-well plate in duplicates and 500 ng/ml Dox was added to one well. Cells were incubated for 48 hours, harvested, mRNA was extracted, cDNA was synthesized as described before followed by qRT-PCR analysis. This was followed by single cell selection using limited dilution and 18 single cell clones were obtained. Single cell clones were analyzed for RETNLB mRNA expression as described before. Glucose concentration in cell culture supernatant was measured using a Nova Bioprofiler FLEX (Nova Biomedical).

H.2.2. Generation of pTRE3G-RETNLB plasmid

The RETNLB clone from the lentiviral human ORF expression library (Škalamera et al. 2012) was obtained from the ARVEC facility at the University of Queensland Diamantina Institute. The RETNLB gene was amplified by PCR into a pBluescript vector and transformed into *E.coli*. A white colony containing the vector with insert was selected using blue/white screening induced by X-gal and IPTG. The RETNLB gene was than digested from the pBluescript clone and ligated into the pTRE3G vector. Clones were screened for the presence of the insert by restriction digest. The final construct was submitted to AGRF (AGRF Brisbane) for sequencing to ensure that correct RETNLB sequence is present in pTRE3G-RETNLB plasmid.

H.2.3. qRT-PCR

A Rotor-Gene 3000A (Corbett Research) and SsoAdvanced SYBR Green Supermix (Bio-Rad) were used according to manufacturer's instructions for qRT-PCR. The following primer pairs were used.

Table H1: Primer pairs used for qRT-PCR

Tet-On 3G F1	5'- CCG TGG GCC ACT TTA CAC -3'
Tet-On 3G R1	5'- AAA AGG AAG GCA GGT TCG -3'
Tet-On 3G F2	5'- CAA CGC CAA GTC ATA CCG -3'
Tet-On 3G R2	5'- ACG CAG CCC AGT GTA AAG -3'
YWHAZ F	5'- ACT TTT GGT ACA TTG TGG CTT CAA -3'
YWHAZ R	5'- CCG CCA GGA CAA ACC AGT AT-3'
RETNLB F1	5'- CCG GGG AGT ACT CAG TGT TCC T -3'
RETNLB R1	5'- TGA CAC TAG CAC ACG AGA GCT -3'
RETNLB F2	5'- GTC AAA AGC CAA GGC AGA CCG -3'
RETNLB R2	5'- ACG AAC CAC AGC CAT AGC CAC -3'

H.3. Results and discussion

H.3.1. qRT-PCR of Tet-On transactivator transfected cells

In total 18 single cell clones were tested for Tet-On transactivator mRNA expression using qRT-PCR. The qRT-PCR data was analyzed using the comparative Ct method (also known as the $2^{-\Delta\Delta Ct}$ method) comparing Tet-On transactivator single cell clones with the Tet-On transactivator cell pool. The five single cell clones with the highest Tet-On transactivator mRNA expression compared to the cell pool are shown in Table H2.

Table H2: Clones with highest relative Tet-On transactivator mRNA expression. Clones with highest Tet-On transactivator mRNA expression relative to housekeeping enzyme, YWHAZ, mRNA expression. Two primer pairs were used for Tet-On transactivator mRNA and one primer pair for YWHAZ (Tyrosine 3-Monooxygenase/ Tryptophan 5-Monooxygenase Activation Protein Zeta Polypeptide) mRNA. Ct = cycle threshold.

	Ct Primer Tet-On 1	Ct Primer Tet-On 2	Ct Primer YWHAZ	Mean Fold change ($2^{-\Delta\Delta Ct}$)
7	10.13	9.86	14.55	2.7962
46	11.31	11.13	15.19	1.8690
28	10.68	10.19	13.98	1.3851
22	10.66	10.35	14.39	1.7559
34	10.84	10.37	15.07	2.6208

H.3.2. Luciferase assay

Five clones with high Tet-On transactivator mRNA expression (Table H2) were transiently transfected with pTRE3G-Luc plasmid. 500 ng/ml doxycycline (Dox) was added 4 hours

after transfection to the cell culture, incubated for 24 hours and luciferase assay was performed (Table H3).

Table H3: Luciferase assay results. Five clones with high Tet-On transactivator mRNA expression were analyzed using the luciferase assay. Clone 22 had the highest fold change. RLU = relative light unit.

clone	+Dox RLU	-Dox RLU	fold change
7	8260000	66654	123.92
46	9200000	64320	143.04
28	5660000	103134	54.88
22	8660000	30789	281.27
34	4580000	303751	15.08

Although, all clones showed high Tet-On transactivator mRNA expression, the fold changes in the luciferase assay were quite different. Clone 22 had the highest fold change and was used for transfection with the pTRE3G-RETNLB plasmid and Linear Puromycin Marker.

H.3.3. qRT-PCR and RETNLB sequencing of RETNLB transfected cell pool

After transfection with the pTRE3G-RETNLB plasmid and Linear Puromycin Marker and before single clone selection the cell pool was tested for inducible RETNLB expression. Cells were cultivated with 500 ng/ml Dox for 48 hours or without Dox as control. qRT-PCR gave good signals for RETNLB mRNA in cells treated Dox whereas only a very week signal was obtained from cells cultivated without Dox (Table H4).

Table H4: Relative mRNA expression of RETNLB with and without Dox. RETNLB transfected cell pool was analyzed for RETNLB mRNA expression when cultivated with 500 ng/ml Dox for 48 hours and without Dox. Ct = cycle threshold, YWHAZ = Tyrosine 3-Monooxygenase/ Tryptophan 5-Monooxygenase Activation Protein Zeta Polypeptide.

	Ct Primer RETNLB 1	Ct Primer RETNLB 2	Ct Primer YWHAZ
22	33.41	30.3	14.62
22 + DOX	20.09	20.43	14.98

Due to the slight difference in Ct of untreated clone 22 and the much higher Ct compared to the treated cells (22 + DOX), the fold changes for primer RETNLB 1 was 13124.73 and for primer pair RETNLB 2 was 1200.98. Therefore, DOX induces RETNLB mRNA expression in the transfected pool 22.

PCR amplified cDNA derived from extracted RNA samples was submitted for sequencing to AGRF (AGRF Brisbane) to ensure transfected RETNLB gene sequence is correct. The resulting sequence showed a 100% match with the RETNLB sequence confirming that no mutations in the RETNLB gene occurred during transfection and subsequent puromycin selection.

A single cell selection followed and 18 clones were obtained and analyzed for RETNLB mRNA expression using 500 ng/ml Dox treatment for 48 hours. One clone, clone 18, showed inducible RETNLB expression (Table H5) with an average fold change of 4775 while the remaining clones tested showed no increased RETNLB expression.

Table H5: Relative mRNA expression of RETNLB with and without Dox. RETNLB transfected cell clone 18 was analyzed for RETNLB mRNA expression when cultivated with 500 ng/ml Dox for 48 hours and without Dox. Ct = cycle threshold, YWHAZ = Tyrosine 3-Monooxygenase/ Tryptophan 5-Monooxygenase Activation Protein Zeta Polypeptide.

	Ct Primer RETNLB 1	Ct Primer RETNLB 2	Ct Primer YWHAZ
Clone 18 + DOX	12.53	12.99	13.21
Clone 18 no DOX	25.98	25.94	14.21

However, the RETNLB mRNA expression in non-induced cells is higher than oberserved in non-induced cell pool (Table H4) indicating that the TRE3G promoter is leaky in clone 18 causing a constant low RETNLB mRNA expression.

H.3.4. Glucose concumption in RETNLB expression induced and non-induced HEK293F cell

Triplcate shake flask cultures of clone 18 with either 500 ng/ml Dox or no Dox (control) were analyzed for glucose consumption. The glucose consumption rates between during exponential growth (16 – 72 hours) are shown in Table H6.

Table H6: Mean glucose consumption rate of RETNLB expression induced and non-induced cells.

500 ng/ml Dox	contol
- 269.55 ± 15.70	-265.31 ± 14.27

No difference in glucose consumption was oberserved between induced and non-induced cells indicating that RETNLB overexpression does not reduce glucose consumption in

HEK293F cells. However, as the system is leaky the result is not conclusive. RETNLB expression at the constant low level detected in non-induced cells may already reduce glucose consumption and further increase in RETNLB expression in induced cells does not lower glucose consumption any further. Further explorations are needed, e.g. comparing glucose consumption of parental cell line and RETNLB transfected cell line.

Appendix I: Summary of studies that investigated DCA's effects on cancer cells in vitro and in vivo

Table I1: Publications investigating DCA's effects on cancer, DCA concentrations used, cell lines and in vivo models, and major effects of DCA.

Reference	DCA conc. used	Cell line used	Major effects of DCA
Bonnet et al. 2007	0.5-5.0 mM	A549, MO59K and MCF-7 cancer cells Healthy SAEC cells	- Reduced lactate production - Depolarized mitochondria in cancer but not healthy cells - DCA is selective for cells with high membrane potential and low K^+ channel Kv1.5 expression - Induced mitochondrial apoptosis in A549 cells - Decreased tumor size in rats
Michelakis et al. 2010	0.5-5.0 mM 6.25-25 mg/kg twice/day	Glioblastoma cells Glioblastoma patients	- Reversed mitochondrial hyperpolarization - Inhibits PDK 2 activity in vivo - Inhibited HIF-1α - Activated p53
Cairns et al. 2007	50 mg/kg	RKO and RKOShHIF1α tumors in mice	- Increased oxygen consumption in RKO tumors from mice - Delayed tumor growth in combination with tirapazamine
Niewisch et al. 2012	250 µM -2 mM	Neuroblastoma: Kelly, SK-N-SH, and LS cells	- Reduced glucose consumption and lactate production - Increased oxygen consumption in Kelly cells - Reduced oxygen consumption in SK-N-SH cells - Only minor induction of apoptosis at 1mM in LS cells
McFate et al. 2008	5.0-20.0 mM	HNSCC cell lines UM-22A and UM-22B	- Decreased PDHα phosphorylation and lactate production only in UM-22A but not in UM-22B cells - toxic in UM-22B cells but not UM-22A cells
Hanberry, Berger & Zastre 2014	0.0001-100 mM	SK-N-BE and Panc-1 cancer cell lines	- DCA reduced mitochondrial membrane potential - DCA reduced cell proliferation
Heshe et al. 2010	0.1-50 mM	18 permanent human tumor cell lines	- only increased apoptotic rate sparsely at 10mM - 80% apoptotic cells at 50mM - Dose- and time-dependent reduction of mitochondrial membrane potential in CCRF-CEM cells
Stockwin et al. 2010	0.5-100 mM 500 mg/kg/day	Panel of normal and cancer cell lines A549 rat xenografts	- DCA depolarizes mitochondria of cancer an normal cells - DCA is not selective for cancer cells - DCA has enhanced activity in cells with defective electron transport chain
Wong et al. 2008	1-10 mM	Panel of endometrial cancer cells	- DCA induced apoptosis in most low to moderately invasive but was ineffective in highly invasive cancer cell tested - Apoptosis was consistent with decreased MMP, decreased Survivin expression, NFAT-Kv1.5-mediated pathways and p53-PUMA-mediated mechanism
Sun et al. 2010	1-5 mM 23-200 mg/kg/day	Panel of breast cancer cell lines Breast cancer in vivo model	- Reduced proliferation without increase in cell death
Madhok et al. 2010	10-100 mM	Panel of colorectal cancer	- DCA decreased proliferation associated with apoptosis and G2 phase cell cycle arrest in cancerous cells but not normal cells
Cao et al. 2008	0.5-1 mM	Prostate cancer cells	- DCA increased apoptotic rate, was associated with G1 cell cycle arrest - DCA sensitized cells to irradiation

Ohashi et al. 2013	2-10 mM 25-100 mg/kg/day	Splenocytes and B16 melanoma cells Panel of mouse strains	- DCA increased antitumor immunotherapeutic activity in CD8+ T cell- and NK cell-sensitive tumor models
Shahrzad et al. 2010	10 mM 150 mg/kg/day	Colorectal cancer cell lines and mouse xenografts	- Induced apoptosis under normoxia - DCA acted as a cytoprotective for some colorectal cancer cells under hypoxic conditions
Sorokina et al. 2011	86 mg/kg	Sarcoma 37 cell mouse xenografts	- DCA increases the cytotoxic activity of arsenic trioxide which correlates with decreased c-Myc , HIF1-α and Bcl-2 expression
Sun et al. 2011	1-5 mM	Panel of breast cancer cells	- Combination of DCA and arsenic trioxide was more effective in inhibiting cell proliferation than either drug alone - DCA alone decreased HIF1α expression but increased ATPβ and Bcl-2 expression - DCA increased PDC activity
Vella et al. 2012	50 mM 2.5 – 25 mg/kg/day	Neuroblastoma cell lines and mouse xenografts	- DCA decreased proliferation without induction of apoptosis in vitro and in vivo - DCA was more effective on very malignant and fully proliferating cells compared to poorly malignant, more differentiated cells
Ayyanathan et al. 2012	1-50 mM	A549 and SCC25 cancer cells	- DCA enhances killing of cells by anticancer drug Sulindac involving ROS production, mitochondrial dysfunction, JNK signalling and induction of apoptosis
Kumar et al. 2012	1-40 mM	Panel of cancer cell lines and T-cell lymphoma cell lines Dalton's lumphoma mouse strain	- DCA induces apoptosis in tumor cells associated with increased ROS - Expression of HIF1-α, HSP70 and Bcl2 were inhibited - Expression of PUMA, p53, caspase-3 and CAD was increased
Kumar A. et al. 2013	112 mg/kg/day	Dalton's lymphoma mouse xenografts	- DCA chemosensitized cells to cisplatin - DCA increased survival of mice, reduced tumor volume, increased number of apoptotic cells, increased number of Annexin-V and TUNEL positive cells, increased ROS
Fiebiger et al. 2011	10 mM	Lung carcenoid cell lines (UMC-11, H727 and H835)	- DCA inhibited cell growth of UMC-1 cells - DCA sensitized UMC-1 cells against novel platinum-based chemotherapeutic drugs
Hur et al. 2013	10-100 mM	Gastric cancer tissues from patients Gastric cancer cell lines	- DCA increased responsiveness to 5-Fluorouracil in cell lines with high expression of PDK-1
Ishiguro et al. 2012	0.45-1.35 mM 50mg/kg/day	HT1080 fibrosarcoma and RKO colon cancer cells HT1080 mouse xenografts	- DCA and omeprazole had higher antitumor activity than DCA alone - Effect of DCA combined with omeprazole was reversed by vitamin E and caspase inhibitor Z-VAD-FMK
Shen et al. 2013	0-60 mM 10-100 mg/kg/day	Hepatocellular carcinoma cell lines and mouse xenografts	- DCA increased ROS and ATP - DCA sensitized sorafenib-resistant cells to sorafenib-induced apoptosis - Combination of DCA and sorafenib resulted in better tumor regression in mice than sorafenib alone
Xie et al. 2011	2-16 mM	HeLa cells	- DCA increased intracellular H_2O_2 and pH levels, decrease in MMP, increase of caspase 3 and 9, increased Kv1.5 expression - Synergistic effect of DCA and Cisplatin